Self-Healing Waterborne Polyurethane Dispersions

Sil Nevejans

Chemical Engineering Group

University of the Basque Country (UPV/EHU)

Donostia – San Sebastián

2018

Supervisors:

Prof. José María Asua (UPV/EHU)
Dr. Bernd Reck (BASF SE)

The research carried out in this thesis is funded by the European Union's Horizon 2020 research and innovation programme under the Marie Sklodowska-Curie grant agreement No. *642514* – TRACKWAY - H2020-MSCA-ITN-2014.

Contents

Chapter I. Introduction & objectives

"Self-healing Materials Market to Reach $2.4 (€2.1) Billion by 2022"[1,2]

I.1. Self-healing polymers

Following the development of the first synthetic plastics in the 20th century, polymers have become an indispensable part of modern life. In fact, plastics have become so widespread in our society that, for the first time since their emergence, people and governments have been forced to realize the impact of plastic waste on the environment, which has become an urgent and global problem. Part of the problem can be linked to the inherent drawback of many polymer materials being relatively prone to damage leading to catastrophic failure after which the polymer cannot perform its function anymore. A protective polymer coating that gets damaged by a small scratch, for instance, becomes instantly useless in preventing corrosion, an issue that alone costs hundreds of billions of dollars a year.[3] Together with the emerging understanding of the issues associated with polymer materials, researchers have been focusing on diminishing material damage and extending product life-time by the development of "self-healing" materials in order to provide a solution to the problems mentioned above.[4–11]

The exponential increase in documents that have been published per year mentioning the terms "self-healing" "materials" (Figure I.1) demonstrates that this is a thriving research field which started at the turn of the 21st century. From the different materials that can be studied, such as ceramics and concrete, polymers have seemingly attracted a lot of attention over the last two decades, accounting for about 50% of the published documents (Figure I.1).[11–14] These trends in academic research have also been reflected by commercial interest, with predictions that the self-healing materials market will reach $2.4 (€2.1) billion by 2022 (Figure I.2) in which healable polymers would still account for 37% of the market.[1,2]

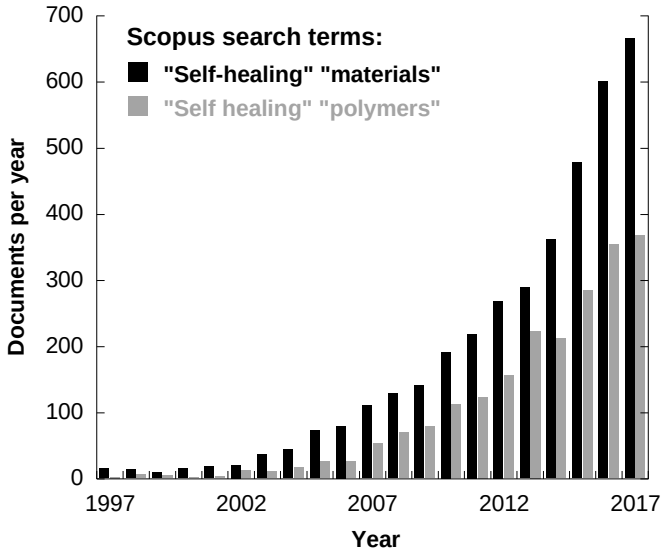

Figure I.1. Published documents per year for "self-healing" "materials" and "polymers" (Scopus).

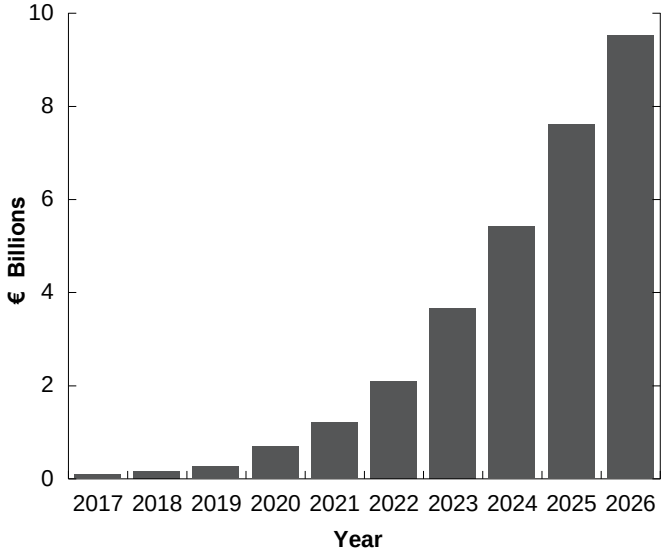

Figure I.2. Total market for self-healing materials predicted by n-tech Research from 2017-2026.[2]

Self-healing materials can be categorized into two types based on the process through which healing is achieved: **extrinsic and intrinsic** (Figure I.3).[15,16] Extrinsically healable materials have active fillers, so called healing agents, such as encapsulated monomers and catalysts embedded in the polymer matrix.[5,17–20] These healing agents are released into the matrix upon rupture and act as fillers which solidify and repair the damaged area. This is a single-use non-reversible process that demands the availability of the healing agents on the damaged interface, *i.e.* a relatively high load of encapsulated agent. This may be a problem in many cases and therefore such materials are likely to be used only in highly specialist applications.

On the other hand, self-healing polymers which can heal intrinsically make use of “built-in” reversible chemical and/or physical bonds to recover from damage and are especially interesting for long term use as they are able to undergo multiple healing events without detriment to the system.[15,16] In case of damage, the polymer network rearranges to bridge the gap thanks to inherent molecular mobility of the polymer chains and reconfigurable bonds within the chain which allow the restoration of the structural integrity of the polymer once the defect is filled.[21–24] Furthermore, since the ability to heal is incorporated through chemical groups, it is possible to preserve the material properties of conventional polymers. For these reasons, intrinsically healing polymers will be the focus of this introduction.

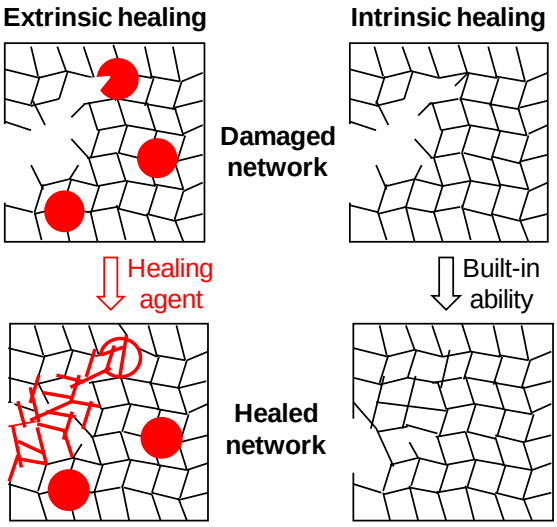

Figure I.3. Different self-healing processes based on extrinsic and intrinsic healing. (Inspired by Teixeira *et al.*[15])

In 1981, already some decades before research on intrinsic self-healing materials became prominent, Wool and O'Connor proposed a **model for crack healing** for conventional non-dynamic polymers involving a sequential process consisting of (a) surface rearrangement and (b) approach, (c) wetting, (d) diffusion and (e) randomization.[25] When considering a damaged object, *e.g.* a scratch or a deep cut (Figure I.4), where no external stimulus is applied, the first driving force for closure of the gap is the reduction of the surface tension. In this case, surface rearrangement (a) and surface approach (b) bring the two fractured interfaces back into close proximity through elastic recovery, the shape memory effect and/or interfacial flow.[23,26–29] Next, wetting or adhesion (c) can be seen as the process in which the two fractured surfaces come into contact so that re-formation of the broken bonds and supramolecular interactions can take place at the interface inducing the recovery of the initial mechanical properties and promoting

the following healing steps.[25,30] Interestingly, under specific conditions, the wetting process was recently described to proceed through a zipper-like cut closure, since the driving force is the inward tension on the crack which diverges at the tip, where the stress field displays a singularity.[31] However, the presence of the tip was found to be crucial, as for brittle fractures that traversed the entire sample and lacked a distinct tip this zipping motion was not observed.

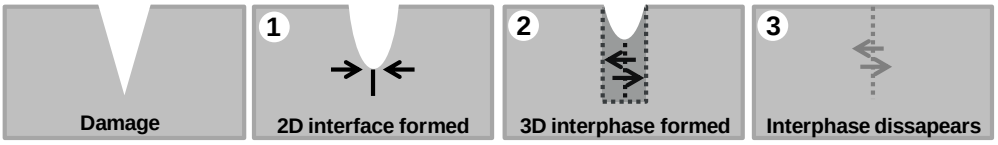

Figure I.4. Process for scratch healing involving (1) movement of material to close the gap, (2) interdiffusion of the polymer across the interface, (3) bond reorganization to fully heal the cut. (Inspired by Susa *et al.*[33])

After good wetting, polymer chains may start to diffuse at the interfacial region from one side to the other, which is called interdiffusion (d). For a linear polymer, the extent of interdiffusion will depend on the mobility of the chains and the time according to the scaling laws developed by Wool and O'Connor.[4,25,32] The mechanical properties of the polymer will be recovered once the length of the chains in both pieces is longer than the characteristic entanglement length of the polymer. On the other hand, for a cross-linked polymer (a thermoset material) interdifussion will be limited to dangling chains, typically shorter than the entanglement length, resulting in a material that is mechanically weaker than the pristine cross-linked network. The static nature of the cross-linked network prevents the further interdiffusion required for complete restoration of mechanical strength. However, when dynamic bonds are incorporated into the polymer backbone, the kinetics of the interdiffusion process can be enhanced. In the case of linear polymers, the rearrangement of the dynamic bonds after modest interpenetration leads to the

formation of polymer chains that extend to both sides of the cut reducing the time needed for the material to recover its mechanical strength (Figure I.5A). Unlike regular thermosets, cross-linked polymers containing dynamic bonds are able to heal and recover their mechanical strength, since the interdiffusion of dangling chains containing dynamic bonds allows the formation of a new cross-linked network at the interface as illustrated in Figure I.5B.

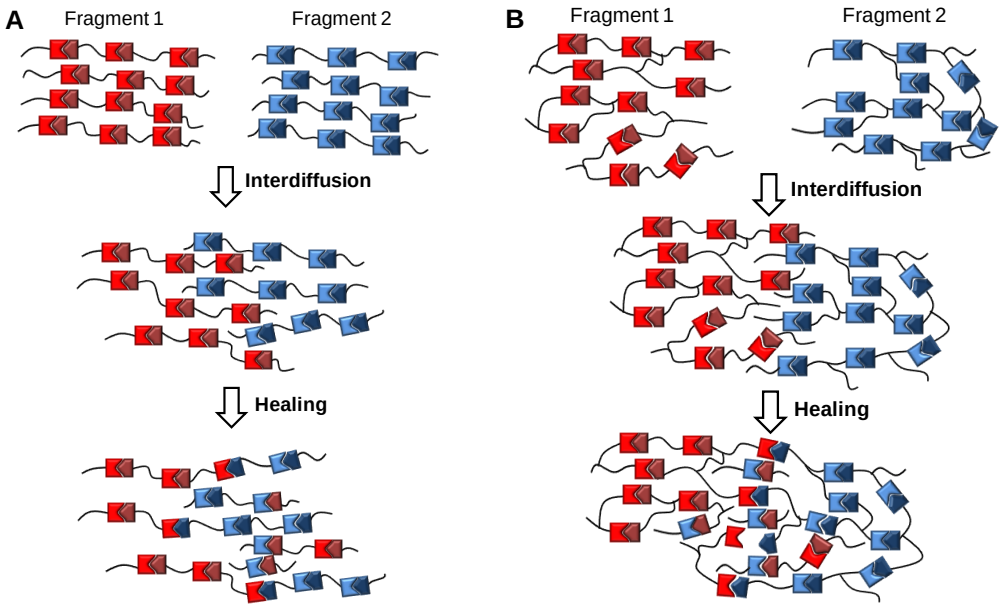

Figure I.5. Healing of a linear (A) and cross-linked (B) polymer containing dynamic bonds following dissection of the polymer chains into two fragments.

It is important to emphasize here that healing of polymer networks is only possible if both interdiffusion and dynamic bond exchange can take place as this induces the last step of the crack healing process described by Wool and O'Conner, namely randomization (e). The

presence of dynamic chemical or physical bonds in the polymer backbone is therefore crucial to complete the healing process as, once all aforementioned steps have been attained, they provide the material with the capability to rearrange and reorganize the polymer network in such a way that the original polymer structure and consequently material properties such as mechanical strength can be recovered.

Summarizing and simplifying the initial crack healing theory, it can be concluded that three series-parallel processes are required to obtain complete healing, which are (1) the movement of the material to close the gap so that a 2D interface is formed (2) interdiffusion of the polymer through the closed gap creating a 3D interphase and (3) dynamic bond exchange leading to rearrangements in the polymer network so that the 3D interphase eventually disappears (Figure I.4).[25,33] A polymer that is capable of both closing the gap and subsequently healing the interface is termed a self-healing polymer. From this model, it becomes clear that the kinetics of self-healing may be controlled by any of these processes and it is therefore of fundamental importance to consider all aspects of the healing process in material design.

With consideration of the mechanism of self-healing outlined above, **polyurethanes** are uniquely placed to provide self-healing polymers. One of the main beneficial properties of polyurethanes is the phase separated microstructure of segmented polyurethanes (Figure I.6), as it enables the production of materials with molecular mobility in the soft phases while preserving physical, structural and mechanical integrity through the presence of hard phases.[23,34] Furthermore, polyurethanes (PUs) have a built-in supramolecular healing ability due to the formation of hydrogen bonds between their backbones which provides the material with a basic level of intrinsic recovery upon damage without the intervention of any other active

element. This particular characteristic reinforces the action of the active moieties included for self-healing,[35–37] and in addition, can guide reactive functionalities allowing them to interact more easily with functional groups in their vicinity.[38–40] Aside from the rheological properties possessed by polyurethanes that make them of interest for self-healing materials, the chemistry involved in polyurethane synthesis is also highly versatile, allowing diverse functional groups to be incorporated.[34] This versatility of polyurethanes and their ease of functionalization has led to the incorporation of almost all possible chemical moieties reported to provide self-healing properties into polyurethane systems which will be discussed in the next section of this introductory chapter.

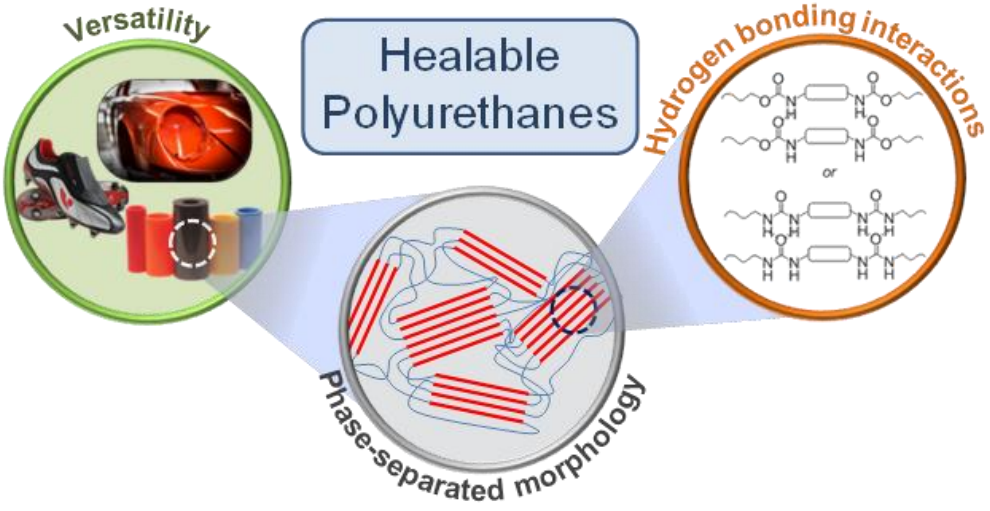

Figure I.6. Dynamic interactions presented in poly(urea-urethane) structures.

I.2. Intrinsically healable polyurethanes

Intrinsic self-healing materials have captured the imagination of polymer chemists leading to the creation of an extensive library of potential bond exchange reactions that can be used to create the basis of such materials. As shown in Figure I.7, two main synthetic pathways towards dynamic bond rearrangements for intrinsically healable polyurethanes have been proposed that can be divided into (1) **supramolecular interactions** and (2) **dynamic covalent reactions**. The incorporation of such structures is responsible for the repair at a molecular level and therefore the understanding of the underlying mechanism as well as the reaction performance is of prime importance. In this section, representative examples of the systems will be given in a short overview.

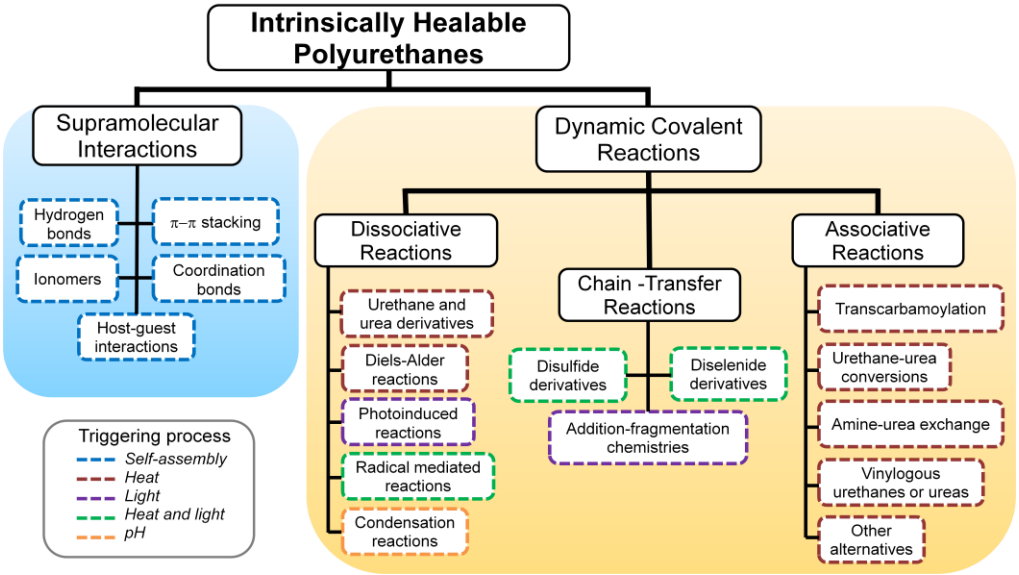

Figure I.7. General classification of intrinsically healable polyurethanes.

I.2.1. Supramolecular interactions

Supramolecular interactions are non-covalent links which are based on the equilibrium between “bound” and “non-bound” states and which present a high stability with time since problems with side reactions can largely be avoided (Figure I.8).[22,41] On the other hand, since the strength of most supramolecular interactions is weaker than a typical covalent bond, these links can be broken with relative ease. Therefore, one of the main objectives when developing strong self-healing PUs is to maximize the strength and number of supramolecular interactions.

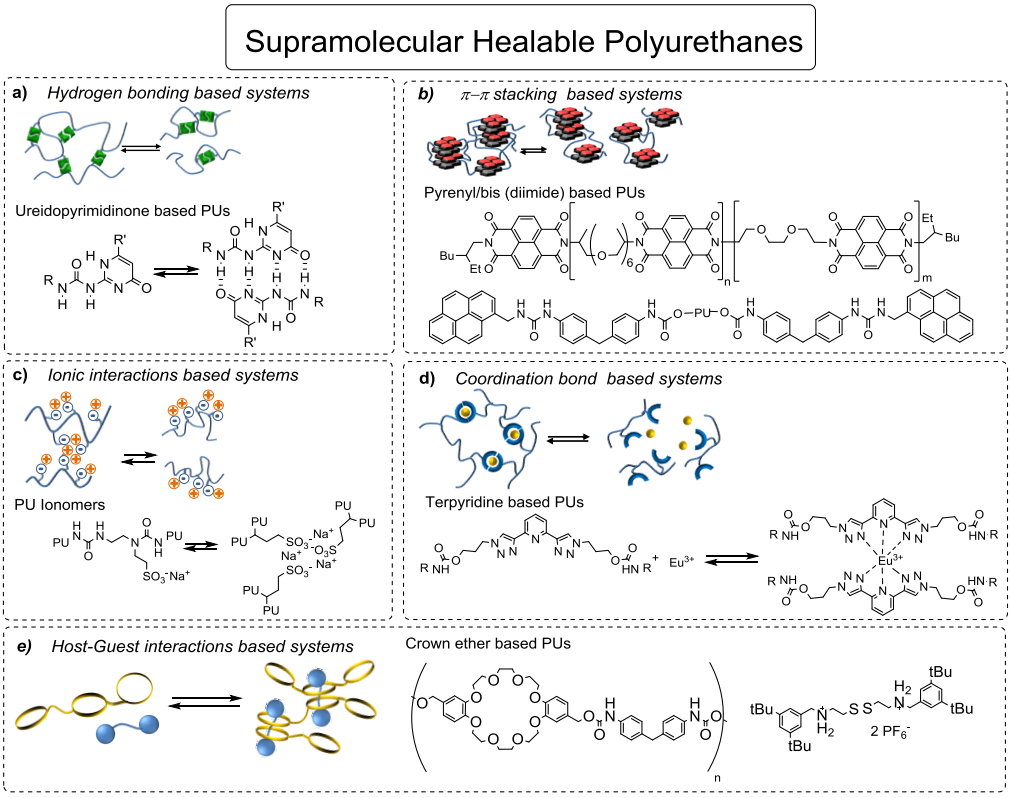

Figure I.8. Schematic representation of the relevant interactions in supramolecular healable PUs.

Hydrogen bonding interactions are one of the most widely used strategies to develop supramolecular healable polyurethanes. In this way, some healable PUs were described just relying on the inherent H-bonding between urethane or (thio)urea units.[35,42] Alternatively, the specific design of self-healing hydrogen bonding networks has been attempted, for instance by introducing multiple substituted and non-substituted urea bonds,[43] or by increasing the strength of active motifs that generate H-bonds such as the well known self-complimentary ureidopyrimidone (UPy) unit (Figure I.8 a).[44–46] The introduction of ***π-π* stacking interactions**, has also been applied in the development of healable PUs (Figure I.8 b).[47,48] However, only a few examples exist introducing these interactions due to the high insolubility of the polymer and the difficulty in finding systems capable of self-assembly by means of π-π interactions. **Ionomers** are polymers that contain a small number of pendent ionic groups which can aggregate and form physical cross-links within the bulk material. Since these supramolecular cross-linking points are dynamic, PU-based ionomers have also been described which demonstrate self-healing behavior for example by the introduction of sulphonate groups (Figure I.8 c),[49] amino and acid groups,[50] or zwitterionic groups.[51] Polymer materials based on **coordination bond interactions** make use of the dynamic cross-linking between ligands and metal ions which are dispersed in the polymer structure to achieve their self-healing ability. The most widely used coordination bond system is based on pyridine derivatives (Figure I.8 d).[52,53] The application of **host-guest interactions** is one of the most recent approaches for intrinsically healable materials, and therefore very few examples have been applied in PU systems (Figure I.8 e).[54,55] The main advantage is the high selectivity of the interaction, which prevents the passivation of the healing process.[56]

I.2.2. Dynamic covalent reactions

Alternatively to supramolecular interaction, intrinsic healable features can also be obtained by introducing dynamic covalent bonds. Contrary to most conventional covalent bonds, these moieties can easily be broken and/or reformed, so that their dynamic equilibrium permits the recovery of the damaged polymer network by forming new covalent bonds. The incorporation of dynamic covalent bonds permits a fundamental change in the way polymers can be used, as incorporating them in a cross-linked network can allow reprocessing, something that is off-limits for conventional thermosets.[43,57,58]

According to the bond exchange mechanism, three main groups of dynamic covalent reactions have been applied in the field of healable polymers termed here dissociative, associative and chain transfer reactions (Figure I.9). During a **dissociative reaction** (Figure I.9 a), the active motif is cleaved into two components which are able to subsequently recombine afterwards. In contrast, the exchange in **associative reactions** (Figure I.9 b) occurs because a free functional group present in the polymer chain reacts with an active motif in its vicinity, generating a new active motif. The third alternative, termed here **chain transfer reactions**, can be considered as a mixture of the other mechanisms (Figure I.9 c). First, an external agent is added (*e.g.* a radical source) or the dynamic bond is activated to produce free reactive species. These reactive species are able to exchange with dynamic bonds in the vicinity, simultaneously producing analogous dynamic bonds in the backbone and new reactive species. The process finishes when the reactive species are terminated by recombination or side reactions. Although the difference between these three cases may appear small, they represent highly different kinetics requiring appropriate selection for certain applications or application conditions.

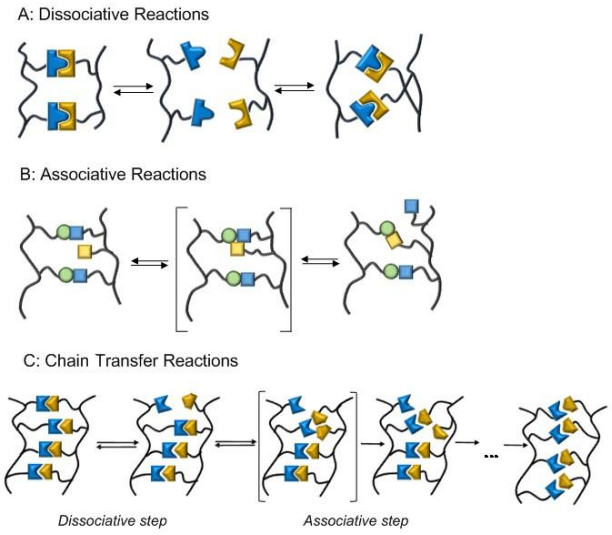

Figure I.9. Schematic of the dynamic covalent reaction mechanisms (Inspired by Denissen *et al.* [58]).

I.2.2.1. Dissociative reactions

Dissociative reactions are based on a dynamic equilibrium involving sequential breaking and reforming of covalent bonds usually requiring an external stimulus, such as heat or light, to shift the equilibrium to the dissociated state so that bond exchange can occur. Since the bond energies of dynamic covalent bonds are usually lower than a typical C-C bond, it is obvious that the introduction of the dynamic bond represents “weak links” in the polymer backbone, which reduces the mechanical properties of the material. Moreover, at elevated temperatures, where the equilibrium is shifted to the dissociated state, the network integrity may be completely lost which causes a serious problem in applications where a minimal strength is required. However, dissociative strategies also are advantageous in that, in most cases, at room temperature the equilibrium is shifted so far to the dormant state that the materials can effectively be considered static which makes them reasonably stable with time.

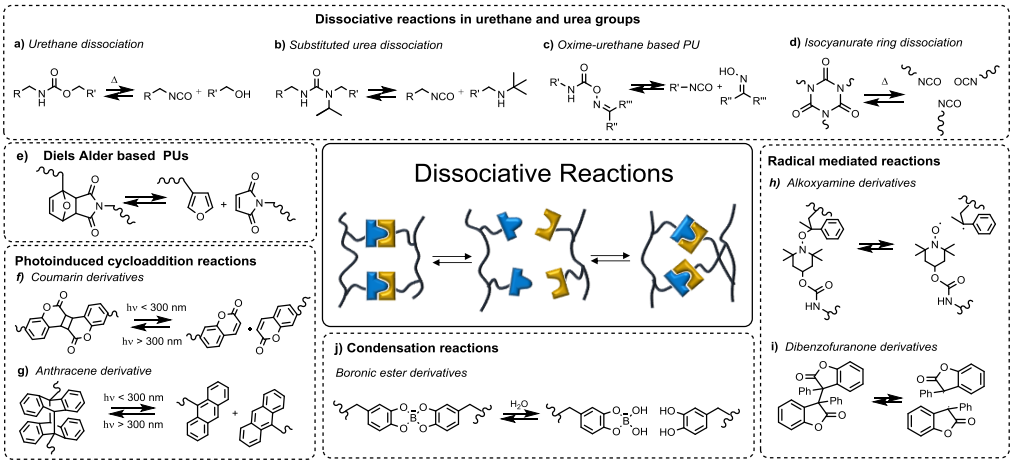

Figure I.10. Dissociative reactions used in the development of healable polyurethanes.

At very high temperatures (T>150ºC), **urethane and urea** groups can undergo dynamic dissociative reactions forming an isocyanate and a hydroxyl or amine group respectively, which usually results in decomposition of the polymer.[59] However, recently, some specifically reversible urethane or urea configurations have been introduced into PUs inducing self-healing at moderate temperatures (Figure I.10 a),[60–63] or even at room temperature in hindered PUUs (Figure I.10 b).[64] Alternatively, dynamic oxime-carbamate bonds (Figure I.10 c),[65] or reversible uretdiones and isocyanurates (Figure I.10 d),[66] have been exploited to obtain healable PUs. An obvious drawback, however, is the formation of toxic isocyanates which are highly reactive towards water (moisture) which would eventually degrade the material with time.

Also **Diels-Alder** (DA) reactions (Figure I.10 e), taking place between a diene and a dienophile *via* a [4+2] cycloaddition, have been employed to reversibly chain extent or cross-link PUs so that the material could recover from damage upon heating.[67–70] However, extensive heating to

temperatures higher than 120ºC are generally necessary for these DA adducts to be reactive which limits their attractiveness for applications. Alternatively, **photoinduced cycloaddition reactions** can also be utilized to stimulate dynamic covalent behavior in PUs, such as the [2+2] cycloaddition reactions involving coumarin derivatives (Figure I.10. f),[71–73] or [4+4] cycloaddition reaction based on anthracene derivatives (Figure I.10 g).[74,75] Although these photoinduced processes are advantageous over heat triggered systems as they present easy spatial and temporal control,[76,77] the application of light obviously restricts the use to transparent and/or thin surfaces and can be problematic in many practical applications where materials are constantly exposed to (sun)light.

Radical mediated dissociative reactions make use of moieties which can provide polymers with a dynamic self-healing behaviour due to the formation of stable free radicals after reversible homolytic scission upon stimulation or damage. Often, alkoxyamine derivatives are used for this purpose in PUs leading even to healing at room temperature (Figure I.10 h),[78–80] but also diarylbibenzofuranones can recover from damage at mild temperatures or with mechanical force (Figure I.10 i).[81,82] Advantageously, these radical reactions are very fast and highly dynamic without provoking complete disintegration of the polymer network, however, their reactivity can also lead to side reactions (*e.g.* with oxygen) and passivation over time. Finally, a **condensation reaction** of dynamic catechol-boronic ester bonds can lead to pH dependent reversible hydrolysis inducing (underwater) healing in specific PUs (Figure I.10 j).[83,84] However, these systems are mostly hydrogels of which the sensitivity to pH and moisture content has to be taken into account towards its applicability.

I.2.2.2. Associative reactions

Associative reactions can be considered as interchange reactions between a dormant center and a reactive functional group within the polymer matrix (Figure I.11), so that, in contrast to dissociative processes, the degree of cross-linking remains constant along the process. The unique mechanism of these reactions has allowed them to be employed in the development of a new generation of materials known as *vitrimers*. They behave as cross-linked materials at low temperatures, but present a glass-like fluidity at high temperatures due to the rapid interchange of functional groups in the polymer network.[57,58] A major drawback of the associative mechanism is its reliance on the reactivity of pendant functional groups, such as hydroxyl or amine groups, which can cause problems in commercial products or might lead to side reactions limiting their long term stability. In addition, bond exchange, even at lower temperatures, leads to creep which could be a significant problem in practical applications.

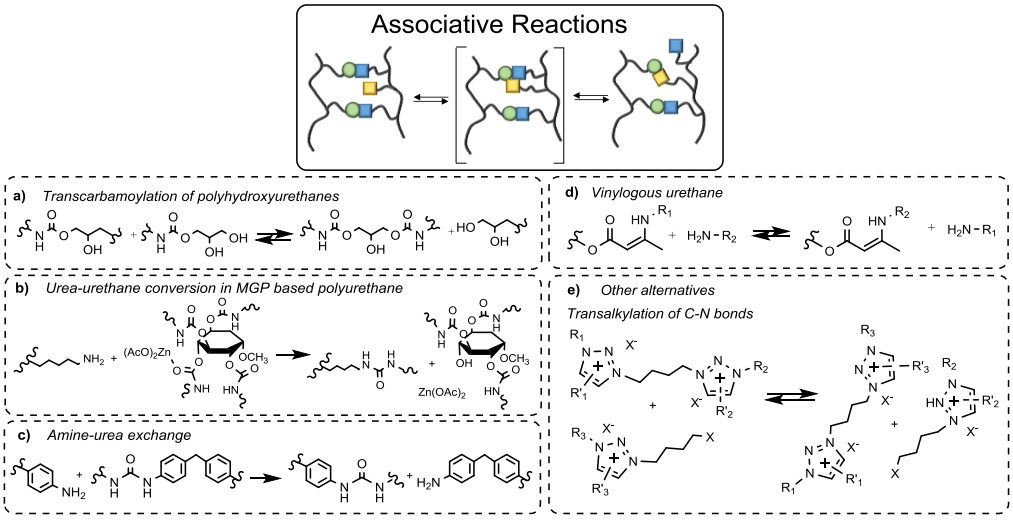

Figure I.11. Dynamic reactions undergoing associative mechanism in healable PUs.

Transcarbamoylation leads to the dynamic exchange of carbamoyl groups with free hydroxyl groups which are present in polyhydroxyurethane based materials which makes reprocessing possible at T>140ºC (Figure I.11 a).[85,86] Transcarbamoylation of carbamates has also been reported to induce dynamic exchange reactions in the material which could be reprocessed at even higher temperatures (T>180ºC).[87] An alternative associative chemistry is based on the **urethane-urea conversion** in methyl α-D-glucopyranoside (MGP) based PU networks in the presence of zinc acetate (Figure I.11 b).[88] This mechanism is distinctive from the general associative mechanism as the free amine groups are only formed upon damage after which they irreversibly react with the urethane groups in the polymer matrix to produce urea linkages and free hydroxyl groups. However, such free amine groups could also be deliberately incorporated into the PUU backbone so that an **amine-urea exchange reaction** could occur leading to recyclable cross-linked materials at T>150ºC and under pressure (Figure I.11 c).[89] Similarly, **vinylogous urethane or urea** based polymer containing amine terminated dangling chains have been developed which are capable of reprocessing and recycling at high temperatures (Figure I.11 d).[90,91] Although the increased reactivity of the vinylogous urethane/urea group is advantageous, the long term stability of amines necessary to induce exchange could cause problems. Finally, there are **alternative associative chemistries** that have yet to be used in polyurethane systems, but have already been able to provide self-healing characteristics to other polymer systems, such as transalkylation of C-N bonds (Figure I.11 e),[92] or boronic esters.[93]

I.2.2.3. Chain transfer reactions

The chain transfer reaction mechanism presents features both from dissociative and associative mechanisms (Figure I.12). The first step involves the generation of active species after which these species react with other dynamic bonds in the vicinity leading to exchange. Generally, chain transfer reactions occur via radical mediated intermediates. It should be highlighted that the potential advantage of this strategy over the purely dissociative radical mechanism is that the number of active species at a given time is comparatively low. However, in this case, the rate of bond exchange can still be fast even when the concentration of active species is low, since all the dynamic bonds present in the backbone are susceptible to react with the formed active species. Nevertheless, the intermediate species can possibly undergo side reactions that may limit their long term stability.

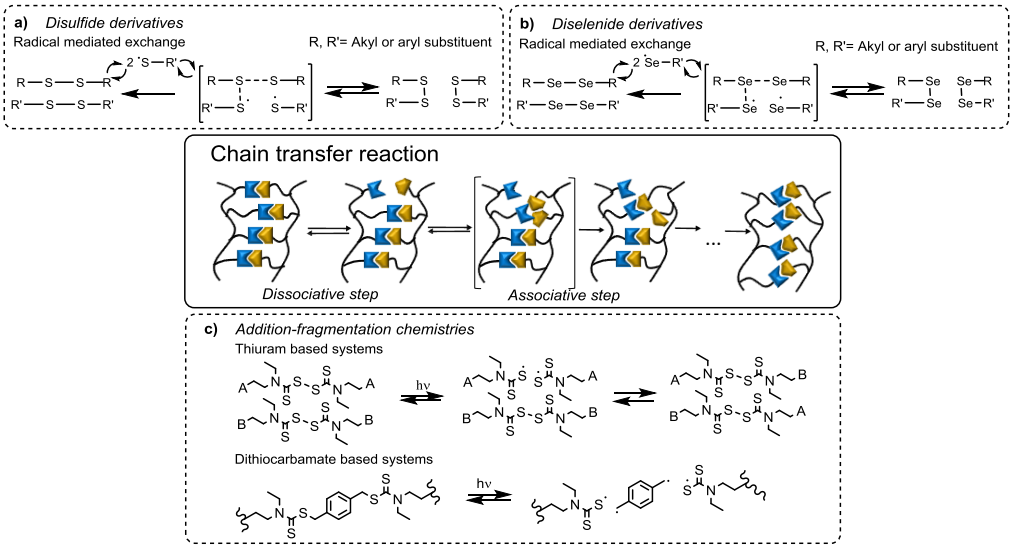

Figure I.12. Chain transfer reactions introduced to develop healable polyurethanes.

Most of the examples of chain transfer reactions are based on **disulfide exchange reactions** as depicted in Figure I.12 a. Already in 1964, the introduction of disulfide and tetrasulfide groups into cross-linked polyurethane elastomers was demonstrated.[94] This early work showed two interesting points; 1) the dynamic nature of the S-S bond allowed for efficient stress relaxation of cross-linked materials, 2) bond exchange was much more rapid in the tetrasulfide linkages than in the disulfide linkage, while the latter showed greater stability in spectroscopic tests.[94] By now, the incorporation of these dynamic aliphatic disulfide bonds into PUs have led to the development of self-healing materials under exposure to heat or light.[95–101] Interestingly, by using aromatic instead of aliphatic disulfides, the development of a cross-linked PUU was described which was able to heal at room temperature without using any catalysts and, in addition, could be reprocessed at elevated temperatures.[102,103] Very recently, the ease of implementation of this chemistry in PUs has attracted (our) attention, leading to alternatives proposing waterborne PU systems[104] and enhanced mechanical strengths.[105,106] Later in this work (Chapter III-V), we will similarly present new waterborne healable PUUs based on the introduction of modified aromatic disulfides leading to even stronger and simultaneously more mobile materials.

Although disulfides are often classed in the same bracket as the associative chemistries, only recently we were able to clarify that the underlying mechanism of disulfide exchange actually occurs through disulfide scission generating sulfur-based radicals followed by bond exchange between the formed radicals and other disulfides, *i.e.* chain transfer, which will be discussed in Chapter II.[107,108] With this radical mediated mechanism, the reasoning for choosing aromatic disulfides over aliphatic ones is twofold. First of all, as the bond dissociation energy of the

disulfide bond in diaryldisulfides is lower (50 kcal.mol^{-1}) than the value in dialkyldisulfides (65 kcal.mol^{-1}) a faster dissociation rate is obtained for the aromatic disulfides.[107,109] Moreover, since phenyl rings give rise to electron delocalization, the formed aromatic S-based radicals are more stable than the aliphatic counterparts.[107] This enhanced stability of the S-based radicals, however, does not limit the exchange reactions in a second step, since recently it was theorectically described that the phenyl rings can lower the energy barrier of the exchange reactions as $\pi - \pi$ stacking stabilize the transition state.[110] It can therefore be concluded that the use of aromatic disulfides is advantageous due to their enhanced dissociation and exchange reaction and additionally since stabilized S-based radicals are formed in the presence of phenyl rings making them attractive towards applications as they supposedly would be less prone to side reactions and therefore could provide more long term stability.

It is noteworthy to mention that due to the underlying radical mediated mechanism, it is not straightforward to incorporate the disulfide bonds in alternative polymer systems which contain radicals or double bonds.[111] For example, recently unusual cross-linking density rather than self-healing was observed when aromatic disulfides were introduced into a polybutadiene based PUU.[112,113] This unexpected behaviour of the disulfides was linked to side reactions, like proton abstraction and radical induced thiol-ene addition, occuring in presence of double bonds which led to chain coupling. In addition to radical-based chain transfer reactions, disulfide moieties can undergo an associative reaction with thiol compounds.[114,115] However, due to the high reactivity of the thiol groups and their tendency to oxidize in ambient conditions their extent of dynamic exchange is reduced with time. Moreover, disulfides can also be induced to undergo exchange by addition of a reducing agent, such as tri-*n*-butylphosphine (TBP), which

leads to the formation of a thiolate anion allowing shuffling of disulfide bonds.[116] Nevertheless, in the presence of water, an irreversible side-reaction of TBP with disulfides can lead to the formation of phosphine oxide and thiols which might be undesirable as this inactivates the catalyst, cleaves the disulfide bonds and ceases the exchange reaction.[116,117]

Alternatively, very recent research has focused on the development of (aromatic) **diselenide and ditelluride** based PUs, in which both enhanced healing kinetics and efficiency have been described due to faster exchange since the bond energy of both Se-Se and Te-Te is lower compared to that of disulfides (Figure I.12 b).[118–120] Nevertheless, it is noteworthy to mention that these weaker bonds also lower the mechanical strength of the PUs and are supposedly less stable with time. Finally, incorporation of **addition-fragmentation chemistries,** such as thiuram,[121] trithiocarbonates,[122,123] and dithiocarbamate units,[124] into PUs similarly allows for bond exchange and healing (Figure I.12 c). However, these mainly photo-activated reactions pose similar drawbacks as the photo-induced dissociative reactions, questioning their stability under long exposure to (sun)light.

I.3. Applicability of intrinsically healable polyurethanes

Having discussed the various chemistries that can be employed to obtain self-healing polyurethanes, it is also important to mention that, since they can act as thermoplastic, elastomeric or thermosetting materials, it possible to use them in various application fields, such as adhesives, elastomers and coatings.[34] Especially the last group has captured a lot of interest, as one of the most widely cited potential applications in academic literature for intrinsically healable polyurethanes is their use in (protective) coatings.[125–127] Nevertheless, only a handful of examples can be found where self-healing (PU) coatings are actually employed in industrial applications, with the biggest interest coming from the car industry. Nissan was one of the first to mention self-healing clear-coats,[125] after which Bayer Materials science (now Covestro) described scratch-resistant and healable topcoats for cars and proposed their usefulness in furniture industry.[128] More recently, also NEI cooperation,[129,130] Croda,[131] and Lubrizol,[132] have been promoting self-healing properties of their commercial products. So why is research on self-healing polymers booming (Figure I.1), while there is almost no existing market for self-healing materials so far (Figure I.2)?

The reason is that for these self-healing polymers to be able to make the transition to industrial applications it is fundamental that they possess analogous properties to the non-healing alternatives, which is not trivial to achieve. For example, self-healing polyurethanes are expected to provide physical strength, *i.e.* limited motion, in order to meet the mechanical requirements of industrial coatings. However, this material property actually imposes a major stumbling block when it comes to their application. In fact, the incorporation of supramolecular interactions or dynamic covalent bonds into the polymer network, to provide dynamics and

mobility of the material enabling healing, tends to lower the mechanical properties of the bulk polymer due the inherent weakness of the dynamic bonds as mentioned above.

These conflicting requirements, with material strength on the one side and network mobility on the other side, have limited the self-healing PU polymers reported in academic literature to attain similar mechanical properties as described for polyurethane coatings in patents so far. With a special focus on the disulfide based PU materials which were described in Section I.2., this issue is exemplified in Figure I.13, where the ultimate tensile strengths in the patent literature of non-healable PU(U) dispersions are above 15 MPa, while almost all academically reported examples of self-healing PU(U)s based on disulfide bonds are below this threshold.

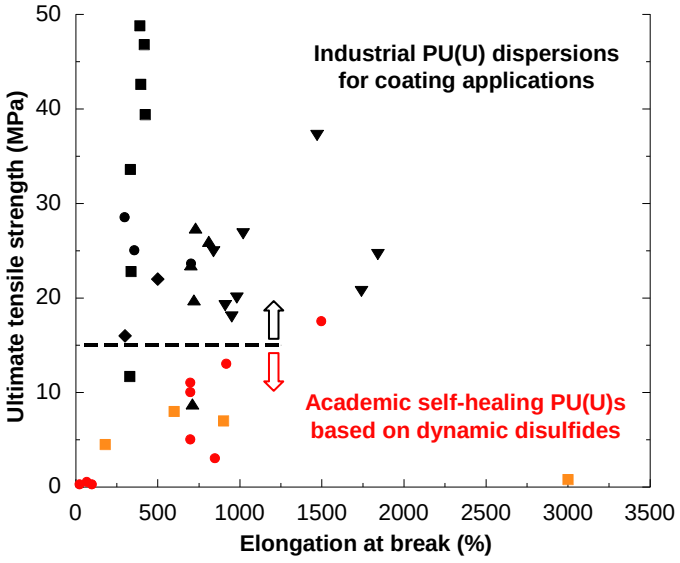

Figure I.13. Tensile properties of PU coatings from the patent literature in black symbols (●: sealing coatings,[133] ■: hardwood floor coatings,[134] ▲,▼: textile/leather coatings,[135,136] ♦: sports floor coating[137]) and for self-healing PUs based on aliphatic disulfides (●),[95–101,114–116] and aromatic disulfides (■),[102–106] described in the literature overview in Section I.2.

Thus, from the above it is clear that in order to overcome the gap that currently exists between academic research and industrial applicability, self-healing PUs with increased mechanical properties need to be developed. Although recently a few studies have recognized this issue and have tried to enhance the strength of healable PU materials based on disulfides,[95,101,105,106] the target region of industrial coatings has not been reached yet (Figure I.13).

It is also important to notice that although in many cases it is attractive to obtain self-healing at room temperature, this inherently demands a certain level of mobility of the polymer which compromises the mechanical properties and can lead to creep as well as a limited ability to withstand wear.[24,138] It may therefore be advantageous to develop a material which shows sufficient mechanical resistance at the service temperature, while self-healing is "triggered" by application of an external stimulus such as heat, which can stimulate both chain dynamics and bond exchange. In order to restrict the heat necessary for activation, obviously the selection of the dynamic system, *i.e.* **the type of reversible chemistry**, is crucial as described in Section I.2. However, taking the crack healing theory described in Section I.1 back into mind, it is clear that the dynamic system mostly plays a role in the last step of randomization through bond reorganization of the polymer network and is not the only factor affecting the healing process.

Another key parameter for successful self-healing is the chain mobility of the polymer. On the one hand, this can easily be enhanced by increasing the temperature above the glass transition temperature (T_g) so that molecular interdiffusion can take place. One the other hand, one can also play with the chain mobility of the material by altering the **polymer architecture**, which has only received limited attention to date as it has often been considered as a secondary factor next to the type of reversible chemistry.[138] In the last few years, however,

researchers have realized the importance of this factor and therefore an increasing effort has been done to study the impact of the polymer structure when developing self-healing polymers. For example, as cross-linked polymers have a high mechanical strength, the impact of the cross-linking density on the healing ability of poly(urethane-urea)s has been studied,[139,140] and alternatively the effect of trapping dynamic disulfides in the hard phase of PU elastomers has been investigated.[95] Other non-PU based work has been directed towards the understanding of influence of polymer composition and physical properties on self-healing polymers,[33,141,142] for example focusing on the effect of the disulfide or tetrasulfide content on the healing ability.[143,144] In these studies, typically scratch closure kinetics were monitored to obtain a first qualitative measure for the healing potential of the polymer. Tensile testing and/or fracture mechanics were performed in order to quantitatively measure the mechanical properties of the material and their recovery after damage and healing. Finally, by combining this information with results from rheological measurements, more insight in the relationship between the polymer dynamics and architecture and the self-healing ability could be obtained. Although more work has been focusing on the influence of the polymer structure recently, it is clear that the understanding of its relationship with healing is still limited compared to the extent of research that has been done on linking the reversible chemistry to healing (Section I.2).

Only if we are able to understand not solely the effect of the reversible chemistries, but also the influence of the polymer architecture on the healing ability of polymers, will we be capable of effectively developing self-healing materials with enhanced mechanical properties that answer the requirements of industrial applications so that the expectations of reaching a $2.4 billion market for self-healing materials by 2022 can be met (Figure I.2).[1,2]

I.4. Main motivation and objectives

As described above, despite the significant efforts that have been done in academic research regarding self-healing polymers, it remains a huge challenge to try and develop a polymer that can meet the demand of industry for high material strength and simultaneously provide the attractive ability to self-heal under mild conditions. In this thesis, the development and characterization of newly synthesized monomers, polymers and polymer coatings will be described with the aim to close the gap between academic and industrial research and produce strong self-healing poly(urethane-urea)s which would be attractive for coating applications. Additionally, since, the coating market is shifting from solvent-based to waterborne coatings, because of environmental concerns and governmental regulations, the synthesis of the described poly(urethane-urea)s will be performed so that they are obtained as aqueous polymer dispersions limiting the use of volatile organic compounds (VOC).

Since aromatic disulfide bonds have the potential of providing enough mechanical strength to the material at room temperature, while offering an easily initiated and fast dynamic exchange at elevated temperatures as described above, we want to incorporate aromatic disulfide bonds into waterborne poly(urethane-urea) materials so that self-healing can be achieved both by supramolecular interactions (H-bonding) and dynamic covalent bonds (disulfide bonds).

However, first, we need to clarify which mechanisms play a role in the disulfide exchange so that we obtain full understanding of the polymer chemistry that will be introduced into the poly(urethane-urea) materials. Afterwards, we aim to investigate the limits of commercially available aromatic disulfide compounds, so that new and improved aromatic disulfides can be

synthesized and incorporated offering stronger and more efficiently healable PU(U)s. Furthermore, we seek to optimize the polymer architecture by playing with the different building blocks so that the materials with an enhanced mechanical strength show sufficient mobility leading to self-healing which would be of interest in coating applications. In other words, we pursue to attain the ultimate goal of getting into the region of scope for the mechanical properties of industrial coatings (Figure I.13), while still showing a certain extent of self-healing. Finally, we desire to test the protective barrier properties of the developed materials at the application level, *i.e.* as coatings.

I.5. Thesis outline

Chapter I gives a general introduction on self-healing materials focusing on the different intrinsic chemistries introduced into polyurethanes to obtain recovery after damage and describing the current issues regarding their applicability. Moreover, the main motivation and objectives of the thesis are specified.

In **Chapter II**, the underlying mechanism of disulfide exchange will be elucidated using a variety of spectroscopic techniques to monitor the model exchange reaction between two aromatic disulfide compounds, so that full understanding of the polymer dynamics can be obtained.

The synthesis of waterborne poly(urethane-urea)s containing dynamic aromatic disulfide bonds will be described in **Chapter III**. Additionally, it will be demonstrated that the incorporation of a new flexible disulfide monomer increases both the mechanical strength and the dynamic behaviour of the materials making them more attractive for self-healing applications. These analyses will be performed mainly using polymer characterization methods, scratch closure tests and rheological measurements.

Chapter IV will focus on the optimization of the polymer microstructure in order to enhance the strength of the poly(urethane-urea)s at room temperature, while obtaining sufficient mobility at elevated temperature, so that healable waterborne coatings can be developed which can overcome the currently existing gap between academic research and industry (Figure I.13). In order to reach this goal, we will not only play with the amount and flexibility of the self-healing

disulfide moiety, but we will also modify the degree of functionality of the chain extender, so that the characteristics of both linear and cross-linked self-healing materials can be compared.

In **Chapter V**, the explicit influence of the dynamic covalent disulfide bonds on the strength, mobility and self-healing ability will be determined for linear poly(urethane-urea)s and cross-linked PUU networks by comparing them with non-dynamic counterparts using fracture mechanics in addition to the other characterization techniques.

Chapter VI will investigate the capability of these healable polymers to protect metal substrates from corrosion in pristine, damaged and healed conditions.

Finally, **Chapter VII** summarizes the most relevant conclusions of this thesis.

In order to avoid too elaborate representations and discussions in the individual chapters, the Supporting Information of Chapter III-V is represented in **Appendixes I-III** respectively, while the **Abbreviations and acronyms** used in the thesis are listed at the very end.

I.6. References

1. Coating World. Breaking News: Self-healing Materials Market to Reach $2.4 Billion by 2022. (2017).
2. n-tech Research. *Markets for Self-healing Materials 2017-2024*. (2017).
3. Hou, B. *et al.* The cost of corrosion in China. *npj Mater. Degrad.* **1,** 1–10 (2017).
4. Wool, R. P. Self-healing materials : A review. *Soft Matter* **4,** 400–418 (2008).
5. Ghosh, S. K. *Self-healing materials: Fundamentals, Design Strategies and Applications*. (Wiley-VCH Verlag GmbH & Co. KGaA, 2009). doi:10.1002/9783527625376
6. Syrett, J. A., Becer, C. R. & Haddleton, D. M. Self-healing and self-mendable polymers. *Polym. Chem.* **1,** 978–987 (2010).
7. Blaiszik, B. J. *et al.* Self-Healing Polymers and Composites. *Annu. Rev. Mater. Res.* **40,** 179–211 (2010).
8. Qiu Zhang, M. & Zhi Rong, M. *Self-Healing Polymers and Polymer Composites*. (Wiley, 2011). doi:10.1002/9781118082720
9. Binder, W. H. *Self-healing polymers*. (Wiley-VCH, 2013). doi:10.1002/9783527670185
10. Yang, Y. & Urban, M. W. Self-healing polymeric materials. *Chem. Soc. Rev.* **42,** 7446–7467 (2013).
11. Hager, M. D., Greil, P., Leyens, C., van der Zwaag, S. & Schubert, U. S. *Self-healing materials*. (Springer, 2016). doi:10.1007/978-3-319-32778-5
12. Wu, M., Johannesson, B. & Geiker, M. A review: Self-healing in cementitious materials and engineered cementitious composite as a self-healing material. *Constr. Build. Mater.* **28,** 571–583 (2012).
13. Lucas, S. S., von Tapavicza, M., Schmidt, A. M., Bertling, J. & Nellesen, A. Study of quantification methods in self-healing ceramics, polymers and concrete: A route towards standardization. *J. Intell. Mater. Syst. Struct.* **27,** 2577–2598 (2016).
14. Zhang, P. & Li, G. Advances in healing-on-demand polymers and polymer composites. *Prog. Polym. Sci.* **57,** 32–63 (2016).
15. Teixeira, R. F. a., Hillewaere, X. K. D., Billiet, S. & Du Prez, F. E. Chemistry of Crosslinking Processes for Self-Healing Polymers. *Self-Healing Polym. From Princ. to Appl.* 215–246 (2013).
16. Billiet, S., Hillewaere, X. K. D., Teixeira, R. F. A. & Du Prez, F. E. Chemistry of Crosslinking Processes for Self-Healing Polymers. *Macromol. Rapid Commun.* **34,** 290–309 (2013).

17. White, S. R. *et al.* Autonomic healing of polymer composites. *Nature* **409,** 794–797 (2001).

18. Toohey, K. S., Sottos, N. R., Lewis, J. A., Moore, J. S. & White, S. R. Self-healing materials with microvascular networks. *Nat. Mater.* **6,** 581 (2007).

19. Zhu, D. Y., Rong, M. Z. & Zhang, M. Q. Self-healing polymeric materials based on microencapsulated healing agents: From design to preparation. *Prog. Polym. Sci.* **49–50,** 175–220 (2015).

20. Hillewaere, X. K. D. & Prez, F. E. Du. Fifteen chemistries for autonomous external self-healing polymers and composites. *Prog. Polym. Sci.* **49–50,** 121–153 (2015).

21. Zhang, M. Q. & Rong, M. Z. Intrinsic self-healing of covalent polymers through bond reconnection towards strength restoration. *Polym. Chem.* **4,** 4878–4884 (2013).

22. Herbst, F., Döhler, D., Michael, P. & Binder, W. H. Self-healing polymers via supramolecular forces. *Macromolecular Rapid Communications* **34,** (2013).

23. Yang, Y., Ding, X. & Urban, M. W. Chemical and physical aspects of self-healing materials. *Prog. Polym. Sci.* **49–50,** (2015).

24. Dahlke, J., Zechel, S., Hager, M. D. & Schubert, U. S. How to Design a Self-Healing Polymer: General Concepts of Dynamic Covalent Bonds and Their Application for Intrinsic Healable Materials. *Adv. Mater. Interfaces* **1800051,** 1–14 (2018).

25. Wool, R. P. & O'Connor, K. M. A theory of crack healing in polymers. *J. Appl. Phys.* **52,** 5953–5963 (1981).

26. Hager, M. D., Bode, S., Weber, C. & Schubert, U. S. Shape memory polymers: Past, present and future developments. *Progress in Polymer Science* **49–50,** (2015).

27. Bose, R. K., Hohlbein, N., Garcia, S. J., Schmidt, A. M. & van der Zwaag, S. Relationship between the network dynamics, supramolecular relaxation time and healing kinetics of cobalt poly(butyl acrylate) ionomers. *Polymer* **69,** 228–232 (2015).

28. Grande, A. M., Bijleveld, J. C., Garcia, S. J. & van der Zwaag, S. A combined fracture mechanical – rheological study to separate the contributions of hydrogen bonds and disulphide linkages to the healing of poly(urea-urethane) networks. *Polymer* **96,** 26–34 (2016).

29. Bode, S. *et al.* Correlation between scratch healing and rheological behavior for terpyridine complex based metallopolymers. *J. Mater. Chem. A* **3,** 22145–22153 (2015).

30. Grande, A. M., Garcia, S. J. & van der Zwaag, S. On the interfacial healing of a supramolecular elastomer. *Polymer* **56,** 435–442 (2015).

31. van der Kooij, H. M., Susa, A., García, S. J., van der Zwaag, S. & Sprakel, J. Imaging the Molecular Motions of Autonomous Repair in a Self-Healing Polymer. *Adv. Mater.* 1701017 (2017). doi:10.1002/adma.201701017

32. Kim, Y. H. & Wool, R. P. A theory of healing at a polymer-polymer interface. *Macromolecules* **16,** 1115–1120 (1983).

33. Susa, A., Bose, R. K., Grande, A. M., van der Zwaag, S. & Garcia, S. J. Effect of the Dianhydride/Branched Diamine Ratio on the Architecture and Room Temperature Healing Behavior of Polyetherimides. *ACS Appl. Mater. Interfaces* **8,** 34068–34079 (2016).

34. Engels, H. W. *et al.* Polyurethanes: Versatile materials and sustainable problem solvers for today's challenges. *Angewandte Chemie - International Edition* **52,** (2013).

35. Kim, Y. J., Huh, P. H. & Kim, B. K. Synthesis of self-healing polyurethane urea-based supramolecular materials. *J. Polym. Sci. Part B Polym. Phys.* **53,** 468–474 (2015).

36. Yamaguchi, M., Ono, S. & Terano, M. Self-repairing property of polymer network with dangling chains. *Mater. Lett.* **61,** 1396–1399 (2007).

37. Yamaguchi, M., Ono, S. & Okamoto, K. Interdiffusion of dangling chains in weak gel and its application to self-repairing material. *Mater. Sci. Eng. B* **162,** 189–194 (2009).

38. He, Y., Xie, D. & Zhang, X. The structure, microphase-separated morphology, and property of polyurethanes and polyureas. *J. Mater. Sci.* **49,** 7339–7352 (2014).

39. Krol, P. Synthesis methods, chemical structures and phase structures of linear polyurethanes. Properties and applications of linear polyurethanes in polyurethane elastomers, copolymers and ionomers. *Prog. Mater. Sci.* **52,** 915–1015 (2007).

40. Formoso, E., Asua, J. M., Matxain, J. M. & Ruiperez, F. The role of non-covalent interactions in the self-healing mechanism of disulfide-based polymers. *Phys. Chem. Chem. Phys.* **19,** 18461–18470 (2017).

41. Brunsveld, L., Folmer, B. J., Meijer, E. W. & Sijbesma, R. P. Supramolecular polymers. *Chem. Rev.* **101,** 4071–4098 (2001).

42. Yanagisawa, Y., Nan, Y., Okuro, K. & Aida, T. Mechanically robust, readily repairable polymers via tailored noncovalent cross-linking. *Science (80-.).* **359,** 72–76 (2018).

43. Cordier, P., Tournilhac, F., Soulié-Ziakovic, C. & Leibler, L. Self-healing and thermoreversible rubber from supramolecular assembly. *Nature* **451,** 977–80 (2008).

44. Sijbesma, R. P. *et al.* Reversible polymers formed from self-complementary monomers using quadruple hydrogen bonding. *Science* **278,** 1601–4 (1997).

45. Beijer, F. H., Sijbesma, R. P., Kooijman, H., Spek, A. L. & Meijer, E. W. Strong Dimerization of Ureidopyrimidones via Quadruple Hydrogen Bonding. *J. Am. Chem. Soc.* **120,** 6761–6769 (1998).

46. Balkenende, D. W. R., Monnier, C. A., Fiore, G. L. & Weder, C. Optically responsive supramolecular polymer glasses. *Nat. Commun.* **7,** 10995 (2016).

47. Burattini, S. *et al.* A Healable Supramolecular Polymer Blend Based on Aromatic π−π Stacking and Hydrogen-Bonding Interactions. *J. Am. Chem. Soc.* **132,** 12051–12058

(2010).

48. Feula, A. *et al.* A Thermoreversible Supramolecular Polyurethane with Excellent Healing Ability at 45 °c. *Macromolecules* **48,** (2015).

49. Xiao, Y., Huang, H. & Peng, X. Synthesis of self-healing waterborne polyurethanes containing sulphonate groups. *RSC Adv.* **7,** 20093–20100 (2017).

50. Comí, M., Lligadas, G., Ronda, J. C., Galià, M. & Cádiz, V. Adaptive bio-based polyurethane elastomers engineered by ionic hydrogen bonding interactions. *Eur. Polym. J.* **91,** 408–419 (2017).

51. Chen, S. *et al.* Development of zwitterionic polyurethanes with multi-shape memory effects and self-healing properties. *J. Mater. Chem. A* **3,** 2924–2933 (2015).

52. Bode, S. *et al.* Self-healing polymer coatings based on crosslinked metallosupramolecular copolymers. *Adv. Mater.* **25,** (2013).

53. Weng, W. *et al.* Multiresponsive supramolecular gels constructed by orthogonal metal-ligand coordination and hydrogen bonding. *Eur. Polym. J.* **49,** 4062–4071 (2013).

54. Nakahata, M., Takashima, Y., Yamaguchi, H. & Harada, A. Redox-responsive self-healing materials formed from host–guest polymers. *Nat Commun* **2,** 511 (2011).

55. Liu, J. *et al.* Tough Supramolecular Polymer Networks with Extreme Stretchability and Fast Room-Temperature Self-Healing. *Adv. Mater.* **29,** 1605325 (2017).

56. Yang, X. *et al.* Self-healing polymer materials constructed by macrocycle-based host–guest interactions. *Soft Matter* **11,** 1242–1252 (2015).

57. Montarnal, D., Capelot, M., Tournilhac, F. & Leibler, L. Silica-Like Malleable Materials from permanent organic networks. *Science (80-.).* **334,** 965–968 (2011).

58. Denissen, W., Winne, J. M. & Du Prez, F. E. Vitrimers: permanent organic networks with glass-like fluidity. *Chem. Sci.* **7,** (2015).

59. Delebecq, E., Pascault, J.-P., Boutevin, B. & Ganachaud, F. On the Versatility of Urethane/Urea Bonds: Reversibility, Blocked Isocyanate, and Non-isocyanate Polyurethane. *Chem. Rev.* **113,** 80–118 (2013).

60. Kuhl, N. *et al.* Urethanes as reversible covalent moieties in self-healing polymers. *Eur. Polym. J.* **104,** 45–50 (2018).

61. Cao, S. *et al.* A thermal self-healing polyurethane thermoset based on phenolic urethane. *Polym J* (2017).

62. Zechel, S. *et al.* Intrinsic self-healing polymers with a high E-modulus based on dynamic reversible urea bonds. *Npg Asia Mater.* **9,** e420 (2017).

63. Fang, Z., Zheng, N., Zhao, Q. & Xie, T. Healable, Reconfigurable, Reprocessable Thermoset Shape Memory Polymer with Highly Tunable Topological Rearrangement Kinetics. *ACS Appl. Mater. Interfaces* **9,** 22077–22082 (2017).

64. Ying, H., Zhang, Y. & Cheng, J. Dynamic urea bond for the design of reversible and self-healing polymers. *Nat. Commun.* **5,** 3218 (2014).

65. Liu, W.-X. *et al.* Oxime-Based and Catalyst-Free Dynamic Covalent Polyurethanes. *J. Am. Chem. Soc.* **139,** 8678–8684 (2017).

66. Zhang, L., Julé, F. & Sodano, H. A. High service temperature, self-mendable thermosets networked by isocyanurate rings. *Polym. (United Kingdom)* **114,** 249–256 (2017).

67. Heo, Y. & Sodano, H. a. Self-healing polyurethanes with shape recovery. *Adv. Funct. Mater.* **24,** 5261–5268 (2014).

68. Irusta, L., Fernández-Berridi, M. J. & Aizpurua, J. Polyurethanes based on isophorone diisocyanate trimer and polypropylene glycol crosslinked by thermal reversible diels alder reactions. *J. Appl. Polym. Sci.* **134,** 44543 (2017).

69. Du, P. *et al.* Slightly crosslinked polyurethane with Diels–Alder adducts from trimethylolpropane. *J. Appl. Polym. Sci.* **133,** 1–8 (2016).

70. Willocq, B. *et al.* One-component Diels-Alder based polyurethanes: a unique way to self-heal. *RSC Adv.* **7,** 48047–48053 (2017).

71. Ling, J., Rong, M. Z. & Zhang, M. Q. Photo-stimulated self-healing polyurethane containing dihydroxyl coumarin derivatives. *Polymer* **53,** 2691–2698 (2012).

72. Rivero, R. S. *et al.* Synthesis and characterization of a photo-crosslinkable polyurethane based on a coumarin-containing polycaprolactone diol. *Eur. Polym. J.* **76,** 245–255 (2016).

73. Aguirresarobe, R. H., Martin, L., Aramburu, N., Irusta, L. & Fernandez-Berridi, M. J. Coumarin based light responsive healable waterborne polyurethanes. *Prog. Org. Coatings* **99,** 314–321 (2016).

74. Van Damme, J. *et al.* Anthracene-based polyurethane networks: Tunable thermal degradation, photochemical cure and stress-relaxation. *Eur. Polym. J.* **105,** 412–420 (2018).

75. Fang, Y., Du, X., Du, Z., Wang, H. & Cheng, X. Light- and heat-triggered polyurethane based on dihydroxyl anthracene derivatives for self-healing applications. *J. Mater. Chem. A* **5,** 8010–8017 (2017).

76. Chatani, S., Kloxin, C. J. & Bowman, C. N. The power of light in polymer science: photochemical processes to manipulate polymer formation, structure, and properties. *Polym. Chem.* **5,** 2187 (2014).

77. Fiore, G. L., Rowan, S. J. & Weder, C. Optically healable polymers. *Chem. Soc. Rev.* **42,** 7278–88 (2013).

78. Yuan, C., Rong, M. Z. & Zhang, M. Q. Self-healing polyurethane elastomer with thermally reversible alkoxyamines as crosslinkages. *Polymer* **55,** 1782–1791 (2014).

79. Takahashi, A., Goseki, R. & Otsuka, H. Thermally Adjustable Dynamic Disulfide Linkages Mediated by Highly Air-Stable 2,2,6,6-Tetramethylpiperidine-1-sulfanyl (TEMPS) Radicals. *Angew. Chemie Int. Ed.* **56,** 2016–2021 (2017).

80. Zhang, Z. P., Rong, M. Z., Zhang, M. Q. & Yuan, C. Alkoxyamine with reduced homolysis temperature and its application in repeated autonomous self-healing of stiff polymers. *Polym. Chem.* **4,** 4648–4654 (2013).

81. Imato, K., Takahara, A. & Otsuka, H. Self-Healing of a Cross-Linked Polymer with Dynamic Covalent Linkages at Mild Temperature and Evaluation at Macroscopic and Molecular Levels. *Macromolecules* **48,** 5632–5639 (2015).

82. Imato, K. *et al.* Repeatable mechanochemical activation of dynamic covalent bonds in thermoplastic elastomers. *Chem. Commun.* **52,** (2016).

83. Cash, J. J., Kubo, T., Bapat, A. P. & Sumerlin, B. S. Room-temperature self-healing polymers based on dynamic-covalent boronic esters. *Macromolecules* **48,** (2015).

84. Xia, N. N., Rong, M. Z. & Zhang, M. Q. Stabilization of catechol-boronic ester bonds for underwater self-healing and recycling of lipophilic bulk polymer in wider pH range. *J. Mater. Chem. A* **4,** 14122–14131 (2016).

85. Fortman, D. J., Brutman, J. P., Hillmyer, M. A. & Dichtel, W. R. Structural effects on the reprocessability and stress relaxation of crosslinked polyhydroxyurethanes. *J. Appl. Polym. Sci.* **134,** 44984 (2017).

86. Chen, X., Li, L., Jin, K. & Torkelson, J. M. Reprocessable polyhydroxyurethane networks exhibiting full property recovery and concurrent associative and dissociative dynamic chemistry via transcarbamoylation and reversible cyclic carbonate aminolysis. *Polym. Chem.* **8,** 6349–6355 (2017).

87. Yan, P. *et al.* Multifunctional polyurethane-vitrimers completely based on transcarbamoylation of carbamates: thermally-induced dual-shape memory effect and self-welding. *RSC Adv.* **7,** 26858–26866 (2017).

88. Yang, Y. & Urban, M. W. Self-healing of glucose-modified polyurethane networks facilitated by damage-induced primary amines. *Polym. Chem.* **8,** 303–309 (2017).

89. Erice, A. *et al.* Reprocessable and recyclable crosslinked poly(urea-urethane)s based on dynamic amine/urea exchange. *Polymer* **145,** 127–136 (2018).

90. Denissen, W. *et al.* Chemical control of the viscoelastic properties of vinylogous urethane vitrimers. *Nat. Commun.* **8,** 14857 (2017).

91. Denissen, W. *et al.* Vinylogous Urea Vitrimers and Their Application in Fiber Reinforced Composites. *Macromolecules* **51,** 2054–2064 (2018).

92. Obadia, M. M., Mudraboyina, B. P., Serghei, A., Montarnal, D. & Drockenmuller, E. Reprocessing and Recycling of Highly Cross-Linked Ion-Conducting Networks through Transalkylation Exchanges of C–N Bonds. *J. Am. Chem. Soc.* **137,** 6078–6083 (2015).

93. Röttger, M. *et al.* High-performance vitrimers from commodity thermoplastics through dioxaborolane metathesis. *Science (80-.).* **356,** 62–65 (2017).

94. Owen, G. D. T., Macknight, W. J. & Tobolsky, A. V. Urethane Elastomers Containing Disulfide and Tetrasulfide Linkages. *J. Phys. Chem.* **68,** 784–786 (1964).

95. Zhang, L., Chen, L. & Rowan, S. J. Trapping Dynamic Disulfide Bonds in the Hard Segments of Thermoplastic Polyurethane Elastomers. *Macromol. Chem. Phys.* **218,** 1600320 (2017).

96. Xu, Y. & Chen, D. A Novel Self-Healing Polyurethane Based on Disulfide Bonds. *Macromol. Chem. Phys.* **217,** 1191–1196 (2016).

97. Xu, W. M., Rong, M. Z. & Zhang, M. Q. Sunlight driven self-healing, reshaping and recycling of a robust, transparent and yellowing-resistant polymer. *J. Mater. Chem. A* **4,** 10683–10690 (2016).

98. Jian, X., Hu, Y., Zhou, W. & Xiao, L. Self-healing polyurethane based on disulfide bond and hydrogen bond. *Polym. Adv. Technol.* **29,** 463–469 (2018).

99. Wan, T. & Chen, D. Synthesis and properties of self-healing waterborne polyurethanes containing disulfide bonds in the main chain. *J. Mater. Sci.* **52,** 197–207 (2017).

100. Wu, X. *et al.* Heat-triggered poly(siloxane-urethane)s based on disulfide bonds for self-healing application. *J. Appl. Polym. Sci.* **135,** 46532 (2018).

101. Wan, T. & Chen, D. Mechanical enhancement of self-healing waterborne polyurethane by graphene oxide. *Prog. Org. Coatings* **121,** 73–79 (2018).

102. Azcune, I. & Odriozola, I. Aromatic disulfide crosslinks in polymer systems: Self-healing, reprocessability, recyclability and more. *Eur. Polym. J.* **84,** 147–160 (2016).

103. Martin, R. *et al.* The processability of a poly(urea-urethane) elastomer reversibly crosslinked with aromatic disulfide bridges. *J. Mater. Chem. A* **2,** 5710–5715 (2014).

104. Aguirresarobe, R. H., Martin, L., Fernandez-Berridi, M. J. & Irusta, L. Autonomic healable waterborne organic-inorganic polyurethane hybrids based on aromatic disulfide moieties. *EXPRESS Polym. Lett.* **11,** 266–277 (2017).

105. Kim, S.-M. *et al.* Superior Toughness and Fast Self-Healing at Room Temperature Engineered by Transparent Elastomers. *Adv. Mater.* **30,** 1705145 (2018).

106. Yang, Y., Lu, X. & Wang, W. A tough polyurethane elastomer with self-healing ability. *Mater. Des.* **127,** 30–36 (2017).

107. Matxain, J. M., Asua, J. M. & Ruipérez, F. Design of new disulfide-based organic compounds for the improvement of self-healing materials. *Phys. Chem. Chem. Phys.* **18,** 1758–1770 (2016).

108. Nevejans, S., Ballard, N., Miranda, J. I., Reck, B. & Asua, J. M. The underlying mechanisms for self-healing of poly(disulfide)s. *Phys. Chem. Chem. Phys.* **18,** 27577–27583 (2016).

109. Dénès, F., Pichowicz, M., Povie, G. & Renaud, P. Thiyl Radicals in Organic Synthesis. *Chem. Rev.* **114,** 2587–2693 (2014).

110. Ruipérez, F., Galdeano, M., Gimenez, E. & Matxain, J. M. Sulfenamides as Building Blocks for Efficient Disulfide-Based Self-Healing Materials. A Quantum Chemical Study. *ChemistryOpen* **7,** 248–255 (2018).

111. Gaulding, J. C., Smith, M. H., Hyatt, J. S., Fernandez-Nieves, A. & Lyon, L. A. Reversible inter- and intra-microgel cross-linking using disulfides. *Macromolecules* **45,** 39–45 (2012).

112. Yarmohammadi, M., Shahidzadeh, M. & Ramezanzadeh, B. Designing an elastomeric polyurethane coating with enhanced mechanical and self-healing properties: The influence of disulfide chain extender. *Prog. Org. Coatings* **121,** 45–52 (2018).

113. Yarmohammadi, M. & Shahidzadeh, M. Evaluation of disulfide chain extender effect on the mechanical properties of unsaturated polyurethane-urea networks. *J. Appl. Polym. Sci.* **135,** 46309 (2018).

114. Canadell, J., Goossens, H. & Klumperman, B. Self-Healing Materials Based on Disulfide Links. *Macromolecules* **44,** 2536–2541 (2011).

115. Pepels, M., Filot, I., Klumperman, B. & Goossens, H. Self-healing systems based on disulfide–thiol exchange reactions. *Polym. Chem.* **4,** 4955 (2013).

116. Lei, Z. Q., Xiang, H. P., Yuan, Y. J., Rong, M. Z. & Zhang, M. Q. Room-Temperature Self-Healable and Remoldable Cross-linked Polymer Based on the Dynamic Exchange of Disulfide Bonds. *Chem. Mater.* **26,** 2038–2046 (2014).

117. Imbernon, L., Oikonomou, E. K., Norvez, S. & Leibler, L. Chemically crosslinked yet reprocessable epoxidized natural rubber via thermo-activated disulfide rearrangements. *Polym. Chem.* **6,** 4271–4278 (2015).

118. Du, W. *et al.* Thermal induced shape-memory and self-healing of segmented polyurethane containing diselenide bonds. *J. Appl. Polym. Sci.* **135,** 46326 (2018).

119. Liu, J., Ma, X., Tong, Y. & Lang, M. Self-healing polyurethane based on ditelluride bonds. *Appl. Surf. Sci.* **455,** 318–325 (2018).

120. An, X. *et al.* Aromatic diselenide crosslinkers to enhance the reprocessability and self-healing of polyurethane thermosets. *Polym. Chem.* **8,** 3641–3646 (2017).

121. Amamoto, Y., Otsuka, H., Takahara, A. & Matyjaszewski, K. Self-healing of covalently cross-linked polymers by reshuffling thiuram disulfide moieties in air under visible light. *Adv. Mater.* **24,** 3975–3980 (2012).

122. Nicolaÿ, R., Kamada, J., Van Wassen, A. & Matyjaszewski, K. Responsive Gels Based on a Dynamic Covalent Trithiocarbonate Cross-Linker. *Macromolecules* **43,** 4355–4361 (2010).

123. Amamoto, Y., Kamada, J., Otsuka, H., Takahara, A. & Matyjaszewski, K. Repeatable

Photoinduced Self-Healing of Covalently Cross-Linked Polymers through Reshuffling of Trithiocarbonate Units. *Angew. Chemie Int. Ed.* **50,** 1660–1663 (2011).

124. Gordon, M. B., French, J. M., Wagner, N. J. & Kloxin, C. J. Dynamic Bonds in Covalently Crosslinked Polymer Networks for Photoactivated Strengthening and Healing. *Adv. Mater.* **27,** 8007–8010 (2015).

125. van Benthem, R. A. T. M., Ming, W. (Marshall) & de With, G. (Bert). in *Self Healing Materials: An Alternative Approach to 20 Centuries of Materials Science* (ed. van der Zwaag, S.) 139–159 (Springer Netherlands, 2007). doi:10.1007/978-1-4020-6250-6_7

126. Zhang, F. *et al.* Self-healing mechanisms in smart protective coatings: a review. *Corros. Sci.* (2018). doi:https://doi.org/10.1016/j.corsci.2018.08.005

127. García, S. J., Fischer, H. R. & van der Zwaag, S. A critical appraisal of the potential of self healing polymeric coatings. *Prog. Org. Coatings* **72,** 211–221 (2011).

128. Wamprecht, C., Mechtel, M. & Klimmasch, T. Coating compositions. US20090247711A1 (2009).

129. Ou, R., Eberts, K. & Skandan, G. Phase separated self-healing polymer coatings. US8987352 B1 (2015).

130. Ou, R. *et al.* Self-healing polymer nanocomposite coatings for use on surfaces made of wood. US8664298 B1 (2014).

131. Smits, A. L. M., Van Triet, R. B., Garcia-Espallargas, S. J. & Dingemans, T. J. WO2014029966A1 Polyimide composition. (2014).

132. Makal, U. G., Day, R. W., Haddleton, D. M. & Summers, J. C. Thermally reversible crosslinked polyurethane. WO2016018956A1. (2014).

133. H. Haberle, W. Temme, R. Bergs, N. Steidl, A. M. Use of aqueous polyurethane dispersions in formulations for crack sealing coating systems. US20030088045A1. (2003).

134. Maier, A. *et al.* Coating system for veneered wood based on polyurethane dispersions method for the production and use thereof. US20030162892A1. (2000).

135. Schütze, D., Kurek, G., Rische, T., Urban, J. & Hassel, T. Polyurethane-polyurea dispersions as coating compositions. US6642303B2. (2003).

136. Rische, T., Casselmann, H., Feller, T., Blum, H. & Kurek, G. Polyurethane-polyurea dispersions and their use as coating compositions. US20070049684A1. (2005).

137. W. Temme, R. Bergs, H. Haberle, A. M. Use of aqueous polyurethane dispersions is formulations for sports floor coverings. US20020004553A1. (2002).

138. Garcia, S. J. Effect of polymer architecture on the intrinsic self-healing character of polymers. *Eur. Polym. J.* **53,** 118–125 (2014).

139. Zhang, L. & Rowan, S. J. Effect of Sterics and Degree of Cross-Linking on the

Mechanical Properties of Dynamic Poly(alkylurea–urethane) Networks. *Macromolecules* **50,** 5051–5060 (2017).

140. Grande, A. M., Martin, R., Odriozola, I., van der Zwaag, S. & Garcia, S. J. Effect of the polymer structure on the viscoelastic and interfacial healing behaviour of poly(urea-urethane) networks containing aromatic disulphides. *Eur. Polym. J.* **97,** 120–128 (2017).

141. Chen, S., Mahmood, N., Beiner, M. & Binder, W. H. Self-Healing Materials from V- and H-Shaped Supramolecular Architectures. *Angew. Chemie Int. Ed.* **54,** 10188–10192 (2015).

142. Bose, R. K. *et al.* Contributions of hard and soft blocks in the self-healing of metal-ligand-containing block copolymers. *Eur. Polym. J.* **93,** 417–427 (2017).

143. AbdolahZadeh, M., C. Esteves, A. C., van der Zwaag, S. & Garcia, S. J. Healable dual organic–inorganic crosslinked sol–gel based polymers: Crosslinking density and tetrasulfide content effect. *J. Polym. Sci. Part A Polym. Chem.* **52,** 1953–1961 (2014).

144. Hernández, M. *et al.* Turning Vulcanized Natural Rubber into a Self-Healing Polymer: Effect of the Disulfide/Polysulfide Ratio. *ACS Sustain. Chem. Eng.* **4,** 5776–5784 (2016).

Chapter II. The underlying mechanisms of disulfide exchange

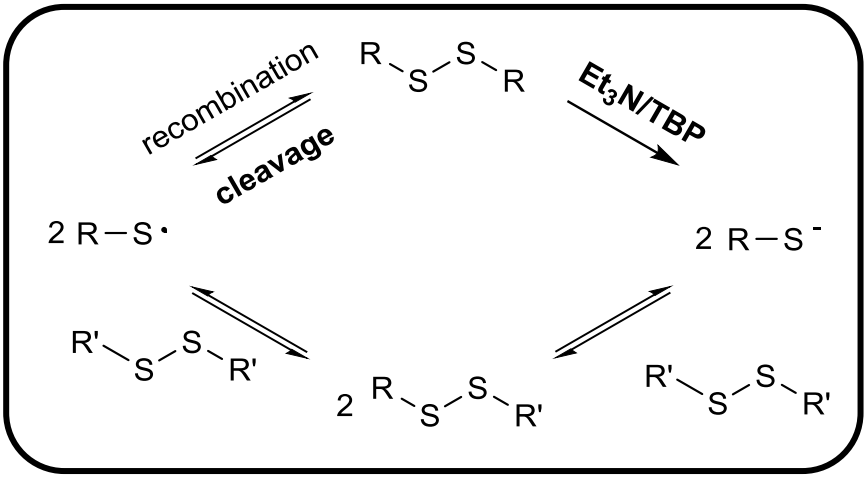

Part of this chapter has been published as:

Nevejans, S., Ballard, N., Miranda, J. I., Reck, B. & Asua, J. M. The underlying mechanisms for self-healing of poly(disulfide)s. *Phys. Chem. Chem. Phys.* **18,** 27577–27583 (2016).

II.1. Introduction

As discussed in Chapter I, self-healing polymers have attracted a lot of attention over the last decades as they provide a potential solution for the persisting problem of material damage, enabling an extended product life-time.[1–7] Especially, self-healing polymers which can heal intrinsically, making use of reversible chemical or physical bonds, are interesting for long-term use as they are able to undergo multiple healing events.[8] In order to develop self-healing materials with a desirable high mechanical strength, it seems advantageous to introduce reversible covalent bonds into the polymer backbone, as they are typically stronger than the supramolecular interactions. Among the broad range of dynamic chemistries that have already been introduced into intrinsically healable polymers (Section I.2.2),[9–12] the dynamic covalent disulfide bonds seem to be particularly interesting due to their versatility, the relatively simple applicability for a large variety of polymers and the fact that they dynamically exchange when exposed to various stimuli, *e.g.* heat, light, redox or pH.[13–15]

Therefore, in this thesis, we will focus on the incorporation of these dynamic disulfide bonds, but before starting to incorporate these bonds into the polymer backbone, it is important to understand the underlying mechanisms involved in this disulfide exchange. Like this, we can obtain more insight in the self-healing event taking place in the polymers incorporating these bonds, so that ideally a more effective development of stronger self-healing materials is possible. However, up till recently, the underlying mechanisms taking place during disulfide exchange were still ambiguous as both metathesis[16–18] and a radical mediated mechanism[19,20] had been described in literature. Moreover, some work had been published in which both mechanisms were used indistinctly to describe the exchange reaction,[21–23] while other research

described the disulfide exchange without specifying the underlying mechanism.[24] Therefore, it was obvious that further analysis of the mechanisms involved in this highly relevant reaction for self-healing was necessary in order to be able to provide a clarifying overview on this topic.

In this context, it is important to emphasize the difference between the [2+2] metathesis reaction mechanism and a [2+1] radical mediated mechanism. As distinctively described by Ruipérez and co-workers, in the first case, the disulfide bonds would break and form simultaneously, while in the radical mediated mechanism, the breaking of one disulfide bond would lead to the formation of sulfur-centered (thiyl) radicals that would eventually attack other disulfide bonds (Figure II.1).[25] These authors theoretically predicted that the main reaction mechanism would go through the formation of sulfur-based radicals and three-membered transition states. In this chapter, we focus on the experimental validation of these theoretical calculations and clarification of the underlying mechanisms of disulfide exchange by investigating the kinetics of the exchange of a mixture of aromatic disulfides.

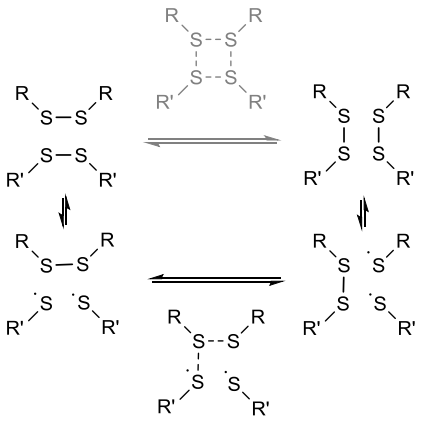

Figure II.1. Schematic representation of the [2+2] metathesis (upper) and [2+1] radical mediated (lower) mechanisms.

First, kinetic studies are performed by quantitative ^{13}C Nuclear Magnetic Resonance (NMR) spectroscopy in order to gain more knowledge about the mechanism of the disulfide exchange reaction. A model exchange reaction of bis(4-aminophenyl)disulfide with diphenyl disulfide is investigated and compared with modified reactions by adding or changing specific reagents (initiator, inhibitor, catalyst, monomer or disulfide compound) or changing the reaction conditions (with or without UV radiation). Additionally, solid-state and solution Electron Paramagnetic Resonance (EPR) measurements are carried out to provide some insight in the presence of radicals in the disulfide bonds of different disulfide compounds and to check the influence of catalysts on the presence of these radicals. Finally, Ellman's reagent (5,5'-dithiobis-(2-nitrobenzoic acid), DTNB) is used to establish the presence of thiolate compounds when certain catalysts are added to the system.

II.2. Experimental

II.2.1. Materials

2,2'-azobis(4-methoxy-2,4-dimethyl valeronitrile) (V70, Wako Pure Chemical Industries, technical grade), 5,5'-dithiobis-(2-nitrobenzoic acid) (DTNB/Ellman's reagent, Sigma Aldrich, ≥98%), 2,2,6,6-tetramethylpiperidine-1-oxyl (TEMPO, Sigma Aldrich, 98%), bis(4-aminophenyl)disulfide (TCI, >98.0%), bis(4-hydroxyphenyl)disulfide (TCI, >98.0%), diethylamine (DEA, Sigma Aldrich, ≥99.5%), diphenyl disulfide (Sigma Aldrich, 99%), methyl methacrylate (MMA, Quimidroga, technical grade), triethylamine (TEA, Sigma Aldrich, ≥99%) and tri-*n*-butylphosphine (TBP, Sigma Aldrich, 97%) were used as received.

II.2.2. Methods

X-band EPR measurements were performed on a Bruker ELEXSYS 500 spectrometer equipped with a super-high-Q resonator ER-4123-SHQ and a maximum available microwave power of 200 mW. Solid samples and solutions were placed in quartz tubes and spectra were recorded at room temperature using typical modulation amplitudes of 0.05-0.1 mT at a frequency of 100 kHz. A NMR probe was used to calibrate the magnetic field and the frequency inside the cavity (~9.4 GHz) was determined with an integrated MW-frequency counter. The liquid NMR spectra were recorded on a Bruker AVANCE 500 spectrometer equipped with a Z-gradient BBO probe. The kinetic studies of the reactions were conducted at 35°C using ^{13}C spectra. The ^{13}C spectra were recorded every 5/15 min for 2/12 h using an inverse gated sequence at 125.13 MHz. A time domain of 64k and a spectral width of 31 kHz were considered, while the interpulse delay was 5 s and the acquisition time 1 s. In some experiments the interpulse delay was changed from 5 s to 20 s. An ultraviolet (UV) chamber (model BS 03, Dr. Gröbel UV-Elektronik GmbH) was used equipped with 20 UV lamps of wavelength range from 315 to 400 nm with a maximum intensity at 368 nm. Ultraviolet-visible (UV–vis) spectra were obtained using a Cary-1 (Varian) spectrophotometer and analyzed using UVProbe as the appropriate software.

II.2.3. Kinetic studies performed by ^{13}C NMR spectroscopy

In a typical reaction, 24.8 mg of bis(4-aminophenyl)disulfide was dissolved in 500 µL of DMSO and brought up to the temperature of 35°C in the NMR spectrometer after which an initial scan was recorded. Subsequently, a solution of 21.8 mg of diphenyl disulfide in 200 µL of DMSO

was added and the NMR tube was mixed briefly before inserting it in the spectrometer. Other reactions were performed and analyzed similarly after adding or varying certain reagents or reaction conditions as described in detail in Table II.1. The degree of product formation for the different reactions was calculated by introducing the integrals of signals a and b (Figure II.3) into equation II.1:

$$X = \frac{I(b)}{\frac{I(a)}{2} + I(b)} \qquad \text{(II.1)}$$

The measured T_1 values of a (1.14 s) and b (1.71 s) are low enough so that, with an interpulse delay of 5 s, the values obtained for the degree of product formation can be considered quantitative. To confirm, these additional experiments with a delay time of 20 s were performed with quantitatively similar results. It should be noted that the carbons c and d as shown in Figure II.3 and Figure II.5 (results and discussion section) have significantly longer relaxation times (T_1=4.01 and 3.22 s for carbons c and d respectively), therefore quantitive comparison is not possible for these signals. Analogously, also the reaction of 21.8 mg of diphenyl disulfide with 175 µL of MMA was followed using ^{13}C NMR spectroscopy in 525 µL DMSO at room temperature. NMR measurements of the mixtures where taken after 2 days at room temperature (RT) and after additional exposure to UV radiation for 1h10min also at RT. Furthermore, the reaction between MMA and diphenyl disulfide (1 eq.) in DMSO and in the presence of 1.4 µL (0.1 eq.) of TEA was followed using ^{13}C NMR spectroscopy, measuring the reaction after 2 d at RT.

II.2.4. EPR measurements

Bis(4-aminophenyl)disulfide and bis(4-hydroxyphenyl) disulfide were analyzed for the presence of radicals by EPR spectroscopy. An amount of 70 mg of each disulfide compound was used to be able to carry out solid-state measurements. Furthermore, to analyze the effect of TEA on the disulfide bond and the presence of radicals in this bond, also measurements in solutions were performed. In 1.5 mL eppendorf tubes, a solution was made of 2 mg of the solid disulfide compound in the required amount of TEA as solvent to reach a total volume of 1.5 mL. Eventually 0.5 mL of mixture was used to perform the solution EPR measurements.

II.2.5. UV-vis measurements in the presence of Ellman's reagent

Quantitative experiments were performed by using UV-vis spectroscopy. In these experiments TEA, DEA and TBP were tested by adding 50 µL of a DTNB solution (4 mg DTNB/ mL DMSO) to a 14.3 mM solution of the reagents in DMSO. These reaction mixtures where then measured by UV-vis spectroscopy in a spectral range varying form 190-700 cm^{-1}.

II.3. Results and discussion

II.3.1. Model exchange reaction

First, the model exchange reaction of bis(4-aminophenyl)disulfide with diphenyl disulfide forming the mixed product (Figure II.2) was followed kinetically for 12 h at 35°C using NMR spectroscopy. The product formation was analyzed through the change of signals in the ^{13}C NMR spectra as depicted in Figure II.3. The signals a and c in Figure II.3 were both assigned to the reactants, while b and d were ascribed to the formed product. The degree of product

formation for the model exchange reaction (i) (Table II.1) was calculated by monitoring the change in the relative integrals of the ^{13}C NMR spectra and is shown in Figure II.4. It can be seen that, after 12 h, the exchange reaction reached a conversion of almost 60%. When experiments were performed under inert conditions (N_2-atmosphere), similar results were obtained which indicated that oxygen has little to no influence on the disulfide exchange reaction. Addition of the radical scavenger TEMPO (0.1 mol eq.) resulted in a complete inhibition of the disulfide exchange (Figure II.5). This inhibition is possible since TEMPO combines with sulfur-based radicals forming an adduct which can also decompose to give inert species.[26] It is particularly important to highlight that complete inhibition of the exchange would not be possible using such a low amount of TEMPO if it is assumed that the exchange proceeds via a simple cleavage and recombination of the disulfide bond.

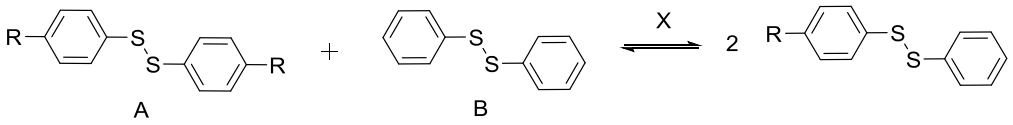

Figure II.2. Exchange reactions studied by ^{13}C NMR spectroscopy.

Table II.1 Detailed description of the exchange reactions studied by ^{13}C NMR spectroscopy.

Reaction	A:B	R	X	Time (h)
i	1:1	$-NH_2$	/	12
ii		$-NH_2$	0.1 mol eq. **TEMPO**	12
iii		$-NH_2$	0.1 mol eq. **V70**	12
iv		$-NH_2$	**UV (10 min)**	12
v		**-OH**	/	12
vi		$-NH_2$	0.1 mol eq. **TEA**	2
vii		$-NH_2$	0.1 mol eq. **TEA +** 0.1 mol eq. **TEMPO**	12
viii		$-NH_2$	0.1 mol eq. **TBP**	2
iv		$-NH_2$	0.1 mol eq. **TBP +** 0.1 mol eq. **TEMPO**	12

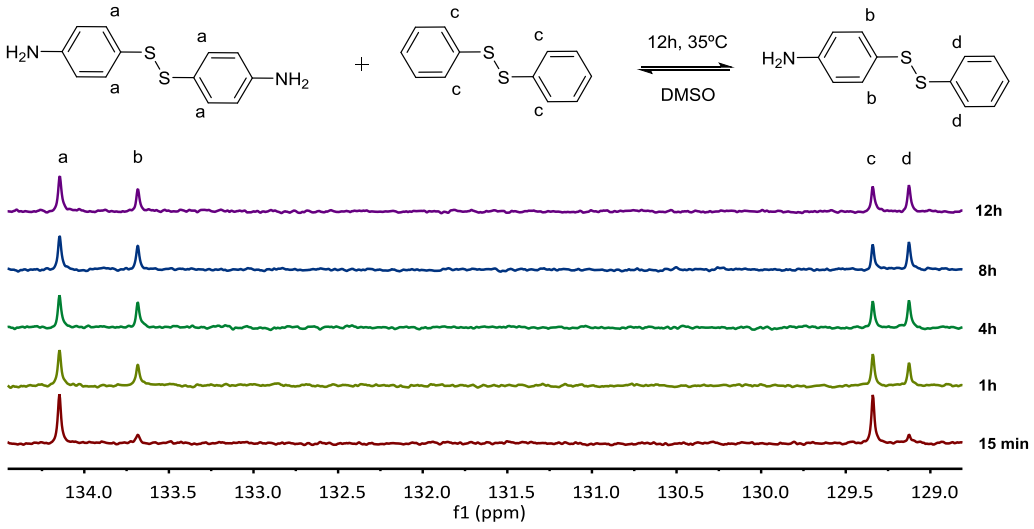

Figure II.3. ^{13}C NMR spectra of the exchange reaction of bis(4-aminophenyl)disulfide with diphenyl disulfide (delay time of 20 s)

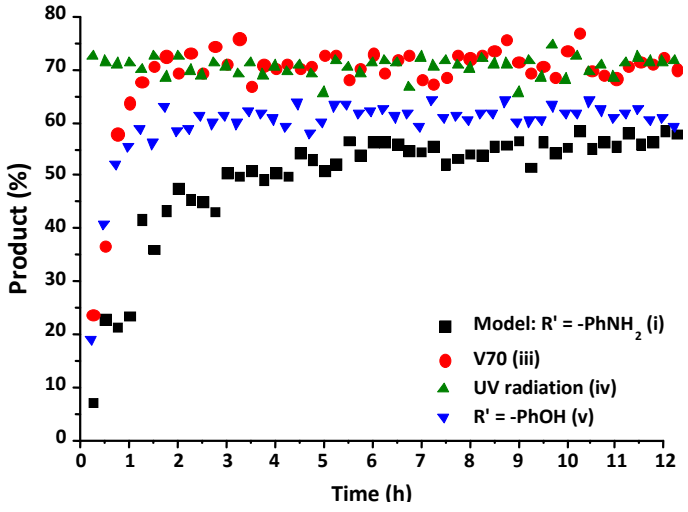

Figure II.4. Formation of the exchange product in function of time for the exchange reactions (i), (iii), (iv) and (v)

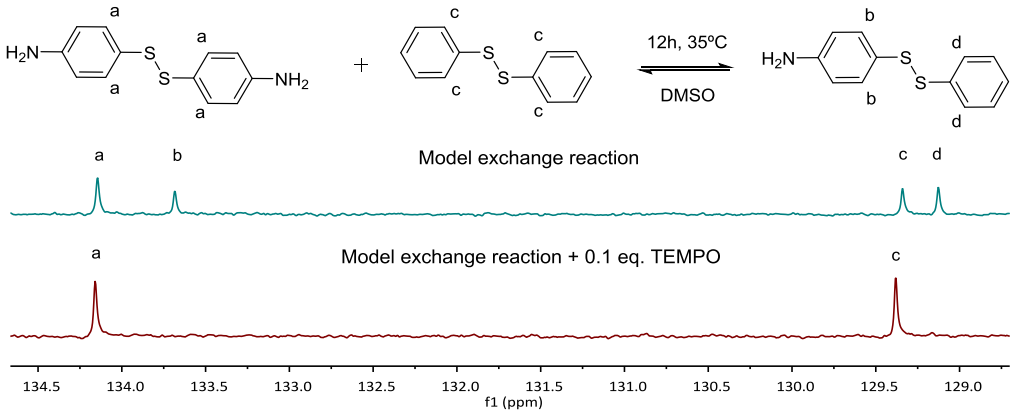

Figure II.5. Formation of the exchange product via the model exchange reaction (i) and in the presence of TEMPO (ii) (delay time of 20 s)

When an initiator with a fast decomposition at low temperature ($t_{1/2}$=10 h at 30°C), V70 (0.5 mol eq.), was introduced into the model reaction mixture, a fast increase to a maximum product formation (70%) at 2 h was observed (Figure II.4 iii). Based on the change in kinetics of the disulfide exchange in the presence of a radical trap and a radical source, it can be presumed that the mechanism for the disulfide exchange is radical mediated as theoretically proposed.[25]

To further confirm the radical mechanism, the reaction conditions of the model exchange experiment were modified. When the reaction mixture was exposed to UV radiation, the exchange reaction was rapid. After exposure for 10 min to UV radiation (iv), the reaction mixture was kinetically studied and the corresponding data obtained by ^{13}C NMR spectroscopy are illustrated in Figure II.4 (iv). This result demonstrates that the exchange reaction had already reached a product formation of 70% at the first measurement of the kinetic study (15 min). This drastic increase in the rate of product formation when conducted under UV radiation further confirmed the proposed mechanism.

In order to investigate the influence of the molecular structure of the disulfide compounds on the exchange reaction, more specifically the effect of alternative substituents on the aromatic ring, the reactant bis(4-aminophenyl)disulfide was replaced by bis(4-hydroxyphenyl)disulfide in the model reaction. As visible in Figure II.4, this exchange reaction (v) reached a conversion of 60% after approximately 2 h in comparison to 12 h in the case of bis(4-aminophenyl)disulfide. The increase in the rate of conversion suggests that the radical generation of bis(4-hydroxyphenyl)disulfide is faster than that of bis(4-aminophenyl)disulfide.

Further confirmation of the radical mediated exchange mechanism was obtained via EPR spectroscopy. Solid-state EPR measurements showed an EPR signal, visible in Figure II.6, for bis(4-hydroxyphenyl)disulfide while no signal could be observed for bis(4-aminophenyl)-disulfide. The isotropic EPR signal with a g-value of 2.0025 affirmed the presence of a (sulfur-based) radical in bis(4-hydroxyphenyl)disulfide which is in strong accordance with the g-value of a sulfur-based radical in a thiuram disulfide diol unit (g=2.004).[19] An explanation for the absence of an EPR signal in the analysis of the bis(4-aminophenyl)disulfide would be the lower radical concentration present in this disulfide compound which is in agreement with the slower rate of product formation as depicted above in Figure II.4 and the limited sensitivity of solid-state EPR spectroscopy which probably prevents the detection of this lower concentration.

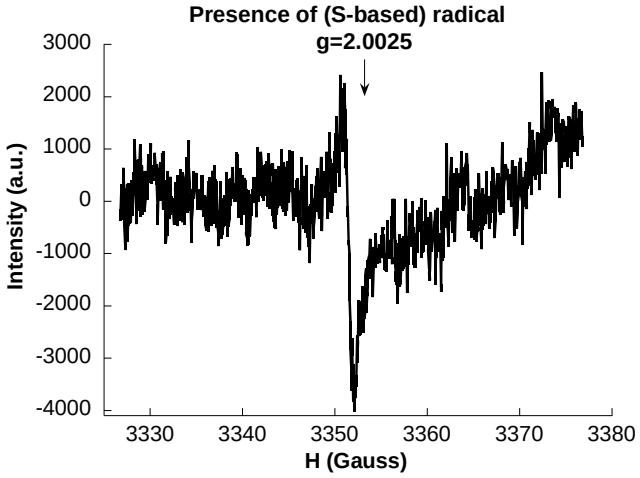

Figure II.6. EPR signal of bis(4-hydroxyphenyl)disulfide.

As a final experiment to validate the presence of radicals in the underlying mechanism of disulfide exchange, diphenyl disulfide was reacted with MMA at RT. Since disulfides can act simultaneously as initiator, transfer agent and terminator (iniferter) in radical polymerization, poly(methyl methacrylate) (PMMA) is expected to be formed with initiator fragments of the disulfide compound as end groups.[27,28] The ^{13}C NMR spectra of the reaction of diphenyl disulfide with MMA after 2 d at RT and after an additional exposure to UV radiation for 10 min and 1h 10 min at RT are depicted in Figure II.7. These spectra show that after 2 d a small amount of PMMA could be observed at the region of 1-0.5 ppm. However, when UV radiation was applied to increase the cleavage of the disulfide compound, larger signals for the formed product were appearing. This proves that UV radiation cleaves the disulfide bond forming S-based radicals which can induce radical polymerization of MMA, since a blank of MMA in DMSO under UV radiation for the same time interval did not show any polymer product.

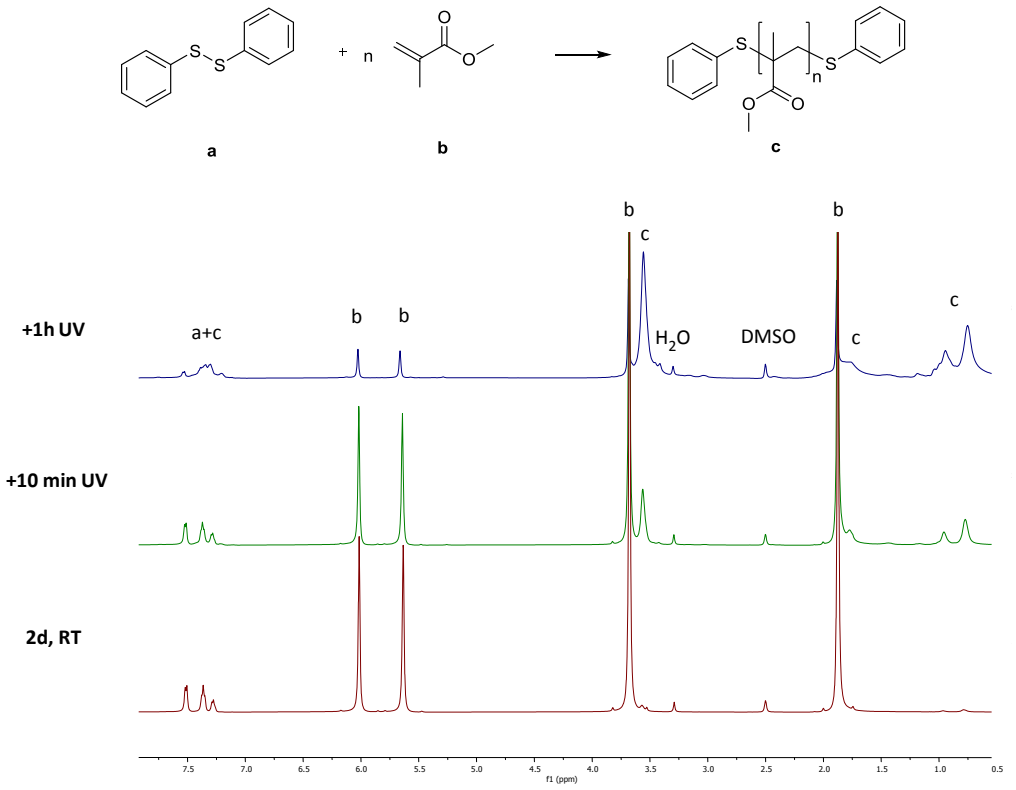

Figure II.7. ^{13}C NMR spectra of the reaction of diphenyl disulfide with MMA.

The suppression of the exchange reaction by the inhibitor, the enhancement by the initiator, by UV radiation and by changing the disulfide and the role of the disulfide as iniferter in the radical polymerization of MMA all suggested that the underlying mechanism for the disulfide exchange reaction is radical mediated. However, the experimental results of the model reaction in the presence of TEMPO showed that a mechanism which only forms radicals via cleavage and recombination could be ruled out, because only 0.1 equivalent of TEMPO was necessary to suppress the formation of the product. Therefore a radical mediated mechanism in which

cleavage leads to the formation of two radicals which can recombine or undergo a chain-transfer reaction can be proposed (Figure II.8). According to this mechanism, only a small amount of radicals have to be formed to achieve extensive disulfide exchange, and hence even a small amount of inhibitor (0.1 mol eq. TEMPO) can kill the possibility of forming any product.

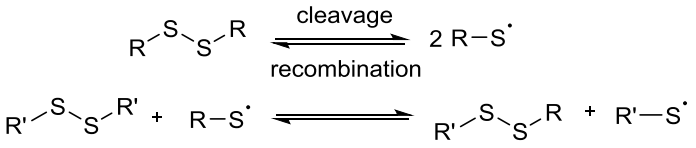

Figure II.8. Probable radical mediated mechanism for the disulfide exchange reaction.

II.3.2. Effect of the addition of catalysts on the model exchange reaction

While the aromatic disulfides undergo spontaneous exchange, other disulfide compounds require the addition of catalysts, such as triethylamine (TEA)[29] and tri-*n*-butylphosphine (TBP),[18] to enhance the disulfide exchange reaction. Kinetic studies were carried out using ^{13}C NMR spectroscopy to verify the enhancing influence of TEA as catalyst on the exchange reaction as described by Rekondo *et al*..[29] Figure II.9 demonstrates that the exchange reaction with the addition of TEA (vi) had already reached a conversion of 70% after approximately 1 h. Similar results were obtained adding TBP (viii) as catalyst to the model exchange reaction. In order to verify the underlying mechanism of this increase, additional solution EPR measurements were carried out in order to examine the effect of a catalyst (TEA) on the presence of radicals in the disulfide bonds of both disulfide compounds. Since the rate enhanced substantially, a corresponding large increase in the EPR signal would be expected when a radical mechanism is assumed. However, no increase in EPR signal was observed in

the presence of the catalyst, indicating that the increase in rate could not be associated with a radical mediated mechanism. Furthermore, addition of TEA had no impact on the extent of polymerization of MMA in the presence of diphenyl disulfide after 2 d at RT, proving that adding catalyst does not lead to an increase in the radical concentration.

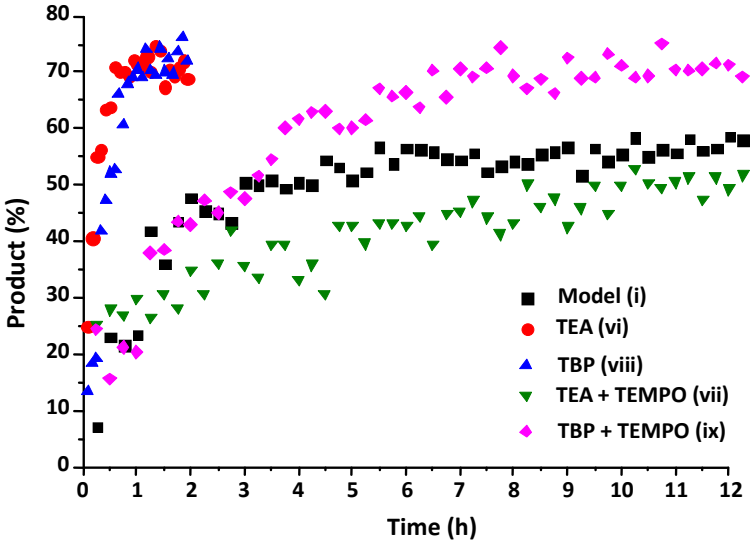

Figure II.9. Formation of the exchange product in function of time for the exchange reactions (i), (vi), (vii), (viii) and (ix).

Since both catalysts, TEA and TBP, are nucleophiles and are known to reduce disulfide compounds, forming thiolate anions, the most probable effect of these catalysts is to enhance the disulfide exchange reaction through the formation of sulfur-based anions.[30] In order to prove this, Ellman's reagent (DTNB), an aromatic disulfide similar in structure to the compounds used in this chapter, was used as a reactant. Upon reduction, 5,5'-dithiobis-(2-nitrobenzoic acid) (DTNB) yields a highly coloured thiolate species, 2-nitro-5-thiobenzoate

(TNB), which can be detected by UV-vis spectroscopy.[31,32] Thus, the disulfide DTNB was reacted with TEA, TBP and DEA in similar concentrations as used in the previous NMR studies and UV-vis spectroscopy was used to measure the formation of the coloured TNB. As can be derived from Figure II.10, the UV-vis signal increased with the nucleophilicity of the catalyst (TBP>DEA>TEA),[33,34] starting from small in the case of TEA, to bigger in the case of DEA and the biggest for TBP as catalyst, confirming that in the presence of nucleophiles aromatic disulfide compounds fragment to yield thiolate anions.

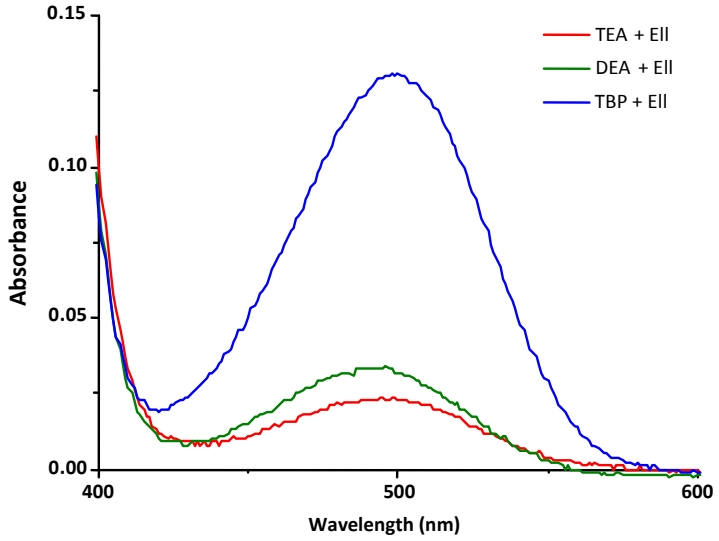

Figure II.10. UV-vis measurements of different catalysts (TBP, TEA, DEA) with DTNB.

Based on these experiments, it would be suggested that in the presence of a catalyst both radical mediated and thiol mediated exchanges occur simultaneously as shown in Figure II.11. In order to confirm this, reactions were conducted in the presence of both catalyst and the

radical scavenger TEMPO. Whilst TEMPO was capable of completely preventing the radical mediated exchange in the absence of catalyst, when a catalyst (TEA or TBP) is added the disulfide exchange still occurs, although at a slower rate than when no TEMPO is present (Figure II.9). The faster relative rate of conversion in the presence of TBP compared to TEA is due to the higher nucleophilicity of the TBP in comparison to TEA, since a higher nucleophilicity enhances the formation of sulfur-based anions and therefore promotes the disulfide exchange.[31] In the presence of TEMPO and catalyst, the radical pathway is blocked, but the exchange can still occur due to the generation of thiols by the catalyst. However, it is noteworthy to mention that when an excess of TEMPO (1 eq.) is added to the model reaction in the presence of TEA (0.1 mol eq.) no product formation was visible. This indicates that TEMPO may also retard the formation of sulfur-based anions formed by the addition of catalysts.[35]

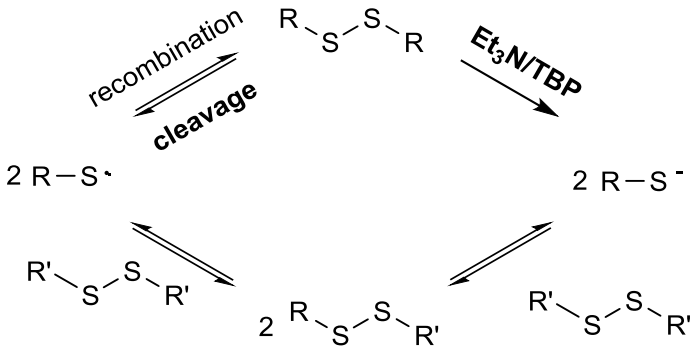

Figure II.11. Disulfide exchange through the formation of S-based radicals and S-based anions.

II.4. Conclusions

In summary, the results presented herein demonstrate that the general mechanism responsible for the self-healing event of disulfide bonds is radical mediated and involves homolytic cleavage of the disulfide bond followed by subsequent radical transfer of sulfur-based radicals. In the presence of nucleophiles, such as TEA and TBP, disulfides yield thiolate anions which can similarly undergo a series of transfer reactions and enhance the rate of the disulfide exchange. It is aspired that this mechanistic picture of the disulfide exchange reaction will enlarge the understanding of the self-healing event in disulfide-based polymers and help the synthesis of new strong self-healing materials as described in Chapter III.

II.5. References

1. Syrett, J. a., Becer, C. R. & Haddleton, D. M. Self-healing and self-mendable polymers. *Polym. Chem.* **1,** 978–987 (2010).
2. Blaiszik, B. J. *et al.* Self-Healing Polymers and Composites. *Annu. Rev. Mater. Res.* **40,** 179–211 (2010).
3. Qiu Zhang, M. & Zhi Rong, M. *Self-Healing Polymers and Polymer Composites*. (Wiley, 2011). doi:10.1002/9781118082720
4. Binder, W. H. *Self-healing polymers*. (Wiley-VCH, 2013). doi:10.1002/9783527670185
5. Yang, Y. & Urban, M. W. Self-healing polymeric materials. *Chem. Soc. Rev.* **42,** 7446–7467 (2013).
6. Zhang, P. & Li, G. Advances in healing-on-demand polymers and polymer composites. *Prog. Polym. Sci.* **57,** 32–63 (2016).
7. Hager, M. D., Greil, P., Leyens, C., van der Zwaag, S. & Schubert, U. S. *Self-healing materials*. (Springer, 2016). doi:10.1007/978-3-319-32778-5
8. Billiet, S., Hillewaere, X. K. D., Teixeira, R. F. A. & Du Prez, F. E. Chemistry of Crosslinking Processes for Self-Healing Polymers. *Macromol. Rapid Commun.* **34,** 290–309 (2013).
9. Denissen, W. *et al.* Chemical control of the viscoelastic properties of vinylogous urethane vitrimers. *Nat. Commun.* **8,** 14857 (2017).
10. Liu, W.-X. *et al.* Oxime-Based and Catalyst-Free Dynamic Covalent Polyurethanes. *J. Am. Chem. Soc.* **139,** 8678–8684 (2017).
11. Zechel, S. *et al.* Intrinsic self-healing polymers with a high E-modulus based on dynamic reversible urea bonds. *Npg Asia Mater.* **9,** e420 (2017).
12. Willocq, B. *et al.* One-component Diels-Alder based polyurethanes: a unique way to self-heal. *RSC Adv.* **7,** 48047–48053 (2017).
13. Garcia, S. J. Effect of polymer architecture on the intrinsic self-healing character of polymers. *Eur. Polym. J.* **53,** 118–125 (2014).
14. Park, I., Sheiko, S. S., Nese, A. & Matyjaszewski, K. Molecular Tensile Testing Machines: Breaking a Specific Covalent Bond by Adsorption-Induced Tension in Brushlike Macromolecules. *Macromolecules* **42,** 1805–1807 (2009).
15. Nevejans, S., Ballard, N., Miranda, J. I., Reck, B. & Asua, J. M. The underlying mechanisms for self-healing of poly(disulfide)s. *Phys. Chem. Chem. Phys.* **18,** 27577–27583 (2016).
16. Belenguer, A. M., Friščić, T., Day, G. M. & Sanders, J. K. M. Solid-state dynamic combinatorial chemistry: reversibility and thermodynamic product selection in covalent

mechanosynthesis. *Chem. Sci.* **2,** 696 (2011).

17. Caraballo, R. Dynamic Sulfur Chemistry: Screening, Evaluation and Catalysis. *KTH Chemical Science and Engineering* (KTH Royal Institute of Technology, 2010).

18. Lei, Z. Q., Xiang, H. P., Yuan, Y. J., Rong, M. Z. & Zhang, M. Q. Room-Temperature Self-Healable and Remoldable Cross-linked Polymer Based on the Dynamic Exchange of Disulfide Bonds. *Chem. Mater.* **26,** 2038–2046 (2014).

19. Amamoto, Y., Otsuka, H., Takahara, A. & Matyjaszewski, K. Self-healing of covalently cross-linked polymers by reshuffling thiuram disulfide moieties in air under visible light. *Adv. Mater.* **24,** 3975–3980 (2012).

20. Fairbanks, B. D., Singh, S. P., Bowman, C. N. & Anseth, K. S. Photodegradable, Photoadaptable Hydrogels via Radical-Mediated Disulfide Fragmentation Reaction. *Macromolecules* **44,** 2444–2450 (2011).

21. Ohishi, T. *et al.* Insertion Metathesis Depolymerization of Aromatic Disulfide-containing Dynamic Covalent Polymers under Weak Intensity Photoirradiation. *Chem. Lett.* **42,** 1346–1348 (2013).

22. Otsuka, H., Nagano, S., Kobashi, Y., Maeda, T. & Takahara, A. A dynamic covalent polymer driven by disulfide metathesis under photoirradiation. *Chem. Commun.* **46,** 1150–1152 (2010).

23. Fritze, U. F. & von Delius, M. Dynamic disulfide metathesis induced by ultrasound. *Chem. Commun.* **52,** 6363–6366 (2016).

24. Sarma, R. J., Otto, S. & Nitschke, J. R. Disulfides, Imines, and Metal Coordination within a Single System: Interplay between Three Dynamic Equilibria. *Chem. – A Eur. J.* **13,** 9542–9546 (2007).

25. Matxain, J. M., Asua, J. M. & Ruipérez, F. Design of new disulfide-based organic compounds for the improvement of self-healing materials. *Phys. Chem. Chem. Phys.* **18,** 1758–1770 (2016).

26. Goldstein, S., Samuni, A. & Merenyi, G. Kinetics of the Reaction between Nitroxide and Thiyl Radicals: Nitroxides as Antioxidants in the Presence of Thiols. *J. Phys. Chem. A* **112,** 8600–8605 (2008).

27. Matyjaszewski, K. Role of initiator-transfer agent-terminator (iniferter) in radical polymerizations: Polymer design by organic disulfides as iniferters. *Macromol. Rapid Commun.* **26,** 135–142 (2005).

28. Otsu, T., Kinoshita, Y. & Imoto, M. The chain transfer mechanism of substituted diphenyl disulfides. *Die Makromol. Chemie* **73,** 225–230 (1964).

29. Rekondo, A. *et al.* Catalyst-free room-temperature self-healing elastomers based on aromatic disulfide metathesis. *Mater. Horizons* **1,** 237–240 (2014).

30. Koval, I. V. The chemistry of disulfides. *Russ. Chem. Rev.* **63,** 735–750 (1994).

31. Ellman, G. L. Tissue sulfhydryl groups. *Arch. Biochem. Biophys.* **82,** 70–77 (1959).

32. Riddles, P. W., Blakeley, R. L. & Zerner, B. in *Methods in Enzymology* **Volume 91,** 49–60 (Academic Press, 1983).

33. Methot, J. L. & Roush, W. R. Nucleophilic Phosphine Organocatalysis. *Adv. Synth. Catal.* **346,** 1035–1050 (2004).

34. Henderson, W. A. & Schultz, C. J. The Nucleophilicity of Amines. *J. Org. Chem.* **27,** 4643–4646 (1962).

35. Antonello, S., Daasbjerg, K., Jensen, H., Taddei, F. & Maran, F. Formation and Cleavage of Aromatic Disulfide Radical Anions. *J. Am. Chem. Soc.* **125,** 14905–14916 (2003).

Chapter III. Self-healing waterborne poly(urethane-urea)s: How high can we push mechanical strength?

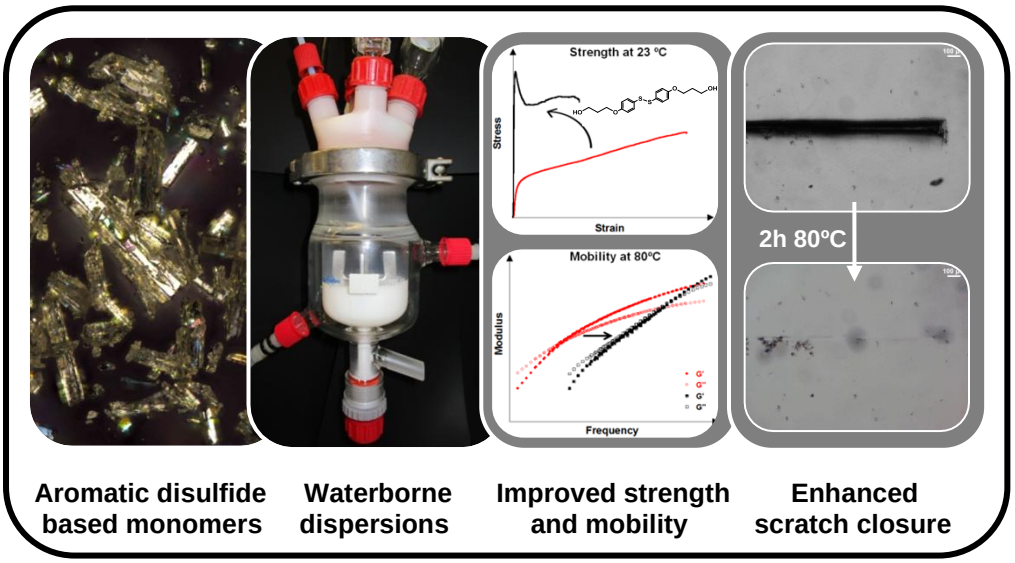

III.1. Introduction

Since the underlying mechanisms of disulfide exchange have been elucidated in Chapter II, we can now introduce this reversible chemistry into polymers so that intrinsically healable materials can be developed. Polyurethanes are perhaps the most attractive candidates to achieve this objective, as clarified in Chapter I, since these versatile materials not only provide strength and mobility due to their phase separated structure, but they also are able to inherently heal due to formation of H-bonds and allow incorporation of additional functional moieties to further enhance recovery from damage.[9,10] Therefore, by incorporating dynamic disulfides into polyurethanes, self-healing materials can be created which provide strength by the unique polyurethane architecture and simultaneously enable healing *via* both supramolecular interactions, i.e. H-bonds, and dynamic covalent bonds, *i.e.* disulfide bonds.

In this way, several PUs have already been developed using the dynamic exchange of linear aliphatic disulfides in order to obtain intrinsically healable polymers under the influence of external stimuli.[16–21] However, by introducing an aromatic disulfide compound, bis(4-aminophenyl)disulfide ($S_2(PhNH_2)_2$, Figure III.1), Rekondo *et al.* described that the dynamic disulfide exchange could be enhanced compared to aliphatic ones, as was demonstrated by the healing of a cross-linked poly(urethane-urea) that could take place at room temperature without the use of any catalysts.[22] The dynamic behaviour of the aromatic disulfide at reduced temperatures has subsequently been explored by several groups in the area of self-healing.[24–26] For example, using the same disulfide, Yang *et al.* synthesized a PU elastomer with improved tensile strength for which self-healing could be induced by heating to 60°C. They observed that for more cross-linked materials a higher tensile strength was obtained, but this

occurred with a concomitant lowering of the ability to self-heal.[27] Kim *et al.* developed a thermoplastic polyurethane with an increased toughness by introducing an aromatic disulfide diol, bis(4-hydroxyphenyl)disulfide ($S_2(PhOH)_2$, Figure III.1), which could also heal at room temperature. Using this system, they reported an ultimate tensile strength of 6.8 MPa, which is at the upper limit of the reported values for self-healing systems at room temperature.[28]

Bis(4-aminophenyl)disulfide $S_2(PhNH_2)_2$ **Bis(4-hydroxyphenyl)disulfide** $S_2(PhOH)_2$

Figure III.1. Chemical structure of bis(4-aminophenyl)disulfide ($S_2(PhNH_2)_2$) and bis(4-hydroxyphenyl)disulfide ($S_2(PhOH)_2$).

However, as already commented in Section I.3, healing at room temperature inherently demands a certain level of mobility of the polymer which compromises the mechanical properties, wear resistance and can lead to creep.[29–31] This is a major issue in polyurethane materials as in many high-end applications the higher cost of polyurethanes is overlooked owing to their superior mechanical strength. For example, while there are a wide variety of polymers that are used in waterborne coatings, few can match polyurethane dispersions for applications requiring strong coatings such as furniture, automotive and floor coatings. As a result, the majority of applications of PU dispersions require high tensile strengths, typically exceeding 15-20 MPa.[32–36] This requirement for high tensile strength puts the constraints of commercial materials beyond the limits of current self-healing polymers (Chapter I, Figure I.13).

To overcome this gap, in Chapter III, we seek to develop waterborne polymer dispersions which show sufficiently high mechanical resistance at room temperature and additionally recover from damage when chain mobility is induced by external stimuli such as heat. In order to meet this objective, the synthesis of waterborne poly(urethane-urea)s containing aromatic disulfide compounds is described.

First, the influence of the hard 2,2-bis(hydroxymethyl)propionic acid (DMPA) monomer, which acts as an internal ionic stabilizing agent upon neutralization in dispersion, on the self-healing ability of linear poly/urethane-urea)s (PUUs) is investigated *via* scratch closure and rheological measurements. Afterwards, the limits for solubility, reactivity and flexibility of the readily available aromatic disulfides, bis(4-aminophenyl)- and bis(4-hydroxyphenyl)disulfide (Figure III.1), in the synthesis of the waterborne PU(U)s is tested. Finally, on the basis of these investigations, a structurally modified aromatic disulfide compound, bis[4-(3'-hydroxypropyloxy)phenyl]disulfide ($S_2(Ph(CH_2)_3OH)_2$), is synthesized and introduced to a higher extent into the polymer backbone so that a waterborne PU(U) material is developed with an increased strength and mobility. Hence, incorporation of the modified aromatic disulfide compound enlarges the efficiency of developing stronger self-healing polymers of interest for applications requiring strength, such as coatings.

III.2. Experimental

III.2.1. Materials

Acetone (Sigma-Aldrich, ≥99.5%), bis(4-aminophenyl)disulfide ($S_2(PhNH_2)_2$, TCI, >98.0%), bis(4-hydroxyphenyl)disulfide ($S_2(PhOH)_2$,TCI, >98%), 2,2-bis(hydroxymethyl)propionic acid (DMPA, Sigma-Aldrich, 98%) 3-bromo-1-propanol (Apollo Scientific, 96%), bromophenol blue (Fluka), dibutyltin dilaurate (DBTL, Sigma-Aldrich, 95%), diethylamine (DEA, Sigma-Aldrich, ≥99.5%), ethyl acetate (EtOAc, ACROS Organics, ≥99.5%), hexane (Fisher Chemicals, >99%), hydrochloric acid 1N (HCl, Panreac), isophorone diisocyanate (IPDI, Sigma-Aldrich, 98%), methyl ethyl ketone (MEK, ACROS Organics, >99%), polytetrahydrofuran (PolyTHF, BASF, 2000 $g.mol^{-1}$), potassium carbonate (K_2CO_3, Sigma-Aldrich, ≥99%), sodium chloride (NaCl, Sigma-Aldrich, ≥99.5%), sodium sulfate (Na_2SO_4, Sigma-Aldrich, ≥99%), tetrahydrofuran (THF, Scharlab), triethylamine (TEA, ACROS Organics, 99%) were used as received.

III.2.2. Synthesis of bis[4-(3'-hydroxypropoxy)phenyl]disulfide $S_2(Ph(CH_2)_3OH)_2$

Inspired by the synthetic method reported by Ohishi *et al.*,[37] a mixture of bis(4-hydroxyphenyl)disulfide (100 g, 0.40 mol), 3-bromo-1-propanol (51 mL, 1.00 mol) and potassium carbonate (554 g, 4.01 mol) in THF (100 wt% of the solid reagents) as solvent was stirred at 60°C for 48 h under N_2-atmosphere (Figure III.2), in a jacketed glass reactor equipped with a mechanical stirrer and a condenser. Afterwards, the reaction mixture was filtered and washed with EtOAc. The obtained organic filtrate was washed with 1N HCl and brine, after which it was dried over anhydrous Na_2SO_4. The solvent was removed from the

product under vacuum and the residue material was purified by recrystallization in an EtOAc:Hexane-mixture (3:5). Finally, the product was dried at 50°C under vacuum to give bis[4-(3'-hydroxypropyloxy)phenyl]disulfide $S_2(Ph(CH_2)_3OH)_2$ [IUPAC: ((disulfanediylbis(4,1-phenylene))bis(oxy))bis(propan-1-ol)].

Yield: 70.5 g (64 mol%). Pale yellow powder. FTIR (neat, cm^{-1}): 3319.19, 2945.40, 2870.80, 1883.87, 1589.02. m.p.: 60.3 - 61.2ºC. ^{1}H NMR (500 MHz, Chloroform-*d*) δ 7.44 – 7.37 (d, *J* = 8.79 Hz, 2H), 6.89 – 6.82 (d, *J* = 8.80 Hz, 2H), 4.12 (t, *J* = 6.0 Hz, 2H), 3.87 (t, *J* = 5.9 Hz, 2H), 2.05 (m, *J* = 5.9 Hz, 2H), 1.81 (s, 1H (O*H*)) (Figure A I.1, Appendix I). ^{13}C NMR (126 MHz, Chloroform-*d*) δ 159.31, 132.82, 128.77, 115.36, 77.50, 77.25, 76.99, 65.88, 60.40, 32.12 (Figure A I.2). Anal. Calcd. for $C_{18}H_{22}O_4S_2$: C 58.99, H 6.05, S 17.50. Found: C 58.96, H 6.01, S 17.42. HRMS (ESI) for $C_{18}H_{22}O_4S_2$ calculated $[M+H]^+$: 366.0960. Found: 366.0960.

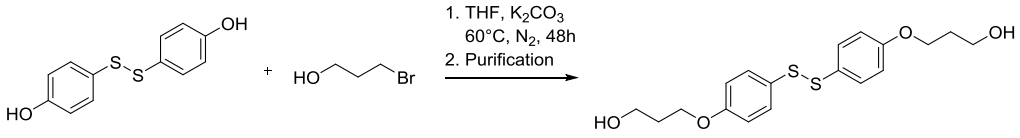

Figure III.2. Claisen etherification to obtain bis[4-(3'-hydroxypropoxy)phenyl]disulfide.

III.2.3. Synthesis of waterborne poly(urethane-urea) dispersions

III.2.3.1. Synthesis of the waterborne PUU dispersions based on bis(4-aminophenyl)disulfide $S_2(PhNH_2)_2$

In order to obtain the prepolymer, PolyTHF (M_n=2000 $g.mol^{-1}$), DMPA and IPDI were fed together into a 100 mL jacketed glass reactor equipped with a mechanical stirrer and a condenser. Next, DBTL (0.2-0.4 wt% of reactants) as catalyst and acetone (45-60 wt%) as

solvent were added and the mixture was stirred for 2 h at 56ºC under refluxing conditions. A first series of PUUs was prepared varying the amount of DMPA added to the reaction mixture from 3 to 7 wt% of reactants. The formulation for the syntheses of these different pre-polymers can be found in Table III.1. After 2 h, the isocyanate concentration had reduced to the theoretical level as determined by back titration and the mixture was cooled down to room temperature so that bis(4-aminodiphenyl)disulfide (0.33 mol eq. of IPDI) could be added into the vessel to react with the residual free NCO-groups of the prepolymer for 4 h. Finally, the mixture was neutralized with TEA (1 mol eq. of DMPA) after which deionized water (100-150 wt%) was added dropwise to obtain a dispersion. Acetone was removed from the filtered dispersion by evaporation using a rotary evaporator at 556 mbar so that a solids content of 30-35 wt% was obtained. A summary of the synthetic process is shown in Figure III.3.

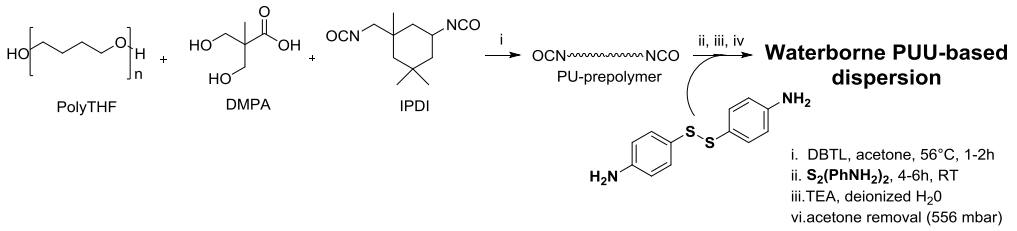

Figure III.3. Synthetic procedure of waterborne PUU dispersions.

For the second series of PUUs based on $S_2(PhNH_2)_2$, a constant amount of DMPA was used (3 wt% of reactants), while a variable amount of bis(4-aminophenyl disulfide) was added to the prepolymer for incorporation into the PUU backbone as is depicted in Table 1. Due to the variable amount of disulfide and therefore varying necessity of free NCO-groups, the prepolymer reaction times were 2 h, 1.5 h and 1 h for PUU-3D-0.33S, PUU-3D-0.44S and

PUU-3D-0.53S, respectively. Subsequently, a reaction time of 6 h instead of 4 h was required for PUU-3D-0.44S and PUU-3D-0.53S to assure full incorporation of the larger amount of bis(4-aminophenyl disulfide) before neutralization, dispersion and evaporation could be carried out.

Table III.1. Formulation of different PUU syntheses performed varying the amount of DMPA and bis(4-aminophenyl disulfide) (wt% based on the total amount of reactants).

Run	Sample	Unit	DMPA	IPDI	PolyTHF	$S_2(PhNH_2)_2$
1	**PUU-3D-0.33S**	wt%	**3**	19	71	**7**
		mol eq.	**0.25**	1	0.42	**0.33**
2	**PUU-4D-0.33S**	wt%	**4**	21	67	8
		mol eq.	**0.31**	1	0.36	0.33
3	**PUU-5D-0.33S**	wt%	**5**	22	64	8
		mol eq.	**0.35**	1	0.32	0.33
4	**PUU-6D-0.33S**	wt%	**6**	24	61	9
		mol eq.	**0.38**	1	0.28	0.33
5	**PUU-7D-0.33S**	wt%	**7**	26	57	10
		mol eq.	**0.42**	1	0.24	0.33
6	**PUU-3D-0.44S**	wt%	3	22	64	**11**
		mol eq.	0.23	1	0.33	**0.44**
7	**PUU-3D-0.53S**	wt%	3	24	58	**14**
		mol eq.	0.21	1	0.27	**0.53**

III.2.3.2. Synthesis of the waterborne PU dispersion based on bis(4-hydroxyphenyl)disulfide $S_2(PhOH)_2$

PolyTHF (M_n=2000 g.mol^{-1}, 8.40 g, 4.20 mmol), DMPA (1.16 g, 8.63 mmol), IPDI (6.00 g, 27.00 mmol) and bis(4-hydroxyphenyl)disulfide (3.55 g, 14.18 mmol) were fed together into a 100 mL jacketed glass reactor equipped with a mechanical stirrer and a condenser. Next, DBTL (0.3 wt% of reactants) and MEK (55 wt%) were added into the vessel and the mixture was stirred for 60 h at 80ºC under refluxing conditions. The mixture was cooled down to room temperature

and neutralized with TEA (1.20 mL, 8.63 mmol) after which deionized water (100 wt%) was added dropwise to obtain a dispersion. MEK was removed from the filtered dispersion by evaporation using a rotary evaporator at 243 mbar so that a solids content of about 30 wt% was obtained.

III.2.3.3. Synthesis of the waterborne PU dispersions based on bis[4-(3'-hydroxypropoxy)phenyl]disulfide ($S_2(Ph(CH_2)_3OH)_2$)

PolyTHF (M_n=2000 $g.mol^{-1}$), DMPA, IPDI and bis[4-(3'-hydroxypropoxy)phenyl]disulfide ($S_2(Ph(CH_2)_3OH)_2$) were fed together into a 100 mL jacketed glass reactor equipped with a mechanical stirrer and a condenser. Next, DBTL (0.3 wt% of reactants) and MEK (60 wt%) were added into the vessel and the mixture was stirred for 8h at 80ºC under refluxing conditions. The amount of DMPA added in the synthesis was constant (6 wt% of reactants), while the amount of $S_2(Ph(CH_2)_3OH)_2$ was varied as shown in Table III.2. Finally, the mixture was neutralized with TEA (1 mol eq. of DMPA) after which deionized water (100 wt%) was slowly added dropwise to obtain a dispersion. MEK was removed from the filtered dispersion by evaporation using a rotary evaporator at 243 mbar giving a solids content of about 30 wt%.

Table III.2. Formulation of different PUs and PUUs based on bis[4-(3'-hydroxypropoxy)phenyl]disulfide (wt% based on the total amount of reactants).

Run	Sample	Unit	DMPA	IPDI	PolyTHF	$S_2(Ph(CH_2)_3OH)_2$
8	**PU-6D-0.33S**	wt%	6	25	54	**14**
		mol eq.	0.42	1	0.24	**0.33**
9	**PU-6D-0.44S**	wt%	6	27	46	**20**
		mol eq.	0.37	1	0.19	**0.44**
10	**PU-6D-0.53S**	wt%	6	30	38	**26**
		mol eq.	0.33	1	0.14	**0.53**

III.2.3.4. Synthesis of the waterborne PUU dispersion containing both $S_2(PhNH_2)_2$ and $S_2(Ph(CH_2)_3OH)_2$

The dispersion termed PUU-6D-0.53S-MIXED was obtained by first feeding PolyTHF (M_n=2000 g mol^{-1}, 5.30 g, 2.65 mmol), DMPA (0.79 g, 5.90 mmol), IPDI (4.00 g, 18.00 mmol) and bis[4-(3'-hydroxypropoxy)phenyl]disulfide (2.08 g, 5.67 mmol) together into a 100 mL jacketed glass reactor equipped with a mechanical stirrer and a condenser. Next, DBTL (0.3 wt% of reactants) and MEK (60 wt%) were added into the vessel and the mixture was stirred for 3 h at 80ºC under refluxing conditions. Afterwards, the mixture was cooled down to room temperature and bis(4-aminodiphenyl)disulfide (0.94 g, 3.78 mmol) was added into the vessel to react with the residual free NCO-groups of the prepolymer for 6 h. Finally, the mixture was neutralized with TEA (0.82 mL, 5.90 mmol) after which deionized water (100 wt%) was slowly added dropwise to obtain a dispersion. MEK was removed from the filtered dispersion by evaporation using a rotary evaporator at 243 mbar so that a solid content of approximately 30 wt% was obtained.

III.2.4. Characterization

III.2.4.1. Monomer characterization

Infrared spectra were recorded on an FTIR spectrometer (Bruker). All melting points were determined in a Büchi Melting Point B-540. The NMR spectra were recorded at 500 MHz for ^{1}H-NMR, and 126 MHz for ^{13}C{H}-NMR in $CDCl_3$ at room temperature. The data are reported as s = singlet, d = doublet, t = triplet, m = multiplet, coupling constant(s) in Hz, integration. Elemental analysis was carried out using a TruSpec Micro (LECO) analyzer. HRMS-analysis was performed with an LC/Q-TOF with Agilent Jet Stream ESI ionization source.

III.2.4.2. Prepolymer and dispersion characterization

To determine the NCO content of the PU prepolymer, a back titration of the excess of diethylamine (DEA) molecules, which were added to neutralize the free NCO-groups of the PU, with HCl was performed.[38,39] The Z-average diameter of the polymer particles was measured by dynamic light scattering (DLS) using a Malvern Zetasizer Nano ZS (Malvern Instruments). Samples were prepared by diluting a fraction of the latex with deionized water, and the analyses were carried out at 25°C.

III.2.4.3. Polymer characterization

Films with a final thickness of 0.50-0.75 mm were obtained by casting the dispersion in silicon molds (25 x 55 mm^2). The casted films were first dried for 1 day at 23°C and subsequently for 3 days at 60°C after which they were equilibrated for 3 days at 23°C while maintaining 55% RH. The molecular weight of the dried films dissolved in THF was determined by Size Exclusion Chromatography/Gel Permeation Chromatography (SEC/GPC). The instrument consisted of a pump (LC-20A, Shimadzu), an autosampler (Waters 717), a differential refractometer (Waters 2410), a UV detector measuring at 262nm (Waters 2487) and three columns in series (Styragel HR2, HR4 and HR6, with pore sizes ranging from 102-106 Å). Chromatograms were obtained at 35 °C using a THF flow rate of 1 $mL.min^{-1}$. A series of polystyrene (PS) standards in the range of 580–3 848 000 $g.mol^{-1}$ were used to obtain the calibration curve which provided molecular weights of the polymer relative to polystyrene. Thermogravimetric analysis (TGA) was performed in a temperature range of 40-800 ºC at 10ºC/min under a nitrogen atmosphere with a TA Instruments Q500. Dynamic mechanical analysis (DMA) measurements were carried

out in a Triton 2000 DMA (Triton Technology) or on a TA Instruments DMA Q800 (only for sample PUU-6D-0.53S-MIXED) equipped with a liquid nitrogen cooling system. The measurements were performed in tension mode at a single frequency of 1 Hz. The samples were cooled down to ≈-150 ºC and heated with a rate of 4ºC.min^{-1} till the temperature at which the minimum dynamic force of 0.01 N was hit. Stress-strain measurements were carried out on dumbbell type specimen under controlled conditions (23ºC and 55% RH) on a tensile apparatus (Stable Micro System TA HD Plus Texture Analyzer) with a crosshead velocity of 25 mm min^{-1}. For each experiment, the average of 3-6 replicate measurements is reported. For the scratch closure experiments, scratches were made with a depth of roughly 75% of the thickness (±0.7 mm) of the films using a razor blade with a thickness of 0.40 mm and subsequently closure at 80ºC was followed using an optical microscope (Nikon Eclipse LV100ND). The rheological data were obtained from a stress-controlled Anton Paar Physica MCR101 rheometer using parallel plate geometry (plate ø = 8mm, disk-shaped specimens of approximately 10 mm in diameter and 0.50-0.75 mm in thickness). Frequency sweeps (0.001-20 Hz) at a strain of 0.5% were conducted at fixed temperatures ranging from 50-120ºC.

III.3. Results and discussion

III.3.1. Waterborne PUU dispersions based on diamine-terminated disulfide compounds

III.3.1.1. Dispersion and polymer characteristics

A series of poly(urethane-urea) dispersions containing varying amounts of bis(4-aminophenyl)disulfide ($S_2(PhNH_2)_2$) and the DMPA were synthesized using the formulations

described in Table III.1 and the process outlined in Figure III.3 which can be found in the experimental section of this chapter. Through the variation of DMPA and aromatic disulfide content, the objective was to explore the balance between material strength and chain mobility in order to obtain mechanically strong self-healing polymers. In a first set of experiments (Runs 1-5, Table III.1), the amount of IPDI and disulfide compound was kept constant, while the DMPA content varied from 3 to 7 wt%. In a second set of experiments (Runs 1, 6 and 7), the amount of IPDI and DMPA was kept constant, but here the amount of bis(4-aminophenyl)disulfide varied from 7 to 14 wt%.

In agreement with the function of DMPA as ionic stabilizer, Table III.3 shows that the particle sizes (d_p) of dispersions decreased when the amount of DMPA increased. In contrast, when the amount of the disulfide compound was increased, the particle size increased significantly and broad particle size distributions were obtained. It is noteworthy to mention that, due to the high amount of disulfide compound added for the synthesis of PUU-D3-0.53S, the prepolymer was no longer a homogeneous solution, but a highly viscous and optically turbid mass, which may explain the large particle sizes. The presence of large particles additionally led to sedimentation of PUU-3D-0.44S and PUU-3D-0.53S (Series 6 and 7). The characteristics of the waterborne PUU dispersions are also reflected in the films formed after casting the dispersions, as can be seen in Figure III.4. PUU-3D-0.33S yielded a rather transparent and homogeneous film, while PUU-3D-0.44S showed a more turbid film and PUU-3D-0.53S formed an even more turbid and inhomogeneous film. This puts a limit on the amount of disulfide that can be introduced into the system, since unfavorable dispersions and film properties are obtained for too high levels of the self-healing moiety.

Table III.3. Dispersion and polymer characteristics of PUUs based on $S_2(PhNH_2)_2$.

Run	Sample	DLS measurement		GPC measurement (RI)			TGA
		d_p (nm)	PDI	M_n (kDa)	M_w (kDa)	Đ	T_d (°C) (5 wt% loss)
1	**PUU-3D-0.33S**	125	0.07	18	34	1.9	262
2	**PUU-4D-0.33S**	71	0.06	16	33	2.0	255
3	**PUU-5D-0.33S**	55	0.07	15	27	1.8	244
4	**PUU-6D-0.33S**	47	0.10	14	26	1.9	236
5	**PUU-7D-0.33S**	42	0.10	12	21	1.7	230
6	**PUU-3D-0.44S**	260	0.80	11	23	2.0	255
7	**PUU-3D-0.53S**	520	0.83	8	16	2.0	253

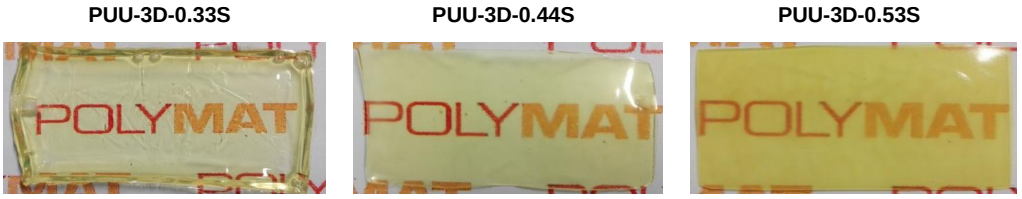

Figure III.4. Films cast from dispersions with an increasing disulfide $S_2(PhNH_2)_2$ content.

When looking at the molecular weights (M_w) shown in Table III.3, it can be noted that the M_w decreased with DMPA. This was due to the fact that when keeping the level of IPDI/$S_2(PhNH_2)_2$ constant, an increase of DMPA inevitably means a decrease of the macrodiol PolyTHF, and therefore lower molecular weights at similar degree of polymerization were obtained. Similarly, the values obtained for the molecular weights of the PUUs with a variable amount of disulfide compound, show that the M_w decreased drastically with increasing disulfide content, although in this case the decrease was significantly greater. Moreover, the molecular weight distributions (MWD) of these PUUs showed the presence of low molecular weight polymer in the case of PUU-3D-0.53S (Figure III.5). The lower molecular weight PUU chains were most probably a result of a less effective incorporation of the disulfide compound due to the solubility problems

observed at high concentrations of disulfide. Moreover, while PUU-3D-0.33S and PUU-3D-0.44S had almost complete incorporation of the disulfide, from the molecular weight distribution obtained by GPC using an UV absorption detector, it could be calculated that PUU-3D-0.53S still had 2.5% of unreacted disulfide compound with respect to the total amount of disulfide added. As a result, the degree of conversion was lower and therefore a lower M_w of the polymer was observed.

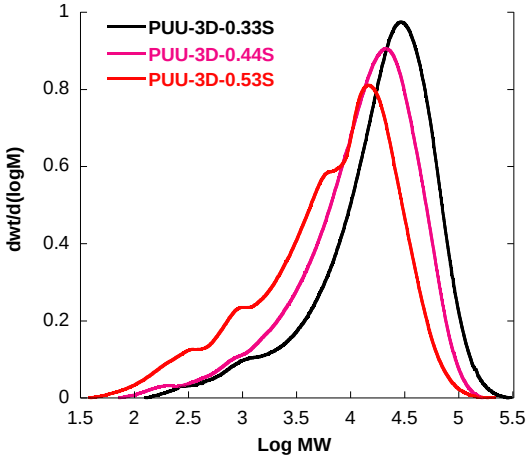

Figure III.5. MWD distribution obtained by GPC (RI) of the PUUs with varying amount of $S_2(PhNH_2)_2$.

III.3.1.2. Thermal and mechanical properties of the PUUs

Regarding the thermal properties of the PUUs, it can be stated that although all polymers are stable up to 230°C, it seems that an increasing amount of DMPA or disulfide decreases the thermal stability of the material, as shown by the thermal degradation temperatures (T_d) presented in Table III.3. Thus, increasing the incorporated DMPA or disulfide content, not only leads to a lower molecular weight of the PUU, but also seems to decrease its thermal stability.

The dynamic mechanical properties of the PUUs were analyzed by DMA (Figure III.6). It is noteworthy to mention that a peak can be observed for the curves of the loss modulus at the lowest temperatures, around -140°C. Such a relaxation at low temperatures in the glassy state of the PUUs is comparable to the ones which have already been described in literature for bisphenol A polycarbonate and can therefore be linked to secondary relaxation processes due to the presence of closely interconnected aromatic rings, in this case linked through dynamic disulfide bonds.[40,41] The most obvious relaxation, located around -70ºC for all the samples, is linked to the glass transition temperature of PolyTHF (T_g = -77ºC). At high temperatures, a broad relaxation is observed for PUU-5D-0.33S, PUU-6D-0.33S and PUU-7D-0.33S, which can reflect segmental motions of the hard parts of the PUUs. This high temperature relaxation shifts to higher temperatures with the amount of DMPA (Figure III.6 A) or disulfide content (Figure III.6 B), *i.e.* as the amount of soft PolyTHF is reduced and the number of hard units increased. Since the high temperatures relaxation is not observed for PUU-3D-0.33S and PUU-4D-0.33S, it can be deduced that a minimum of hard units of PUU is necessary for this relaxation.

Additionally, this has a relevant influence on the overall mechanical properties of the samples, because the presence of organized hard units also provokes a considerable increase of the storage modulus E', in particular close to room temperature. Moreover, as can be seen in Figure III.6, E' decreases severely with temperature above the T_g of -70ºC in the case of PUU-3D-0.33S and PUU-4D-0.33S, which is due to the absence of organized hard units in these samples.

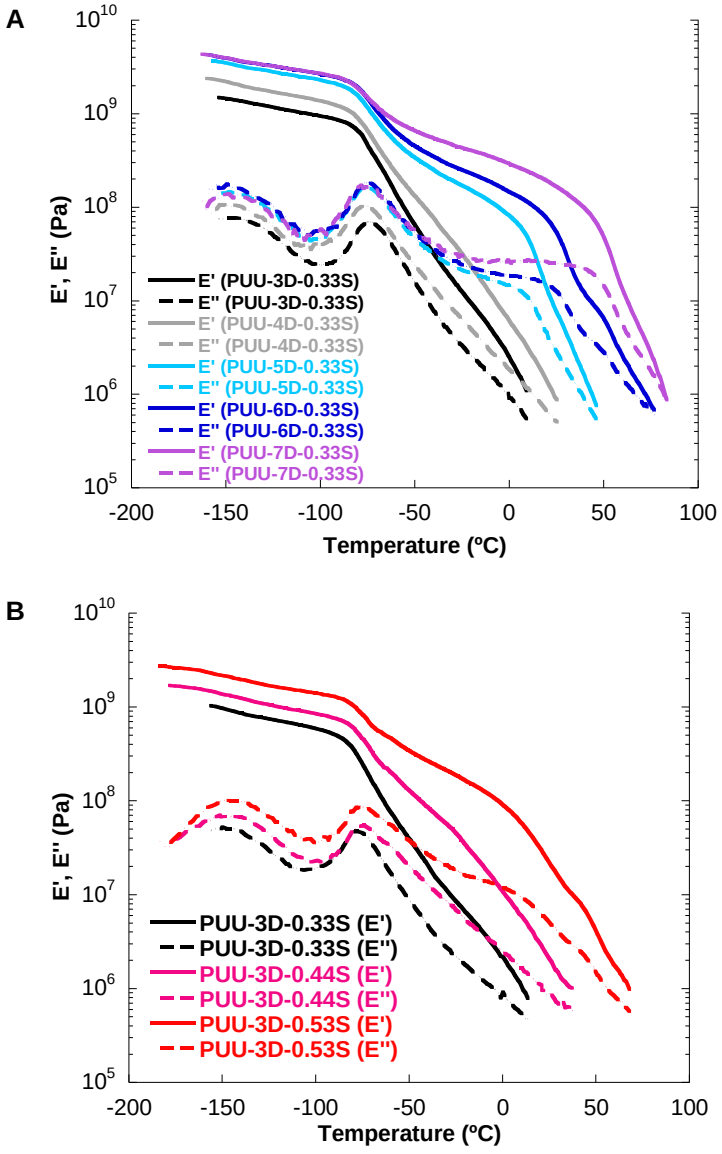

Figure III.6. DMA results of PUUs based on a varying DMPA (A) or $S_2(PhNH_2)_2$ (B) content.

Tensile test results obtained at room temperature were also affected by the presence of hard units. Figure III.7 and Table III.4 show that increasing the amount of DMPA or disulfide in the PUU backbone led to an enhancement of both the Young's modulus and ultimate tensile strength (UTS). The unexpected lower tensile strength for the PUU-7D-0.33S (Figure III.7A) might be explained either by the lower M_w of the material compared to the other PUUs or alternatively due to the higher T_g of the material (Figure III.6) which could lead to a restricted film formation. It is noteworthy to mention that the values obtained for the tensile strength of these PUUs are significantly higher (UTS ≈ 17 MPa at a strain rate of 25 mm.min^{-1}) than those obtained for self-healing elastomers based on bis(4-aminophenyl)disulfide (UTS ≈ 0.8 MPa at 500 mm.min^{-1}),[22] and for waterborne organic-inorganic hybrids with the same self-healing moiety (UTS ≈ 4.5 MPa at 20 mm.min^{-1}).[24] Even when comparing with values of the "tough" self-healing polyurethane elastomers reported previously (UTS ≈ 7.7 MPa at 500 mm.min^{-1} and 6.8 MPa at 100 mm.min^{-1}),[27,28] it can be concluded that the PUUs presented here are significantly stronger, especially considering the low strain rate employed for the tensile tests.

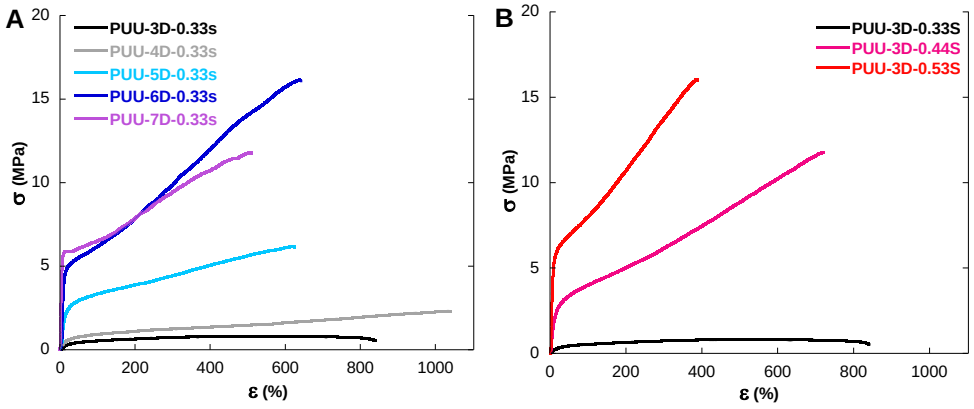

Figure III.7. Stress-strain (σ-ε) curves of PUUs with varying DMPA (A) and disulfide (B) content.

Table III.4. Tensile testing results of PUUs with varying DMPA and disulfide content.

Run	Sample	Young's modulus (MPa)	UTS (MPa)	ε_f (%)
1	**PUU-3D-0.33S**	2.7 ± 0.3	0.9 ± 0.1	850 ± 10
2	**PUU-4D-0.33S**	5.0 ± 0.6	2.4 ± 0.5	970 ± 110
3	**PUU-5D-0.33S**	26.2 ± 1.8	6.3 ± 0.3	610 ± 20
4	**PUU-6D-0.33S**	85.8 ± 2.6	16.5 ± 0.2	680 ± 30
5	**PUU-7D-0.33S**	141.5 ± 4.2	11.3 ± 0.3	470 ± 20
6	**PUU-3D-0.44S**	33.0 ± 1.1	11.3 ± 0.4	680 ± 25
7	**PUU-3D-0.53S**	128.0 ± 2.8	16.7 ± 0.5	400 ± 15

III.3.1.3. Scratch closure

Although for coating applications damage resistance and therefore strength is required, the polymer chains still need to show some mobility in order to repair the damage and allow recovery of broken bonds and interactions. As a qualitative method to check the overall mobility of the chains, the scratch closure of the PUUs was optically monitored. In order to reach the terminal or flow zone of the viscoelastic response, and so induce chain mobility, the films were heated up to a temperature of 80°C, well above the glass transition temperature of all the samples. Figure III.8 A shows that increasing the amount of DMPA, scratch closure was slower, because the material became stiffer as reflected by the higher values of E' (Figure III.6) and Young modulus (Figure III.7 A). An increase in disulfide content, that also provided polymers with higher rigidity, led to the same effect in scratch closure (Figure III.8 B). It is worth emphasizing that these results show that self-healing is the result of the interplay between rheology and bond exchange and that for self-healing moieties that affect both characteristics, the use of higher quantities of the self-healing moiety may have a negative effect on the healing process.

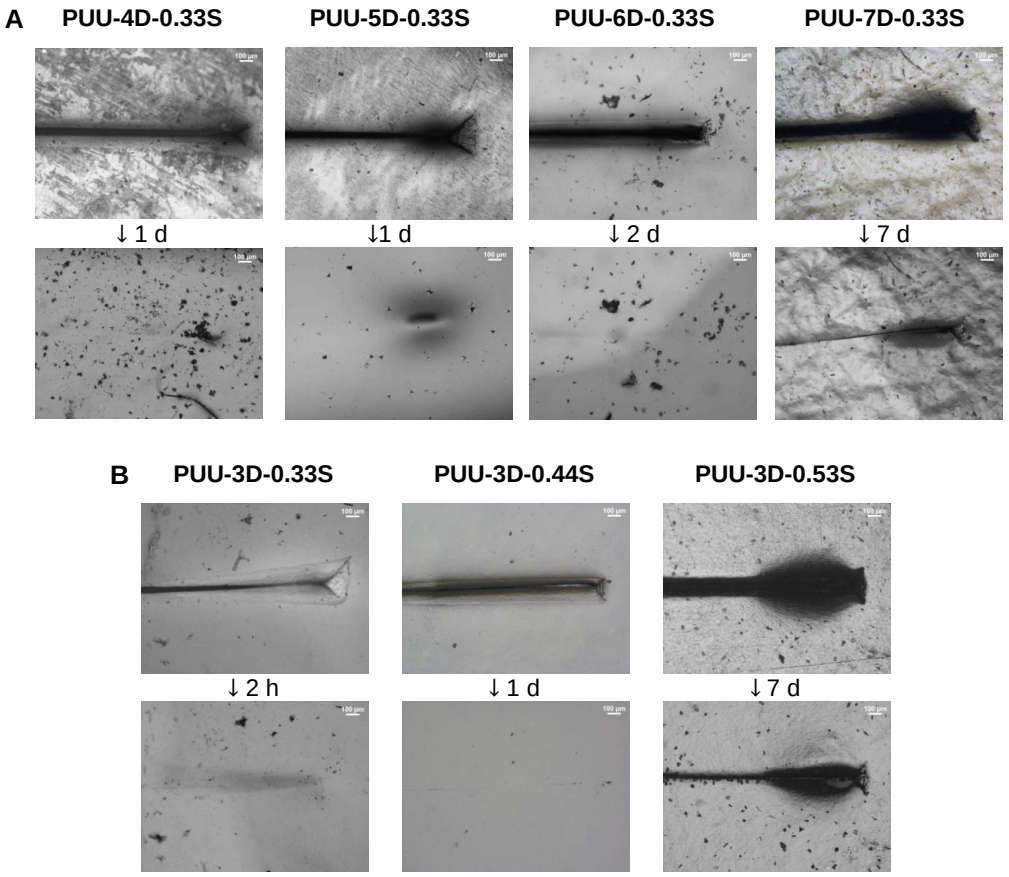

Figure III.8. Scratch closure at 80°C of PUUs based on a varying amount of DMPA (A) or $S_2(PhNH_2)_2$ content (B).

III.3.1.4. Rheological behaviour of the PUUs

The scratch closure measurements demonstrated that a certain degree of chain mobility is generated in these rather stiff materials. Contrary to the local or segmental motions, the global mobility of the chains is only detected in the terminal viscoelastic zone, at which parameters involving large scale motions can be measured. A representative parameter of the mobility of

the chains is the so-called terminal relaxation time (τ_d), that for a given temperature is the inverse of the frequency ($\omega_d=1/\tau_d$) at which the crossover between the storage (G') and the loss (G'') moduli occurs.[42–45] Figure III.9 presents the master curves of G' and G'' at a reference temperature of 80°C. In order to obtain these curves, the viscoelastic behaviour of the PUUs was studied by performing frequency sweep measurements at temperatures ranging from 50 to 120ºC and afterwards applying the time-temperature superposition (TTS) principle.

However, this principle is only valid for materials that do not change their microstructure upon exposure to temperature, which is not always the case for polymers based on dynamic bonds.[46–55] A way to verify if the TTS principle is applicable is using the van-Gurp-Palmen-plot (vGP-plot), in which the phase angle δ of the measured rheological data is depicted versus the corresponding absolute value of the complex shear modulus $|G^*|$. If the isothermal frequency curves merge into a common line, the principle holds.[56] For all PUUs, a good overlap of these different curves was obtained (Figures A I.5 and A I.6 in Appendix I), which shows that the TTS principle is applicable for these materials, at least for temperatures above the high temperature relaxation (Figures III.6) associated to the hard units of the PUUs.

The relaxation times (τ_d) of the different PUUs presented in Table III.5 follow the same trend as the scratch closure times with the harder materials presenting the longer relaxation times. However, comparison with the results in Figure III.8 shows that the times required for scratch closure were much longer than the relaxation times. Likely the different time scales are due to the fact that scratch closure requires the creep deformation of the polymer over relatively large times, which is a complex viscoelastic process that implies a spectrum of retardation times.[46]

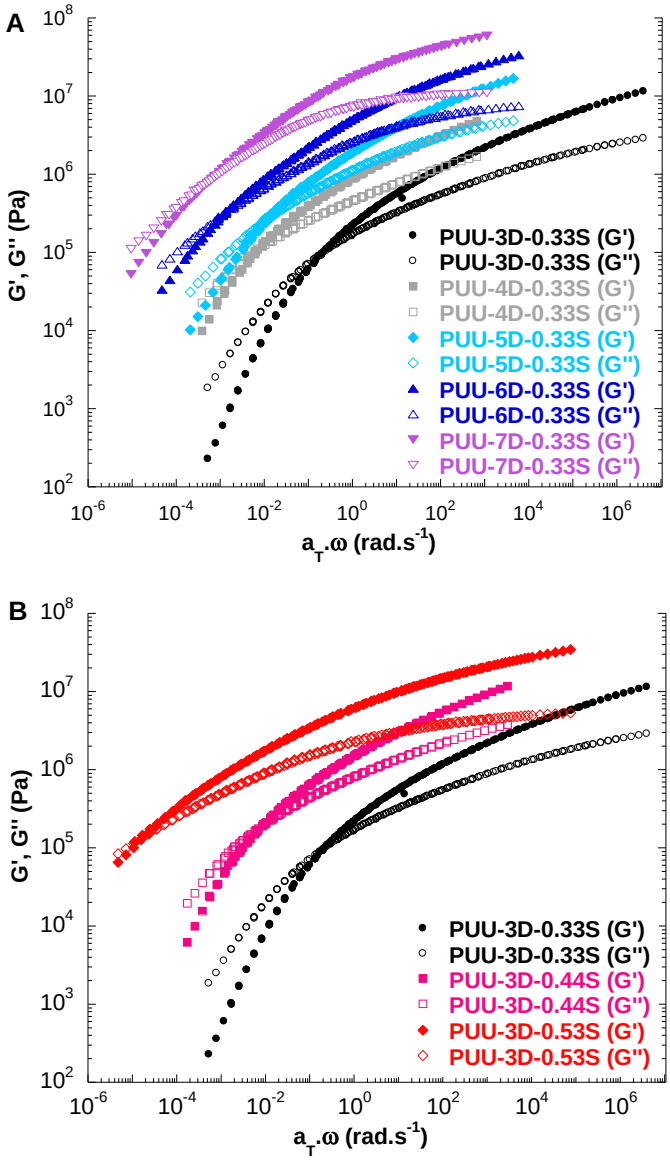

Figure III. 9. Master curves (T_{ref}=80ºC) for the PUUs based on $S_2(PhNH_2)_2$ with varying DMPA (A) and disulfide content (B) obtained by applying TTS using horizontal shift factors (a_T).

Table III.5. Characteristic values for G'-G'' crossover in the master curves (T_{ref}=80ºC) of PUUs based on $S_2(PhNH_2)_2$ with varying amount of DMPA and disulfide.

Run	Sample	ω_d (rad.s^{-1})	τ_d
1	**PUU-3D-0.33S**	0.2315	30 s
2	**PUU-4D-0.33S**	0.0062	17 min
3	**PUU-5D-0.33S**	0.0089	12 min
4	**PUU-6D-0.33S**	0.0013	1.5 h
5	**PUU-7D-0.33S**	0.0005	3.5 h
6	**PUU-3D-0.44S**	0.0082	13 min
7	**PUU-3D-0.53S**	0.00001	7 d

It is clear from the preceding that the use of bis(4-aminophenyl)disulfide presents a number of issues. First, due to the relatively low solubility in the polymerization reaction, the amount of bis(4-aminophenyl)disulfide that can be incorporated is limited, influencing the MW of the PUU that can be obtained. Furthermore, a significant increase in bis(4-aminophenyl)disulfide renders the PUU dispersion instable. In addition, increasing the amount of the self-healing moiety in the PUU backbone makes the material stiffer limiting its mobility which hampers self-healing. Therefore, there is a need for alternative self-healing moieties that still contain reactive aromatic disulfides, but that additionally provide enough flexibility so the self-healing ability is not hindered by the rigidity of the material.

III.3.2. Waterborne PU(U) dispersions based on diol-terminated disulfide compounds

III.3.2.1. Polymer synthesis

In the search for other aromatic disulfide compounds, the commercially available bis(4-hydroxyphenyl)disulfide was considered as an interesting alternative. Due to the lower reactivity of alcohols towards isocyanates, the reaction was performed at 80 ºC using MEK as

solvent. However, even at the high reaction temperature and with the prolonged reaction times (60 h), more than 15% of the bis(4-hydroxyphenyl)disulfide was not incorporated into the PU-backbone, as shown by the molecular weight distribution obtained by GPC using an UV absorption detector in Figure A I.7 (Appendix I). This incomplete incorporation was due to the fact that the reactivity of phenolic OH-groups towards isocyanates is significantly lower than that of water.[57,58]

Since the commercially available diamine- and diol-terminated disulfides showed the aforementioned problems, bis[4-(3'-hydroxypropoxy)phenyl]disulfide ($S_2(Ph(CH_2)_3OH)_2$, Figure III.2 in the experimental section) was synthesized. The reactivity of the primary alcohols was expected to increase sufficiently so that full incorporation of the self-healing moiety would be possible in acceptable reaction times. Moreover, by introducing an alkyl chain consisting of three carbon atoms onto the aromatic rings, the flexibility of alkyl chain can counteract the rigid aromatic rings of the disulfide compound and therefore a more mobile polymer was anticipated. Additionally, the alkyl chain would also increase the solubility of the polymer in the reaction mixture, providing the opportunity to increase the disulfide content into the PU-backbone without encountering solubility issues.

Advantageously, bis[4-(3'-hydroxypropoxy)phenyl]-disulfide was added to the reactor together with the other diols (DMPA and PolyTHF) reacting together in one step to form a polyurethane (PU) in MEK at 80°C, as depicted in Figure III.10. After that, the waterborne PU dispersion could be obtained through neutralization with TEA and addition of deionized water.

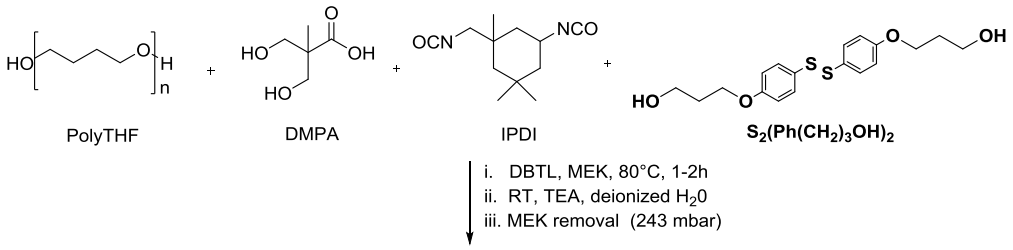

Figure III.10. Scheme of synthesis procedure of waterborne PU dispersion

For the series of PUs synthesized by introducing $S_2(Ph(CH_2)_3OH)_2$, the amount of IPDI and the DMPA content (6 wt%) were kept constant. The higher DMPA content was used so that the polymer had acceptable rigidity for coating applications. The amount of $S_2(Ph(CH_2)_3OH)_2$ varied from 0.33 mol eq. of IPDI (14 wt%) for PU-6D-0.33S and 0.44 mol eq. of IPDI (20 wt%) for PU-6D-0.44S to a maximum of 0.53 mol eq. of IPDI (26 wt%) for PU-6D-0.53S (Table III.2, experimental section). For the same number of molar equivalents, the weight fraction of $S_2(Ph(CH_2)_3OH)_2$ was higher than in the previous cases due to the higher molecular weight. Unlike the aromatic diamine disulfide, during the synthesis of the series of PUs with increasing amounts of $S_2(Ph(CH_2)_3OH)_2$, no solubility issues of the polymer in the solvent were observed.

Additionally, a mixed disulfide polymer, PUU-6D-0.53S-MIXED, was synthesized by introducing both $S_2(Ph(CH_2)_3OH)_2$ and $S_2(PhNH_2)_2$ as self-healing moieties into the PUU backbone. The formulation of the mixed disulfide polymer was chosen with the intention that the amounts of IPDI, PolyTHF and DMPA were similar to the amounts used in the synthesis of PU-6D-0.53S, described in detail in the experimental section of this chapter, so that direct comparison of PU-6D-0.53S with PUU-6D-0.53S-MIXED was possible.

III.3.2.2. Dispersion and polymer characteristics

For all PUs and the mixed disulfide polymer (PUU-6D-0.53S-MIXED) nearly complete incorporation of disulfide compound was obtained even for the highest disulfide content. In addition, stable dispersions of small particle size and relatively narrow PDI were obtained (Table III.6). The films cast from the PU(U) dispersions were homogeneous, transparent and almost colourless (Figure III.11) even though the amount of disulfide was substantially higher than that used for the PUUs that yielded yellowish films (Figure III.4). PUU-6D-0.53S-MIXED is slightly more yellow due to the presence of $S_2(PhNH_2)_2$. The molecular weights obtained for the PUs were similar to that of PUU-6D-0.33S (Table III.6). Moreover, contrary to the PUUs based on $S_2(PhNH_2)_2$, the M_w of the polymer did not decrease with the amount of DMPA or disulfide.

Table 0.6. Dispersion and polymer characteristics of PUs and PUUs based on $S_2(Ph(CH_2)_3OH)_2$.

Run	Sample	DLS		GPC (RI)			TGA
		d_p (nm)	PDI	M_n (kDa)	M_w (kDa)	Đ	T_d (°C) (5 wt% loss)
4	**PUU-6D-0.33S**	47	0.10	14	26	1.9	235
8	**PU-6D-0.33S**	35	0.18	11	22	1.9	243
9	**PU-6D-0.44S**	32	0.15	13	23	1.8	244
10	**PU-6D-0.53S**	36	0.14	11	27	2.4	241
11	**PUU-6D-0.53S-MIXED**	50	0.11	14	26	1.8	230

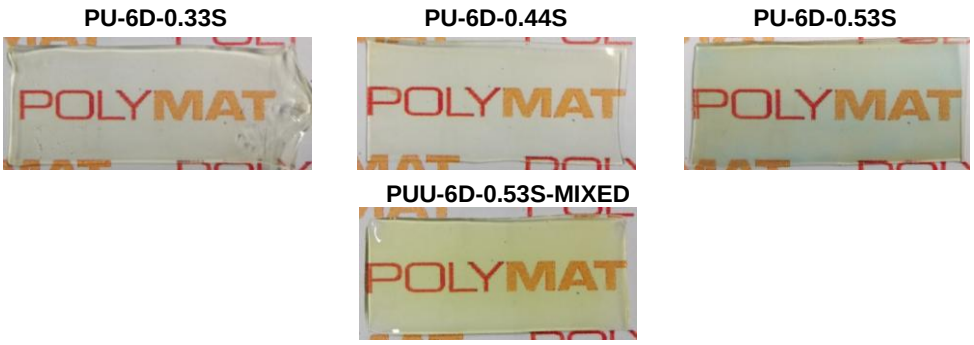

Figure III.11. Films from dispersions PUs based on $S_2(Ph(CH_2)_3OH)_2$ and PUU-6D-0.53S-MIXED.

III.3.2.3. Thermal and mechanical properties of the PU(U)s

The thermal stabilities obtained for the PUs were similar to that of PUU-6D-0.33S and were not seemingly affected by the amount disulfide (Table III.6). The dynamic mechanical properties of the PU series were analyzed by DMA (Figure III.12). Similar to the PUUs reported above, the secondary relaxation of closely interconnected aromatic rings led to a peak in E'' modulus at around -140ºC. Additionally, also here, a low temperature T_g was observed at -70°C in all samples and a broad relaxation, which probably reflects segmental motions of the hard units of the system, was observed at temperatures close to room temperature. As could be expected, with increasing amounts of disulfide the T_g was shifted to higher values. Therefore, the general interpretation of the results of Figure III.12 is the same as those of Figure III.6. However, the values obtained for the PUs were lower than those of PUU-6D-0.33S, due to the introduction of a more flexible self-healing moiety into the backbone and the absence of urea groups that reduced H-bonding, which decreased the rigidity of the PUs.

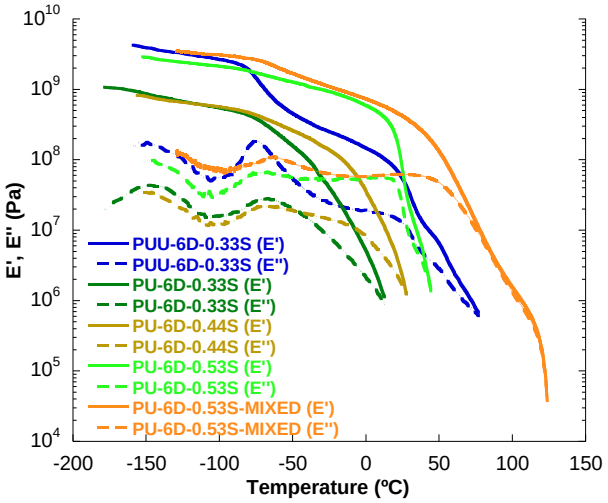

Figure III.12. DMA results of PU(U)s based on a varying $S_2(Ph(CH_2)_3OH)_2$ content.

The results obtained from the tensile tests are presented in Figure III.13 and Table III.7. It can be seen that the Young's modulus and the ultimate tensile strength (UTS) increased, and the elongation at break (ε_f) decreased with the $S_2(Ph(CH_2)_3OH)_2$ content. The PUs show a more ductile behaviour after reaching a yield point in which the stress does not increase above the yield strength anymore. When replacing 21 mol% of $S_2(Ph(CH_2)_3OH)_2$ by $S_2(PhNH_2)_2$ (PUU-6D-0.53S-MIXED), a significant increase of the Young's modulus and ultimate tensile strength was obtained compared to PU-6D-0.53S, although the measured strain was similar for both materials. This highlights the effect of the flexibility offered by the alkyl chain on the aromatic rings of the PUs and that of the urea groups. These effects are also evident when all these polymers are compared with PUU-6D-0.33S which displays a strong and non-ductile behaviour without a significant yield point.

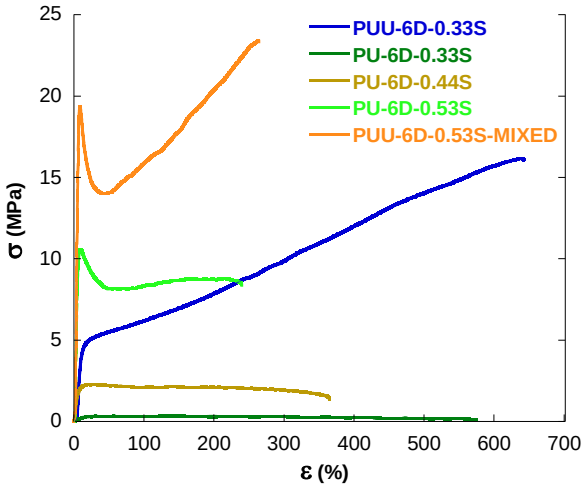

Figure III.13. Stress-strain (σ-ε) curves of PU(U)s based on varying $S_2(Ph(CH_2)_3OH)_2$ content.

Table III.7. Tensile testing results of PU(U)s based on variable amount of $S_2(Ph(CH_2)_3OH)_2$.

Run	Sample	Young's modulus (MPa)	UTS (MPa)	ε_f (%)
4	**PUU-6D-0.33S**	85.8 ± 2.6	16.5 ± 0.2	680 ± 30
8	**PU-6D-0.33S**	2.8 ± 0.4	0.3 ± 0.1	520 ± 35
9	**PU-6D-0.44S**	53.0 ± 3.8	2.3 ± 0.1	385 ± 10
10	**PU-6D-0.53S**	321.0 ± 7.8	10.2± 0.2	210 ± 10
11	**PUU-6D-0.53S-MIXED**	577.4± 11.4	23.1± 0.5	260± 10

III.3.2.4. Rheological behaviour of the PU(U)s

Figure III.14 presents the master curves of G' and G'' at a reference temperature of 80 ºC of the polymers based on a variable amount of $S_2(Ph(CH_2)_3OH)_2$ in comparison with PUU-6D-0.33S. These curves were obtained from frequency sweep measurements carried out at different temperatures using the TTS principle.

In this case, however, the isothermal frequency curves in the van-Gurp-Palmen-plots did not merge into a single line (Figure A I.8) indicating that the materials showed some local change with temperature. This behavior was not unexpected, since the dynamic disulfide bonds can be activated at higher temperatures and therefore would give rise to a change in the microstructure. The reason why this effect appears for these materials, but could not be observed for the PUUs based on $S_2(PhNH_2)_2$, could possibly be explained by the fact that $S_2(Ph(CH_2)_3OH)_2$ generated a softer PU backbones where the dynamic disulfide exchange can act more freely than in the more rigid PUU backbone where additionally H-bonds between the urea groups physically cross-link the material and further lock the ability of the disulfide bonds to exchange. Although the TTS principle does not hold as strongly as for the PUUs based on

$S_2(PhNH_2)_2$, using both horizontal (a_T) and vertical shift factors (b_T) acceptable superposition could be achieved to obtain the master curves in Figure III.14.

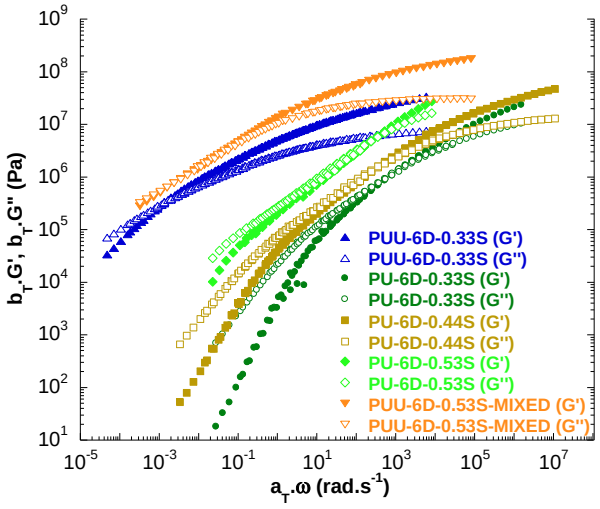

Figure III.14. Master curves (T_{ref}=80ºC) of PU(U)s based on varying $S_2(Ph(CH_2)_3OH)_2$ content.

Table III.8. Characteristic values for G'-G'' crossover in the master curves (T_{ref}=80ºC) of PU(U)s based on varying $S_2(Ph(CH_2)_3OH)_2$ content.

Run	Sample	ω_d (rad.s^{-1})	τ_d
4	**PUU-6D-0.33S**	0.0013	1.5 h
8	**PU-6D-0.33S**	784	0.008 s
9	**PU-6D-0.44S**	240	0.026 s
10	**PU-6D-0.53S**	12	0.524 s
11	**PUU-6D-0.53S-MIXED**	0.1 – 0.001	1 min - 2 h

The relaxation times (τ_d) calculated from the crossover points in Figure III.14 are presented in Table III.8. It can be seen that the relaxation time increases with the $S_2(Ph(CH_2)_3OH)_2$ content, because the polymer becomes stiffer. Similarly, the incorporation of $S_2(PhNH_2)_2$ in the PUU-6D-0.53S-MIXED resulted in a further increase of the relaxation time. The broader crossover

region observed in PUU-6D-0.53S-MIXED was attributed to the fact that a less homogeneous polymer was obtained as two different aromatic disulfide compounds were introduced into the PUU-backbone which broadens the time frame at which the different segments of the polymer relaxed. Nevertheless, for the considerably stiffer PUU-6D-0.53S-MIXED, the frequency at which G' and G'' start crossing over is higher than for PUU-6D-0.33S, indicating a higher molecular mobility for some part of the polymer. However, for PUU-6D-0.53S-MIXED to start flowing completely, almost the same relaxation time (τ_d) has to be considered as PUU-6D-0.33S (Table III.8).

III.3.2.5. Scratch closure

Scratch closure of the PUs and the mixed disulfide PUU was optically monitored at 80°C (Figure III.15). It can be seen that the time needed for scratch closure ($t_{scratch}$) increases with the relaxation time, but as in the case of the $S_2(PhNH_2)_2$-based PUUs, in all cases $t_{scratch} >> \tau_d$, because as explained above, creep deformation of the polymer is needed for scratch closure. The scratch closure times correlate quite well with the storage modulus (E') at the temperature at which the test was carried out (80ºC) as can be observed in Figure III.16 A. In order to construct this figure, the values of the storage modulus at 80ºC were obtained from the data in Figures III.6 and III.12, while the values of $t_{scratch}$ were roughly estimated from Figures III.7 and III.15. Although the use of the approximate interrelations among viscoelastic functions, which allows estimating creep from dynamic viscoelastic results, is out of the scope of this thesis, it is known that E' is inversely proportional to the creep compliance function D(t).[46] Therefore, increasing the storage modulus E' should give rise to a lower compliance or deformation capacity, which leads to higher scratch closure times.

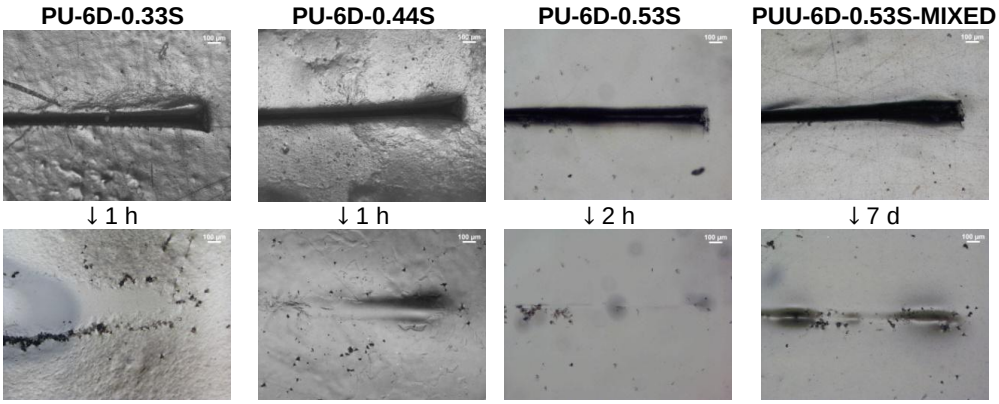

Figure III.15. Scratch closure at 80°C of PU(U)s based on varying amount of $S_2(Ph(CH_2)_3OH)_2$.

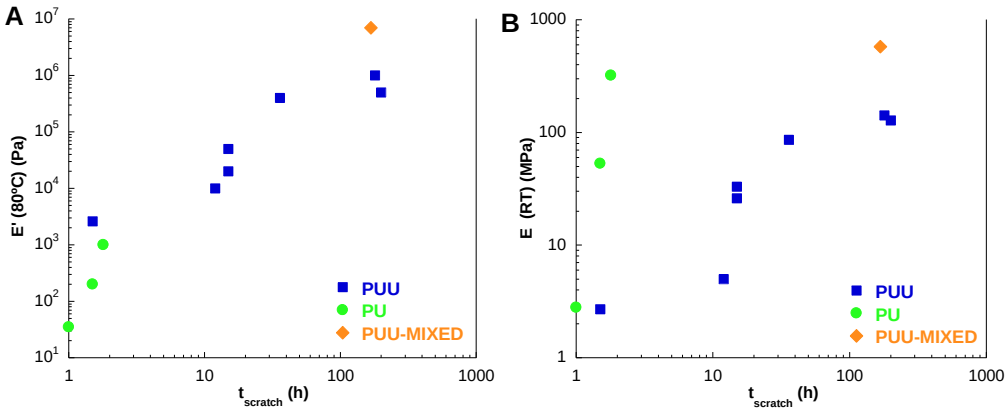

Figure III.16. Relationship between the storage modulus E' (T=80ºC) (A) or the Young's modulus E (RT) (B) and the time for scratch closure $t_{scratch}$ (T=80ºC) for all PU(U)s.

From a practical point of view, short times for scratch closure at the healing temperature and good mechanical properties at the service temperature (usually RT) are required. Therefore, Figure III.16 B compares the Young's modulus (E) determined in the tensile tests carried out at room temperature with $t_{scratch}$ at 80ºC for all of the synthesized polymers. It can be seen that for the same $t_{scratch}$, the PUs present much better mechanical properties than the PUUs, with the

additional advantage of having a higher concentration of disulfide groups. The reason for the high E-value of the PUs at room temperature is that the absence of the strong H-bonds provided by the urea groups is compensated by the reduction of the soft PolyTHF content. On the other hand, at the healing temperature, the alkyl moiety of the disulfide unit of the PUs allows a certain mobility of the hard segments lowering the storage modulus below that of the PUUs. These results highlight the importance of playing not only with the dynamic moieties, but also with the polymer microstructure to develop attractive self-healing materials.

The combination of good mechanical properties at the service temperature with considerable mobility at easily reachable healing temperatures marks a significant improvement on previous self-healing PUs and potentially allows the production of strong yet healable coatings systems. Interestingly, to best of our knowledge, the strongest self-healing PU elastomers based on aromatic disulfides described in literature so far were developed by Kim *et al.*,[28] presenting stress-strain curves with an ultimate tensile strength of 6.8 MPa at a 100mm.min^{-1} strain rate. With this in mind, the unique mechanical properties of the developed PU(U)s are obvious as PU-6D-0.53 has a yield strength of 10 MPa and PUU-6D-0.53S-MIXED has an ultimate tensile strength of 23 MPa at 25 mm.min^{-1}, whilst demonstrating complete scratch closure at 80ºC.

It seems clear from the presented results that a material with a mechanical strength required for high-end applications cannot be expected to undergo healing at the room temperature, since the short relaxation time of the material would inevitably lead to creep which limits its practical utility. However, through careful tuning of rheological behaviour of the polymer *via* designed synthesis, it appears possible for a material to show a marked transition from a strong material at room temperature, to a softer, healable material at elevated temperatures.

III.4. Conclusions

In summary, a series of waterborne PU(U) dispersions were synthesized with varying amount of hard monomers, namely DMPA and aromatic disulfide compounds, incorporated into the polymer backbone. By increasing the DMPA content, PUUs with better mechanical properties could be obtained (UTS $\leq$ 17 MPa), however, this limited the mobility of the polymer that could be observed in scratch closure and which was confirmed by longer relaxation times in frequency sweep measurements. Furthermore, it could be demonstrated that, contrary to the intuition of a chemist, an increasing amount of the self-healing moiety does not necessarily offer a higher mobility of the material which is crucial to obtain self-healing. Since the incorporation of both the commercial bis(4-aminophenyl)- and bis(4-hydroxyphenyl)disulfide into the PU(U) backbone was restricted due to limitations towards solubility, reactivity and mobility, the more flexible bis[4-(3'-hydroxypropoxy)phenyl]disulfide was introduced in order to obtain waterborne PU materials. In this way, it was possible to increase the amount of the self-healing moiety incorporated in the backbone, without compromising the mechanical properties of the materials reaching ultimate tensile strengths in the range of 10 to 23 MPa, at the service temperature and providing good mobility at the healing temperature.

This proved the fact that, next to the presence of dynamic bonds or supramolecular interactions, the polymer architecture and in this case the structure of the introduced disulfides plays a crucial role in the mobility and consequently self-healing ability of the material. Further optimization of the developed waterborne PU(U) materials, incorporating more flexible aromatic disulfides, may therefore lead to more efficient self-healing polymers which can serve in coating applications requiring higher mechanical strength which will be the focus of Chapter IV.

III.5. References

1. Syrett, J. a., Becer, C. R. & Haddleton, D. M. Self-healing and self-mendable polymers. *Polym. Chem.* **1,** 978–987 (2010).
2. Blaiszik, B. J. *et al.* Self-Healing Polymers and Composites. *Annu. Rev. Mater. Res.* **40,** 179–211 (2010).
3. Qiu Zhang, M. & Zhi Rong, M. *Self-Healing Polymers and Polymer Composites*. (Wiley, 2011). doi:10.1002/9781118082720
4. Binder, W. H. *Self-healing polymers*. (Wiley-VCH, 2013). doi:10.1002/9783527670185
5. Yang, Y. & Urban, M. W. Self-healing polymeric materials. *Chem. Soc. Rev.* **42,** 7446–7467 (2013).
6. Zhang, P. & Li, G. Advances in healing-on-demand polymers and polymer composites. *Prog. Polym. Sci.* **57,** 32–63 (2016).
7. Hager, M. D., Greil, P., Leyens, C., van der Zwaag, S. & Schubert, U. S. *Self-healing materials*. (Springer, 2016). doi:10.1007/978-3-319-32778-5
8. Billiet, S., Hillewaere, X. K. D., Teixeira, R. F. A. & Du Prez, F. E. Chemistry of Crosslinking Processes for Self-Healing Polymers. *Macromol. Rapid Commun.* **34,** 290–309 (2013).
9. Yang, Y., Ding, X. & Urban, M. W. Chemical and physical aspects of self-healing materials. *Prog. Polym. Sci.* **49–50,** (2015).
10. Engels, H. W. *et al.* Polyurethanes: Versatile materials and sustainable problem solvers for today's challenges. *Angewandte Chemie - International Edition* **52,** (2013).
11. Denissen, W. *et al.* Chemical control of the viscoelastic properties of vinylogous urethane vitrimers. *Nat. Commun.* **8,** 14857 (2017).
12. Xiao, Y., Huang, H. & Peng, X. Synthesis of self-healing waterborne polyurethanes containing sulphonate groups. *RSC Adv.* **7,** 20093–20100 (2017).
13. Sun, P. *et al.* Facile Preparation of Mussel-Inspired Polyurethane Hydrogel and Its Rapid Curing Behavior. *ACS Appl. Mater. Interfaces* **6,** 12495–12504 (2014).
14. Yang, X. *et al.* Self-healing polymer materials constructed by macrocycle-based host-guest interactions. *Soft Matter* **11,** 1242–1252 (2015).
15. Nevejans, S., Ballard, N., Miranda, J. I., Reck, B. & Asua, J. M. The underlying mechanisms for self-healing of poly(disulfide)s. *Phys. Chem. Chem. Phys.* **18,** 27577–27583 (2016).
16. Zhang, L., Chen, L. & Rowan, S. J. Trapping Dynamic Disulfide Bonds in the Hard Segments of Thermoplastic Polyurethane Elastomers. *Macromol. Chem. Phys.* **218,** 1600320 (2017).

17. Xu, Y. & Chen, D. A Novel Self-Healing Polyurethane Based on Disulfide Bonds. *Macromol. Chem. Phys.* **217,** 1191–1196 (2016).

18. Xu, W. M., Rong, M. Z. & Zhang, M. Q. Sunlight driven self-healing, reshaping and recycling of a robust, transparent and yellowing-resistant polymer. *J. Mater. Chem. A* **4,** 10683–10690 (2016).

19. Jian, X., Hu, Y., Zhou, W. & Xiao, L. Self-healing polyurethane based on disulfide bond and hydrogen bond. *Polym. Adv. Technol.* **29,** 463–469 (2018).

20. Wan, T. & Chen, D. Synthesis and properties of self-healing waterborne polyurethanes containing disulfide bonds in the main chain. *J. Mater. Sci.* **52,** 197–207 (2017).

21. Wu, X. *et al.* Heat-triggered poly(siloxane-urethane)s based on disulfide bonds for self-healing application. *J. Appl. Polym. Sci.* **135,** 46532 (2018).

22. Rekondo, A. *et al.* Catalyst-free room-temperature self-healing elastomers based on aromatic disulfide metathesis. *Mater. Horizons* **1,** 237–240 (2014).

23. Matxain, J. M., Asua, J. M. & Ruipérez, F. Design of new disulfide-based organic compounds for the improvement of self-healing materials. *Phys. Chem. Chem. Phys.* **18,** 1758–1770 (2016).

24. Aguirresarobe, R. H., Martin, L., Fernandez-Berridi, M. J. & Irusta, L. Autonomic healable waterborne organic-inorganic polyurethane hybrids based on aromatic disulfide moieties. *EXPRESS Polym. Lett.* **11,** 266–277 (2017).

25. Yarmohammadi, M., Shahidzadeh, M. & Ramezanzadeh, B. Designing an elastomeric polyurethane coating with enhanced mechanical and self-healing properties: The influence of disulfide chain extender. *Prog. Org. Coatings* **121,** 45–52 (2018).

26. Yarmohammadi, M. & Shahidzadeh, M. Evaluation of disulfide chain extender effect on the mechanical properties of unsaturated polyurethane-urea networks. *J. Appl. Polym. Sci.* **135,** 46309 (2018).

27. Yang, Y., Lu, X. & Wang, W. A tough polyurethane elastomer with self-healing ability. *Mater. Des.* **127,** 30–36 (2017).

28. Kim, S.-M. *et al.* Superior Toughness and Fast Self-Healing at Room Temperature Engineered by Transparent Elastomers. *Adv. Mater.* **30,** 1705145 (2018).

29. Dahlke, J., Zechel, S., Hager, M. D. & Schubert, U. S. How to Design a Self-Healing Polymer: General Concepts of Dynamic Covalent Bonds and Their Application for Intrinsic Healable Materials. *Adv. Mater. Interfaces* **1800051,** 1–14 (2018).

30. Garcia, S. J. Effect of polymer architecture on the intrinsic self-healing character of polymers. *Eur. Polym. J.* **53,** 118–125 (2014).

31. García, S. J., Fischer, H. R. & Van Der Zwaag, S. A critical appraisal of the potential of self healing polymeric coatings. *Prog. Org. Coatings* **72,** 211–221 (2011).

32. H. Haberle, W. Temme, R. Bergs, N. Steidl, A. M. Use of aqueous polyurethane

dispersions in formulations for crack sealing coating systems. US20030088045A1. (2003).

33. Maier, A. *et al.* Coating system for veneered wood based on polyurethane dispersions method for the production and use thereof. US20030162892A1. (2000).

34. D. Schütze, G. Kurek, T. Rische, J. Urban, T. H. Polyurethane-polyurea dispersions as coating compositions. US6642303B2. (2003).

35. Rische, T., Casselmann, H., Feller, T., Blum, H. & Kurek, G. Polyurethane-polyurea dispersions and their use as coating compositions. US20070049684A1. (2005).

36. P. H. Markusch, J. W. Rosthauser, M. C. B. Stable, aqueous dispersions of polyurethane-ureas. US4501852A. (1985).

37. Ohishi, T. *et al.* Insertion Metathesis Depolymerization of Aromatic Disulfide-containing Dynamic Covalent Polymers under Weak Intensity Photoirradiation. *Chem. Lett.* **42,** 1346–1348 (2013).

38. Hamzehlou, S. *et al.* Mechanistic investigation of the simultaneous addition and free-radical polymerization in batch miniemulsion droplets: Monte Carlo simulation versus experimental data in polyurethane/acrylic systems. *Polymer* **55,** 4801–4811 (2014).

39. Mehravar, S., Ballard, N., Agirre, A., Tomovska, R. & Asua, J. M. Relating polymer microstructure to adhesive performance in blends of hybrid polyurethane/acrylic latexes. *Eur. Polym. J.* **87,** 300–307 (2017).

40. Jho, J. Y. & Yee, A. F. Secondary relaxation motion in bisphenol A polycarbonate. *Macromolecules* **24,** 1905–1913 (1991).

41. Delbreilh, L., Bernès, A. & Lacabanne, C. Secondary Retardation/Relaxation Processes in Bisphenol A Polycarbonate: Thermostimulated Creep and Dynamic Mechanical Analysis Combined Investigations. *Int. J. Polym. Anal. Charact.* **10,** 41–56 (2005).

42. Stukalin, E. B., Cai, L. H., Kumar, N. A., Leibler, L. & Rubinstein, M. Self-Healing of Unentangled Polymer Networks with Reversible Bonds. *Macromolecules* **46,** 7525–7541 (2013).

43. Chen, S., Mahmood, N., Beiner, M. & Binder, W. H. Self-Healing Materials from V- and H-Shaped Supramolecular Architectures. *Angew. Chemie Int. Ed.* **54,** 10188–10192 (2015).

44. Hackelbusch, S., Rossow, T., van Assenbergh, P. & Seiffert, S. Chain Dynamics in Supramolecular Polymer Networks. *Macromolecules* **46,** 6273–6286 (2013).

45. Bode, S. *et al.* Correlation between scratch healing and rheological behavior for terpyridine complex based metallopolymers. *J. Mater. Chem. A* **3,** 22145–22153 (2015).

46. Ferry, J. D. *Viscoelastic Properties of Polymers*. (Wiley, 1980).

47. Seiffert, S. & Sprakel, J. Physical chemistry of supramolecular polymer networks. *Chem. Soc. Rev.* **41,** 909–930 (2012).

48. Müller, M., Seidel, U. & Stadler, R. Influence of hydrogen bonding on the viscoelastic properties of thermoreversible networks: analysis of the local complex dynamics. *Polymer* **36,** 3143–3150 (1995).

49. Stadler, F. J. *et al.* Linear Viscoelastic Rheology of Moderately Entangled Telechelic Polybutadiene Temporary Networks. *Macromolecules* **42,** 6181–6192 (2009).

50. Feldman, K. E., Kade, M. J., Meijer, E. W., Hawker, C. J. & Kramer, E. J. Model Transient Networks from Strongly Hydrogen-Bonded Polymers. *Macromolecules* **42,** 9072–9081 (2009).

51. Callies, X. *et al.* Linear rheology of bis-urea functionalized supramolecular poly(butylacrylate)s: Part I – weak stickers. *Polymer* **69,** 233–240 (2015).

52. Abdolah Zadeh, M., Grande, A. M., van der Zwaag, S. & Garcia, S. J. Effect of curing on the mechanical and healing behaviour of a hybrid dual network: a time resolved evaluation. *RSC Adv.* **6,** 91806–91814 (2016).

53. Grande, A. M., Bijleveld, J. C., Garcia, S. J. & van der Zwaag, S. A combined fracture mechanical – rheological study to separate the contributions of hydrogen bonds and disulphide linkages to the healing of poly(urea-urethane) networks. *Polymer* **96,** 26–34 (2016).

54. Bose, R. K. *et al.* Contributions of hard and soft blocks in the self-healing of metal-ligand-containing block copolymers. *Eur. Polym. J.* **93,** 417–427 (2017).

55. Grande, A. M., Martin, R., Odriozola, I., van der Zwaag, S. & Garcia, S. J. Effect of the polymer structure on the viscoelastic and interfacial healing behaviour of poly(urea-urethane) networks containing aromatic disulphides. *Eur. Polym. J.* **97,** 120–128 (2017).

56. Trinkle, S., Walter, P. & Friedrich, C. Van Gurp-Palmen Plot II – classification of long chain branched polymers by their topology. *Rheol. Acta* **41,** 103–113 (2002).

57. Mark, H. F. *Encyclopedia of Polymer Science and Technology, Concise*. (Wiley, 2013).

58. Delebecq, E., Pascault, J.-P., Boutevin, B. & Ganachaud, F. On the Versatility of Urethane/Urea Bonds: Reversibility, Blocked Isocyanate, and Non-isocyanate Polyurethane. *Chem. Rev.* **113,** 80–118 (2013).

Chapter IV. Flexible aromatic disulfide monomers for self-healable linear and cross-linked poly(urethane-urea) coatings

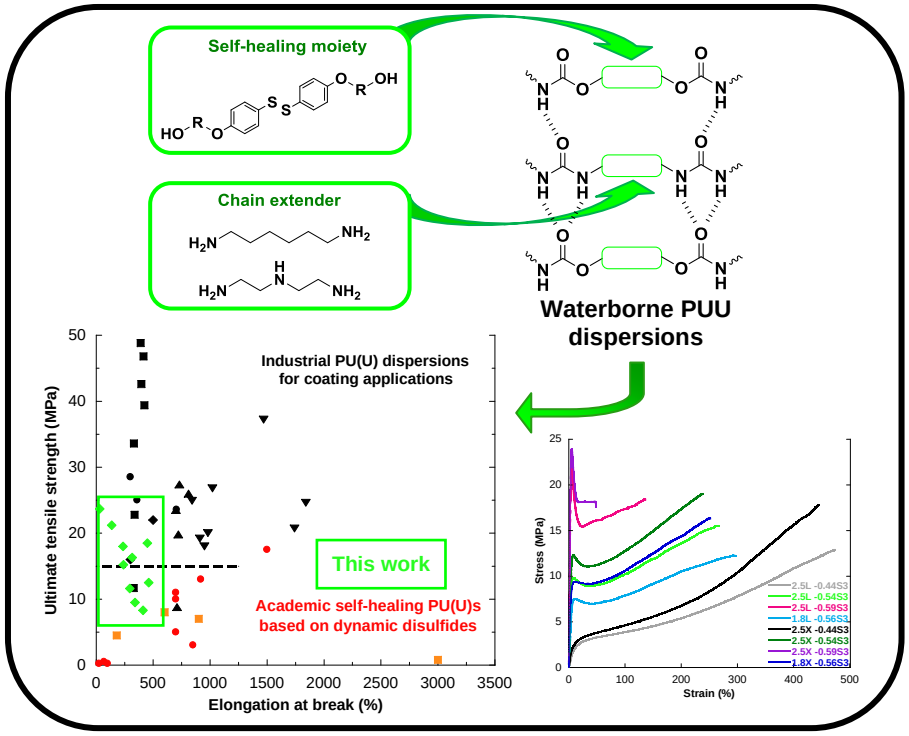

IV.1. Introduction

As already mentioned in Chapter III, the main challenge self-healing materials are facing is to meet the requirements imposed by the applications, particularly in the case of coatings, where damages leave the substrate unprotected against the initiation and rapid propagation of corrosion processes. A strategy to achieve self-healing in materials which still provide damage resistance, minimize dirt pickup and improve blocking (so that undesired adhesion of the coated surface with any other surface can be avoided), was described in Chapter III. PU(U)s were developed with a microstructure that offers mechanical strength at the service temperature and that undergoes a conformational change upon exposure to external stimuli, in this case heat, so that it became mobile enough to allow scratch closure and bond exchange. This mobility was made possible due to both supramolecular H-bonding between the urethane and urea units and the incorporation of dynamic aromatic disulfide moieties with an enhanced mobility. Moreover, considering environmental concerns and governmental regulations, the polymer was additionally synthesized in an aqueous dispersed system, where the coating is the result of coalescence of individual particles after water evaporation.

In comparison with other self-healing waterborne PU(U)s, based on dynamic sulphonate groups (8 MPa, strain rate not disclosed),[1] light-responsive coumarin derivatives (2 MPa at cross-head speed of 20 $mm.min^{-1}$),[2] or other aliphatic (18 MPa at 200 $mm.min^{-1}$),[3,4] and aromatic disulfide moieties (4.5 MPa at strain rate of 20 $mm.min^{-1}$),[5] it is clear that for the waterborne PU(U)s of Chapter III attractive ultimate tensile strengths reaching up to 10-23 MPa (cross-head velocity of 25 $mm.min^{-1}$) could be obtained that would be of interest for coating applications. However, it is still possible to further optimize the self-healing ability of these

linear PU(U) materials while achieving higher mechanical strength by introducing more flexible aromatic disulfides which do not hinder the mobility when incorporated to a higher extent, as demonstrated in Chapter III.

A first way to induce a higher strength and a better water resistance of the PU materials based on the diol-terminated disulfide moiety $S_2(Ph(CH_2)_3OH)_2$, synthesized in Chapter III, is by terminating the PU synthesis with the implemention of diamine-terminated chain extenders so that also urea units are incorporated into the polymer backbone. In this way, poly(urethane-urea)s are obtained providing additional H-bonding between the urea motifs which further enhance the self-healing that can occur through supramolecular interactions.

Moreover, as cross-linked polymers typically provide a higher mechanical strength than their linear counterparts and even thermoset polymers containing dynamic bonds can be reprocessed,[6–8] they may be an interesting alternative to consider for the development of healable coatings. Moreover, the impact of the cross-linking density on the ability of a polymer to heal has been the focus of several recent studies.[9–12] For example, García and co-workers recently described the effect of the polymer structure of a self-healing PUU on the viscoelastic and interfacial healing behaviour by performing rheological measurements and fracture mechanical tests and correlating them to healing tests.[13] They produced polymeric networks with different cross-linking densities, while retaining the same amount of reversible bonds through the introduction of an aromatic disulfide compound. Although the polymers containing lower cross-linking densities showed high viscoelastic and healing properties, only low tensile strength could be obtained in that case, showing that finding a good balance between mechanical properties and a high healing ability is not straightforward.

In this chapter, we will mainly focus on the effect of the polymer microstructure/architecture on mechanical properties and self-healing ability of the waterborne poly(urethane-urea) dispersions based on aromatic disulfide moieties with an enhanced flexibility. The structural modifications studied here are the concentration and flexibility of the aromatic disulfide units and the effect of cross-linking. More specifically, the two disulfide compounds incorporated into the PUU backbone are $S_2(Ph(CH_2)_3OH)_2$ (S3), which was already discussed in Chapter III, and the more flexible alternative $S_2(Ph(CH_2)_6OH)_2$ (S6). Linear polymers were obtained using a bifuntional chain extender (hexane-1,6-diamine, HDA) and trifunctional chain extenders (diethylenetriamine, DETA) were used to form polymer networks. The effects and limits of these structural changes on the mechanical properties of the polymers and their healing ability will be determined *via* a combination of DMA measurements, tensile tests, and rheological and scratch closure experiments.

IV.2. Experimental

IV.2.1. Materials

Bis(4-hydroxyphenyl)disulfide ($S_2(PhOH)_2$, Enamine, 95%), 2,2-bis(hydroxymethyl)-propionic acid (DMPA, GEO specialty chemicals, >96%), 3-bromo-1-propanol (Apollo Scientific, 96%), 6-bromo-1-propanol (Apollo Scientific, 96%), dibutylamine 0.1N in xylol (DBA, Bernd Kraft), dibutyltin dilaurate (DBTL, TCI, >95%), ethyl acetate (EtOAc, Brenntag, >98%), diethylene triamine (DETA, Merck KGaA, ≥98%), hexane-1,6-diamine (HDA, Sigma-Aldrich, 98%), hexane (Brenntag, 100%), hydrochloric acid 1N in water (HCl, Bernd Kraft), isophorone diisocyanate (IPDI, Bayer Material Science, >99%), N-methylpyrrolidon (NMP, Honeywell, ≥99.9%), methyl ethyl ketone (MEK, Honeywell, ≥99.5%), polytetrahydrofuran (PolyTHF, BASF, 2000 $g.mol^{-1}$),

potassium carbonate (K_2CO_3, Sigma-Aldrich, ≥99%), sodium chloride (NaCl, Sigma-Aldrich, ≥99.5%), sodium sulfate (Na_2SO_4, Honeywell, ≥99%), tetrahydrofuran (THF, Scharlab), triethylamine (TEA, Sigma-Aldrich, ≥99%) were used as received.

IV.2.2. Synthesis of modified aromatic disulfide compounds

The synthesis of bis[4-(3'-hydroxypropyloxy)phenyl]disulfide ($S_2(Ph(CH_2)_3OH)_2$ or S3, Figure IV.1) was implemented as already described in Chapter III (Section III.2.2). Additionally, a newly modified aromatic disulfide compound with longer alkyl chain, bis[4-(6'-hydroxyhexoxy)phenyl]disulfide ($S_2(Ph(CH_2)_6OH)_2$ or S6) (Figure IV.1), was synthesized based on the same synthesis procedure. A mixture of bis(4-hydroxyphenyl)disulfide (53.5 g, 0.21 mol), 6-bromo-1-hexanol (68.6 mL, 0.52 mol), potassium carbonate (290.0 g, 2.10 mol) in THF (120 wt% of solid reagents) as solvent was stirred at 60°C for 120h under N_2-atmosphere in a jacketed glass reactor equipped with a mechanical stirrer and a condenser. Afterwards, the reaction mixture was filtrated and washed with EtOAc. The obtained organic filtrate was washed with 1N HCl and brine, after which it was dried over anhydrous $NaSO_4$. The solvent was removed from the product under vacuum and the residue material was purified by recrystallization in an EtOAc:Hexane-mixture (3:5). Finally, the product was dried at 50°C under vacuum to give bis[4-(6'-hydroxyhexoxy)phenyl]disulfide $S_2(Ph(CH_2)_6OH)_2$ (S6) [IUPAC: 6,6'-((disulfanediylbis(4,1-phenylene))bis(oxy))bis-(hexan-1-ol)].

Yield: 30.3g (32 mol%). Pale yellow powder. FTIR (neat, cm^{-1}): 3424.97, 3372.48, 2937.83, 2925.88, 2864.63, 1735.82, 1589.27. m.p. 59.4 – 60.6 ºC. ^{1}H NMR (500 MHz, Chloroform-*d*): δ 7.33 – 7.26 (d, *J* = 8.7 Hz, 2H), 6.76 – 6.71 (d, *J* = 8.8 Hz, 2H), 3.86 (t, *J* = 6.5 Hz, 2H), 3.58 (t,

J = 6.6 Hz, 2H), 1.76 – 1.66 (m, 2H), 1.57 – 1.48 (m, 2H), 1.47 – 1.30 (m, 4H + 1H (OH)). ^{13}C NMR (126 MHz, Chloroform-*d*): δ 159.67, 132.95, 132.71, 128.45, 115.35, 77.50, 77.25, 76.99, 68.20, 63.11, 32.89, 29.38, 26.09, 25.75. (The ^{1}H, ^{13}C, g-COSY, g-HSQC NMR spectra of S6 are depicted in Figures A II.1-4 in Appendix II) Anal. Calcd. for $C_{24}H_{34}O_4S_2$: C 63.97, H 7.60, S 14.23. Found: C 63.72, H 7.54, S 14.05. HRMS (ESI) for $C_{24}H_{34}O_4S_2$ calculated $[M + H]^+$: 450.1899. Found: 450.1896.

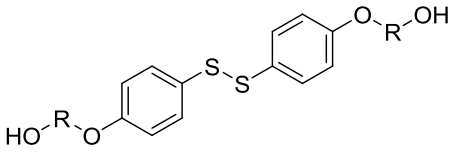

S3 = $S_2(Ph(CH_2)_3OH)_2$: R= -$(CH_2)_3$-
S6 = $S_2(Ph(CH_2)_6OH)_2$: R= -$(CH_2)_6$-

Figure IV.1. Chemical structure of bis[4-(3'-hydroxypropyloxy)phenyl]disulfide (S3) and bis[4-(6'-hydroxyhexoxy)phenyl]disulfide (S6).

IV.2.3. Synthesis of waterborne polyurethane-urea dispersions

The synthesis of the PUU dispersions was carried out as summarized in Figure IV.2 using the formulation in Table IV.1. In order to obtain the disulfide-containing prepolymer, PolyTHF (M_w=2000 g.mol^{-1}), DMPA, IPDI and $S_2(Ph(CH_2)_3OH)_2$ (S3) or $S_2(Ph(CH_2)_6OH)_2$ (S6) were fed together into a 100 mL jacketed glass reactor equipped with a mechanical stirrer and a condenser. Next, DBTL (0.7-0.9 wt% of reactants) as catalyst and MEK (55-65 wt%) as solvent were added and the mixture was stirred for 105-140 min (depending on the formulation as shown in Table IV.1) at 80ºC under refluxing conditions. The amount of DMPA added in the synthesis was constant (3 wt% of reactants), while the amount of S3 or S6 varied as shown in

Table IV.1. After the prepolymer synthesis, the isocyanate concentration reduced to the theoretical level as determined by back titration and the mixture was cooled down to room temperature and neutralized with TEA (1 mol eq. of DMPA). Then, deionized water (100 wt%) was added dropwise to obtain a dispersion. Finally, the chain extender was added to react with the residual NCO groups of the dispersed prepolymer for 30min. MEK was removed from the filtered dispersion by evaporation using a rotary evaporator at 243 mbar so that approximately 45 mL of a waterborne PUU dispersion was obtained with a solids content of 30 wt%.

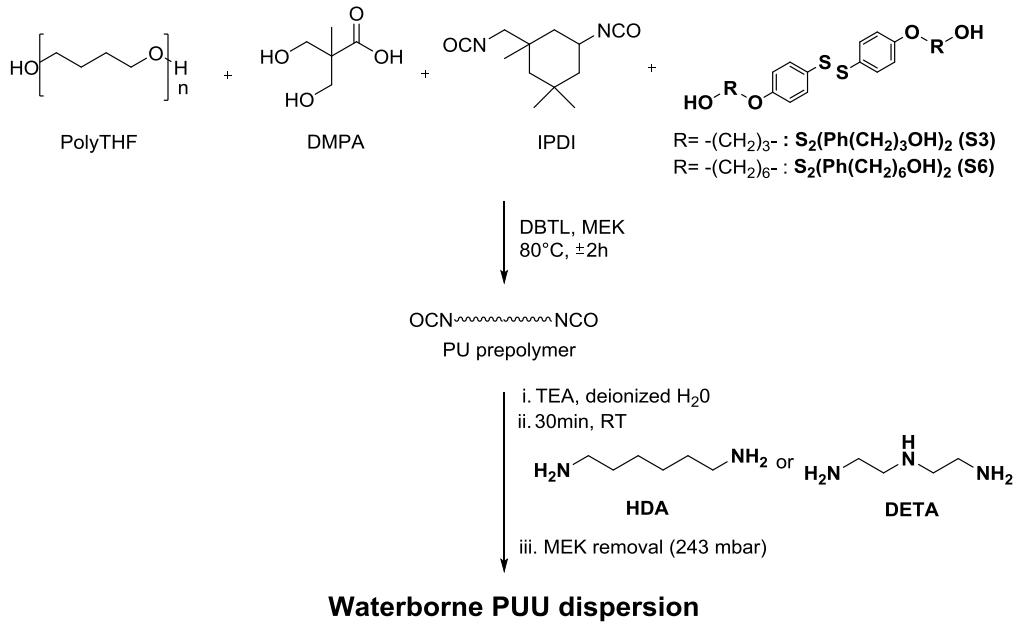

Figure IV.2. Scheme of synthesis procedure of waterborne PUU dispersion.

The dispersions were named according to their varying amount and type of chain extender, L (linear obtained with HDA) and X (cross-linked obtained with DETA) followed by an indication

of the amount and type of disulfide $S_2(Ph(CH_2)_3OH)_2$ (S3) or $S_2(Ph(CH_2)_6OH)_2$ (S6). For example, a sample called 1.8X-0.56S3 contains 1.8 wt% of DETA combined with 0.56 mol eq. of IPDI of the aromatic disulfide $S_2(Ph(CH_2)_3OH)_2$ (S3), while 1.8X-0.56S6 has the same formulation where the alternative aromatic disulfide $S_2(Ph(CH_2)_6OH)_2$ (S6) with longer alkyl chain is introduced instead.

Table IV.1. Formulation (based on mol equivalents) of the different PUU syntheses.

Sample		DMPA	IPDI	PolyTHF	S3	S6	HDA	DETA	t (min)
L-S3	**2.5L-0.44S3**	0.18	1	0.20	0.44	/	0.18	/	120
	2.5L-0.54S3	0.16	1	0.13	0.54	/	0.17	/	105
	2.5L-0.59S3	0.15	1	0.10	0.59	/	0.16	/	110
	1.8L-0.56S3	0.17	1	0.15	0.56	/	0.13	/	130
L-S6	**1.8L-0.56S6**	0.17	1	0.15	/	0.56	0.13	/	140
X-S3	**2.5X-0.44S3**	0.18	1	0.20	0.44	/	/	0.18	120
	2.5X-0.54S3	0.16	1	0.13	0.54	/	/	0.17	105
	2.5X-0.59S3	0.15	1	0.10	0.59	/	/	0.16	110
	1.8X-0.56S3	0.17	1	0.15	0.56	/	/	0.13	130
X-S6	**1.8X-0.56S6**	0.17	1	0.15	/	0.56	/	0.13	140

Two series of dispersions were synthesized. In a first series, linear polymers were prepared. Using $S_2(Ph(CH_2)_3OH)_2$ (S3) as the self-healing moiety, three linear (L-S3) PUUs were synthesized varying the amount of S3 from 0.44 mol eq. of IPDI for 2.5L-0.44S3 and 0.54 mol eq. for 2.5L-0.54S3 to 0.59 mol eq. for 2.5L-0.59S3, but keeping the amount of HDA (2.5 wt%) constant (Table IV.1). In order to obtain a softer material and understand the influence of the urea groups, an additional linear PUU (1.8L-0.56S3) was obtained by lowering the amount of HDA to 1.8 wt% of reactants, while keeping the amount of IPDI and DMPA constant. Another polymer dispersion (1.8L-0.56S6) was obtained by using the more flexible self-healing moiety

$S_2(Ph(CH_2)_6OH)_2$ (S6) for the same formulation of the S3-based alternative (1.8L-0.56S3). The second series of polymer dispersions is formed by the cross-linked versions of the first series that were obtained by changing the chain extender from HDA to DETA. A schematic overview of the different series is depicted in Figure IV.3.

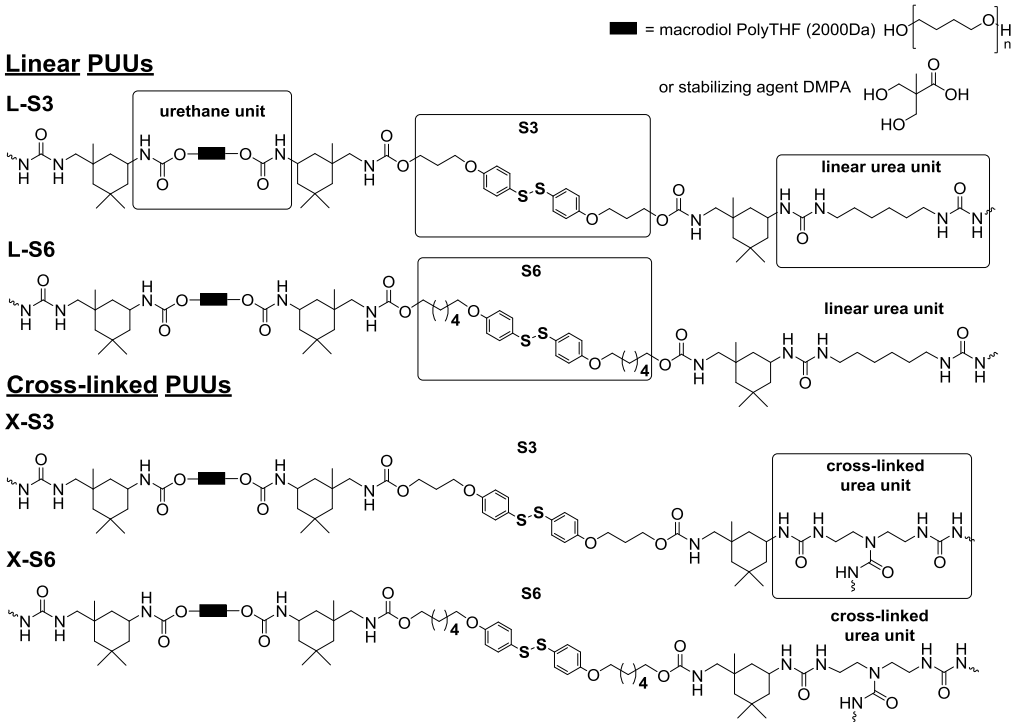

Figure IV.3. Schematic of linear PUUs (L-S3 and L-S6) and cross-linked PUUs (X-S3 and X-S6).

IV.2.4. Characterization

IV.2.4.1. Monomer characterization

Infrared spectra were recorded in a FTIR spectrometer (Bruker). All melting points were measured in a Büchi Melting Point B-540. The NMR spectra were recorded at 500 MHz for ^{1}H-NMR, and 126 MHz for ^{13}C{H}-NMR in $CDCl_3$ at room temperature. The data are reported as s = singlet, d = doublet, t = triplet, m = multiplet, coupling constant(s) in Hz, integration. Elemental analysis was carried out using a TruSpec Micro (LECO) analyzer. HRMS-analysis was performed with a LC/Q-TOF with Agilent Jet Stream ESI ionization source.

IV.2.4.2. Monomer, prepolymer and dispersion characterization

The NCO content of the PU prepolymer was determined by means of a back titration with HCl of the excess of dibutylamine (DBA) molecules, which were added to neutralize the free NCO-groups of the PU.[14–16] The particle sizes and distributions were measured by hydrodynamic chromatography (HDC) with a Matec CHDF3000 instrument equipped with UV detector operating at 254 nm and a PL-PSDA Type 2 (Agilent) column using a carrier flux of 1 $mL.min^{-1}$. For these measurements, samples were diluted to 1% solids content, passed through a 1.2 µm nylon filter and injected with an autosampler (25 µL). The eluent was an aqueous solution of sodium dihydrogenphosphate (0.24 $g.L^{-1}$), sodium dodecyl sulfate (0.5 $g.L^{-1}$), Brij35 (poly alkylenglycolether, 2 $g.L^{-1}$) and sodium azide (0.2 $g.L^{-1}$) was used. Periodic calibration of the system was performed using narrowly dispersed polystyrene standards.

IV.2.4.3. Polymer characterization

Films with a thickness of 0.50-0.75 mm were obtained by casting the dispersion in silicon molds (25x55 mm^2). The films were first dried for 1 day at 25°C and subsequently for 2 days at 60°C after which they were equilibrated for 3 days at 25°C.

The molecular weights of the dried films which could completely dissolve in THF after 1h were determined by injecting them into a Size Exclusion Chromatography/Gel Permeation Chromatography (SEC/GPC) instrument after filtering them. The instrument consisted of a pump (LC-20A, Shimadzu), an autosampler (Waters 717), a differential refractometer (Waters 2410), a UV detector measuring at 262nm (Waters 2487) and three columns in series (Styragel HR2, HR4 and HR6, with pore sizes ranging from 102-106 Å). Chromatograms were obtained at 35 °C using a THF flow rate of 1 $mL.min^{-1}$. A series of polystyrene (PS) standards in the range of 580–3 848 000 $g.mol^{-1}$ were used to obtain the calibration curve which provided molecular weights of the polymer relative to PS. It is perhaps worth emphasizing here that longer dissolution times than 1h in THF should be avoided for the GPC measurements of the PUU materials, since immersion into solvents like THF or MEK led to the cleavage of the polymer chain resulting in lower molecular weights of the PUUs, as was demonstrated for 0.18L-0.56S3 depicted in Figure A II.5 (Appendix II).

For the water resistance tests, samples of 5 x 5 x 0.5mm^3 were weighted (M_0) and immersed in 10 ml of deionized water at room temperature. At specific times t, the films were weighed (M_t) after smoothly blotting with a filter paper and put back again in the deionized water. Finally, the

water uptake was calculated in relation to the initial dry weight of the sample based on the following equation IV.1:

$$\text{Water uptake (\%)} = \frac{(M_t - M_0)}{M_0} .100 \qquad \text{(IV.1)}$$

Thermogravimetric analysis (TGA) was performed in a temperature range of 40-800 ºC at 10ºC/min under a nitrogen atmosphere with a TA Instruments Q500. Dynamic mechanical analysis (DMA) was carried out in a TA Instruments DMA Q800 equipped with a liquid nitrogen cooling system. The measurements were performed in tensile geometry at a fixed frequency of 1 Hz, an initial static force of 0.35 N and a constant strain of 0.03% with the static force 20% larger than the dynamic one. The samples (typical size = 10 x 10 x 0.5 mm^3) were cooled down to -150/-100ºC and heated with a rate of 4ºC.min^{-1} till the temperature at which the minimum dynamic force of 0.01 N was hit.

Stress-strain measurements were carried out on dumbbell type specimen at 23ºC and 50%RH, meeting the requirements of ISO 291-23/50-class 1, on a universal testing machine Z050/zmart.pro with testcontrol by Zwick GmbH at a 25 mm.min^{-1} strain rate. The averages of 3-5 replicate measurements are reported. For the scratch closure experiments, scratches were made with a depth of roughly 75% of the thickness ($\pm$0.7 mm) of the films using a razor blade with a thickness of 0.40 mm and subsequently closure at 80ºC was followed using an optical microscope (Nikon Eclipse LV100ND). The rheological data were obtained from a stress-controlled Anton Paar Physica MCR101 rheometer using parallel plate geometry (plate ∅ = 8mm, disk-shaped specimens with ∅ = 10 mm and a thickness of 0.50-0.75 mm). Frequency sweeps (0.001-20 Hz) at 0.5% strain were conducted at fixed temperatures from 70-130ºC.

IV.3. Results and discussion

IV.3.1. Dispersion and polymer characteristics

All synthesized PUU dispersions were stable and coagulum free. The particle size distributions (Figures A II.6-7, Appendix II), determined by HDC, show a broad variation with average particle sizes in the range of 50 to 300 nm, since the chain extension step that was performed after dispersion of the PUU in water is more difficult to control on this small scale. However, homogeneous and transparent films were obtained in all cases (Figure IV.4). By increasing the disulfide content, the molecular weights of the linear S3-based (L-S3) PUUs decreased (Table IV.2). This was due to the fact that an increase of disulfide inevitably implies a decrease of the macrodiol PolyTHF (Table IV.1, experimental section) and therefore lower molecular weights were obtained at a similar degree of polymerization. On the other hand, the molecular weight increased when S6 was used instead S3, which might be due to the higher flexibility of S6 that could lead to better availability of the alcohol functionalities when long chain lengths were obtained during polymerization leading to higher conversion levels that yield higher molecular weights.

Furthermore, less than 20% of water uptake could be measured for all PUUs after 1 month of immersion in water (Figure A II.8, Appendix II), which is a significant improvement compared to the PUs of Chapter III which already partially disintegrate after 5 d in water. This might be due to a low degree of H-bonding in the PUs, as the water uptake tests demonstrate that a higher level of chain extender or changing from linear PUUs to networks leads to less water uptake, since more physical and/or chemical cross-linked materials are generally more water resistant.

Figure IV.4. Films from the dispersions which show the broadest PSD in Figures A II.6-7.

Table IV.2. Polymer characteristics of PUUs based on $S_2(Ph(CH_2)_{3/6}OH)_2$ (S3/S6).

Sample		GPC (IR)			TGA	DMA
		M_n (kDa)	M_w (kDa)	Đ	T_d (°C) (5 wt% loss)	T_g (°C) (=T_{max} Tan δ)
L-S3	2.5L-0.44S3	34	65	1.9	265	43
	2.5L-0.54S3	23	44	1.9	258	67
	2.5L-0.59S3	20	39	1.9	262	75
	1.8L-0.56S3	22	45	2.1	267	59
L-S6	1.8L-0.56S6	35	71	2.0	263	27
X-S3	2.5X-0.44S3	Insoluble in THF			259	53
	2.5X-0.54S3				256	73
	2.5X-0.59S3				254	77
	1.8X-0.56S3				263	64
X-S6	1.8X-0.56S6				259	33

IV.3.2. Thermal and mechanical properties of the PUUs

Regarding the thermal properties of the PUUs, it can be concluded that all materials show a high T_d > 250°C, while the cross-linked materials show lower thermal stability in comparison with the linear counterparts (Table IV.2). The DMA results of the PUUs are depicted in Figures IV.5-6. First of all, a secondary relaxation linked to the presence of closely interconnected aromatic rings can be observed around -140°C, similarly to the PU(U)s described in Chapter III.[17,18] Additionally, also here, two different glass transition regions can be observed for all

PUUs based on S3 (Figure IV.5 B and D). While the low T glass transition temperature (T_g) is situated again around -70ºC, a second broader transition could be observed at higher temperatures. This high temperature glass transition, which can be followed easily by looking at the peak of the tan δ as this is also considered as a measure for the T_g, differed significantly between samples as depicted in Figure IV.5 and in Table IV.2.

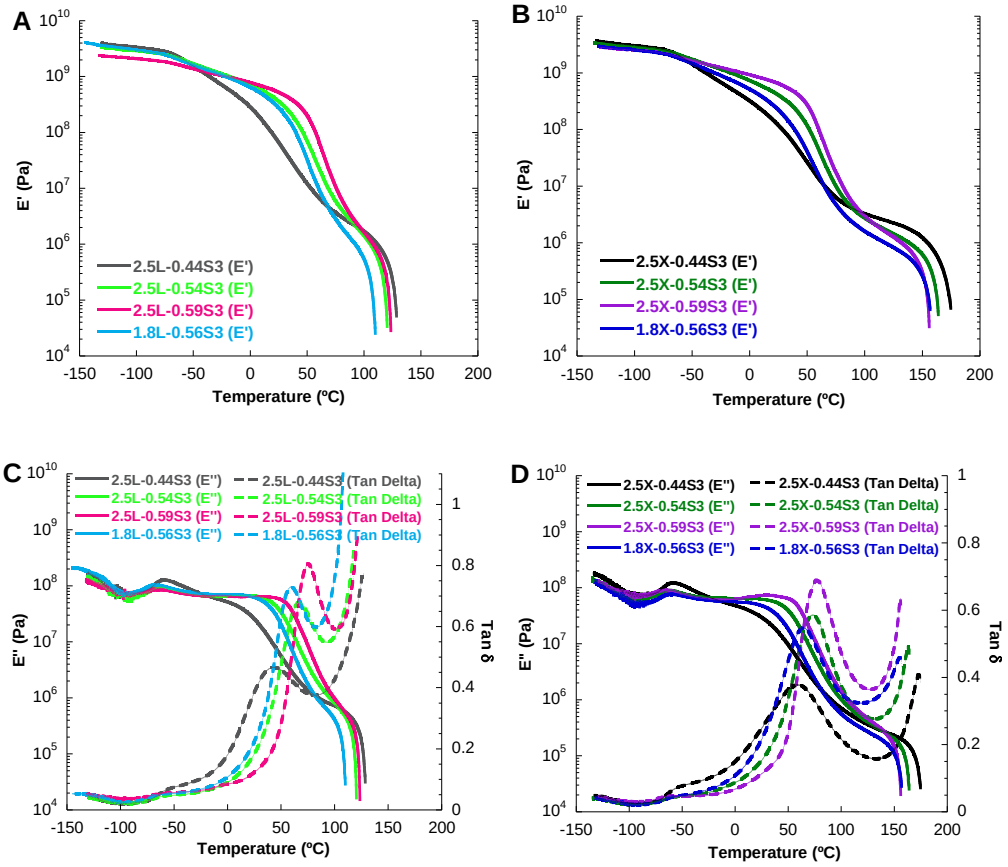

Figure IV.5. Storage modulus (E'), loss modulus (E'') and Tan δ vs. T, of linear (A; C) and cross-linked (B; D) PUUs based on S3.

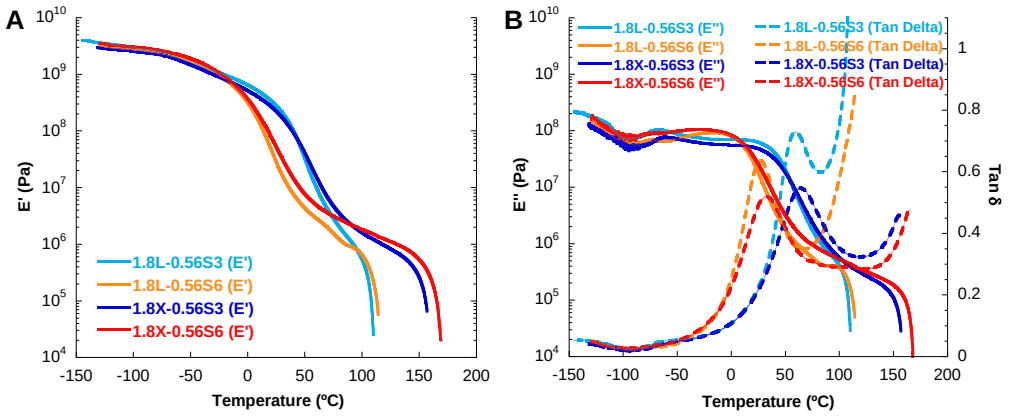

Figure IV.6. Storage modulus (E') (A), loss modulus (E'') and Tan δ (B) vs. T of 1.8L/X-0.56S3 in comparison with 1.8L/X-0.56S6.

In the samples containing the same amount of chain extender, the high temperature T_g increased with the content of S3 in the polymer, in accordance to what could be observed in Chapter III, because more aromatic moieties were incorporated into the backbone. In addition, the T_g increased with the content of chain extender because of the augmentation of the urea groups that led to a higher degree of H-bonding. Figure IV.5 also shows that cross-linking led to an increase of the high temperature T_g and to a rubbery plateau, which is a fingerprint of the polymer network, at higher temperatures. Moreover, Figure IV.6 depicts that the storage modulus at room temperature and the high temperature T_g strongly decreased when the more flexible disulfide moiety S6 was incorporated instead of S3.

Alternatively, the polymer structure also influenced the tensile test results as can be seen in Table IV.3 and Figure IV.7. By increasing the amount of the self-healing moiety (S3) or chain extender or by introducing cross-linking points into the PUU material, the rigidity and strength of the material increased, as can be seen at the increasing value of the Young's modulus, yield

strength (σ_y) and tensile strength at fracture (σ_f). However, at the same time they decreased the elongation at fracture (ε_f), which is most obvious for the most rigid PUU 2.5X-0.59S3 (Figure IV.7 A). On the other hand, by introducing the more flexible self-healing moiety (S6) into the polymer backbone, the strength and rigidity of the PUUs decreased (Figure IV.7 B). Additionally, Figure IV.7 shows that several of the PUUs synthesized in this chapter showed tensile strengths at fracture in the range of 16-18.5 MPa, which are improved values compared to the ones that were obtained in Chapter III. There, values up to 17 MPa could be reached for the PUUs based on the diamine-terminated disulfide compound, but these materials only gave limited mobility, while the PUs based on $S_2(Ph(CH_2)_3OH)_2$ (S3), without the use of a diamine-terminated chain extender which was introduced in an additional synthesis step in this chapter, could only achieve ultimate tensile strengths of 10 MPa.

Table IV.3. Tensile testing results of PUUs based on $S_2(Ph(CH_2)_3OH)_2$ (S3) or $S_2(Ph(CH_2)_6OH)_2$ (S6).

Sample		Young's modulus (MPa)	σ_y (MPa)	σ_f (MPa)	ε_f (%)
L-S3	**2.5L-0.44S3**	31.2 ± 1.9	/	12.5 ± 0.7	460 ± 10
	2.5L-0.54S3	321.2 ± 1.1	10.3 ± 0.3	15.2 ± 0.5	240± 20
	2.5L-0.59S3	707.8 ± 11.6	21.2 ± 0.5	17.7 ± 0.4	135 ± 10
	1.8L-0.56S3	207.2 ± 6.8	7.2 ± 0.2	11.6 ± 0.3	295 ± 10
L-S6	**1.8L-0.56S6**	15.1 ± 1.1	/	8.3 ± 0.3	410 ± 5
X-S3	**2.5X-0.44S3**	41.0 ± 2.7	/	18.5 ± 0.5	450 ±5
	2.5X-0.54S3	340.3 ± 6.4	11.7 ± 0.6	18.0 ± 1.0	235 ± 10
	2.5X-0.59S3	751.9 ± 12.9	23.7 ± 0.4	13.6 ± 3.0	30 ± 10
	1.8X-0.56S3	278.5 ± 7.2	9.3 ± 0.1	16.3 ± 0.3	315± 35
X-S6	**1.8X-0.56S6**	27.9 ± 1.9	/	9.5 ± 0.2	340 ± 10

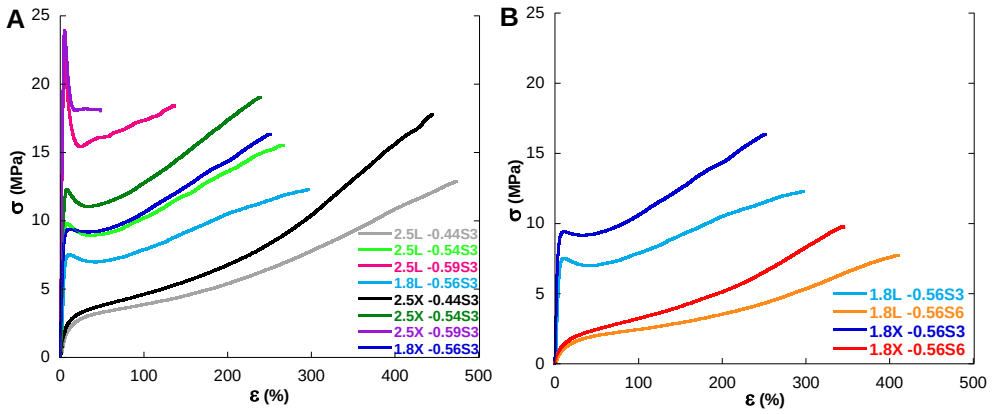

Figure IV.7. Stress-strain curves measured of PUUs based on S3 (A) and PUUs based on S6 (B) obtained at 23ºC using a cross-head velocity of 25 mm.min^{-1}.

IV.3.3. Rheological behaviour of the PUUs

The results discussed above show that the combination of aromatic disulfides of different flexibility (S3 *versus* S6) and chain extenders with different functionalities (HDA *versus* DETA) allows the synthesis of PUUs with a wide range of mechanical properties. However, the self-healing ability of these materials should also be characterized which can be carried out by studying the molecular mobility of the PUUs by performing frequency sweep measurements in a similar fashion as described in Chapter III.

Also for the PUU materials presented here, the van-Gurp-Palmen-plots were constructed in order to check the applicability of the TTS principle to construct the master curves of G' and G'' (Figures A II.9-10 in Appendix II). These plots showed that, similar to what was described for the PUs in Chapter III, the depicted isothermal frequency curves did not completely merge to a single line indicating that the materials underwent some change with temperature, likely due to

the activation of the dynamic disulfide bonds at higher temperatures. This also explains the growing divergence between the isothermal frequency curves as the amount of disulfide compound S3 increased (Figure A II.9, Appendix II). However, by using horizontal (a_T) and vertical shift factors (b_T), an acceptable superposition could be achieved for the linear PUUs and the cross-linked 1.8X-0.56S3 and 1.8X-0.56S6. For these polymers, the master curves were constructed using 80 ºC as reference temperature. This temperature was chosen because it is high enough so the T_g of all PUUs is surpassed and the materials are able to molecularly interdiffuse (Figure IV.5-6), but simultaneously it is low enough to avoid any possible degradation (*e.g.* by cleavage of urethane linkages ≥ 150ºC).[35] For the other cross-linked PUUs, superposition was not good enough to obtain acceptable master curves at 80ºC.

The master curves at 80 ºC for the linear polymers and the cross-linked 1.8X-0.56S3 and 1.8X-0.56S6 are presented in Figure IV.8. The values of the crossover frequency ω_d, at which G' and G'' intersect and which is indicated with an arrow (Figure IV.8), as well as those of the relaxation time τ_d are reported in Table IV.4. From the values obtained from the master curves of the L-S3 (Figure 8 A), it is clear that the mobility of the material decreased by either a too low amount of the self-healing moiety (S3) (*e.g.* soft 2.5L-0.44S3), as only a limited amount of disulfide bonds are present, or a too high disulfide content (S3) (e.g. rigid 2.5L-0.59S3), since dynamic exchange is restricted by the stiffness of the PUU backbone. This is a different trend than the one that was described in Chapter III which only demonstrated a decrease in mobility of the PUs by an increasing amount of disulfide units. This can be explained by the fact that the PUUs described here additionally contain urea units which induce a higher degree of H-bonding and physical cross-linking. Therefore, sufficient disulfide bonds are required for

dynamic exchange to be able to enhance the mobility in the PUU backbone. Once enough disulfide bonds have been incorporated, a similar trend as for the PUs of Chapter III can be demonstrated. Additionally, the mobility also decreased with the content of the chain extender (HDA) as again more H-bonds led to a more rigid and less mobile structure.

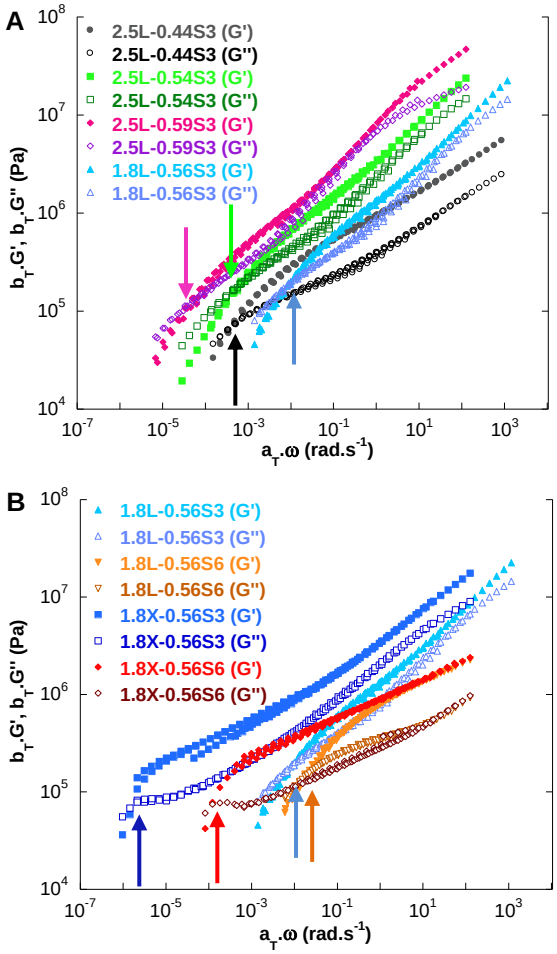

Figure IV.8. Master curves (T_{ref}=80°C) of the L-S3 series (A) and 1.8L/X-0.56S3 *vs.* 1.8L/X-0.56S6 (B).

Table IV.4. Characteristic values for G'-G'' crossover in the master curves (T_{ref}=80ºC) of the PUUs.

Sample		ω_d (rad.s^{-1})	τ_d
L-S3	**2.5L-0.44S3**	$4*10^{-4}$	4.5 h
	2.5L-0.54S3	$6*10^{-4}$	3 h
	2.5L-0.59S3	$5*10^{-5}$	1.5 d
	1.8L-0.56S3	0.008	13 min
L-S6	**1.8L-0.56S6**	0.016	6.5 min
X-S3	**1.8X-0.56S3**	$2*10^{-6}$	36 d
X-S6	**1.8X-0.56S6**	$1*10^{-4}$	17.5 h

Furthermore, it is remarkable that some of the cross-linked PUUs showed a G'-G'' crossover point at 80 ºC. Generally, for cross-linked polymers, no G'-G'' crossover point is expected as the network prevents the material from flowing. However, when activated by temperature, the dynamic disulfide bonds present in the PUU backbone break the polymer chains between cross-linking points allowing the rearrangement of the network structure and therefore inducing some flow. This was the reason for the presence of G'-G" crossover in the PUUs cross-linked with the lowest DETA concentration (1.8 %, samples 1.8X-0.56S3 and 1.8X-0.56S6). However, when the DETA concentration was increased to 2.5% (samples 2.5X-0.44S3, 2.5X-0.54S3 and 2.5X-0.59S3), the network was so densely cross-linked that the exchange of some disulfide bonds did not allow sufficient flow of the material at 80ºC. In any case, Table IV.4 shows that, even for 1.8X-0.56S3 and 1.8X-0.56S6, the network reduced the mobility of the polymer.

A way to overcome these restrictions in the mobility of the PUUs, is by using the more flexible disulfide (S6) as shown in Figure IV.8 B and Table IV.4. It is particularly remarkable that in the case of the cross-linked PUUs the relaxation time was reduced by a factor of 50, whereas in the linear polymers τ_d decreased only by a factor of 2, when comparing the S6-based materials

to their S3-based counterparts. This clearly indicates that dynamic covalent bonds placed in flexible moieties facilitate the rearrangement of polymer networks making the healing of cross-linked polymers possible under moderate conditions. From these results, it can therefore be concluded that although mechanical properties can influence the mobility of the system, ultimately the polymer architecture with the possibility of incorporating intramolecular interactions, dynamic bonds, cross-linking points and/or more or less flexible monomers has a decisive role on determining the final mobility and thus healing ability of the material.

IV.3.4. Scratch closure

All the polymers in Table IV.4 showed mobility and flow at 80 ºC although the relaxation time τ_d varied from a few minutes to days. In order to test if the mobility of these PUUs also leads to self-healing, scratch closure tests were performed as a simple method to macroscopically assess the healing ability of materials. In Figures IV.9 and 10, the evolution of the scratches is depicted which showed that complete closure of the scratches could be achieved, although in most cases the time required ($t_{scratch}$) was considerably longer than the relaxation time τ_d. This could be expected as scratch closure requires creep deformation, as explained in Chapter III, which is a complex viscoelastic process with a spectrum of retardation times.[28] Interestingly, there is a linear relationship between $t_{scratch}$ and τ_d (Figure IV.11). Nevertheless, it is noteworthy to mention that, contrary to the other examples, $t_{scratch}$ seemed shorter than the relaxation time τ_d for 1.8X-0.56S3. This might be explained by the fact that the higher cross-linking degree induces a delayed elastic recovery at higher temperatures leading to a strong scratch closing behaviour after already 1 d, which supposedly promotes scratch closure in shorter times.[36–38]

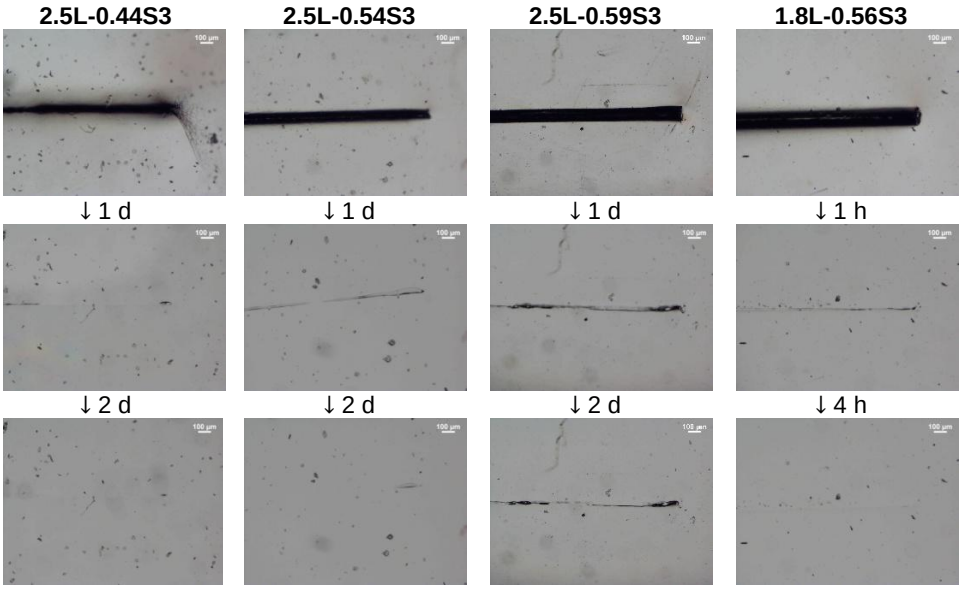

Figure IV.9. Scratch closure at 80°C of linear PUUs based on $S_2(Ph(CH_2)_3OH)_2$ (S3).

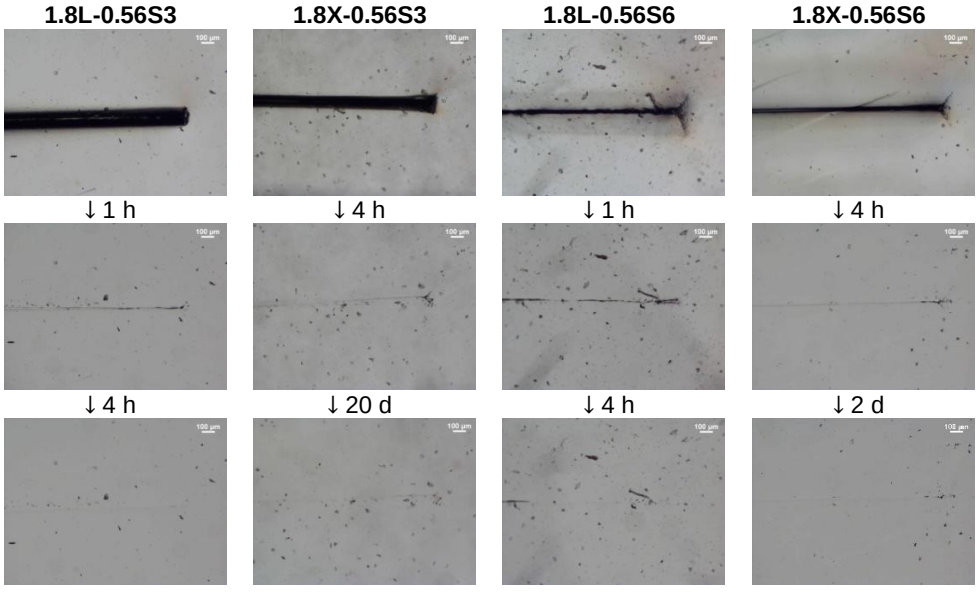

Figure IV.10. Scratch closure at 80°C of PUUs based on S6 *vs.* S3.

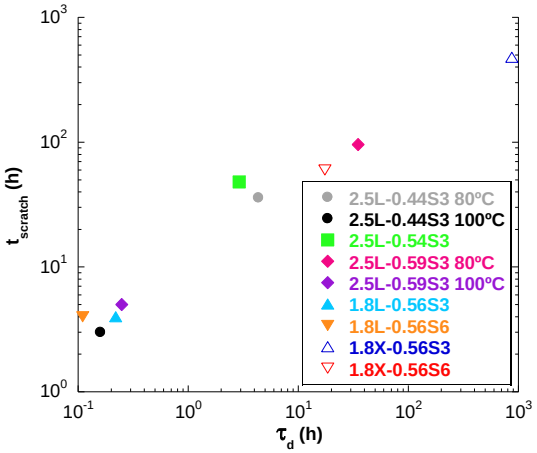

Figure IV.11. Relationship between the time needed for scratch closure ($t_{scratch}$) and the relaxation time (τ_d) at 80ºC for the linear PUUs and the cross-linked 1.8X-0.56S3 and 1.8X-0.56S6.

As the long scratch closure times needed at 80 ºC may be an issue when considering the application of these materials, the effect of the healing temperature on the relaxation time was explored by using the TTS principle (Figure IV.12). Using the soft 2.5L-0.44S3 and relatively hard 2.5L-0.59S3 as examples, increasing the healing temperature to 100 ºC decreased their relaxation times to 560 s (0.16h) and 900 s (0.25h), respectively. Using Figure IV.11 as a reference, $t_{scratch}$ is expected to decrease from days to about a few hours, which could also be confirmed experimentally showing a $t_{scratch}$ of 3h and 5h for the soft and hard example, respectively (Figure A II.11, Appendix II). This result shows that the linear relationship between $t_{scratch}$ and τ_d (Figure IV.11) can be considered as a master curve, as also 2.5L-0.44S3 and 2.5L-0.59S3 demonstrated this trend even at a temperature of 100ºC. Next to playing with the flexibility of the polymer microstructure, further increasing the healing temperature might therefore be another way to overcome the mobility restrictions in order to develop stronger polymer networks with more efficient self-healing abilities.

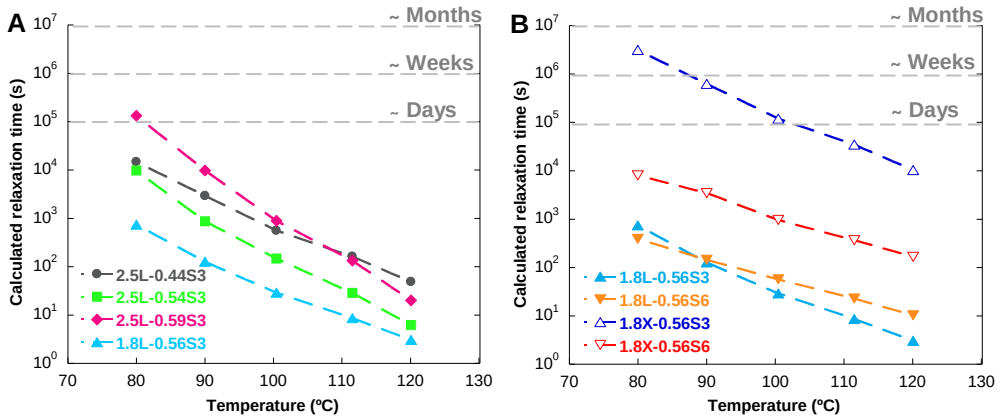

Figure IV.12. Calculated relaxation times in function of T for the linear PUUs based on S3 (A) and for 1.8L/X-0.56S3 versus 1.8L/X-0.56S6 (B).

IV.4. Conclusions

For this new series of waterborne PUU dispersions based on the more flexible aromatic disulfide moieties and chain extended with amine-terminated compounds, the effect of the polymer microstructure on the mechanical properties, rheological behaviour and scratch closing ability of the material could be systematically studied. Although incorporation of a sufficiently high amount of the self-healing moiety was necessary to introduce enough mobility into the PUU backbone, higher amounts of aromatic disulfide increased the rigidity to a level that it limited the disulfide exchange. Nevertheless, reducing the amount of chain extender and thus the formation of urea moieties and their associated H-bonds, allowed the incorporation of sufficient disulfide compound, so that materials with significant strength as well as mobility could be obtained since the disulfide exchange is less hindered by physical interactions.

Additionally, by changing the chain extender from a difunctional amine (HDA) into a trifunctional amine (DETA), cross-linking points could be introduced into the PUU material which strongly decreased the mobility of the polymer. Interestingly, since dynamic disulfide bonds are present in the network, a crossover point could still be observed in the master curves (T_{ref}=80ºC) obtained by TTS, showing a relaxation time significantly above the levels of those of the linear PUUs.

However, replacing the disulfide $S_2(Ph(CH_2)_3OH)_2$ (S3) by its more flexible alternative $S_2(Ph(CH_2)_6OH)_2$ (S6) increased the mobility of the material to an even higher extent, so that possibly by incorporating more self-healing moiety even stronger and simultaneously more mobile materials could be developed.

This proved the fact that varying and optimizing the various building blocks involved in the polymer synthesis can give rise to a polymer architecture which is necessary to obtain self-healing materials which present high mechanical properties with tensile strengths up to roughly 20 MPa, while showing sufficient mobility at moderate temperatures. In Figure IV.13, the results obtained in this chapter can now be compared with the previously discussed results of Chapter I, showing the limited mechanical strength of academic self-healing PU(U)s based on disulfide bonds compared to industrial PU(U) dispersions for coatings. From this plot, it becomes clear that with these materials we tend to overcome the gap that currently exists between academic research and industry. Finally, in Chapter V, the focus will be on the quantitative determination of the recovery upon damage of these strong polymers in comparison with the counterpart materials lacking dynamic covalent bonds in their PUU backbone.

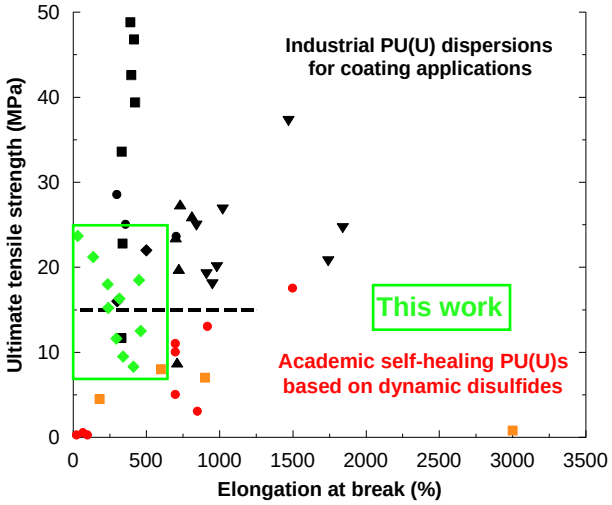

Figure IV.13. Indication of the results obtained for this chapter in green added to the already discussed Figure I.13 of Chapter I.

IV.5. References

1. Xiao, Y., Huang, H. & Peng, X. Synthesis of self-healing waterborne polyurethanes containing sulphonate groups. *RSC Adv.* **7,** 20093–20100 (2017).
2. Aguirresarobe, R. H., Martin, L., Aramburu, N., Irusta, L. & Fernandez-Berridi, M. J. Coumarin based light responsive healable waterborne polyurethanes. *Prog. Org. Coatings* **99,** 314–321 (2016).
3. Wan, T. & Chen, D. Synthesis and properties of self-healing waterborne polyurethanes containing disulfide bonds in the main chain. *J. Mater. Sci.* **52,** 197–207 (2017).
4. Wan, T. & Chen, D. Mechanical enhancement of self-healing waterborne polyurethane by graphene oxide. *Prog. Org. Coatings* **121,** 73–79 (2018).
5. Aguirresarobe, R. H., Martin, L., Fernandez-Berridi, M. J. & Irusta, L. Autonomic healable waterborne organic-inorganic polyurethane hybrids based on aromatic disulfide moieties. *EXPRESS Polym. Lett.* **11,** 266–277 (2017).
6. Lafont, U., Van Zeijl, H. & Van Der Zwaag, S. Influence of cross-linkers on the cohesive and adhesive self-healing ability of polysulfide-based thermosets. *ACS Appl. Mater. Interfaces* **4,** 6280–6288 (2012).
7. Ruiz de Luzuriaga, A. *et al.* Epoxy resin with exchangeable disulfide crosslinks to obtain reprocessable, repairable and recyclable fiber-reinforced thermoset composites. *Mater. Horiz.* **3,** 241–247 (2016).
8. Erice, A. *et al.* Reprocessable and recyclable crosslinked poly (urea-urethane) s based on dynamic amine / urea exchange. *Polymer* **145,** 127–136 (2018).
9. Zhang, L. & Rowan, S. J. Effect of Sterics and Degree of Cross-Linking on the Mechanical Properties of Dynamic Poly(alkylurea–urethane) Networks. *Macromolecules* **50,** 5051–5060 (2017).
10. AbdolahZadeh, M., C. Esteves, A. C., van der Zwaag, S. & Garcia, S. J. Healable dual organic–inorganic crosslinked sol–gel based polymers: Crosslinking density and tetrasulfide content effect. *J. Polym. Sci. Part A Polym. Chem.* **52,** 1953–1961 (2014).
11. Abdolah Zadeh, M., Grande, A. M., van der Zwaag, S. & Garcia, S. J. Effect of curing on the mechanical and healing behaviour of a hybrid dual network: a time resolved evaluation. *RSC Adv.* **6,** 91806–91814 (2016).
12. García-Huete, N. *et al.* Effect of the blend ratio on the shape memory and self-healing behaviour of ionomer-polycyclooctene crosslinked polymer blends. *Eur. Polym. J.* **98,** 154–161 (2018).
13. Grande, A. M., Martin, R., Odriozola, I., van der Zwaag, S. & Garcia, S. J. Effect of the polymer structure on the viscoelastic and interfacial healing behaviour of poly(urea-urethane) networks containing aromatic disulphides. *Eur. Polym. J.* **97,** 120–128

(2017).

14. O. S. Henze, R. Steinberger, R. Krech, N. Pohlmann, C. Beckmann, J. D. Isocyanate-Containing Thermoplastic Polyurethane. US20080207846A1. BASF Aktiengesellschaft Patents, Trademarks and Licenses. (2008).

15. Hamzehlou, S. *et al.* Mechanistic investigation of the simultaneous addition and free-radical polymerization in batch miniemulsion droplets: Monte Carlo simulation versus experimental data in polyurethane/acrylic systems. *Polymer* **55,** 4801–4811 (2014).

16. Mehravar, S., Ballard, N., Agirre, A., Tomovska, R. & Asua, J. M. Relating polymer microstructure to adhesive performance in blends of hybrid polyurethane/acrylic latexes. *Eur. Polym. J.* **87,** 300–307 (2017).

17. Jho, J. Y. & Yee, A. F. Secondary relaxation motion in bisphenol A polycarbonate. *Macromolecules* **24,** 1905–1913 (1991).

18. Delbreilh, L., Bernès, A. & Lacabanne, C. Secondary Retardation/Relaxation Processes in Bisphenol A Polycarbonate: Thermostimulated Creep and Dynamic Mechanical Analysis Combined Investigations. *Int. J. Polym. Anal. Charact.* **10,** 41–56 (2005).

19. Kim, S.-M. *et al.* Superior Toughness and Fast Self-Healing at Room Temperature Engineered by Transparent Elastomers. *Adv. Mater.* **30,** 1705145 (2018).

20. Yang, Y., Lu, X. & Wang, W. A tough polyurethane elastomer with self-healing ability. *Mater. Des.* **127,** 30–36 (2017).

21. Richeton, J., Ahzi, S., Vecchio, K. S., Jiang, F. C. & Adharapurapu, R. R. Influence of temperature and strain rate on the mechanical behavior of three amorphous polymers: Characterization and modeling of the compressive yield stress. *Int. J. Solids Struct.* **43,** 2318–2335 (2006).

22. Sahin, S. & Yayla, P. Effects of testing parameters on the mechanical properties of polypropylene random copolymer. *Polym. Test.* **24,** 613–619 (2005).

23. Stukalin, E. B., Cai, L. H., Kumar, N. A., Leibler, L. & Rubinstein, M. Self-Healing of Unentangled Polymer Networks with Reversible Bonds. *Macromolecules* **46,** 7525–7541 (2013).

24. Hackelbusch, S., Rossow, T., van Assenbergh, P. & Seiffert, S. Chain Dynamics in Supramolecular Polymer Networks. *Macromolecules* **46,** 6273–6286 (2013).

25. Bode, S. *et al.* Correlation between scratch healing and rheological behavior for terpyridine complex based metallopolymers. *J. Mater. Chem. A* **3,** 22145–22153 (2015).

26. Seiffert, S. & Sprakel, J. Physical chemistry of supramolecular polymer networks. *Chem. Soc. Rev.* **41,** 909–930 (2012).

27. Trinkle, S., Walter, P. & Friedrich, C. Van Gurp-Palmen Plot II – classification of long

chain branched polymers by their topology. *Rheol. Acta* **41,** 103–113 (2002).

28. Ferry, J. D. *Viscoelastic Properties of Polymers*. (Wiley, 1980).

29. Müller, M., Seidel, U. & Stadler, R. Influence of hydrogen bonding on the viscoelastic properties of thermoreversible networks: analysis of the local complex dynamics. *Polymer* **36,** 3143–3150 (1995).

30. Stadler, F. J. *et al.* Linear Viscoelastic Rheology of Moderately Entangled Telechelic Polybutadiene Temporary Networks. *Macromolecules* **42,** 6181–6192 (2009).

31. Feldman, K. E., Kade, M. J., Meijer, E. W., Hawker, C. J. & Kramer, E. J. Model Transient Networks from Strongly Hydrogen-Bonded Polymers. *Macromolecules* **42,** 9072–9081 (2009).

32. Callies, X. *et al.* Linear rheology of bis-urea functionalized supramolecular poly(butylacrylate)s: Part I – weak stickers. *Polymer* **69,** 233–240 (2015).

33. Grande, A. M., Bijleveld, J. C., Garcia, S. J. & van der Zwaag, S. A combined fracture mechanical – rheological study to separate the contributions of hydrogen bonds and disulphide linkages to the healing of poly(urea-urethane) networks. *Polymer* **96,** 26–34 (2016).

34. Bose, R. K. *et al.* Contributions of hard and soft blocks in the self-healing of metal-ligand-containing block copolymers. *Eur. Polym. J.* **93,** 417–427 (2017).

35. Delebecq, E., Pascault, J.-P., Boutevin, B. & Ganachaud, F. On the Versatility of Urethane/Urea Bonds: Reversibility, Blocked Isocyanate, and Non-isocyanate Polyurethane. *Chem. Rev.* **113,** 80–118 (2013).

36. García, S. J., Fischer, H. R. & van der Zwaag, S. A critical appraisal of the potential of self healing polymeric coatings. *Prog. Org. Coatings* **72,** 211–221 (2011).

37. Garcia, S. J. Effect of polymer architecture on the intrinsic self-healing character of polymers. *Eur. Polym. J.* **53,** 118–125 (2014).

38. Bose, R. K., Hohlbein, N., Garcia, S. J., Schmidt, A. M. & van der Zwaag, S. Connecting supramolecular bond lifetime and network mobility for scratch healing in poly(butyl acrylate) ionomers containing sodium, zinc and cobalt. *Phys. Chem. Chem. Phys.* **17,** 1697–1704 (2015).

Chapter V. How do dynamic covalent bonds influence the self-healing and mechanical strength of PUU materials?

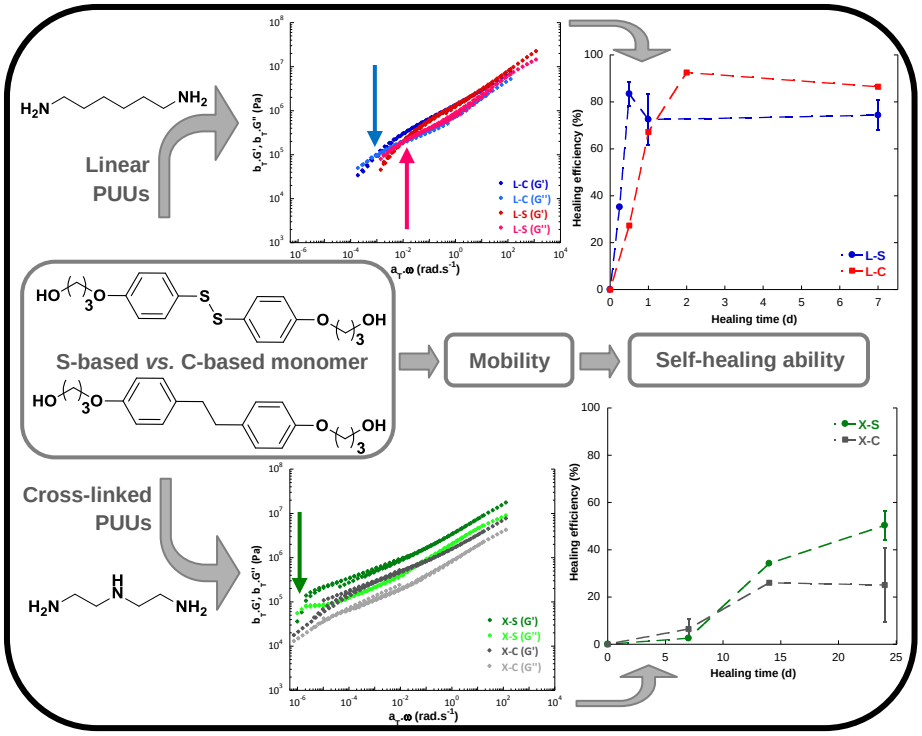

V.1. Introduction

In the previous chapters, disulfide containing PUUs were developed which are able to simultaneously provide high strength at room temperature and show mobility at moderate healing temperatures making them attractive for waterborne coating applications. These characteristics could be obtained due to the presence of three types of dynamic bonds with different interaction or bond strengths: the reversible covalent disulfide bonds which give rise to dynamic disulfide exchange, the H-bonding between the urethane units and the stronger H-bonds formed between the urea moieties.[1–3] However, the quantitative differentiation between the effect of these dynamic disulfide bonds and the influence of H-bonding on the mechanical strength and healing ability of the developed PUUs has not yet been discussed in this thesis.

Looking into literature, the influence of these dynamic disulfide bonds on self-healing of cross-linked PUU elastomers has been studied by comparing the self-healing efficiency of PUUs containing aromatic disulfide groups with PUUs of the same polymer structure but in which the disulfide bond was substituted by a C-C bond.[4,5] For a relatively open network and using the recovery of the toughness (area under the stress-strain curve obtained by tensile testing) as a measure of the self-healing efficiency, a recovery of 80% could be achieved at room temperature in only 2 h, while this recovery was nearly complete after 24 h.[4] On the other hand, the healing efficiency obtained for the cross-linked PUUs lacking disulfide motifs (but showing the same mechanical strength) was about 50% after 24 h, which was attributed to the contribution of the H-bond between the urea groups. The increase in recovery from 50 to 100% was thus attributed to the disulfide moieties, but the mechanism that led to this enhancement was not discussed. Alternatively, the effect of substituting the aromatic disulfide bonds by C-C

bonds was also studied for more densely cross-linked elastomers using fracture mechanics to measure self-healing efficiency.[5] It was found that the PUU containing aromatic disulfide groups showed a recovery of about 30% after 6 h at 90 ºC, whereas the PUU with similar strength but lacking the disulfide groups did not show any significant recovery even after 24 h at 120 ºC. These differences upon heating were attributed to the fact that strong covalent disulfide bonds could be reformed at the healing interface, while the material without these disulfide moieties could only re-establish reversible weak bonds that provided a limited recovery of the original fracture properties. Therefore, both the aforementioned works suggest that the formation of strong disulfide bonds at the healing zone is the main reason for the higher healing efficiency in PUU elastomers.

In this chapter, we want to investigate if this is also the case for the stronger self-healing PUU materials that were developed in Chapter IV. For this, linear and cross-linked waterborne PUU dispersions containing either disulfide groups or C-C bonds were synthesized. Disulfide groups are incorporated using the previously described bis[4-(3'-hydroxypropyloxy)phenyl]disulfide ($S_2(Ph(CH_2)_3OH)_2$), while the second polymer incorporates a similar monomer in which the disulfide bond is replaced by a C-C bond, namely 1,2-[4-(3-hydroxypropoxy)phenyl]ethane ($C_2(Ph(CH_2)_3OH)_2$). In the same way as described in Chapter IV, the linear PUUs were obtained using hexane-1,6-diamine (HDA) as chain extender and the cross-linked ones using diethylene triamine (DETA). In this chapter, a thorough study of the mechanical properties, rheological behaviour and self-healing ability of these polymers will be carried so that the influence of the dynamic disulfide bonds additional to the H-bonds, already inherently present in the PUUs, can be demonstrated in linear as well as cross-linked materials.

V.2. Experimental

V.2.1. Materials

Bibenzyl-4.4'-diol ($S_2(PhOH)_2$, Interchim, >95%), bis(4-hydroxyphenyl)disulfide ($S_2(PhOH)_2$, Enamine, 95%), 2,2-bis(hydroxymethyl)-propionic acid (DMPA, GEO specialty chemicals, >96%), 3-bromo-1-propanol (Apollo Scientific, 96%), dibutylamine 0.1N in xylol (DBA, Bernd Kraft), dibutyltin dilaurate (DBTL, TCI, >95%), ethyl acetate (EtOAc, Brenntag, >98%), diethylenetriamine (DETA, Merck KGaA, ≥98%), hexane-1,6-diamine (HDA, Sigma-Aldrich, 98%), hydrochloric acid 0.1N in water (HCl, Bernd Kraft), isophorone diisocyanate (IPDI, Bayer Material Science, >99%), N-methylpyrrolidon (NMP, Honeywell, ≥99.9%), methyl ethyl ketone (MEK, Honeywell, ≥99.5%), polytetrahydrofuran (PolyTHF, BASF, 2000 $g.mol^{-1}$), potassium carbonate (K_2CO_3, Sigma-Aldrich, ≥99%), sodium chloride (NaCl, Sigma-Aldrich, ≥99.5%), sodium sulfate ($NaSO_4$, Honeywell, ≥99%), tri-n-butylphosphine (TBP, Sigma-Aldrich, 97%), triethylamine (TEA, Sigma-Aldrich, ≥99%), tetrahydrofuran (THF, Scharlau), were used as received.

V.2.2. Synthesis of alternative carbon-based aromatic compound

Similar to the in Chapter III (Section III.2.2) described synthesis of bis[4-(3'-hydroxypropyloxy)phenyl]disulfide ($S_2(Ph(CH_2)_3OH)_2$), a carbon-based counterpart compound was synthesized, 1,2-[4-(3-hydroxypropoxy)phenyl]ethane ($C_2(Ph(CH_2)_3OH)_2$), in which the disulfide bond of $S_2(Ph(CH_2)_3OH)_2$ was replaced by a C-C bond (Figure V.1). A mixture of bibenzyl-4,4'-diol (79.0 g, 0.37 mol), 3-bromo-1-propanol (83.4 mL, 0.92 mol), potassium carbonate (509.6 g, 3.69 mol) in THF (120 wt% of solid reagents) as solvent was stirred at

60°C for 95h under N_2-atmosphere in a jacketed glass reactor equipped with a mechanical stirrer and a condenser. Afterwards, the reaction mixture was filtrated and washed with EtOAc. The obtained organic filtrate was washed with 1M HCl and saturated aqueous NaCl solution, after which it was dried over anhydrous $NaSO_4$. The solvent was removed from the product under vacuum and the residue material was purified by recrystallization in EtOAc. Finally, the product was dried at 50°C under vacuum to give 1,2-[4-(3-hydroxypropoxy)phenyl]ethane $C_2(Ph(CH_2)_3OH)_2$ [IUPAC: 3,3'-((ethane-1,2-diylbis(4,1-phenylene))bis(oxy))bis(propan-1-ol)].

Yield: 44.6 g (37 mol%). Pale brown powder. FTIR (neat, cm-1): 3249.02, 2908.08, 2870.14, 1878.29, 1611.05, 1582.41. m.p. 138.9-140.4 ºC. ^{1}H NMR (500 MHz, DMSO-d_6) δ 7.13 – 7.06 (d, *J* = 8.6 Hz, 2H), 6.85 – 6.78 (d, *J* = 8.6 Hz, 2H), 4.54 (t, *J* = 5.1 Hz, 1H (O*H*)), 3.98 (t, *J* = 6.4 Hz, 2H), 3.55 (t, *J* = 6.2 Hz, 2H), 2.76 (s, 2H), 1.84 (p, *J* = 6.3 Hz, 2H). ^{13}C NMR (126 MHz, DMSO) δ 157.28, 133.80, 129.72, 114.58, 64.88, 57.82, 40.48, 40.32, 40.15, 39.98, 39.81, 39.65, 39.48, 36.95, 32.66. (The ^{1}H, ^{13}C, g-COSY, g-HSQC NMR spectra are depicted in Figures A III.1-4 in Appendix III) Anal. Calcd. for $C_{20}H_{26}O_4$: C 72.70, H 7.93, S 0. Found: C 72.89, H 7.86, S 0. HRMS (ESI) for $C_{20}H_{26}O_4$ calculated $[M + H]^+$: 330.1831. Found: 330.1822

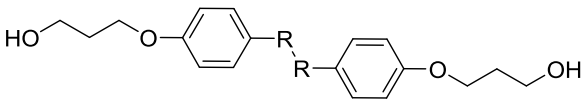

$S_2(Ph(CH_2)_3OH)_2$ (S): R = S
$C_2(Ph(CH_2)_3OH)_2$ (C): R = CH_2

Figure V.1. Chemical structure of bis[4-(3'-hydroxypropyloxy)phenyl]disulfide $S_2(Ph(CH_2)_3OH)_2$ and 1,2-[4-(3-hydroxypropoxy)phenyl]ethane $C_2(Ph(CH_2)_3OH)_2$.

V.2.3. Synthesis of the waterborne PUU dispersions based on sulfur-based and carbon-based monomers

The synthesis procedure for the PUU dispersions was similar to the one described in Chapter IV using the formulations described in Table V.1. In order to obtain the S-containing or C-based prepolymers, PolyTHF (M_w=2000 $g.mol^{-1}$), DMPA, IPDI and $S_2(Ph(CH_2)_3OH)_2$ or $C_2(Ph(CH_2)_3OH)_2$ were fed together into a 100 mL jacketed glass reactor equipped with a mechanical stirrer and a condenser. Next, DBTL (0.8 wt% of reactants) and MEK (60 wt%) were added and the mixture was stirred for 130 min at 80ºC under refluxing conditions. The mixture was cooled down to room temperature and neutralized with TEA (1 mol eq. of DMPA) after which deionized water (100 wt%) was slowly added dropwise to obtain a dispersion. In the last synthesis step, a constant amount (13 mol%) of chain extender (HDA or DETA) was added into the vessel to react with the residual free NCO-groups of the dispersed prepolymer for 30 min. MEK was removed from the filtered dispersion by evaporation using a rotary evaporator at 243 mbar. The waterborne PUU dispersion had a solids content of 25 wt%.

The samples were named according to their varying type of chain extender, L (linear) for HDA and X (cross-linked) for DETA, followed by an indication of the incorporation of the disulfide compound $S_2(Ph(CH_2)_3OH)_2$ (S) or the C-based monomer $C_2(Ph(CH_2)_3OH)_2$ (C) into PUU backbone as depicted in Figure V.2. The formulations for the S-based PUUs are equal to the ones of 1.8L-0.56S3 and 1.8X-0.56S3 described in Chapter IV and are simplified in this chapter by naming them L-S and X-S, respectively. Their C-based counterparts are synthesized using the same formulation (based on mol equivalents), but replacing $S_2(Ph(CH_2)_3OH)_2$ by $C_2(Ph(CH_2)_3OH)_2$, and are respectively named L-C and X-C.

Table V.1 Formulation of PUU syntheses performed based on S_2- or $C_2(Ph(CH_2)_3OH)_2$.

Sample	Data	DMPA	IPDI	PolyTHF	S	C	HDA/DETA
L/X-S	wt%	3	29	38	27	/	1.9/1.7
	mol eq.	0.17	1	0.15	0.56	/	0.13
L/X-C	wt%	3	30	39	/	25	2.0/1.7
	mol eq.	0.17	1	0.15	/	0.56	0.13

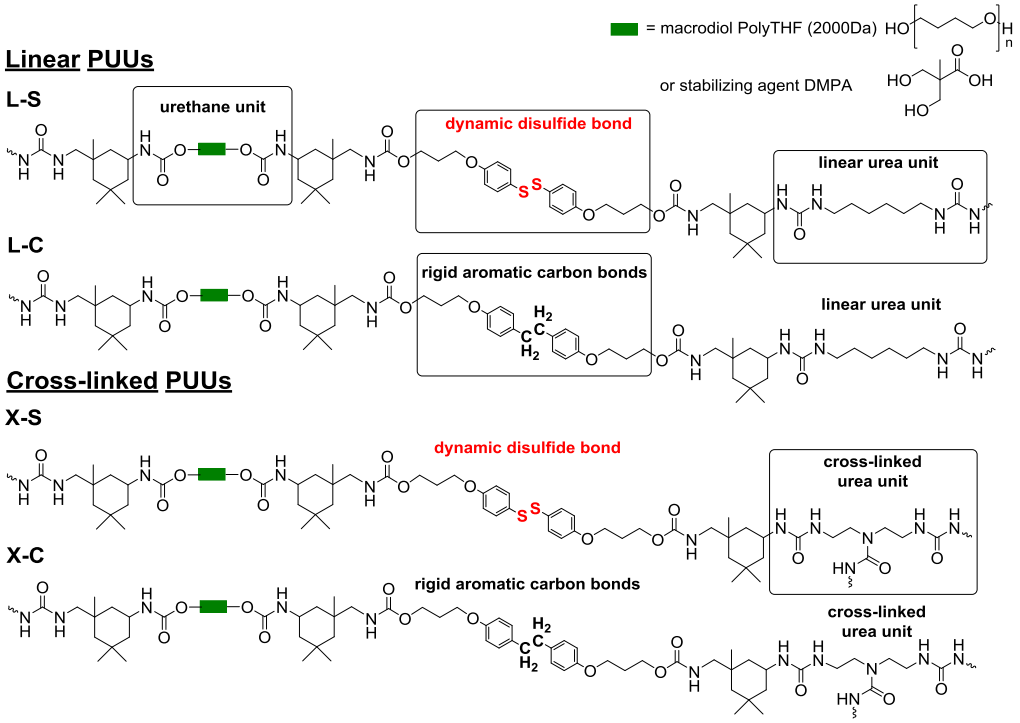

Figure V.2. Schematic of linear PUUs (L-S and L-C) and cross-linked PUUs (X-S and X-C).

V.2.4. Characterization

V.2.4.1. Polymer characterization

The same standard monomer, prepolymer and dispersion characterization techniques as in Chapter IV were used (Section IV.2.4.1-2). The films were dried and GPC, TGA and DMA were carried out as described in Chapter IV (Section IV.2.4.3). The gel content of the materials was defined by immersing small samples cut from the polymer films during 24 h in MEK. Afterwards, the films were filtered from the solvent and dried overnight at 60ºC under vacuum to make sure all the residual MEK evaporated. The gel content could then be calculated as the ratio of the weight of the different samples after drying and before immersion. Stress-strain measurements were carried out on dumbbell type specimen at 23ºC and 50%RH, meeting the requirements of ISO 291-23/50-class 1, on a universal testing machine Z050/zmart.pro with testcontrol by Zwick GmbH at a crosshead velocity of 25 $mm.min^{-1}$. For each experiment, the average results of 3-5 replicate measurements are reported here. It is noteworthy to mention that due to the high toughness of the C-based materials, breaking in the clamp or slippage occurred in some tensile measurements and therefore the results that could be obtained with this tensile apparatus only give an estimate of the absolute strength of the C-based polymers. As an alternative technique to tensile testing, fracture mechanics were performed, so that the absolute difference in toughness between the S-based and C-based materials could be obtained. Differential scanning calorimetry (DSC) was performed using a TA Instruments Q2000. The samples were heated from -70ºC to 150ºC with a heating rate of 20ºC/min during a first heating cycle after they were cooled again to -70ºC during a cooling cycle. Finally, they were heated during a second heating cycle from -70ºC to 150ºC.

The rheological data were obtained from a stress-controlled Anton Paar Physica MCR101 rheometer using parallel plate geometry (plate ø = 8mm, disk-shaped specimens with ø = 10 mm and 0.50-0.75 mm in thickness). Frequency sweeps (0.001-20 Hz) at a strain of 0.5% were conducted at fixed temperatures ranging from 70-150ºC. Creep measurements were performed on a stress-controlled ARG2 (TA Instrument) rheometer. A nominal stress of 35 Pa was applied at 120ºC during 30 min after which the stress was removed from the sample and the residual strain behaviour was measured during an additional 30 min. The relaxation experiments were performed using a strain-controlled ARES (TA Instrument) rheometer at a temperature of 120ºC for which a 0.05% strain was applied, and the resulting stress was monitored over time.

V.2.4.2. Scratch closure and fracture mechanics tests

For the scratch closure experiments, scratches were made with a depth of roughly 75% of the thickness (±0.7 mm) of the films using a razor blade with a thickness of 0.40 mm and subsequently closure at 80ºC was followed using an optical microscope (Nikon Eclipse LV100ND). Fracture experiments were performed on Single Edge Notch Tensile (SENT) specimens (70x20x2 mm) at room temperature using a MTS (model 810) testing machine fitted with a 15 kN load cell. The SENT specimens were cut using a rectangular die from flat polymeric sheets which were obtained from casting the dispersion in the silicon molds (60 x 75 mm) and drying the first layer for 1 d at 23°C, 3 d at 50°C and 1 d at 60ºC while maintaining a relative humidity of 50%, after which a second layer was formed in a similar fashion and the obtained specimens with a residual thickness of ±2 mm were further dried for 2 d at 60ºC and 3 d at 25°C. For the pristine samples, a pre-notch with a length of 10 mm was introduced into the center of the longest side, perpendicular to the tensile direction, of the specimens using a

sharp razor blade. The pre-notched pristine specimens were then clamped in the tensile machine using a gauge length of 40 mm and stretched until failure. For the healing experiments, new samples were cut completely in the center of the longest side, perpendicular to the tensile direction, using a sharp razor blade. Afterwards, the fractured parts were accurately positioned in Teflon moulds (70x20x2 mm) using a thin (0.065 mm) Teflon film to retain an unhealed pre-notch of approximately 10 mm. The fractured samples were healed at 80ºC and the effect of the healing time (6 h, 12 h, 1 d, 2 d, 7 d, 14 d or 24 d) on the recovery of the fracture properties was investigated. After an equilibration at room temperature for at least 1h, the healed samples were tested following the same SENT fracture procedure. A constant cross-head separation velocity of 10mm.min^{-1} was employed in each experiment and force and displacement data were collected. The low cross-head speed was applied so that the crack initiation and evolution could be accurately recorded by a camera positioned in the front of the rectangular samples, as depicted for a typical sequence (*e.g.* L-C) in Figure V.3.

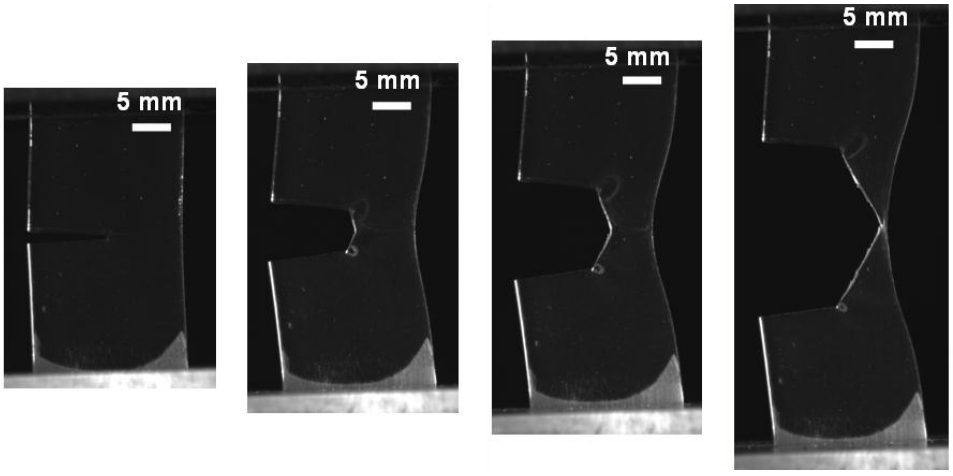

Figure V.3. Image sequence for fracture tests on SENT specimen taking pristine L-C as example.

V.3. Results and discussion

V.3.1. Dispersion and polymer characteristics

The particle size of the dispersions determined by hydrodynamic chromatography (HDC, Table 2) show that in general small particle sizes ($d_p \leq 100$ nm) were obtained with narrow particle size distributions (PSD) in which no obvious effect of changing the monomer from $S_2(Ph(CH_2)_3OH)_2$ to $C_2(Ph(CH_2)_3OH)_2$ or altering the polymer structure from linear to network could be observed. Comparable molecular weights were obtained for the linear PUUs (L-S and L-C) when performing GPC measurements (RI) after dissolution of 1 h in THF.

Table V.2. Dispersion and polymer characteristics of PUUs based on S_2 – and $C_2(Ph(CH_2)_3OH)_2$.

Sample	HDC		GPC (IR)		
	d_p (nm)	PSD	M_n (kDa)	M_w (kDa)	Đ
L-S	40 - 85	Sligtly bimodal	22	45	2.1
L-C	100	Gauss	26	49	1.9
X-S	70	Monomodal	Insoluble in THF		
X-C	45 - 100	Bimodal			

These molecular weights are higher than the critical molecular weights (M_c) for entanglements (L-S ≈ 5.5 kDa, L-C ≈ 7 kDa), based on the entanglement molecular weight ($M_e \approx M_c/2$) which could be calculated from the plateau modulus ($G_N = \rho RT/ M_e$) obtained from rheological data.[6] Due to the insolubility of the cross-linked films in THF on a short timeframe, the molecular weight of X-S and X-C could not be determined by GPC. In order to be able to compare the cross-linking degree of the networks, the gel content measured for both polymers and showed to be in the range of around 50-60 % demonstrating that the polymers were not completely

cross-linked, likely due to the low reactivity of the secondary amine of the DETA. Moreover, since similar molecular weights between the cross-links could be calculated from rheological data for X-S (9.5 kDa) and X-C (10.5 kDa), it could be confirmed that similar networks were formed for both materials.

V.3.2. Thermal and mechanical properties of the PUUs

The mechanical behaviour of the PUUs in both linear and non-linear regimes was studied by means of DMA and tensile tests, respectively. From the DMA results of the PUUs represented in Figure V.4, it is clear that for both linear and cross-linked systems, the S-based and C-based PUUs show a very similar behaviour for the storage modulus E', loss modulus E'' and tan δ (E''/E') in function of temperature. This already makes these polymers of interest to compare them towards their healing ability as will be discussed below. For all materials, a secondary relaxation can be observed for the loss modulus at around -140°C, which is linked to the presence of closely interconnected aromatic rings as discussed in the previous chapters. Also for these PUUs, a low temperature T_g that can be seen around -70ºC, and a second broader transition appeared at higher T, related to the glass transition of the hard phase of the material.

This broad glass transition showed a slight shift to higher temperatures for the cross-linked polymers which could also be observed in the DSC results (Figure A III.5, Appendix III). Nevertheless, the cross-linked materials are clearly distinguishable from the linear PUUs due to the presence of a rubbery plateau at temperatures higher than 70 °C. In a temperature range starting from 150ºC, the urethane linkages begin to degrade leading to a loss in mechanical integrity, as can be observed in the DMA results of the cross-linked PUUs (Figure V.4).[7]

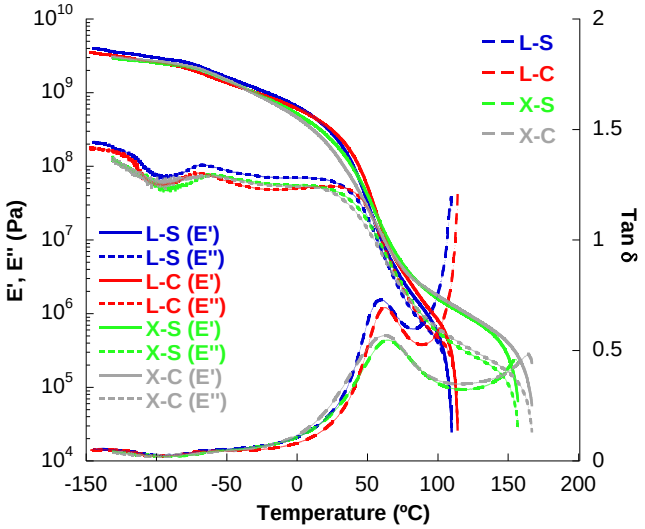

Figure V.4. DMA results of PUUs: storage modulus (E'), loss modulus (E'') and tan δ *versus* T.

DMA measures the mechanical response in the linear regime over a wide range of temperatures, which was seen to be same for both the S- and C-based monomers. In order to explore the mechanical properties in the non-linear regime, tensile tests were carried out at room temperature as shown in Table V.3 and Figure V.5. In this case, significant differences were observed between the C-based and S-based materials regarding their toughness. Although the Young's modulus (E) and the yield strength (σ_y) show similar values for all materials, it is clear that the tensile strength (σ_f) and strain (ε_f) at fracture are lower for the S-based materials. Comparing in particular L-S and L-C, it seems that at first, the materials are behaving similarly, as may be expected based on the DMA results in the linear regime, but as the strain (ε) surpasses 150%, L-S shows less strain hardening than L-C and breaks at lower stress σ_f and strain ε_f. This suggests that the disulfide bonds broke when subjected to high stress (strain). This clear difference in strength between the S-based and C-based materials

was not observed for the softer elastomeric PUUs described above that was subjected to tensile tests.[4,5] Although the bond energy of covalent disulfides is greater than the energy of H-bonds of the urethane and urea groups,[2] the higher number of the latter H-bonding interactions in the strong coating makes the disulfide bonds to be the weak point in the PUU.

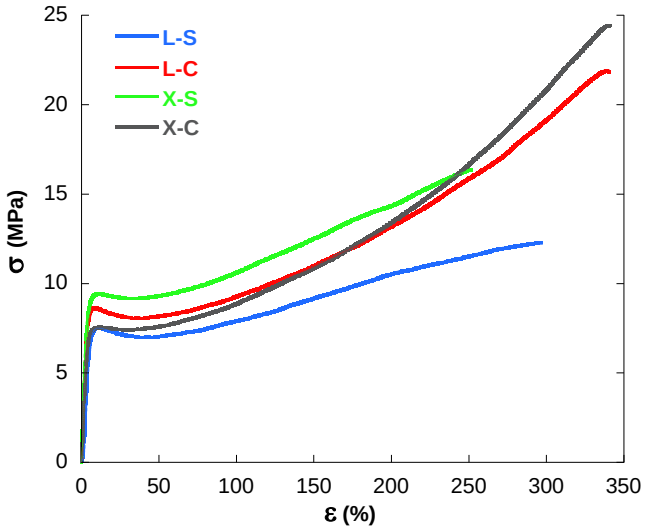

Figure V.5. Stress-strain (σ-ε) curves of PUUs based on $S_2(Ph(CH_2)_3OH)_2$ *versus* $C_2(Ph(CH_2)_6OH)_2$ obtained at 23ºC using a crosshead velocity of 25mm.min^{-1}.

Table V.3. Tensile testing results of PUUs based on $S_2(Ph(CH_2)_3OH)_2$ *versus* $C_2(Ph(CH_2)_3OH)_2$.

Sample	E (MPa)	σ_y (MPa)	σ_f (MPa)	ε_f (%)
L-S	207.2 ± 6.8	7.2 ± 0.2	11.6 ± 0.3	295 ± 10
L-C	264.6 ± 18.4	8.6± 0.1	24.5 ± 2.6	360 ± 25
X-S	278.5 ± 7.2	9.3 ± 0.1	16.3 ± 0.3	315± 35
X-C	259.2 ± 14.5	8.1± 0.4	28.8 ± 2.8	395 ± 40

V.3.3. Rheological behaviour of the PUUs

In order to analyze the mobility of the PUUs on the molecular level, master curves of the storage modulus G' and loss modulus G'' were constructed, by applying the time-temperature superposition (TTS) principle. The van-Gurp-Palmen-plots were constructed in order to check the applicability of the TTS principle to construct the master curves of G' and G'' (Figures A III.7 in Appendix III). These plots showed that, similarly as what was described in the previous chapters, the isothermal frequency curves do not completely merge in a common line which indicates that the TTS principle does not hold equally well for all these polymers.[8] Nevertheless, using both horizontal (a_T) and vertical shift factors (b_T), an acceptable superposition of G' and G'' could be achieved for all PUUs to obtain the master curves that are presented in Figure V.6 for a reference temperature of 80ºC. This temperature was chosen because it is above the T_g of all polymers and comfortably away from temperatures where cleavage of urethane/urea groups could also take place (Figure V.4).[7] In this way, it is possible to distinguish the influence of the presence of the dynamic disulfide bonds in the S-based PUUs compared to the C-bonds in L-C and X-C on the mobility of the material without the interference of any effects of the degradation of urethane/urea moieties.

Figure V.6 shows that in the high frequency region, the linear polymers (L-S and L-C) display an almost identical rheological behaviour. However, at lower frequencies, both PUUs show a transition where the material goes from exhibiting an elastic behaviour (G'>G'') to a region where the viscous response is dominating (G'<G''). The crossover frequency ω_d defines the characteristic relaxation time τ_d of the material, which gives an indication of the time needed for the material to flow.[5,9,10] As can be seen in Figure V.6 A, the G'-G'' crossover point (marked

with arrows) for L-S takes place at a higher crossover frequency than for L-C, *i.e.* in a shorter relaxation time (about 13 min for L-S *versus* more or less 2 h for L-C) which indicates that at 80 ºC the disulfide bonds undergo some exchange enhancing the mobility of the system.

Alternatively, cross-linked materials show a fundamental difference in behaviour compared to linear polymers. In general, no G'-G'' crossover point is expected for completely cross-linked polymers as the network prevents the material from flowing. However, both X-S and X-C contained some linear chains that may provide some mobility. Figure V.6 B shows that X-S presented a crossover point at around 10^{-6} rad.s^{-1}, while X-C lacks a similar crossover point for even lower frequencies. The crossover point for X-S could be explained by the presence of disulfide bonds inserted in the chains between cross-linking points although some help of the linear chains cannot be excluded. These disulfide bonds are able to undergo exchange inducing dynamic reorganization of the network and thus flow of the cross-linked material at elevated temperature. Although this dynamic process was very slow (relaxation time τ_d of roughly 36 d for X-S). This crossover point and thus rearrangement could not be observed for X-C showing that the permanent network which lacks these dynamic bonds determined its rheological behaviour.

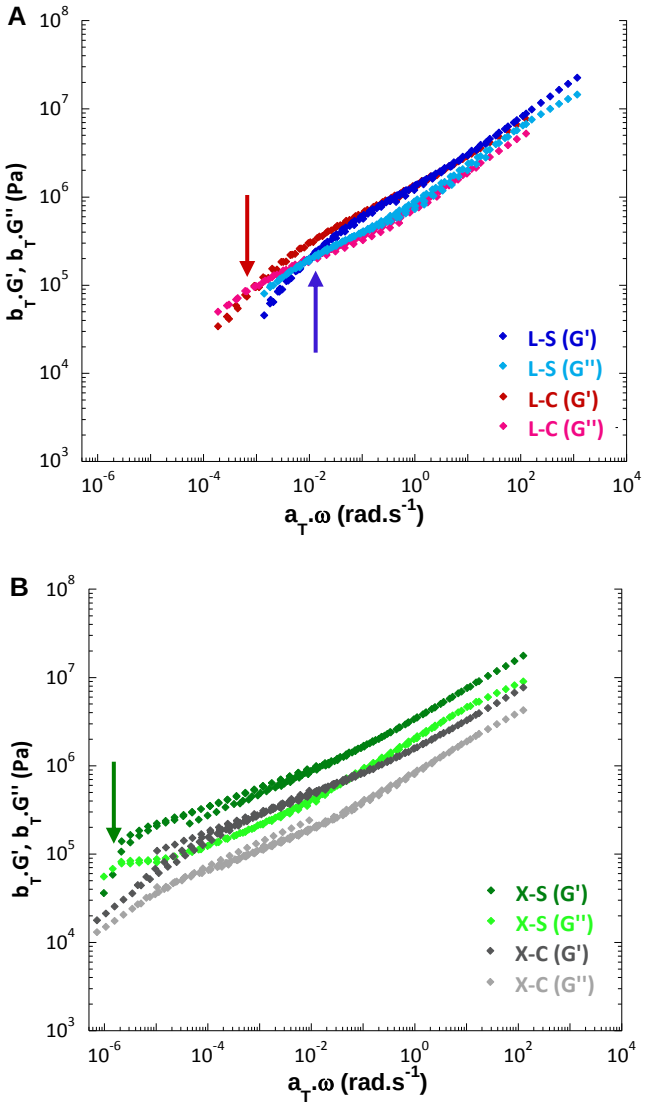

Figure V.6. Master curves (T_{ref}=80ºC) for the linear (A) and cross-linked (B) PUUs.

The cross-linked polymers were further analyzed by means of the stress relaxation and creep experiments. In the stress-relaxation experiment, a strain is applied and the variation of the stress with time is monitored (Figure V.7 A). On the other hand, in the creep experiment, a constant stress is applied for a certain time (30 min in Figure V.7 B) and the evolution of the strain is measured both during the application of the stress and afterwards. The experiments were carried out at 120 ºC in order to have an acceptable time frame for the measurement. The relaxation time τ_d for X-S decreases from roughly 36 d at 80 ºC to more or less 10 min at 120 ºC (Figure A III.8, Appendix III). This temperature is below the degradation temperature (T_d) of the materials (T_d = 265±5ºC at 5 wt% weight loss) as depicted in the TGA curves in Figure A III.6 in Appendix III.

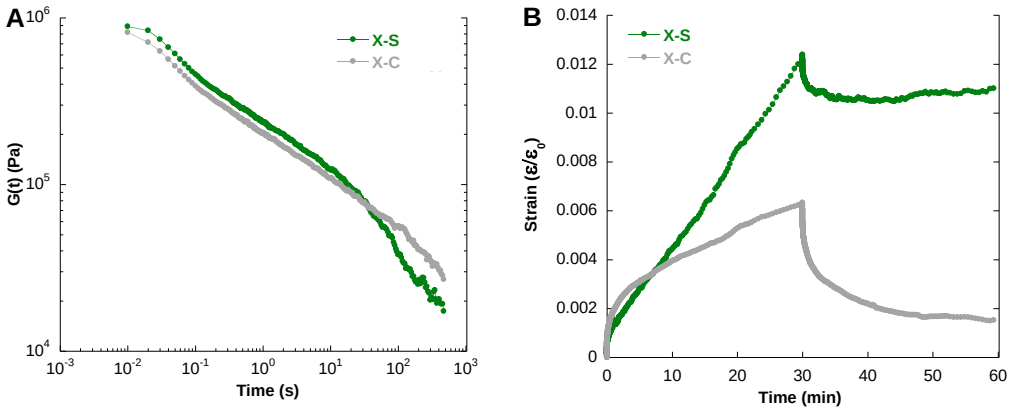

Figure V.7. Stress-relaxation (A) and creep (B) experiments at 120ºC for X-S and X-C.

Figure V.7 A shows that up to 10 s, X-C and X-L behave equally, but for later X-S showed a significant decrease in the shear modulus G(t) when compared to X-C. This indicates that, due to network reoganization, X-S behaves more as a viscoelastic liquid, while X-C shows the behaviour of a viscoelastic solid. Similar conclusions could be drawn from creep experiments

(Figure V.7 B). It can be seen that, under stress, X-S deformed to a greater extent and faster than X-C. When the stress was removed after 30 min of measurement, X-S maintained a high strain level which shows that X-S could withhold the deformation. This strongly indicates that the structure of the network changed during the experiment adapting itself to the form that resulted from the strain of the sample. This was possible because the disulfide bonds were located in the chains connecting the cross-linking points. On the other hand, X-C showed the typical response of a viscoelastic solid and recovered most of the original form, which is a clear indication that the network was not modified during the creep experiment and that it was the network and not the fraction of polymer with lower molecular weight which controlled the response of the material to creep. It is noteworthy to mention that the creep observed at 120ºC would be negligible at the service temperature of the material, as even at 80ºC the mobility of X-C is very small.

V.3.4. Healing behaviour after scratch and fracture damage

When a coating is damaged, complete healing involves scratch closure and the restoration of the polymer strength, so that the closed scratch does not represent a weak point in the material. Scratch closure is mainly a rheological problem, as described already in the previous chapters, which will be followed optically. However, in order to obtain a quantitative measure of the restoration of the polymer which involves formation of new bonds, the investigation of the interfacial healing is required which will be measured using fracture mechanics tests.

V.3.4.1. Scratch closure

The closure of scratches, made with a razor blade, was optically monitored at 80 ºC (Figure V.8). This temperature was selected to allow a direct comparison with relaxation times obtained from the master curves (Figure V.6). For the linear PUUs, after 2 h almost complete closure could be observed for L-S, while the scratch of L-C was still visible to a larger extent.

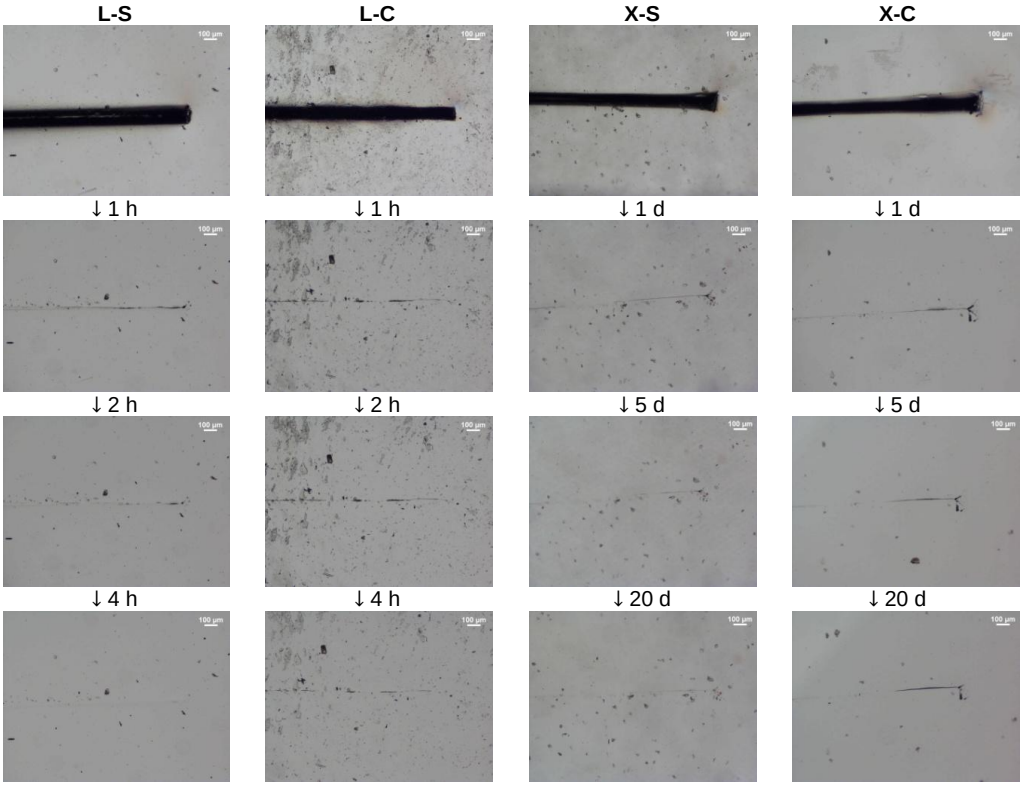

Figure V.8. Scratch closure at 80°C of PUUs based on $S_2(Ph(CH_2)_3OH)_2$ *versus* $S_2(Ph(CH_2)_3OH)_2$.

Regarding the cross-linked materials, scratch closure for X-S was almost complete after 20 d, while still a part of the scratch was visible for X-C. The fact that the time necessary for scratch

closure is shorter than the relaxation time τ_d might be due to the higher cross-linking degree inducing a delayed elastic recovery at higher temperatures, as explained in Chapter IV, leading to a strong scratch closing behaviour after already 1 d for both cross-linked materials and supposedly promoting shorter healing times.[11–13] These experiments support the idea that the disulfide bonds are important for the rheological behaviour of the polymers allowing faster flow at the healing temperature. However, they do not demonstrate to what extent the mechanical strength of the material could be recovered, hence, this will be the focus in the next section.

V.3.4.2. Fracture mechanics

In order to investigate if new bonds are created at the fractured interface after the scratch closure and therefore the closed scratch does not represent a weak region in the material, fracture mechanics experiments on Single Edge Notch Tensile (SENT) samples were performed as depicted in Figure V.3 in the experimental part. In these experiments, the pre-notched geometry ensures stress localization at the crack tip zone, contrary to the widely used tensile tests, where samples are loaded with a quasi-homogeneous stress distribution.[10] In this way, fracture mechanics have shown to provide more reliable measurements of the real degree of healing, *i.e.* the recovery of the original polymer network, when comparing the results of the healing efficiencies to those obtained by tensile testing.[14] Since short relaxation times were predicted in the rheological measurements and short scratch closure times were measured for the linear PUUs, these polymers were healed at 80 ºC with a varying healing time up to 7 d to ensure complete recovery. The cross-linked materials that showed an almost complete scratch closure in 20 d were exposed to 80ºC during longer healing times up to 24 d.

The load-displacement curves (corrected for the thickness of the materials) are depicted in Figure V.9 (repeated measurements in Figure A III.10-11, Appendix III). First of all, it is worth emphasizing that the PUUs synthesized here were significantly stronger (loads up to 100-150 N/mm thickness) than the elastomers already discussed in literature using fracture mechanics.[5,10,14] In addition, remarkable recovery levels for the load-displacements curves after healing could be obtained. Furthermore, it can be noticed that the S-based materials reached lower values for load and completely fractured at lower displacement compared to the C-based PUUs. This is related to what was observed in the tensile test results (Figure V.5) and could also be explained by the presence of the weaker disulfide bonds in both L-S and X-S.

From the data obtained by fracture mechanics, it is also possible to quantify the recovery by calculating the healing efficiency based on the fracture energy value (J). Applying the J-integral analysis method, the J-integral values for each sample could be obtained from the load/thickness-displacement curves in Figure V.9 according to the following equation V.1:

$$J\ (kJ/m^2) = \left.\frac{0.001\eta U}{(w-a)}\right|_u \qquad (V.1)$$

where U is the energy per unit length of thickness (N) calculated as the area under the curves in Figure V.9 at different levels of displacement u, η is the proportionality factor related to sample geometry (0.9 used for this SENT geometry), w is the sample width (0.020 m) and a is the pre-notch length (0.010 m).[5,10,14–17] Based on these values, the healing efficiency (HE) can then be calculated as the ratio of the fracture energy after healing (J^{healed}) and the fracture energy of the pristine material ($J^{pristine}$) as represented by equation V.2.[5,10,14]

$$\text{Healing efficiency HE (\%)} = \frac{J^{healed}}{J^{pristine}} \cdot 100 \qquad (V.2)$$

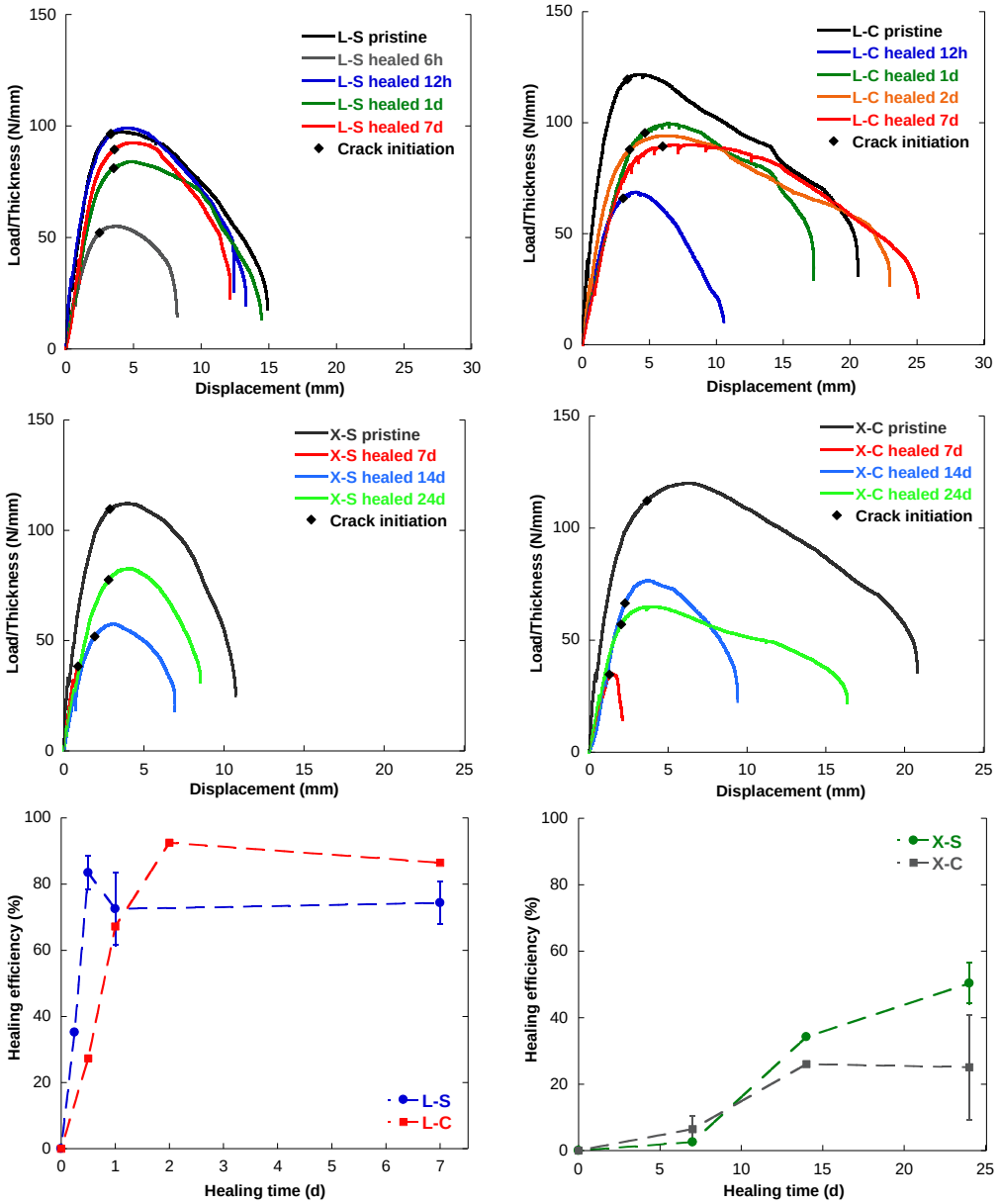

Figure V.9. Load/Thickness-displacement curves (A: L-S, B: L-C, C: X-S and D: X-C) and the healing efficiencies of L-S and L-C (E) and X-S and X-C (F) in function of healing time at 80°C.

As the three different J-integrals calculated in this chapter, based on crack initiation (J_{ci}), crack propagation (J_{prop}) and complete fracture (J_{tot}), gave a similar trend in healing efficiencies over time (as described in the fracture mechanics section in Appendix III), only the healing efficiencies obtained from the simplified calculations of J-integral values that are based on complete fracture (J_{tot}) were depicted in Figure V.9 for the linear (E) and cross-linked (F) PUUs.

Based on the load/thickness-displacement plots of the linear PUUs, it is clear that L-S shows almost complete recovery of the strength of the pristine material after 12 h, showing that after scratch closure complete interfacial healing could take place (Figure V.9 A). On the other hand, L-C showed a substantial recovery, but it required longer times than for L-S and even after long healing times fracture propagated at lower loads than the pristine material (Figure V.9 B). At first sight, in line with the reports in literature for elastomers,[4,5] the higher recovery of the L-S could be attributed to the formation of disulfide bonds at the healing zone. However, it is worth pointing out that the total energy for fracture propagation, that per unit of thickness is the area under the curves in Figure V.9, was greater for L-C than for L-S. This means that although the recovery of L-C was not complete, the material was mechanically stronger than L-S.

Specifically quantifying these results, by calculating the healing efficiencies of L-S and L-C using J_{tot} in equation V.2, demonstrates that the linear materials can obtain recoveries up to 80-100% (Figure V.9 E). Moreover, the trends observed for the healing efficiency confirm the aforementioned faster kinetics for the L-S compared to L-C on short term. However, it is noteworthy to mention that L-C could show healing efficiencies up to 100% after 2 d and 7 d of healing according to calculations based on complete facture. This can be explained by the fact that, although the crack initiated at the edge of the fractured interface and thus lower recovery

in the load-displacement curves was obtained (Figure V.9 B), the crack did not propagate entirely through the fractured interface, but slightly below in the pristine material (Figure V.10). This fracture propagation behaviour has not been described in literature before when using fracture mechanics for self-healing materials. However, theoretically, this can eventually be expected for all linear materials which are sufficiently mobile and are given enough time to interdiffuse, so that due to randomization full restoration of polymer properties can be achieved as already explained in Chapter I (Section I.1).

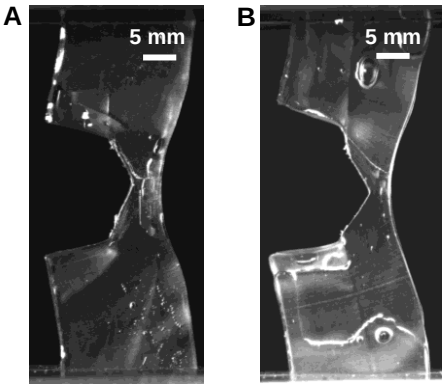

Figure V.10. Crack propagation in fracture test of L-C after 2d (A) and 7d (B) healing at 80ºC.

The results obtained for the linear PUUs indicate that the mechanical strength of the healed region at the service temperature (room temperature) was not determined by the reformation of disulfide covalent bonds, but by the H-bonds, as L-C appeared to be mechanically stronger than L-S upon recovery. Therefore, the main role of the disulfide groups seems to be the enhancement of the mobility of the polymer chains when the material is brought to the healing temperature.

The load/thickness-displacement curves of the cross-linked materials are presented in Figures V.9 C and D. First of all, it can be noticed that a significantly lower recovery of the mechanical strength was obtained compared to the linear materials, because the networks are less mobile as already shown in the rheological data (Figure V.6). For a healing time of 7 d, only very low recovery levels could be obtained for X-S and X-C as these materials were unable to undergo any significant flow during the limited healing time. At longer healing times (14 and 24 d) a clear differentiation between the materials can be observed. In the latter case, X-S shows a continuous increase of the recovery, while X-C did not recover further after the extent of recovery observed for the first 14 d of healing. It is possible that the linear polymer chains in X-C might contribute to the recovery observed in the first 14 d. However, here again, the total energy for fracture after 24 d was higher for the polymer lacking the disulfide groups (X-C).

The same trends can again be observed when considering the healing efficiency values obtained for X-S, showing a maximum of 40-50% after 24d, and those for X-C, already reaching a maximum of 20-30% after 14 d (Figure V.9 F). It is clear that this is considerably lower than the ones obtained for the linear counterpart, however, these healing efficiencies are high considering the high toughness of these materials when comparing these values with those of soft elastomeric PU(U)s already discussed in literature using fracture mechanics.[5,10,14]

Finally, also the trends observed for cross-linked materials further support the idea that for strong coatings the dynamic disulfide groups enhance the mobility of the polymer chains during healing, but the mechanical strength at service temperature is mainly due to the H-bonds.

V.4. Conclusions

In this chapter, the role of the dynamic disulfide covalent bonds in the self-healing of PUU coatings, namely polymers that are strong at room temperature but can flow at a moderate healing temperature, was investigated. For this, linear and cross-linked waterborne PUU dispersions containing either aromatic disulfide groups or C-C bonds were synthesized. These materials were compared by means of thermal, mechanical, rheological and fracture mechanical analysis.

In this way, we were able to demonstrate that in the case of linear materials, dynamic disulfides induce faster healing kinetics and make the reorganization of the polymer possible giving rise to complete recovery of the original polymer network. However, for the same healing conditions, the linear polymers lacking disulfide groups showed to be mechanically stronger upon recovery than the materials with S-S bonds. On the one hand, this means that for the coating the mechanical strength of the healed region was not determined by the reformation of disulfide covalent bonds, but by the H-bonds. On the other hand, it is noteworthy to mention that although dynamic bonds can significantly contribute to reducing the time scale of healing, they are not a necessary precondition to achieve self-healing in linear materials as sufficient mobility enables complete randomization and eventually strength recovery.

For cross-linked PUUs the disulfide bonds provide mobility to the network, through reorganization *via* disulfide exchange, which facilitates healing. The cross-linked PUUs lacking these disulfide groups (X-C) behave as an elastic solid showing a limited capability for self-healing, which in part could be due to the fraction of linear chains. However, even under these

conditions X-C presented a total energy of fracture greater than that of the cross-linked polymer with disulfide group.

Therefore, in this chapter it could be demonstrated that, for the strong PUU developed in this thesis, the main role of the dynamic disulfide bonds is to enhance the mobility of the polymer chains and networks allowing interpenetration of polymer through the interface and the formation of H-bonds, while the latter provide the mechanical strength to the coating. It is thus worth emphasizing that the limited mechanical strength that can be obtained for these self-healing materials based on reversible covalent bonds is a factor that has to be taken into account when aiming at coating applications.

V.5. References

1. Mattia, J. & Painter, P. A Comparison of Hydrogen Bonding and Order in a Polyurethane and Poly(urethane−urea) and Their Blends with Poly(ethylene glycol). *Macromolecules* **40,** 1546–1554 (2007).
2. Matxain, J. M., Asua, J. M. & Ruipérez, F. Design of new disulfide-based organic compounds for the improvement of self-healing materials. *Phys. Chem. Chem. Phys.* **18,** 1758–1770 (2016).
3. Ruipérez, F., Galdeano, M., Gimenez, E. & Matxain, J. M. Sulfenamides as Building Blocks for Efficient Disulfide- Based Self- Healing Materials. A Quantum Chemical Study. *ChemistryOpen* **7,** 248–255 (2018).
4. Rekondo, A. *et al.* Catalyst-free room-temperature self-healing elastomers based on aromatic disulfide metathesis. *Mater. Horizons* **1,** 237–240 (2014).
5. Grande, A. M., Bijleveld, J. C., Garcia, S. J. & van der Zwaag, S. A combined fracture mechanical – rheological study to separate the contributions of hydrogen bonds and disulphide linkages to the healing of poly(urea-urethane) networks. *Polymer* **96,** 26–34 (2016).
6. Ferry, J. D. *Viscoelastic Properties of Polymers*. (Wiley, 1980).
7. Delebecq, E., Pascault, J.-P., Boutevin, B. & Ganachaud, F. On the Versatility of Urethane/Urea Bonds: Reversibility, Blocked Isocyanate, and Non-isocyanate Polyurethane. *Chem. Rev.* **113,** 80–118 (2013).
8. Trinkle, S., Walter, P. & Friedrich, C. Van Gurp-Palmen Plot II – classification of long chain branched polymers by their topology. *Rheol. Acta* **41,** 103–113 (2002).
9. Feula, A. *et al.* A Thermoreversible Supramolecular Polyurethane with Excellent Healing Ability at 45 °c. *Macromolecules* **48,** (2015).
10. Grande, A. M., Martin, R., Odriozola, I., van der Zwaag, S. & Garcia, S. J. Effect of the polymer structure on the viscoelastic and interfacial healing behaviour of poly(urea-urethane) networks containing aromatic disulphides. *Eur. Polym. J.* **97,** 120–128 (2017).
11. García, S. J., Fischer, H. R. & van der Zwaag, S. A critical appraisal of the potential of self healing polymeric coatings. *Prog. Org. Coatings* **72,** 211–221 (2011).
12. Garcia, S. J. Effect of polymer architecture on the intrinsic self-healing character of polymers. *Eur. Polym. J.* **53,** 118–125 (2014).
13. Bose, R. K., Hohlbein, N., Garcia, S. J., Schmidt, A. M. & van der Zwaag, S. Connecting supramolecular bond lifetime and network mobility for scratch healing in poly(butyl acrylate) ionomers containing sodium, zinc and cobalt. *Phys. Chem. Chem. Phys.* **17,** 1697–1704 (2015).

14. Grande, A. M., Garcia, S. J. & van der Zwaag, S. On the interfacial healing of a supramolecular elastomer. *Polymer* **56,** 435–442 (2015).

15. Ramorino, G., Agnelli, S., De Santis, R. & Riccò, T. Investigation of fracture resistance of natural rubber/clay nanocomposites by J-testing. *Eng. Fract. Mech.* **77,** 1527–1536 (2010).

16. Bode, S. *et al.* in *Self-healing materials* (eds. Hager, M. D., van der Zwaag, S. & Schubert, U. S.) **273,** 113–142 (Springer, 2016).

17. Agnelli, S., Ramorino, G., Passera, S., Karger-Kocsis, J. & Riccò, T. Fracture resistance of rubbers with MWCNT, organoclay, silica and carbon black fillers as assessed by the J-integral: Effects of rubber type and filler concentration. *Express Polym. Lett.* **6,** 581–587 (2012).

Chapter VI. Characterization of the passive corrosion protection by healable PUU coatings

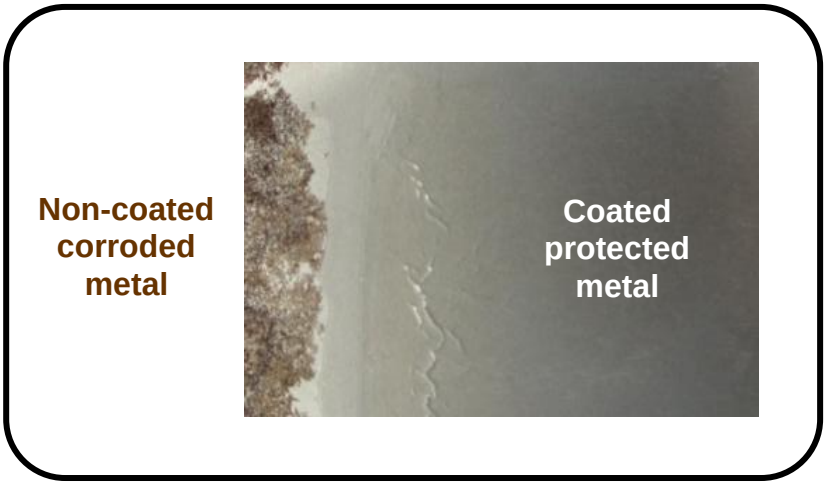

VI.1. Introduction

In this thesis, waterborne PU(U) dispersions containing disulfide bonds were developed aiming at their use as healable protective coatings. As commented in the previous chapters, several attempts to prepare this type of materials have been reported.[1–7] An important application of coatings is the use of these thin layers as protection of metals against corrosion.[8–12] Generally, electrochemical characterization methods are used to evaluate the protective performance of the coating, due to the electrochemical nature of corrosion processes. Recently, an AC/DC/AC accelerated electrochemical procedure has been used to evaluate the protective performance of cross-linked coatings after healing of scratches.[13]

AC/DC/AC consists of a first application of an alternating current (AC) (Figure VI.1, Phase I), *i.e.* an electrochemical impedance spectroscopy (EIS) step, for the evaluation of the initial state of the coating system. In this stage, the impedance (Z) of a system, *i.e.* the resistance of a circuit to the flow of an AC when it is immersed in an electrolyte, is measured over a desired frequency range.[14] Afterwards, a constant potential, *i.e.* direct current (DC), is applied in order to cathodically polarize the sample, so that local cathodic reactions can possibly be stimulated at the metal-coating interface leading to the formation of blisters, coating delamination and further corrosion processes around existing deffects (Figure VI.1, Phase II). Afterwards, the open circuit potential (OCP) of the coating is monitored during a specified relaxation period (Figure VI.1, Phase III). Finally, an alternating current is applied again to measure the new state of the coating (Figure VI.1, Phase IV). This procedure was repeated for 6 cycles, so that an accelerated aging of the coating was promoted and information on the persistence or failure of the coating could be obtained in the restricted time of the 24 h test, avoiding long-term

experiments such as EIS measurements.[13–17] An additional advantage for using this procedure instead of non-destructive methods like EIS is because AC/DC/AC facilitates coating failure at its weakest point, *i.e.* the healed interface, by applying an additional cathodic polarization step.[13] In this way, the method enables the analysis of the ability of coatings to restore their protective function after healing the scratch damage, even detecting the slightest failure points in a (partially) healed interface, which would not be detected optically or by EIS.

In this chapter, the application of the AC/DC/AC procedure will be described as an efficient electrochemical technique for the evaluation of the passive corrosion protection of the cross-linked PUUs developed in Chapter V.

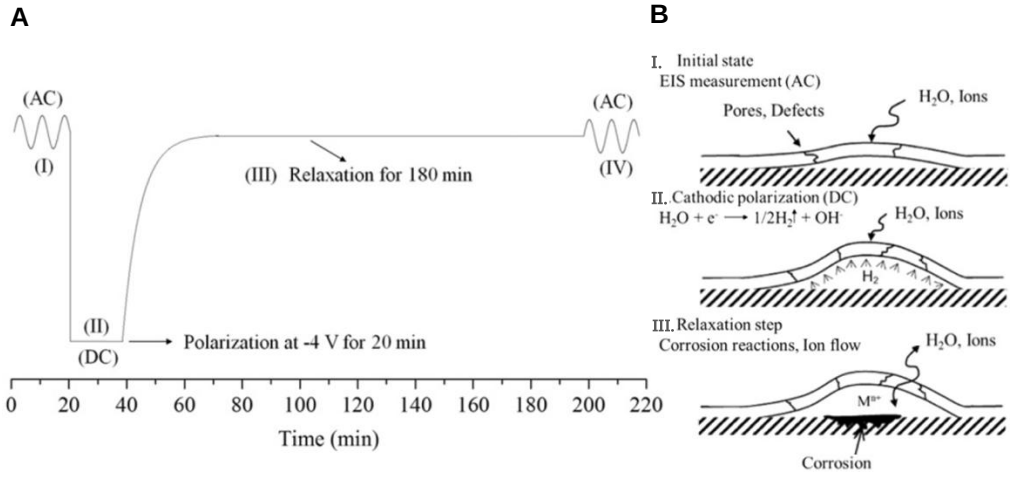

Figure VI.1 Schematic representation of an AC/DC/AC cycle (A) and the associated failure mechanism (B) of the coating due to the AC/DC/AC test procedure.
Reprinted from Abdolah Zadeh *et al.*,[13] Copyright (2016), with permission from Elsevier.

VI.2. Experimental

VI.2.1. Materials

The cross-linked dispersions, X-S and X-C, synthesized in Chapter V were used. Clad AA2024-T3 with a thickness of 1 mm was received at the TU Delft from Salomon's Metalen and used as a metallic substrate.

VI.2.2. Coating preparation

Prior to application of the coating, the AA2024-T3 panels were degreased with ethanol and rinsed with acetone. Afterwards, the metallic substrates were dried and coated with the dispersions using a calibrated aluminum single doctor blade. The coated samples were dried at room temperature for at least 1 h and afterwards for 12 h at 60ºC to assure that no residual water was trapped in the coating. Transparent, homogeneous and colorless coatings with an average dry thickness of 60±5 or 150±5 μm were obtained. To evaluate the sealing and healing efficiency of the cross-linked coatings, 5 mm long scratches were created at a rate of 10 mm.min^{-1}, using a sharp razor blade, so that an average scratch width of roughly 100 μm was obtained. In order to make sure that the coating was scratched across the complete thickness, the penetration depth of the razor blade was adapted so that the metallic substrate was reached. The scratched coatings were examined after damage and healing using a Keyence VHX-2000 series digital microscope in reflection mode with a 500x objective.

VI.2.3. Coating characterization *via* AC/DC/AC

The intact, scratched and healed coating systems were electrochemically characterized *via* AC/DC/AC measurements at room temperature following the reported procedures.[13,17,18] The measurements were performed in a conventional three-electrode cell configuration consisting of a saturated Ag/AgCl reference electrode, a carbon black rod of 5 mm diameter as the counter-electrode and the coated AA2024-T3 metallic samples as the working electrode. The samples were placed horizontally in the electrochemical cell with an area of 0.8 cm^2 exposed to the stagnant 0.5 M NaCl aqueous solution in equilibrium with air as testing electrolyte. This set-up was placed in a Faraday cage in order to avoid any interference of external electromagnetic fields with the tests.

The tests were carried out using an Autolab PGSTAT 302 N potentiostat which was coupled to a frequency analyser (FRA). For the first AC measurement (Figure VI.1, Phase I), 10 data points were acquired per frequency decade in the frequency range of 10^{-1} – 10^5 Hz, with a 10 mV root mean square (RMS) sinusoidal perturbation with respect to the open circuit potential OCP. After the first AC run was completed, the samples were cathodically polarized for 20 min at a constant potential of -4.0 V *versus* the Ag/AgCl reference electrode (Figure VI.1, Phase II). Subsequently, the variation in OCP versus time was monitored during a potential relaxation period of 3 h (Figure VI.1, Phase III). Finally, the cycle was completed with a new AC run (Figure VI.1, Phase IV). This AC/DC/AC cycle was repeated 6 times in order to observe accelerated aging of the coating in a total testing time of 24 h.

VI.3. Results and discussion

VI.3.1. Intact coating performance

First of all, the pristine samples of metal covered by a X-S or X-C coating with a thickness of 60 µm were tested. The results for the pristine samples are depicted in Figure VI.2, which shows that after 6 consecutive AC/DC/AC cycles there were no visible signs of delamination or corrosion (A).

Furthermore, Figure VI.2 B presents the Bode plots of the pristine coatings, in which both the total impedance |Z| and the phase angle are plotted on the Y-axes in function of the frequency on the X-axis. It can be observed that high impedance values were obtained at low frequencies for the initial cycle, which indicates both the X-S and X-C offer a good passive barrier.[13,16,18] In addition, it is clear that over the course of the 6 cycles the impedance remains high and no significant changes in the behaviour of the phase could be observed.

The evolution of the OCP in function of time (Figure VI.2 C) shows that the OCP value gradually goes back to the original OCP of the Clad AA2024-T3 metallic surface (-0.5 V) during the relaxation period of 3 h for all cycles. These results confirm the absence of any corrosion or delamination processes taking place after exposure to destructive conditions (NaCl-solution and repeated cathodic polarization). This demonstrates the good adhesion and passive protective barrier properties of both X-S and X-C coatings which are comparable to other healable PU coatings,[19–21] emphasizing that the present coatings are waterborne and provide a considerably high strength.

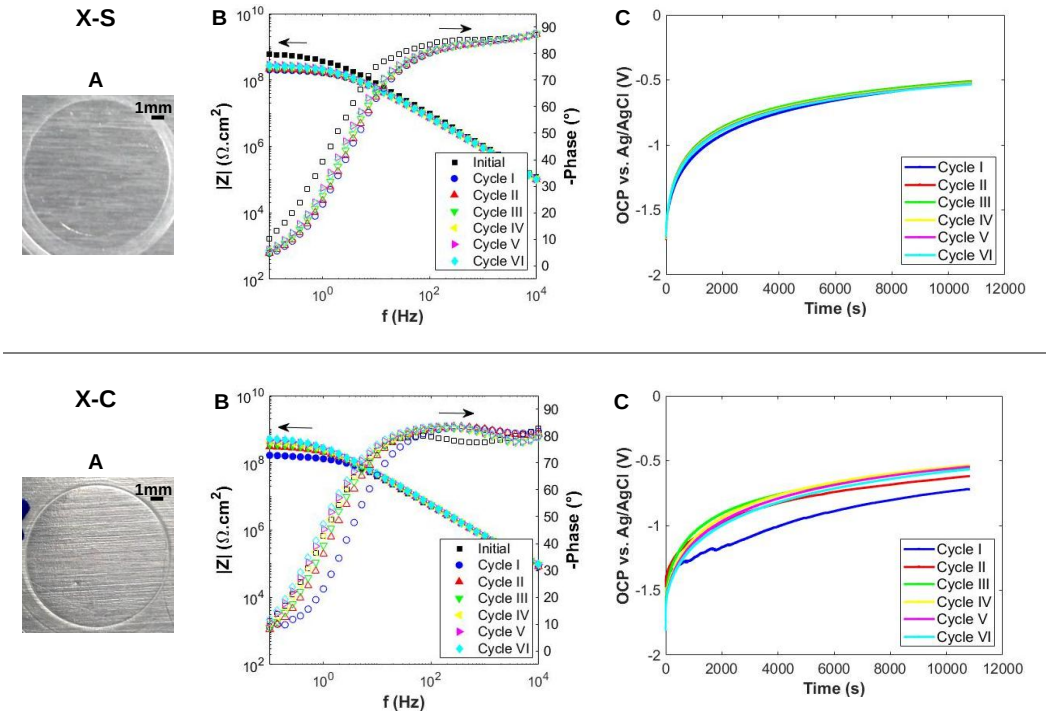

Figure VI.2. Results of AC/DC/AC testing for pristine coatings (60 µm) (X-S and X-C) showing sample (A), Bode plots (B) and evolution of open circuit potential (OCP) vs. time (C) for 6 cycles.

VI.3.2. Damaged and healed coating performance

However, when the 60 µm X-S and X-C coatings were damaged by an artificial scratch of a width of 100 µm penetrating the complete coating thickness and making contact with the metallic substrate, major defects could be observed macroscopically after 6 cycles of the AC/DC/AC procedure. It is clear in Figure VI.3 A that delamination of the coating took place and even corrosion products could be detected in and around the scratch. The Bode plots (Figure VI.3 B) show that the coatings failed in their function of providing a protective barrier in

the presence of a scratch as the impedance decreased during the subsequent cycles. In addition, a fluctuating OCP (Figure VI.3 C) indicates that massive corrosion processes and delamination took place during the AC/DC/AC measurement. It is noteworthy to mention that some cycles were removed in the representations of the results, because extreme fluctuations in values for the impedance and phase shift were obtained due to intense corrosion activities.

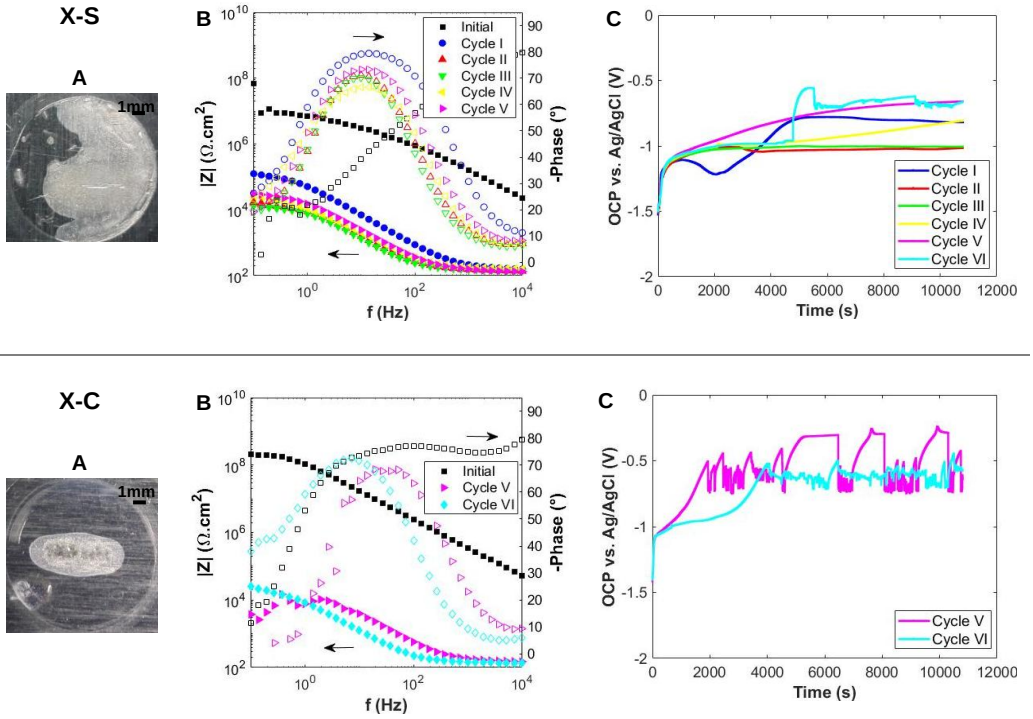

Figure VI.3. Results of AC/DC/AC testing for scratched coatings (60 µm) (X-S and X-C) tested just after damage showing sample (A), Bode plots (B) and evolution of OCP vs. time (C) for 6 cycles.

Alternatively, the scratched 60 µm thick coatings were healed at 80 ºC for 14 d and subjected to the AC/DC/AC test. Figure VI.4 A shows that delamination and corrosion could be observed visually. This was confirmed by the loss of impedance in the Bode plots and the fluctuations of OCP in time in Figures VI.4 B and C, which demonstrates that the damaged coatings were unable to recover the protective performance of the pristine coating.

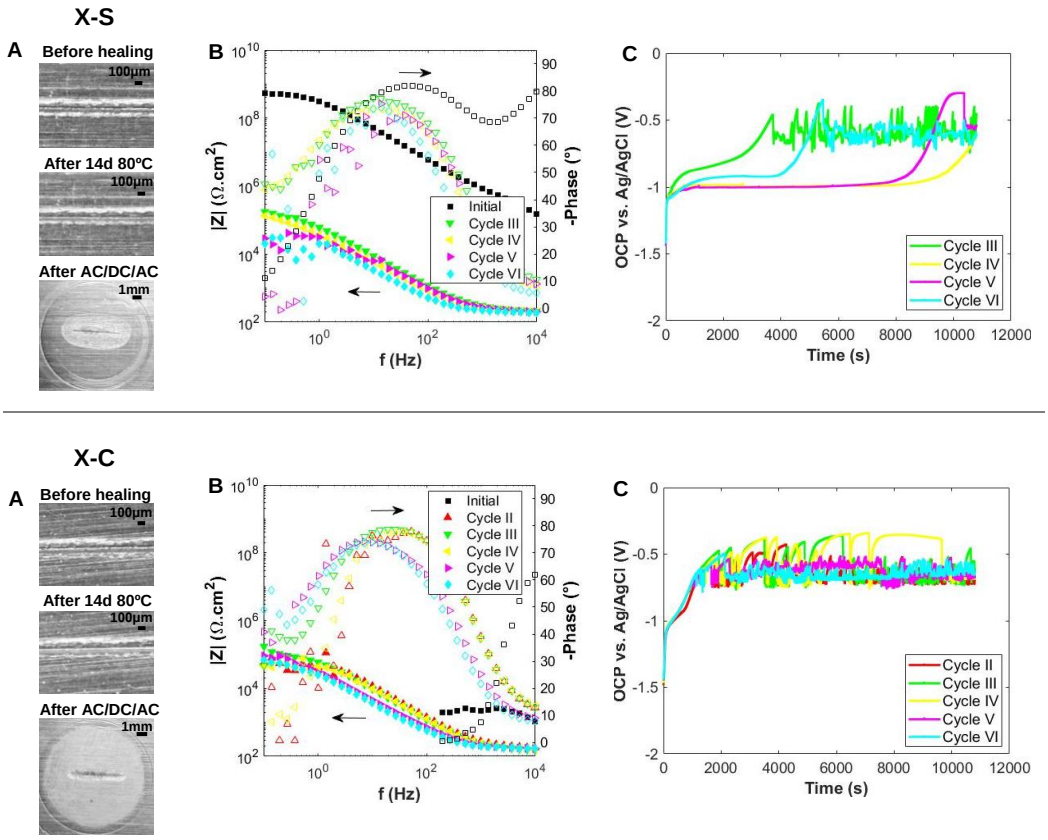

Figure VI.4. Results of AC/DC/AC testing for coatings (60 µm) (X-S and X-C) healed for 14d at 80ºC showing sample (A), Bode plots (B) and evolution of the OCP vs. time (C) for 6 cycles of AC/DC/AC.

As fracture mechanics experiments presented in Chapter V showed an increased healing efficiency of 40-50% for X-S and 20-30% for X-C after 24 d of healing at 80ºC, the scratched coatings were also healed for 24d at 80ºC and analyzed by AC/DC/AC. However, even after 24 d, no significant scratch closure could be observed and additionally again corrosion and delamination took place (Figure VI.5).

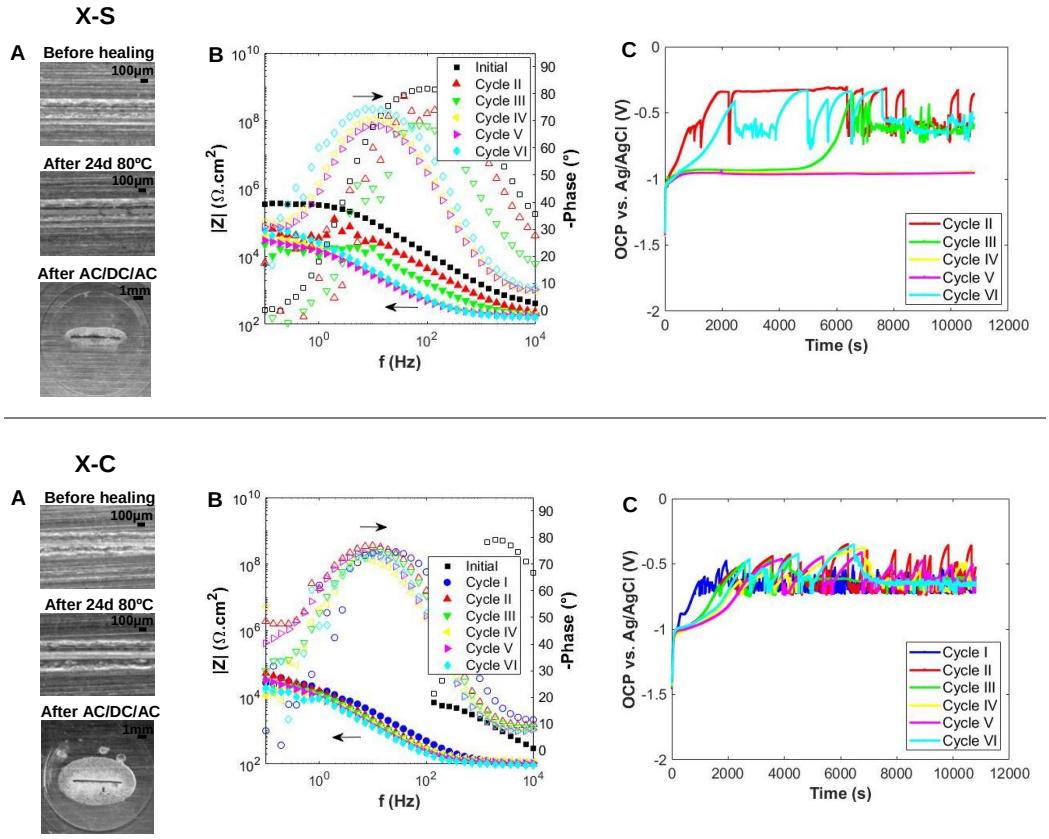

Figure VI.5. Results of AC/DC/AC testing for coatings (60 µm) (X-S and X-C) healed for 24 d at 80ºC showing sample (A), Bode plots (B) and evolution of the OCP vs. time (C) for 6 cycles.

This lack of healing in the 60 µm coatings compared to some degree of self-healing demonstrated for thick fracture specimens could be due to the fact that there was not enough material in the thin film to fill a scratch gap of 100 µm that was larger than the coating thickness of 60 µm. This effect has already been described for other healable cross-linked protective coatings by Abdolah Zadeh *et al.*, who stated that the healed (under slight pressure) coating exhibited long-term corrosion protection if the scratch width was smaller than the coating thickness, while only short-term closure of the scratch-induced interface could be obtained when the coating thickness was larger than the scratch width.[22] In this way, they confirmed that the metallic substrate had a restrictive effect on the polymer's macroscopic flow and healing ability, especially when the created gap is bigger than the coating thickness. Finally, it is important to mention that, as described by Rey *et al.*, not only the thickness plays a role in the scratch closure, as factors such as the elasticity of the material also affect the mobility of the coating.[23]

VI.3.3. Effect of the film thickness on coating performance

In order to check the effect of the coating thickness on the healing ability of the thin layers, the metals were coated with 150 µm thick films that were subjected to the same test as the 60 µm (100 µm wide scratch and AC/DC/AC applied just after scratching the film). Additionally, in a second sample of X-C, two perpendicular scratches were made in order to increase the possibility for the electrolyte to reach the metal-coating interface.

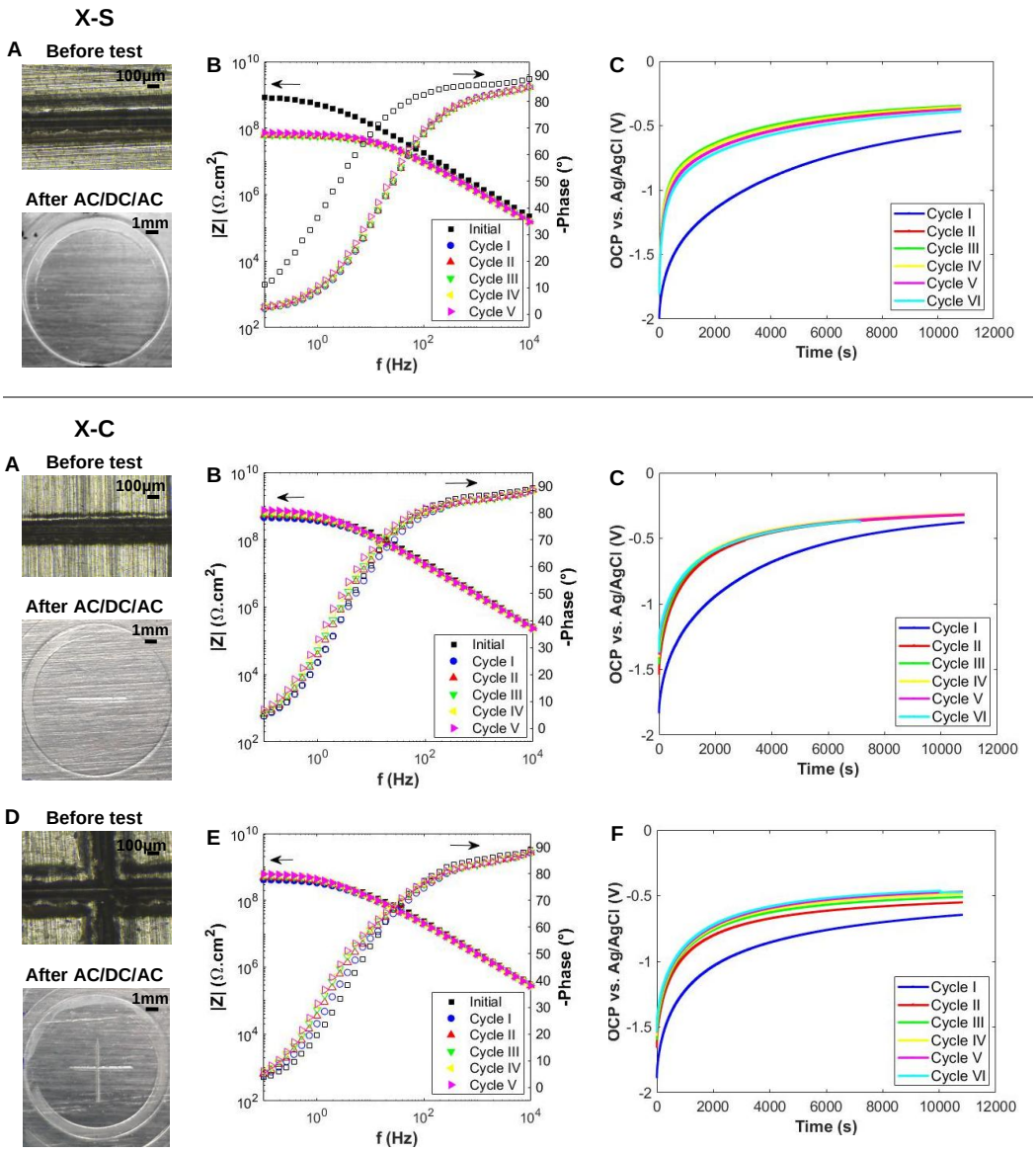

Figure VI.6. Results of AC/DC/AC testing for scratched (but not healed) coatings (150 µm) of X-S (linear) and X-C (linear and perpendicular) showing sample (A), Bode plots (B) and evolution of the OCP vs. time (C) for 6 cycles of the AC/DC/AC procedure.

Figure VI.6 shows that in all cases, neither delamination nor corrosion could be detected visually or by analyzing the AC/DC/AC results obtained after 6 consecutive cycles, as the high impedance values could be retained and the OCP gradually went back to the initial OCP (-0.5 V) during the relaxation period for all cycles. This shows that when the cross-linked coating was thicker than the scratch width, it had sufficient elastic recovery to close the scratch immediately after damage. In this way, the coating could behave as a pristine coating during the AC/DC/AC experiments and could recover its protective function. Contrary to the example of Abdolah Zadeh *et al.*,[22] sufficient sealing performance could be obtained without the need of applying pressure or increasing temperature.

VI.4. Conclusions

In conclusion, from the analysis of the aforementioned AC/DC/AC results, it could be stated that the pristine coatings of X-S or X-C with a thickness of only 60 µm show good adhesion and barrier properties. However, when a scratch with a width greater than the thickness of the coating was created, the barrier was lost and delamination and corrosion could be observed even after 24 d of healing at 80ºC. On the other hand, when the thickness of the coating was greater than the width of the scratch, the elastic recovery of the cross-linked PUUs immediately closed the scratch leading to efficient protection the metallic substrate. These results highlight the challenge of achieving self-healing in thin hard coatings.

VI.5. References

1. Cho, S. H., White, S. R. & Braun, P. V. Self-Healing Polymer Coatings. *Adv. Mater.* **21,** 645–649 (2009).
2. García, S. J., Fischer, H. R. & van der Zwaag, S. A critical appraisal of the potential of self healing polymeric coatings. *Prog. Org. Coatings* **72,** 211–221 (2011).
3. Wan, T. & Chen, D. Synthesis and properties of self-healing waterborne polyurethanes containing disulfide bonds in the main chain. *J. Mater. Sci.* **52,** 197–207 (2017).
4. Wan, T. & Chen, D. Mechanical enhancement of self-healing waterborne polyurethane by graphene oxide. *Prog. Org. Coatings* **121,** 73–79 (2018).
5. Xiao, Y., Huang, H. & Peng, X. Synthesis of self-healing waterborne polyurethanes containing sulphonate groups. *RSC Adv.* **7,** 20093–20100 (2017).
6. Aguirresarobe, R. H., Martin, L., Aramburu, N., Irusta, L. & Fernandez-Berridi, M. J. Coumarin based light responsive healable waterborne polyurethanes. *Prog. Org. Coatings* **99,** 314–321 (2016).
7. Aguirresarobe, R. H., Martin, L., Fernandez-Berridi, M. J. & Irusta, L. Autonomic healable waterborne organic-inorganic polyurethane hybrids based on aromatic disulfide moieties. *EXPRESS Polym. Lett.* **11,** 266–277 (2017).
8. Walter, G. W. A critical review of the protection of metals by paints. *Corros. Sci.* **26,** 27–38 (1986).
9. Stratmann, M., Feser, R. & Leng, A. Corrosion protection by organic films. *Electrochim. Acta* **39,** 1207–1214 (1994).
10. Stankiewicz, A. & Barker, M. B. Development of self-healing coatings for corrosion protection on metallic structures. *Smart Mater. Struct.* **25,** 84013 (2016).
11. AbdolahZadeh, M., van der Zwaag, S. & Garcia, S. J. in *Self-healing Materials* (eds. Hager, M. D., van der Zwaag, S. & Schubert, U. S.) 185–218 (Springer International Publishing, 2016). doi:10.1007/12_2015_339
12. Zhang, F. *et al.* Self-healing mechanisms in smart protective coatings: a review. *Corros. Sci.* (2018). doi:https://doi.org/10.1016/j.corsci.2018.08.005
13. Abdolah Zadeh, M., van der Zwaag, S. & García, S. J. Assessment of healed scratches in intrinsic healing coatings by AC/DC/AC accelerated electrochemical procedure. *Surf. Coatings Technol.* **303,** 396–405 (2016).
14. Bose, R. K., Lafont, U., Vega, J. M., Garcia, S. J. & van der Zwaag, S. in *Self-Healing Polymers* 335–359 (Wiley-VCH Verlag GmbH & Co. KGaA, 2013). doi:10.1002/9783527670185.ch14
15. Rodríguez, M. T., Gracenea, J. J., García, S. J., Saura, J. J. & Suay, J. J. Testing the

influence of the plasticizers addition on the anticorrosive properties of an epoxy primer by means of electrochemical techniques. *Prog. Org. Coatings* **50,** 123–131 (2004).

16. Allahar, K. N., Su, Q., Bierwagen, G. P. & Hyung, L. Do. Monitoring Of The Ac-Dc-Ac Degradation Of Organic Coatings Using Embedded Electrodes. *CORROSION* (2007).

17. García, S. J. & Suay, J. Optimization of deposition voltage of cataphoretic automotive primers assessed by EIS and AC/DC/AC. *Prog. Org. Coatings* **66,** 306–313 (2009).

18. García, S. J. & Suay, J. A comparative study between the results of different electrochemical techniques (EIS and AC/DC/AC): Application to the optimisation of the cataphoretic and curing parameters of a primer for the automotive industry. *Prog. Org. Coatings* **59,** 251–258 (2007).

19. Jorcin, J.-B. *et al.* Investigation of the self-healing properties of shape memory polyurethane coatings with the 'odd random phase multisine' electrochemical impedance spectroscopy. *Electrochim. Acta* **55,** 6195–6203 (2010).

20. Deflorian, F., Rossi, S. & Scrinzi, E. Self-healing supramolecular polyurethane coatings: preliminary study of the corrosion protective properties. *Corros. Eng. Sci. Technol.* **48,** 147–154 (2013).

21. Lutz, A. *et al.* A Shape-Recovery Polymer Coating for the Corrosion Protection of Metallic Surfaces. *ACS Appl. Mater. Interfaces* **7,** 175–183 (2015).

22. Abdolah Zadeh, M., van der Zwaag, S. & Garcia, S. J. Adhesion and Long-Term Barrier Restoration of Intrinsic Self-Healing Hybrid Sol–Gel Coatings. *ACS Appl. Mater. Interfaces* **8,** 4126–4136 (2016).

23. Rey, R., Javierre, E., García, S. J., van der Zwaag, S. & García-Aznar, J. M. Numerical study of the scratch-closing behavior of coatings containing an expansive layer. *Surf. Coatings Technol.* **206,** 2220–2225 (2012).

24. de Gennes, P.-G., Brochard-Wyart, F. & Quere, D. *Capillarity and Wetting Phenomena: Drops, Bubbles, Pearls, Waves*. (Springer, 2004). doi:10.1007/978-0-387-21656-0

Chapter VII. Conclusions

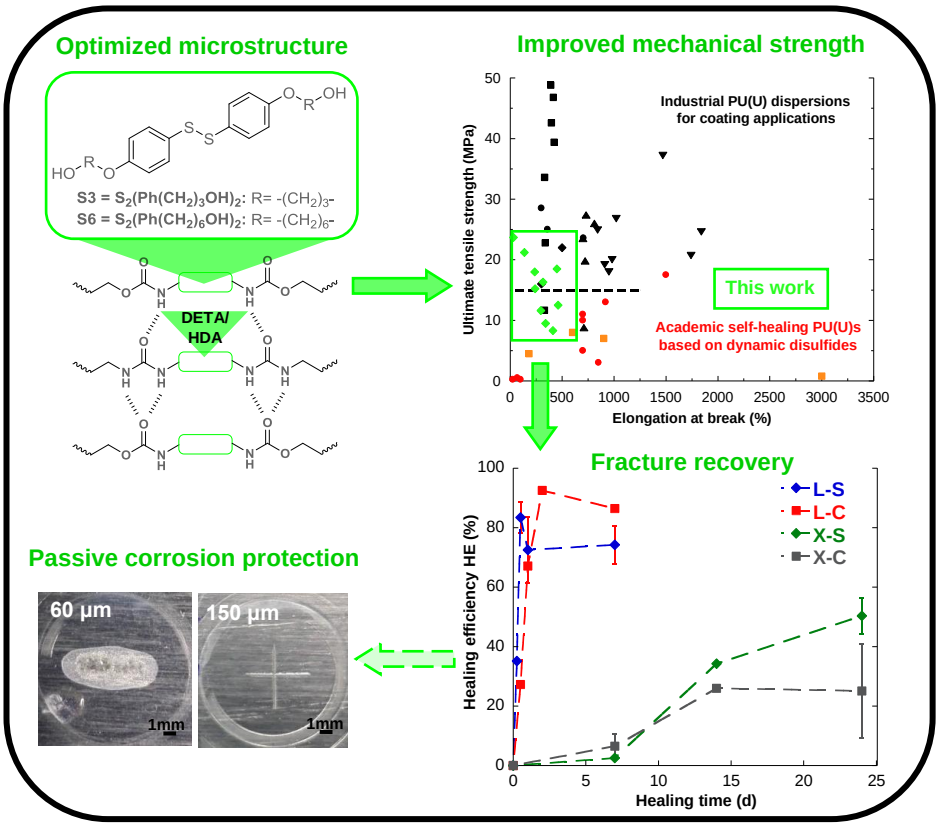

In this thesis, we aimed at closing the gap between academic and industrial research so that strong self-healing materials could be developed which would be attractive for coating applications. We desired to do this by incorporating the rapidly exchanging aromatic disulfide bonds into poly(urethane-urea) backbones, as this combination would allow us to achieve healing through supramolecular interactions as well as dynamic covalent bond exchange, while maintaining enough mechanical strength for further application as described in **Chapter I**.

However, due to the ambiguity regarding the disulfide exchange found in literature, we first needed to clarify the underlying mechanisms for this exchange, so that we could incorporate these disulfide bonds into the PU materials with complete understanding of the self-healing event that they would induce. Using spectroscopic techniques, it was possible to demonstrate that the general exchange mechanism was radical mediated rather than occurring *via* metathesis as described in **Chapter II**. In this mechanism, cleavage of disulfide bonds leads to the formation of two sulfur-based radicals which can recombine or induce exchange by undergoing a chain transfer reaction as depicted in Figure VII.1. However, in the presence of nucleophiles, such as TEA and TBP, this exchange can be enhanced as the disulfides yield thiolate anions which can similarly undergo a series of transfer reactions (Figure VII.1).

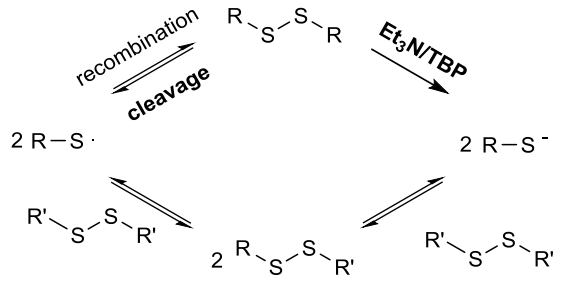

Figure VII.1. Disulfide exchange through the formation of S-based radicals and S-based anions.

After obtaining better insight in the underlying mechanism of disulfide exchange, in **Chapter III**, we could start to incorporate aromatic disulfides into PU backbones so that a series of waterborne PU(U) dispersions was obtained for which the mechanical strength could be increased by playing with the hard building blocks, namely DMPA and aromatic disulfide compounds. More specifically, by increasing the DMPA content, ultimate tensile strengths (UTS) of up to 17 MPa could be obtained. However, scratch closure tests and rheological measurements showed that this limited the mobility of the polymer which would not be advantageous for healing.

Alternatively, also different aromatic disulfide building blocks were introduced (Figure VII.2), which demonstrated the restrictions of the commercial bis(4-aminophenyl)- and bis(4-hydroxyphenyl)disulfide towards solubility, reactivity and especially mobility, as an increasing amount of the self-healing moiety did not offer a higher material mobility which is crucial for self-healing. Therefore, the more flexible bis[4-(3'-hydroxypropoxy)phenyl]disulfide $S_2(Ph(CH_2)_3OH)_2$ was synthesized, so that the amount of the self-healing moiety incorporated in the PU backbone could be increased without compromising the mechanical properties of the materials. The successful implementation of this newly modified aromatic disulfide led to PU materials with an increased mechanical strength (UTS=10-23 MPa) at the service temperature, while a good mobility could be observed at the healing temperature of 80ºC.

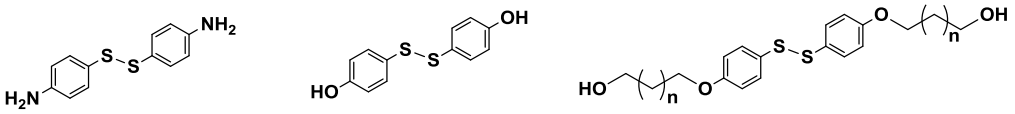

$S_2(PhNH_2)_2$ **$S_2(PhOH)_2$** **n=1: $S_2(Ph(CH_2)_3OH)_2$ (S or S3)** **n=4: $S_2(Ph(CH_2)_6OH)_2$ (S6)**

Figure VII.2. Chemical structure of the different aromatic disulfides incorporated into the PU.

This proved the fact that, next to the reversible chemistries incorporated, also the structure of the building blocks, i.e. the polymer architecture, greatly affects the mobility and healing ability of the material. Therefore, **Chapter IV** mainly focused on this topic in order to further optimize the developed waterborne PU materials of Chapter III. More specifically, amine-terminated chain extenders were introduced after the synthesis of the waterborne PU prepolymer in order to incorporate urea units which give rise to additional H-bonding so that the mechanical strength, water resistance and healing ability of the PUUs could be increase. Additionally, by varying the chain extender from difunctional (HDA) to trifunctional (DETA), the polymer structure could be altered from linear to a network. Although the introduction of cross-linking points strongly decreased the mobility of the polymer, reorganization of the network was still possible due to the presence of dynamic disulfide bonds. Alternatively replacing the disulfide $S_2(Ph(CH_2)_3OH)_2$ (S3) by its more flexible alternative $S_2(Ph(CH_2)_6OH)_2$ (S6) increased the mobility of the material to an even higher extent than could already be obtained, so that possibly by incorporating more self-healing moiety even stronger and simultaneously more mobile materials could be developed.

Thus, by varying and optimizing the various building blocks, a polymer architecture could be developed so that self-healing materials are obtained which present high mechanical properties (UTS up to 20 MPa), while showing an increased mobility at moderate temperatures. Interestingly, these developed PUUs were described to be especially attractive to be applied in coating applications as they tend to overcome the gap that currently exists between industrial PU(U) dispersions for coatings and academic self-healing PU(U)s based on disulfide bonds regarding the tensile strength that can be achieved as depicted in green in Figure VII.3.

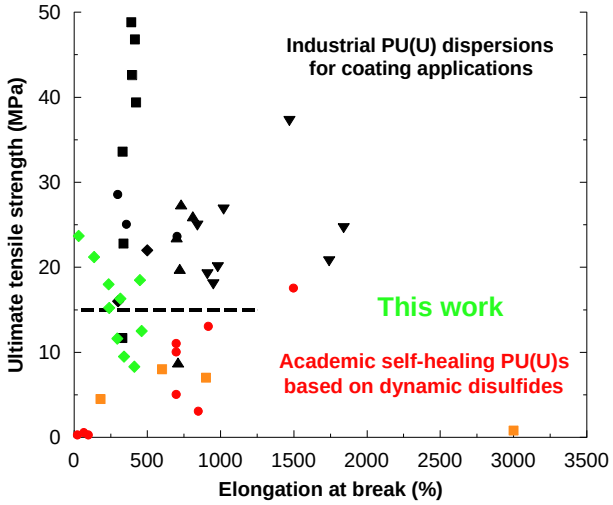

Figure VII.3. The results obtained in Chapter IV (green) compared to the gap existing between other academic self-healable PU(U)s and industrial examples of PU(U) materials.

Subsequently, in **Chapter V**, we focused on the effect of the dynamic covalent bonds in both linear and cross-linked PUUs, by comparing materials containing dynamic disulfide bonds through incorporation of the aromatic $S_2(Ph(CH_2)_3OH)_2$ moiety, with C-based materials which could be obtained by incorporating the counterpart 1,2-[4-(3-hydroxypropoxy)phenyl]ethane ($C_2(Ph(CH_2)_3OH)_2$) compounds that lacks these dynamic bonds. This was carried out *via* thermal, mechanical, rheological and scratch closure analysis of the PUU systems and additionally by quantitative determination of the recovery of their fracture mechanical properties upon healing after damage. In this way, it could be demonstrated that, for the strong PUU developed in this thesis, the main role of the dynamic disulfide bonds is to enhance the mobility of the polymer chains and networks allowing interpenetration of the polymer through the interface and formation of H-bonds, while the latter H-bonds provide the mechanical strength to the coating as was shown for the C-based PUU counterparts.

Finally, in **Chapter VI**, the ability of two (partially) healable cross-linked PUUs to provide passive corrosion protection to a metal substrate was characterized by means of AC/DC/AC measurements. From these results, it could be observed that the intact coatings showed good adhesion and barrier properties. When the coating was damaged and a scratch width (100 µm) greater than the thickness of the coating (60 µm) was created, the barrier was lost and delamination and corrosion processes were observed, even after 24 d of healing at 80ºC. However, when the thickness of the coating (150 µm) was greater than the scratch width (100 µm), elastic recovery of the cross-linked PUUs immediately closed the scratch leading to effective protection of the metallic substrate. The aforementioned results obtained from the fracture mechanical analysis and the accelerated electrochemical method therefore highlight the challenge of achieving self-healing in cross-linked materials which would be of interest for thin hard coatings, where the thickness of the protective layer seemingly plays a crucial role.

In conclusion, new self-healing waterborne PU(U) dispersions were synthesized by incorporating dynamic aromatic disulfide moieties. The microstructure of these PU(U)s was optimized by systematically playing with the building blocks incorporated into the backbone. This eventually improved the mechanical properties of the PU(U)s at room temperature, while achieving sufficient mobility for scratch closure at moderate temperatures. In this way, we showed that the gap which exist between academic research on self-healing PU(U)s and industrial PU(U) coating applications could be overcome. Moreover, it became clear that for such strong coatings the main role of the dynamic disulfide bonds is to enhance the mobility, while H-bonds provide mechanical strength to the coating. Nevertheless, further research is encouraged as still challenges exist in applying strong PUUs as healable protective coatings.

Appendix I. Supporting Information Chapter III

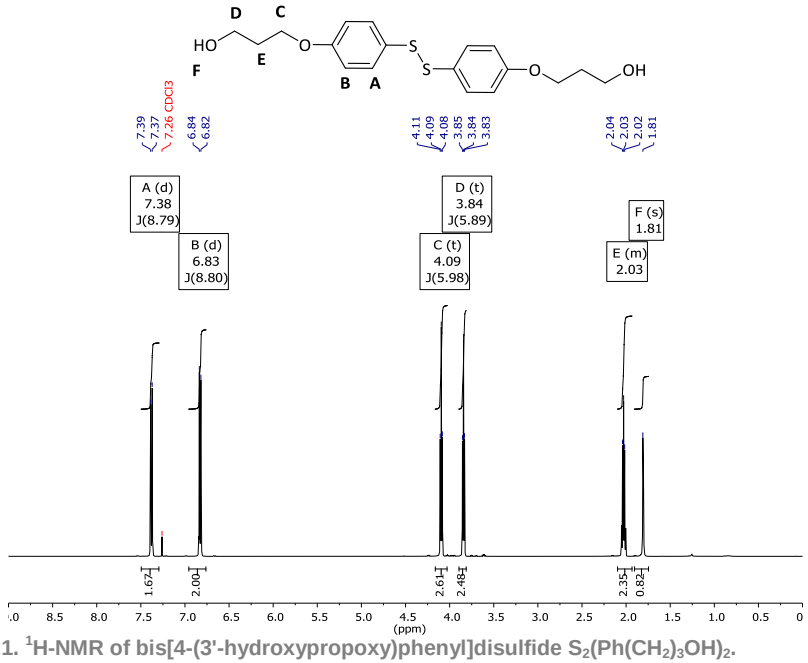

Figure A I.1. ^{1}H-NMR of bis[4-(3'-hydroxypropoxy)phenyl]disulfide $S_2(Ph(CH_2)_3OH)_2$.

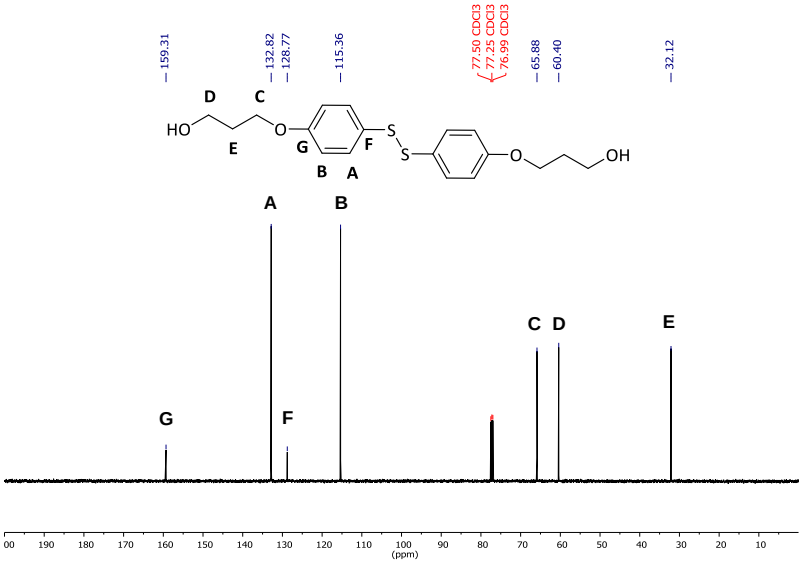

Figure A I.2. ^{13}C{H}-NMR of bis[4-(3'-hydroxypropoxy)phenyl]disulfide $S_2(Ph(CH_2)_3OH)_2$.

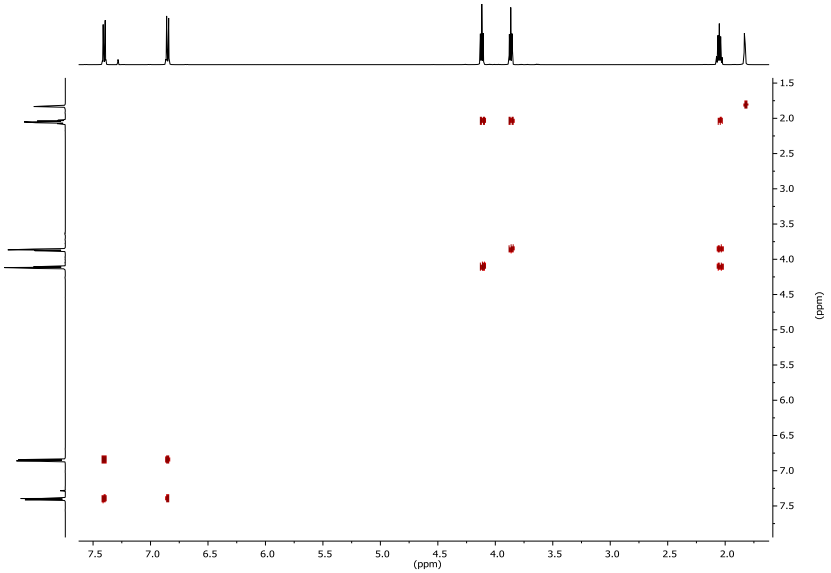

Figure A I.3. g-COSY (correlation spectroscopy) of compound $S_2(Ph(CH_2)_3OH)_2$.

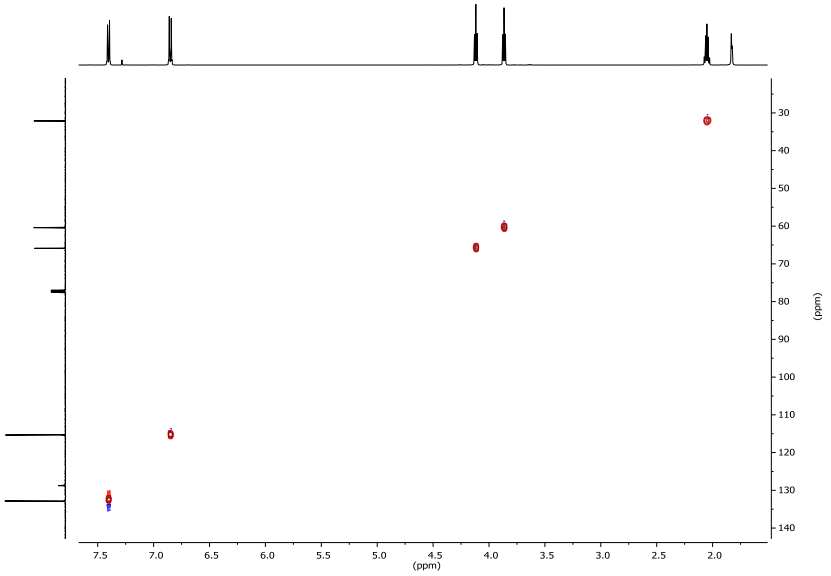

Figure A I.4. g-HSQC (Heteronuclear Single-Quantum Correlation spectroscopy) of compound $S_2(Ph(CH_2)_3OH)_2$.

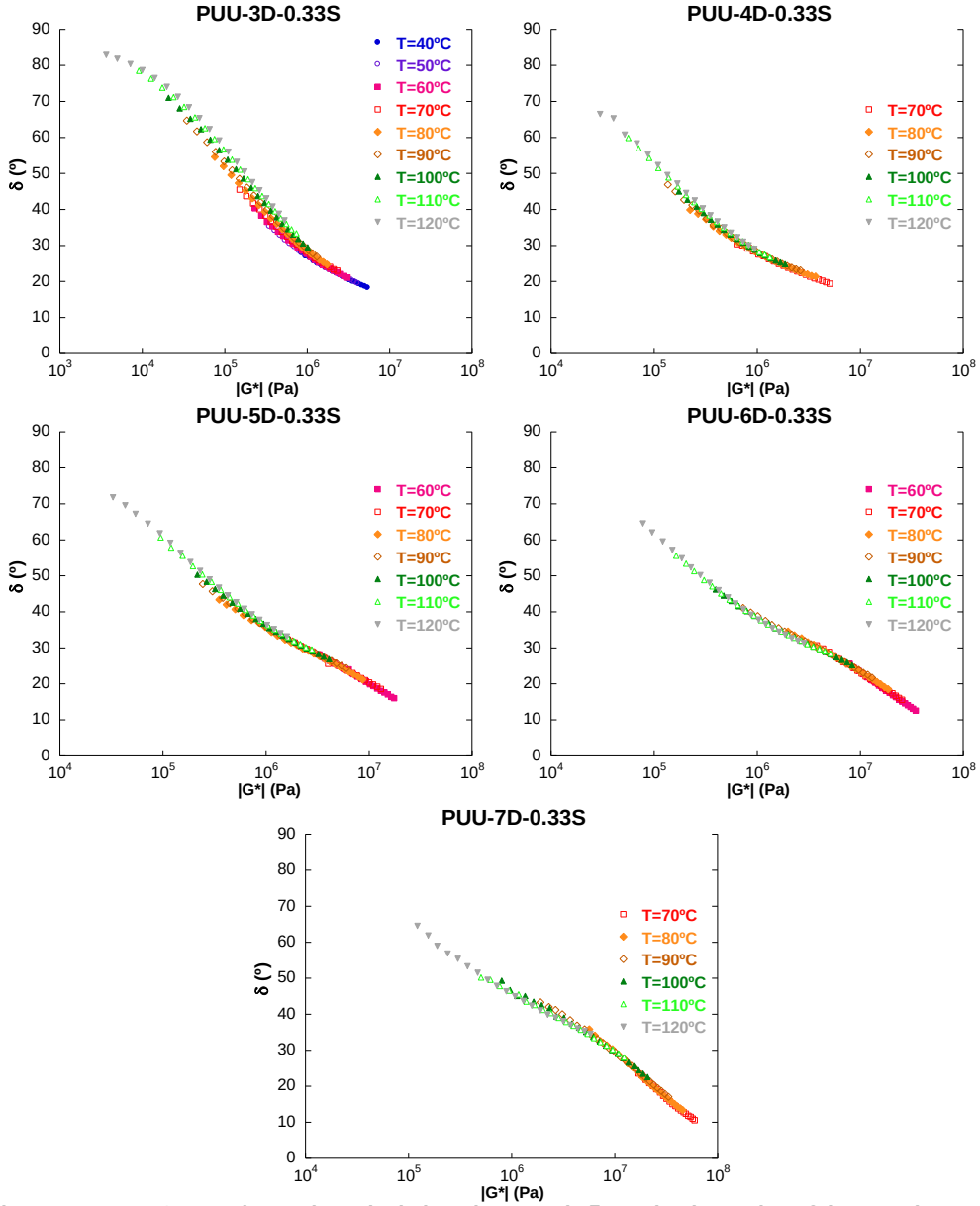

Figure A I.5. van-Gurp-Palmen-plots, depicting phase angle δ *vs.* absolute value of the complex shear modulus $|G^*|$, of PUUs based on $S_2(PhNH_2)_2$ with varying DMPA content.

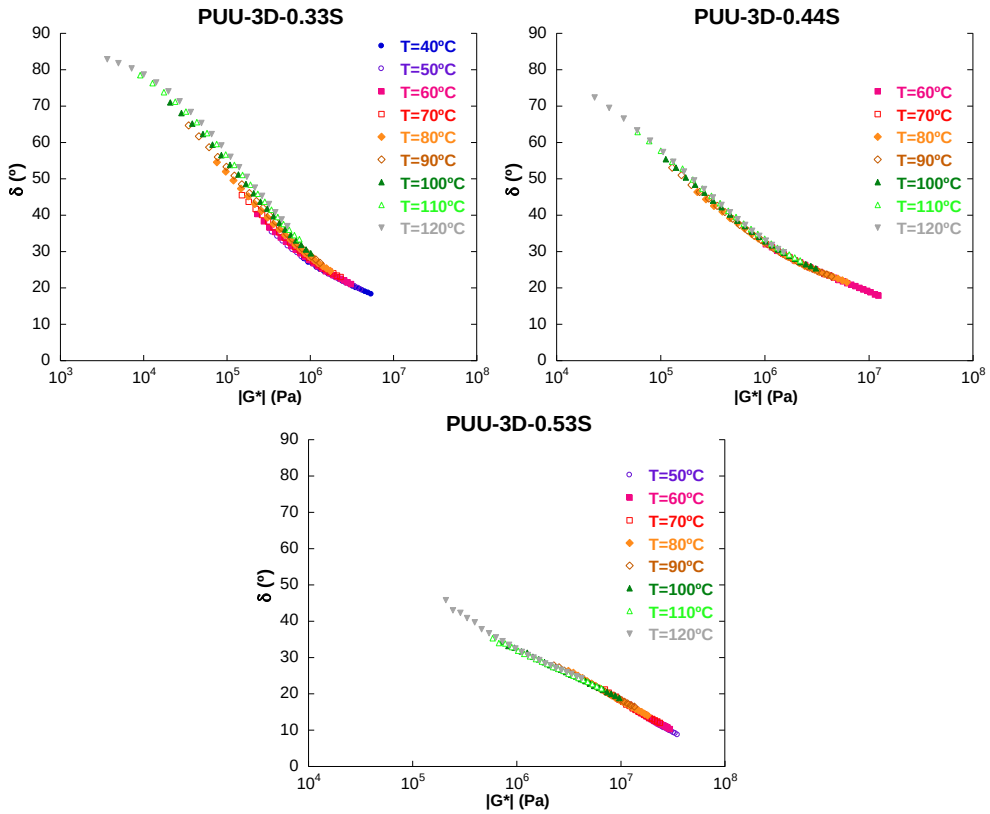

Figure A I.6. van-Gurp-Palmen-plots, depicting phase angle δ *versus* the absolute value of the complex shear modulus $|G^*|$, of PUUs based on a varying amount of $S_2(PhNH_2)_2$.

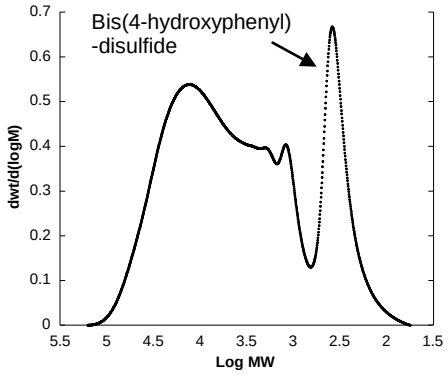

Figure A I.7. MWD obtained by GPC (UV) of PU based on $S_2(PhOH)_2$ after 60h of reaction.

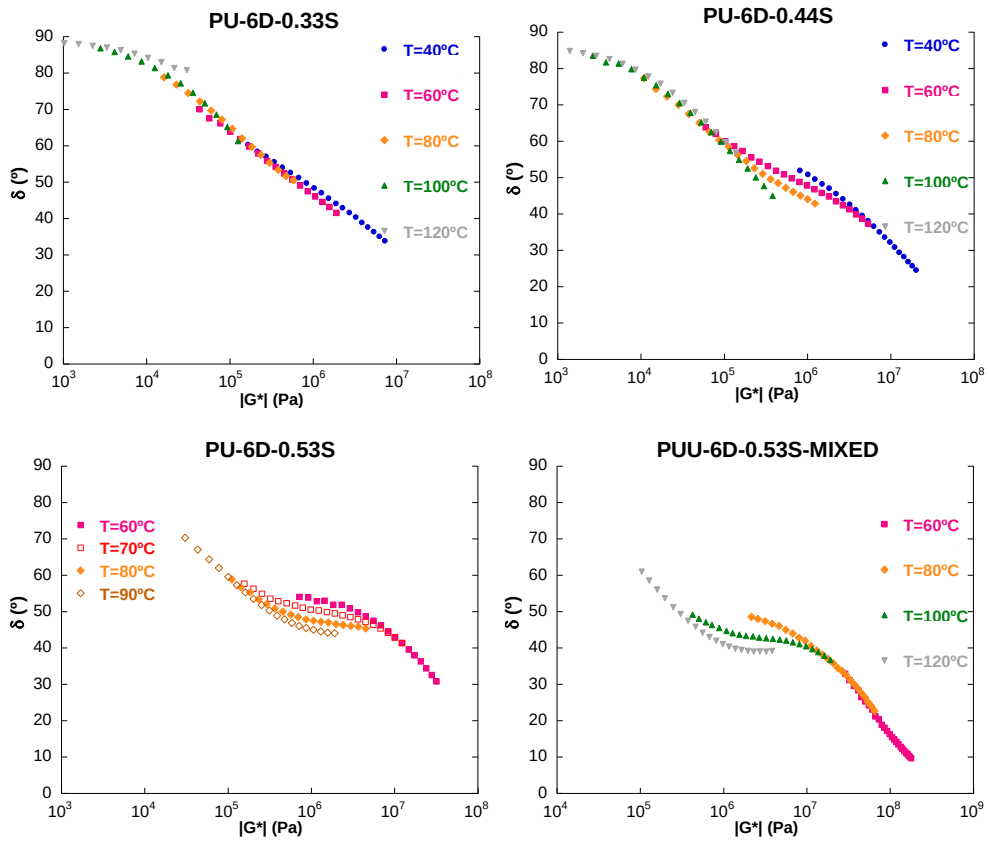

Figure A I.8. van-Gurp-Palmen-plots, depicting phase angle δ *versus* the absolute value of the complex shear modulus $|G^*|$, of PU(U)s with varying amount of $S_2(Ph(CH_2)_3OH)_2$.

Appendix II. Supporting Information Chapter IV

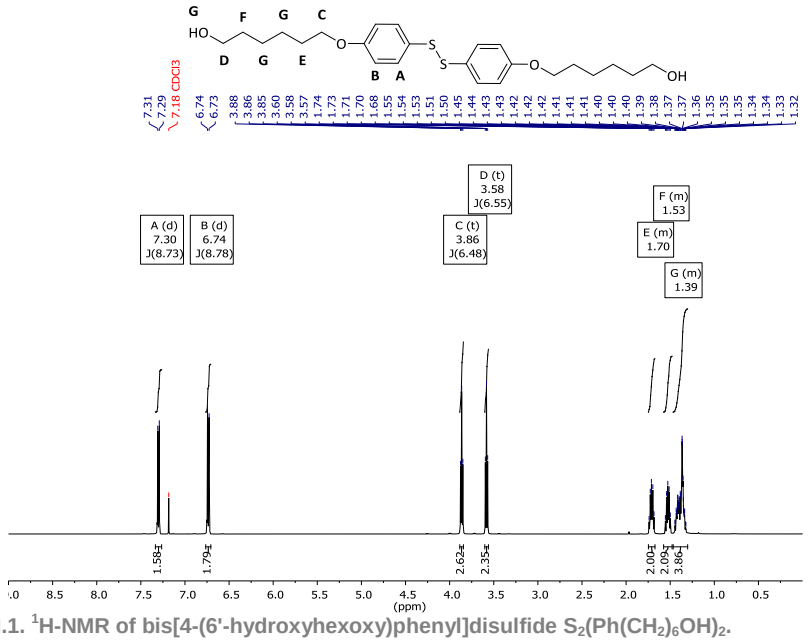

Figure A II.1. ^{1}H-NMR of bis[4-(6'-hydroxyhexoxy)phenyl]disulfide $S_2(Ph(CH_2)_6OH)_2$.

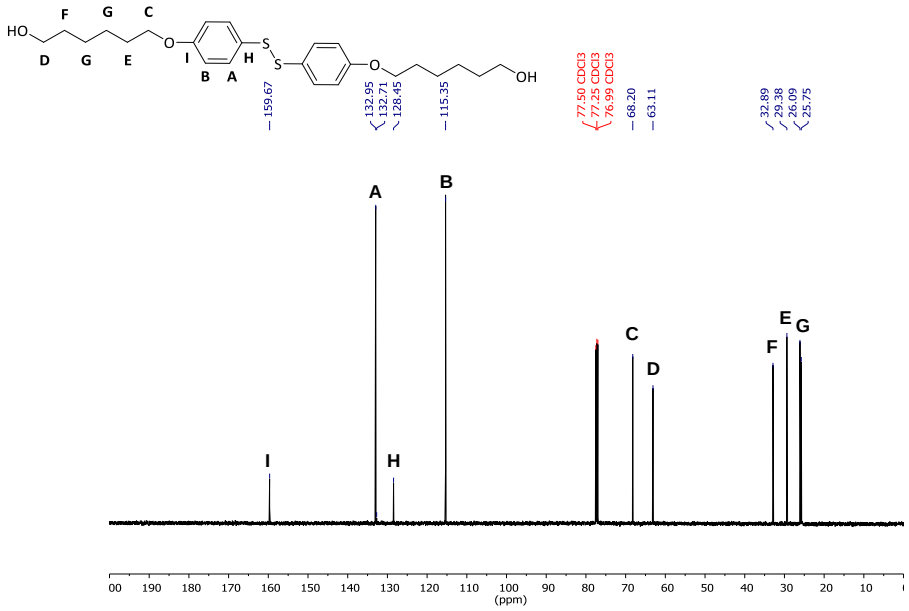

Figure A II.2. ^{13}C{H}-NMR of bis[4-(6'-hydroxyhexoxy)phenyl]disulfide $S_2(Ph(CH_2)_6OH)_2$.

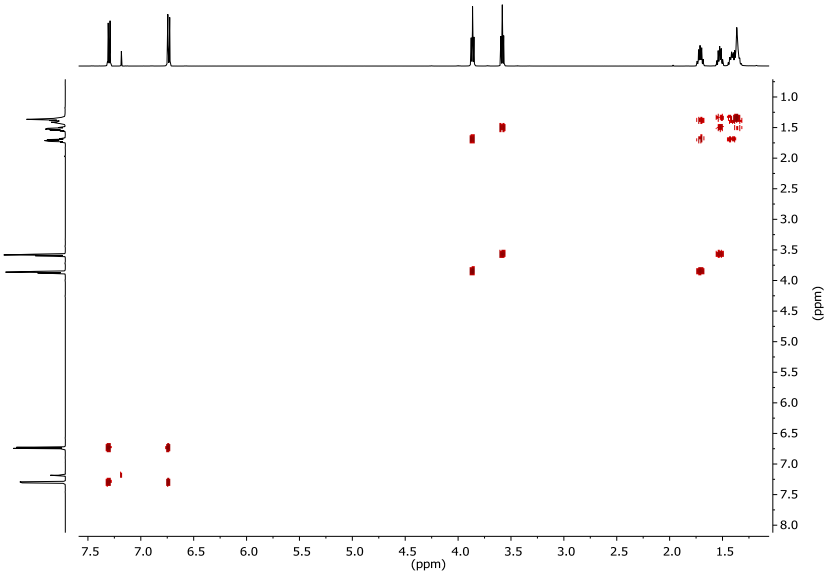

Figure A II.3. g-COSY of bis[4-(6'-hydroxyhexoxy)phenyl]disulfide $S_2(Ph(CH_2)_6OH)_2$.

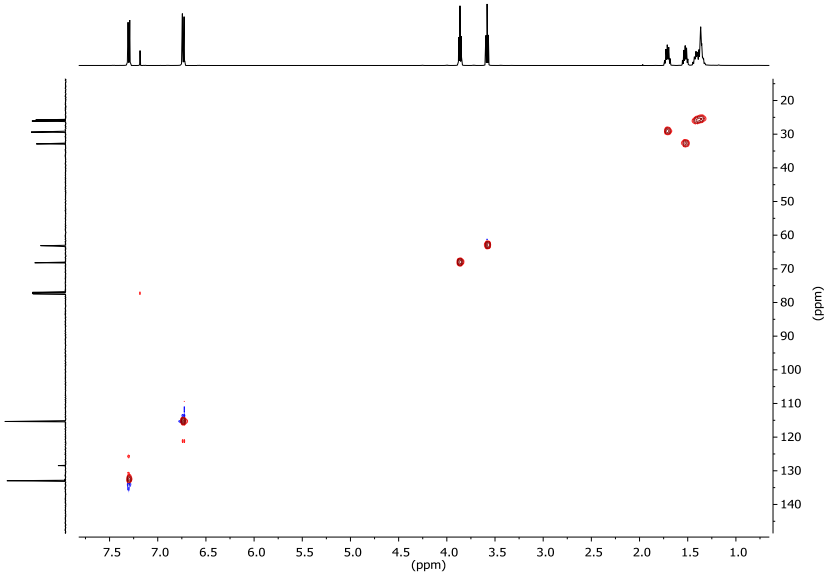

Figure A II.4. g-HSQC of bis[4-(6'-hydroxyhexoxy)phenyl]disulfide $S_2(Ph(CH_2)_6OH)_2$.

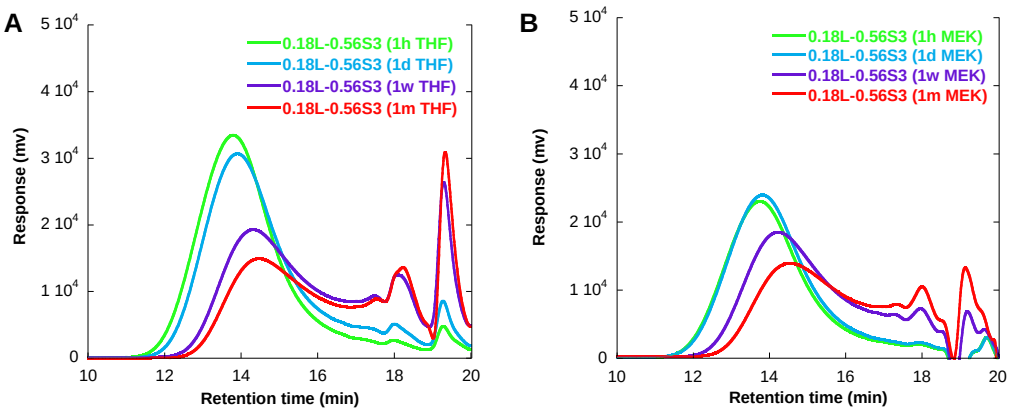

Figure A II.5. Chromatograms obtained by GPC (RI) for a set of dissolution times of 1.8L-0.56S3 in THF (A) and MEK (B).

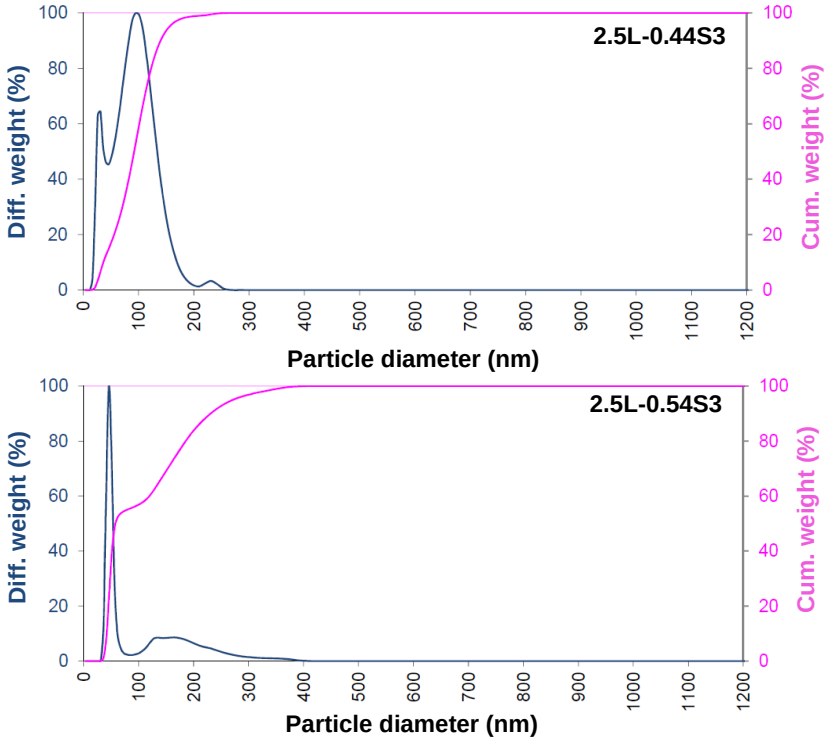

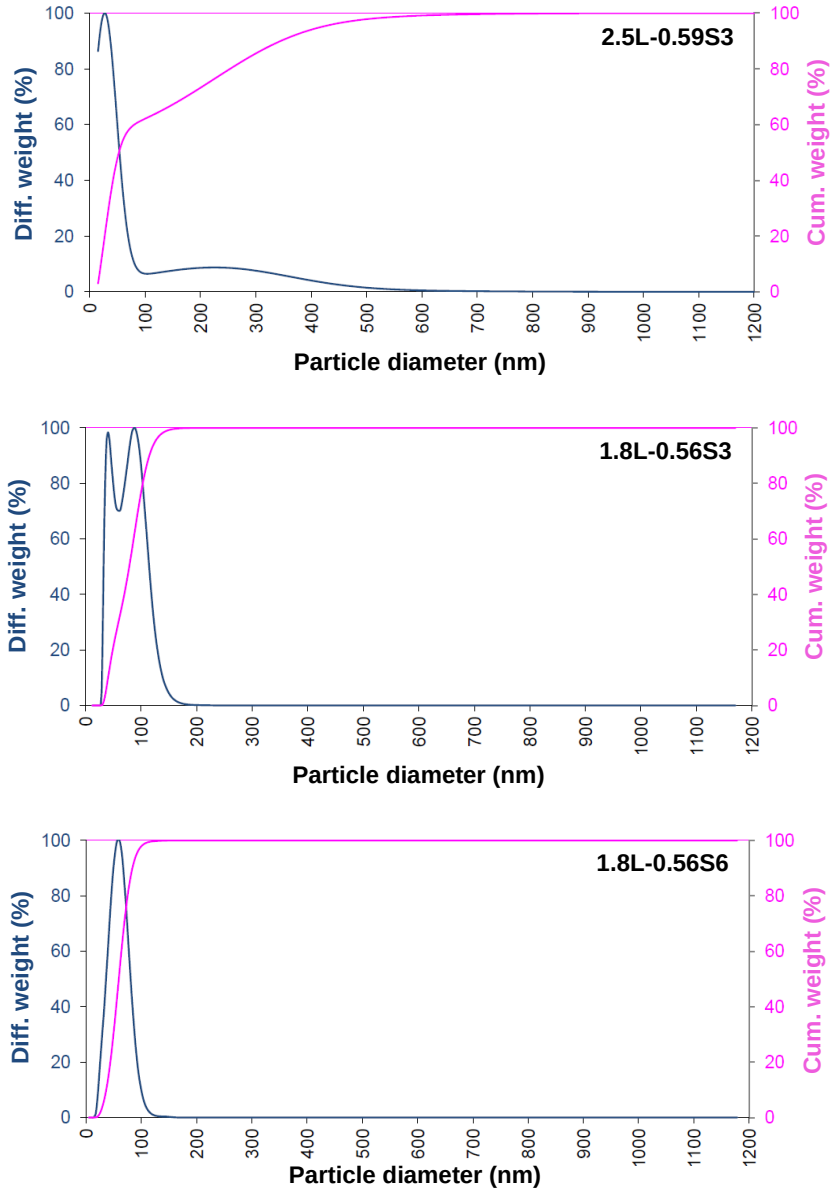

Figure A II.6. Partice size distribution graphs obtained by HDC for the linear PUUs.

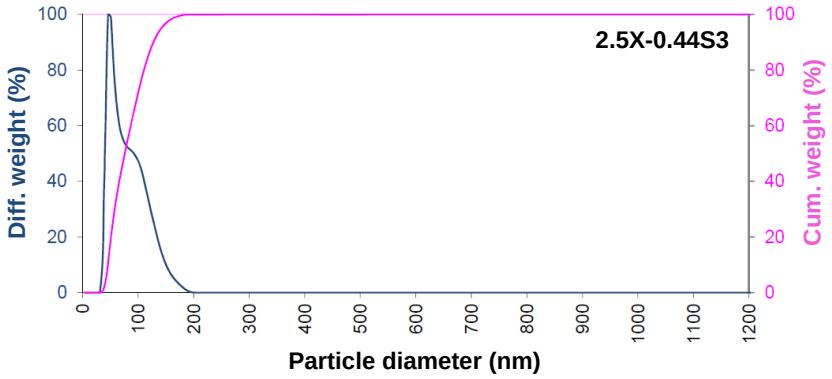
2.5X-0.44S3
Diff. weight (%)
Cum. weight (%)
Particle diameter (nm)
0
20
40
60
80
100
0
100
200
300
400
500
600
700
800
900
1000
1100
1200

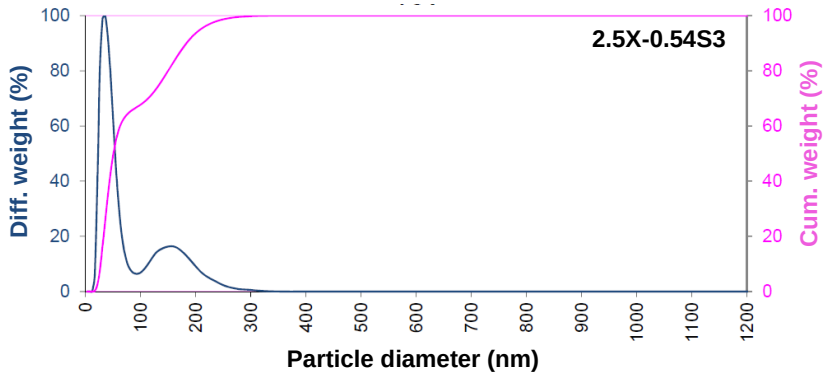
2.5X-0.54S3
Diff. weight (%)
Cum. weight (%)
Particle diameter (nm)
0
20
40
60
80
100
0
100
200
300
400
500
600
700
800
900
1000
1100
1200

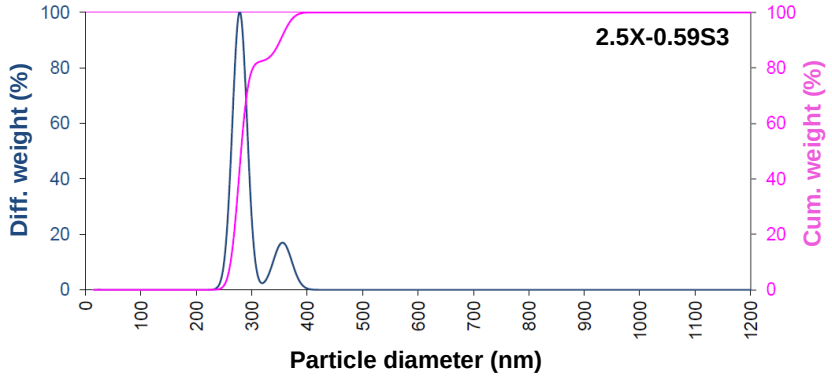
2.5X-0.59S3
Diff. weight (%)
Cum. weight (%)
Particle diameter (nm)
0
20
40
60
80
100
0
100
200
300
400
500
600
700
800
900
1000
1100
1200

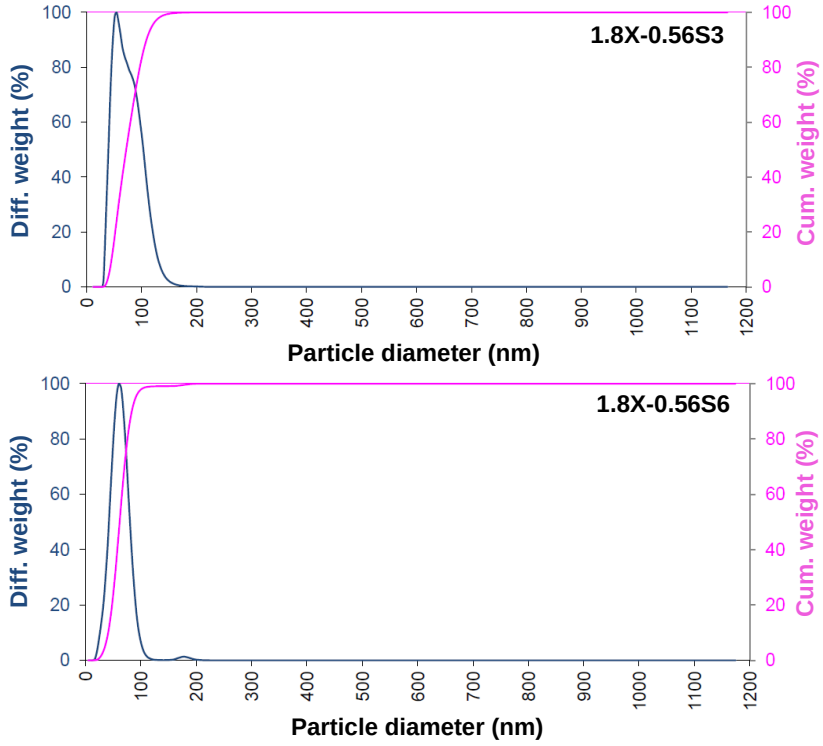

Figure A II.7. Partice size distribution graphs obtained by HDC for the cross-linked PUUs.

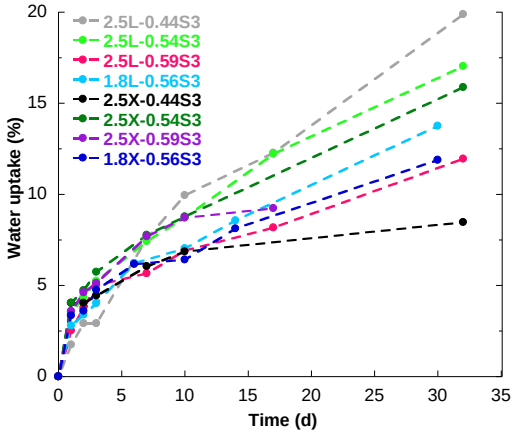

Figure A II.8. Water uptake measurements of both the linear and the cross-linked PUUs.

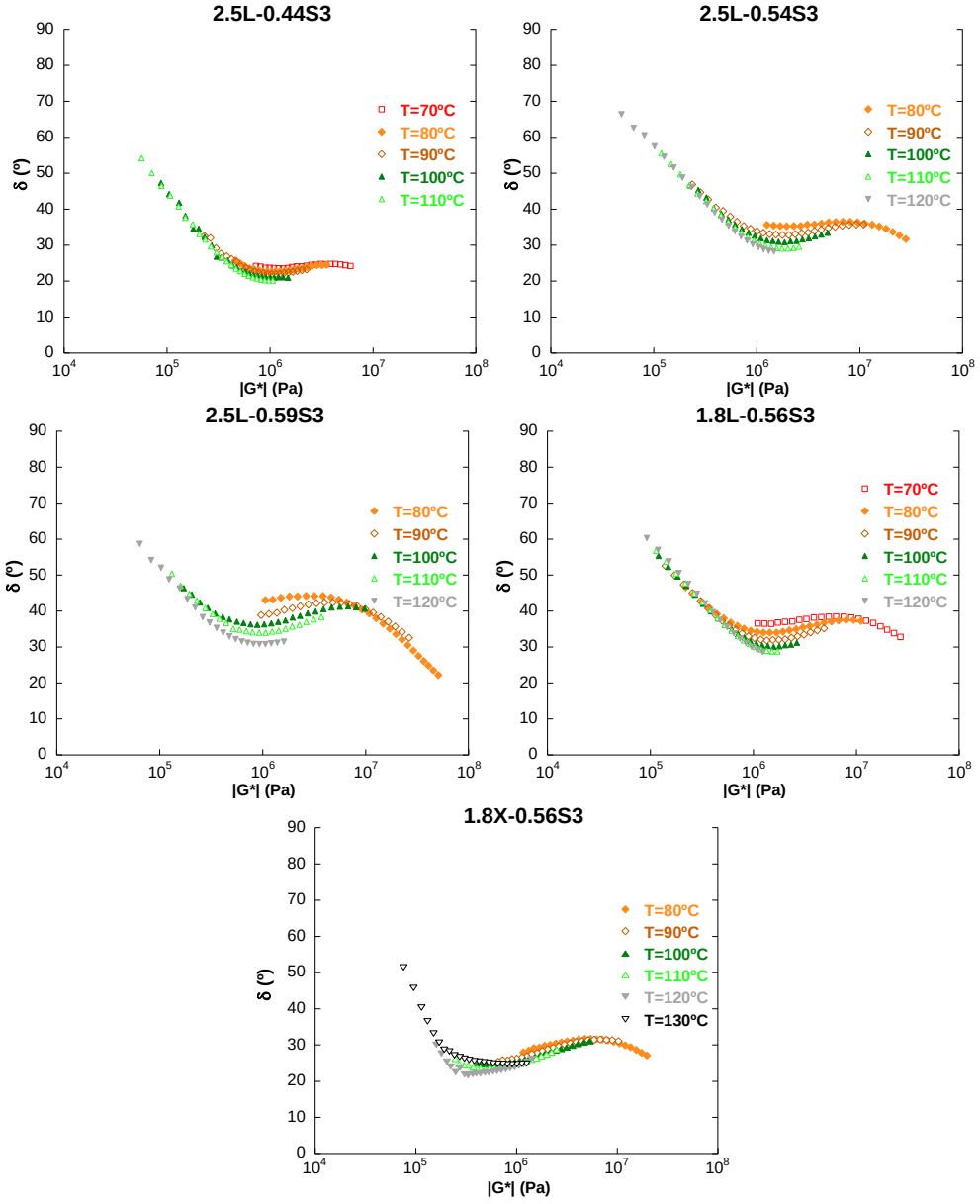

Figure A II.9. van-Gurp-Palmen-plots of PUUs based on $S_2(Ph(CH_2)_3OH)_2$ (S3).

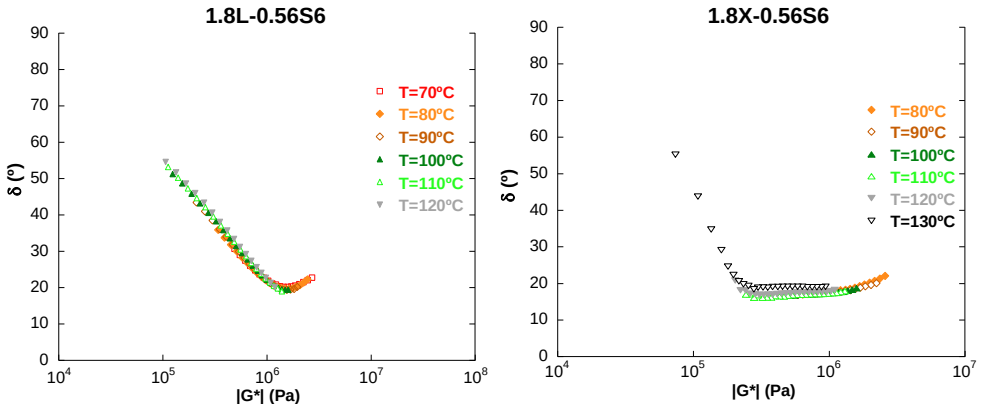

Figure A II.10. van-Gurp-Palmen-plots of PUUs based on $S_2(Ph(CH_2)_6OH)_2$ (S6).

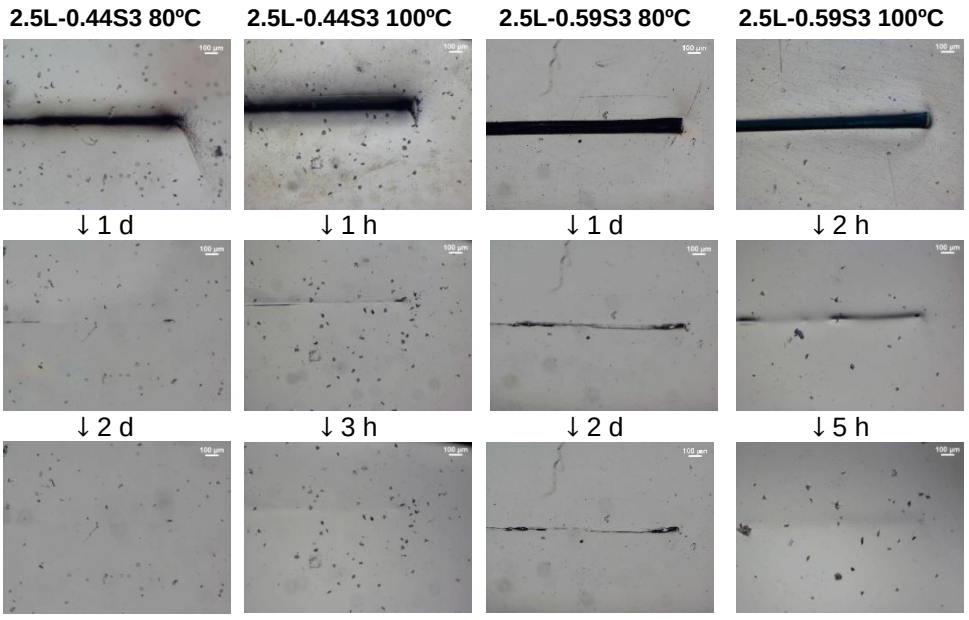

Figure A II.11. Scratch closure at 80°C and 100°C for the soft 2.5L-0.44S3 and hard 2.5L-0.59S3.

Appendix III. Supporting Information Chapter V

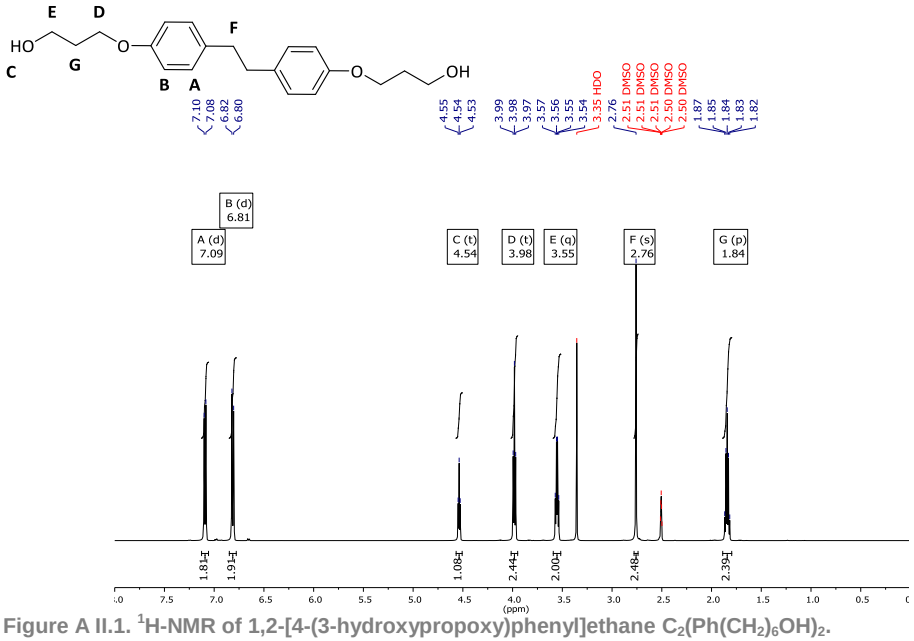

Figure A II.1. ^{1}H-NMR of 1,2-[4-(3-hydroxypropoxy)phenyl]ethane $C_2(Ph(CH_2)_6OH)_2$.

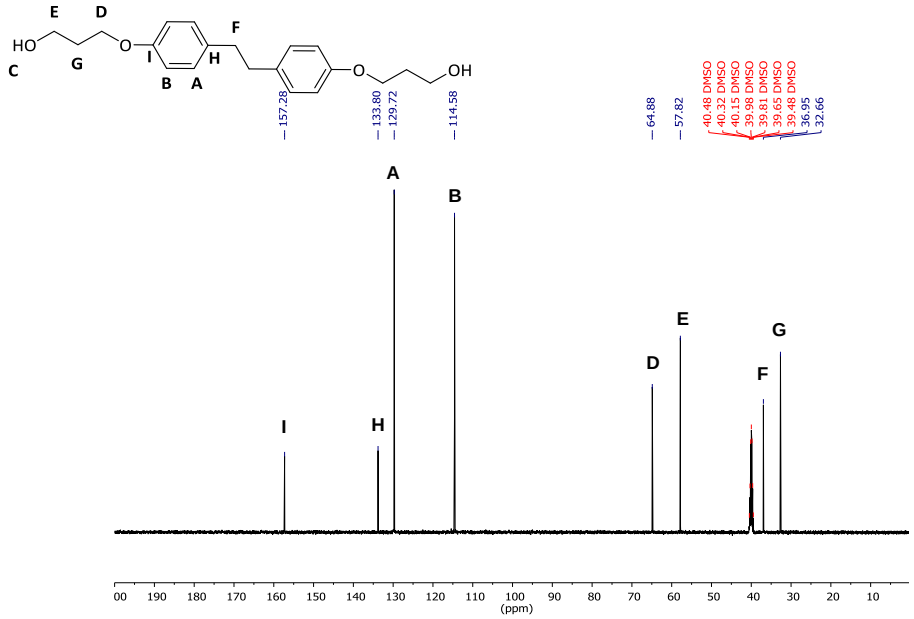

Figure A III.2. ^{13}C{H}-NMR of 1,2-[4-(3-hydroxypropoxy)phenyl]ethane $C_2(Ph(CH_2)_6OH)_2$.

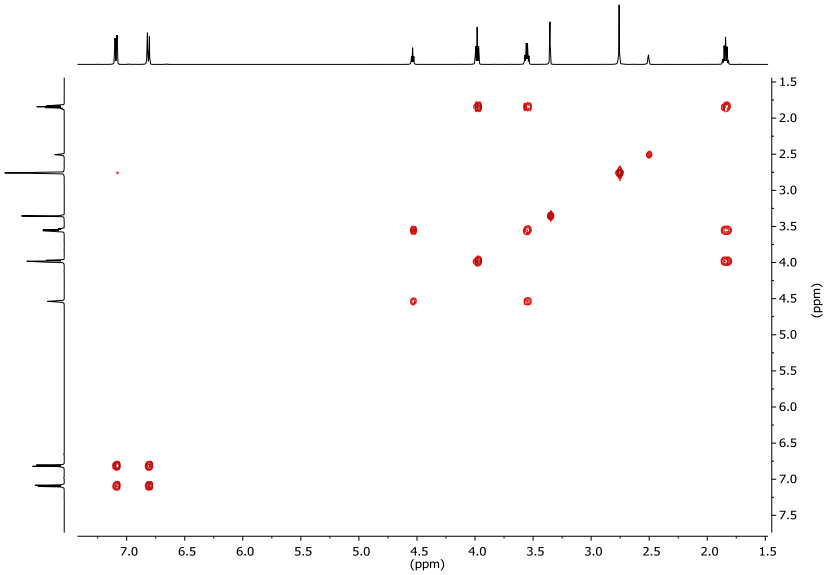

Figure A III.3. g-COSY of 1,2-[4-(3-hydroxypropoxy)phenyl]ethane $C_2(Ph(CH_2)_6OH)_2$.

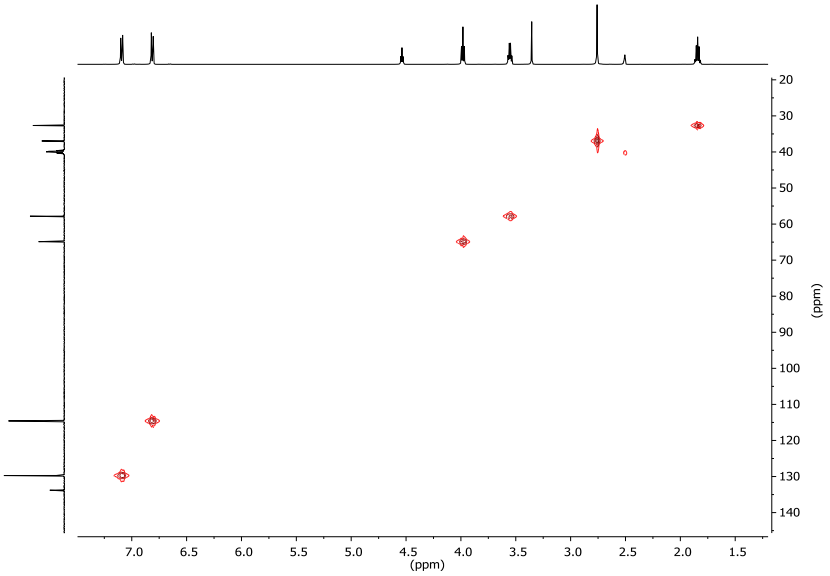

Figure A III.4. g-HSQC of 1,2-[4-(3-hydroxypropoxy)phenyl]ethane $C_2(Ph(CH_2)_6OH)_2$.

Thermal data

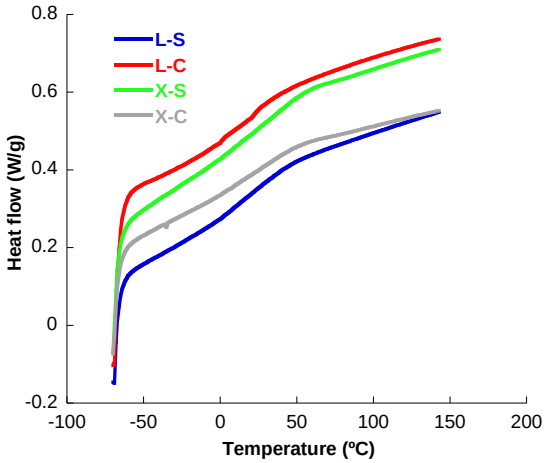

Figure A III.5. DSC results of the series of PUUs showing the heat flow in function of temperature.

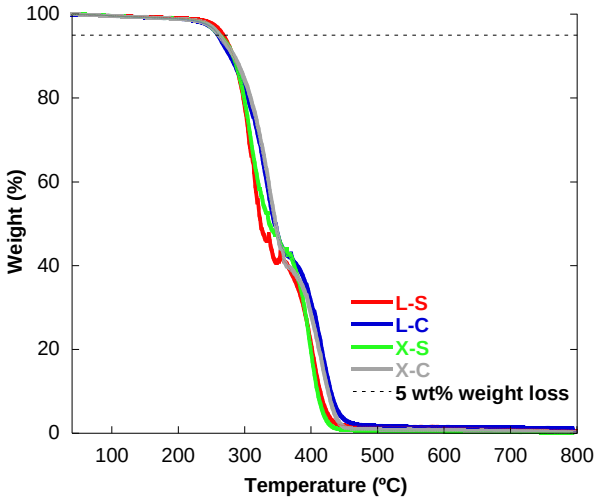

Sample	T_d (5 wt% weight loss)
L-S	267
L-C	260
X-S	263
X-C	262

Figure A III.6. TGA curves of the series of PUUs and the degradation temperature (T_d) at 5 wt% weight loss.

Rheological data

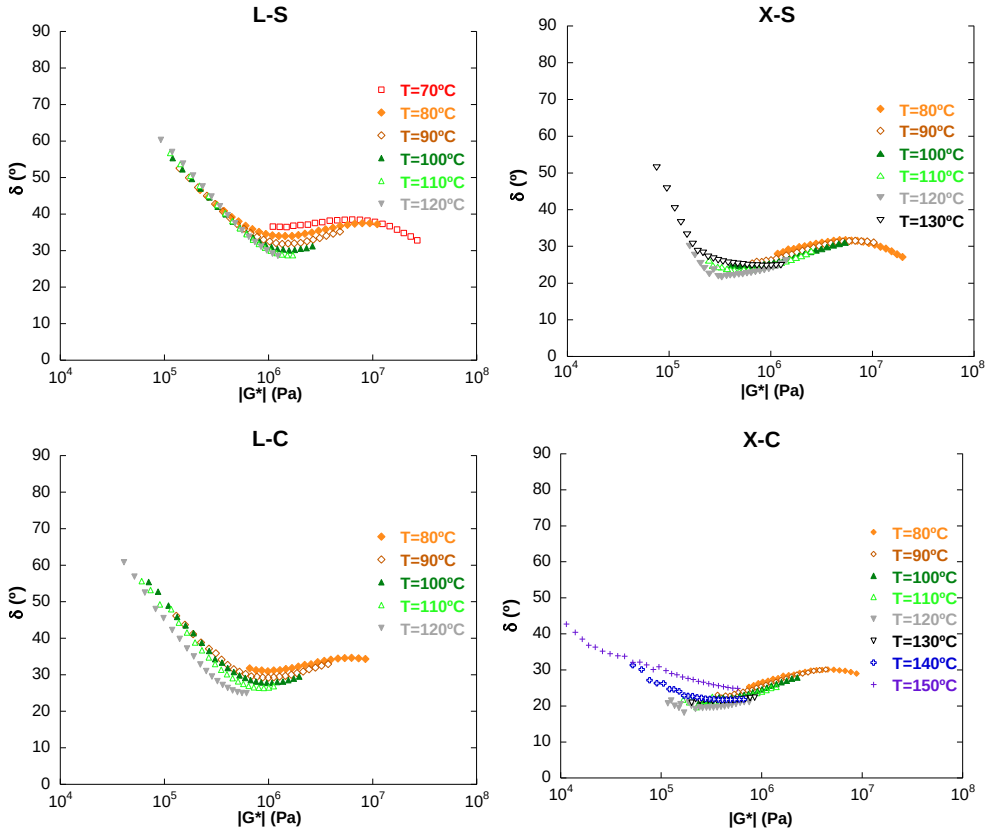

Figure A III.7. van-Gurp-Palmen-plots of the PUUs, depicting phase angle δ *versus* the absolute value of the complex shear modulus $|G^*|$.

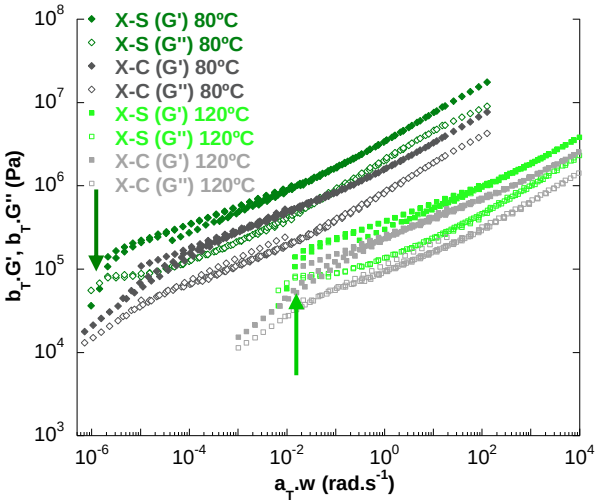

Figure A III.8. Master curves for the cross-linked PUUs at reference temperature of 80ºC and 120ºC.

Fracture mechanics

Three different J values were determined in Chapter V. First, the J-integral based on crack initiation J_{ci} was determined using U_{ci} as the area under the load-displacement curve before crack initiation, depicted as red in Figure A III.9. By combining the load-displacement results with the measured crack tip opening displacement (CTOD) evolution during the fracture tests, the J-integral at crack initiation (J_{ci}), calculated at CTOD=0 mm, could be derived by linear intrapolation of the J-resistance curves functions of the CTOD in the same way as described by van der Zwaag and co-workers.[1] Although the J-integral based on the crack initiation is a common term in fracture mechanics and has been used so far in self-healing properties to determine the healing efficiency, obtaining the value for J_{ci} demands elaborate calculations.[1–3] Therefore, it was favorable to use the J-integral based on complete fracture (J_{tot}) to calculate

the healing efficiencies as this term does not need any additional calculations and can be easily obtained using the equation (1) by introducing U_{tot} as the total area under the load-displacement curve before complete fracture (depicted as the shaded area in Figure A.III.10). It is noteworthy to mention that this is the first time that this can be described using fracture mechanics for healing experiments, as here we can follow the complete crack propagation and fracture of the specimen during the measurement which was not the case for soft elastomers measured with fracture mechanics as they fractured shortly after crack initiation and did not propagate through the complete specimen.[1–3] As a third J-integral, also J_{prop} which is linked to the crack propagation could be calculated as the difference between J_{tot} and J_{ic} and is represented in blue in Figure A III.11. Finally, J_{ic}, J_{prop} and J_{tot} were applied to calculate the healing efficiency (HE) as represented by equation V.2 described in Chapter V..

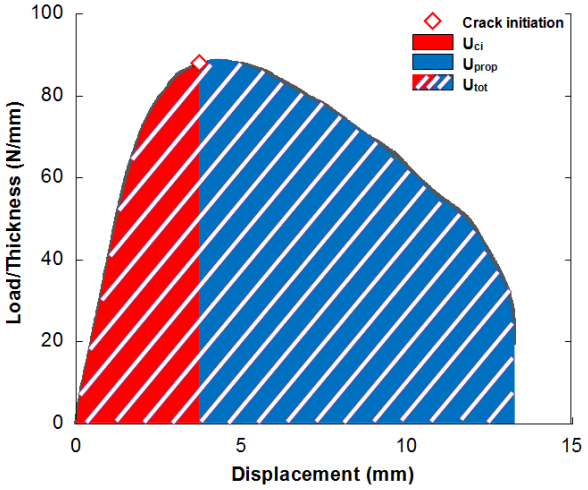

Figure A III.9. Schematic representation of crack initiation (ci), U_{ci}, U_{prop} and U_{tot}.

The healing efficiencies for the PUUs which were obtained using equation V.2 are depicted in function of the healing time for J-integrals based on crack initiation (J_{ic}), crack propagation (J_{prop}) and complete fracture (J_{tot}) are depicted in Figures A III.10 and 11 for the linear and cross-linked PUUs respectively. For these latter results, it is obvious that the healing efficiencies based on J_{prop} and J_{tot} are almost identical, demonstrating that no additional information on the recovery of the materials can be obtained by calculating the healing efficiencies based on the crack propagation. Furthermore, comparing the trends of the healing efficiencies as a function of the healing times obtained from the calculated crack initiation (J_{ci}) and complete fracture (J_{tot}), it can be concluded that although different values were obtained for the healing efficiencies, similar trends are visible for both the linear and cross-linked materials. This demonstrates that the calculation of the J-integral solely based on the readily obtained complete fracture can possibly replace the elaborate calculation of the crack initiation. However, this latter hypothesis would need to be tested for other strong self-healing materials analyzed with fracture mechanics to test the reproducibility and reliability of these statements. For simplification, during further discussion of the results of the healing efficiencies in Chapter V, only those based on complete fracture (J_{tot}) will be considered.

References

1. Grande, A. M., Garcia, S. J. & van der Zwaag, S. On the interfacial healing of a supramolecular elastomer. *Polymer* **56,** 435–442 (2015).
2. Grande, A. M., Bijleveld, J. C., Garcia, S. J. & van der Zwaag, S. A combined fracture mechanical – rheological study to separate the contributions of hydrogen bonds and disulphide linkages to the healing of poly(urea-urethane) networks. *Polymer* **96,** 26–34 (2016).
3. Grande, A. M., Martin, R., Odriozola, I., van der Zwaag, S. & Garcia, S. J. Effect of the polymer structure on the viscoelastic and interfacial healing behaviour of poly(urea-urethane) networks containing aromatic disulphides. *Eur. Polym. J.* **97,** 120–128 (2017).

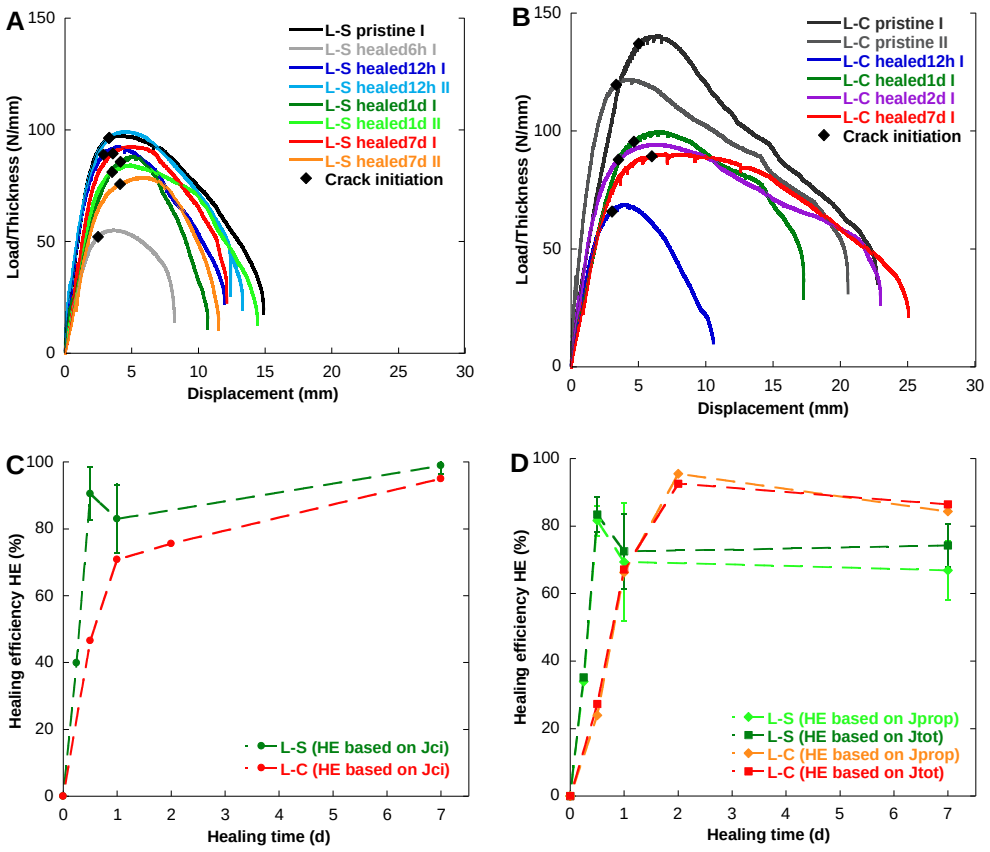

Figure A III.10. Load/Thickness-displacement curves (A: L-S, B: L-C) where crack initiation points for different samples are highlighted; and their healing efficiencies HE based on J_{ci} (C) and J_{prop} and J_{tot}-integrals (D) in function of healing time at 80°C.

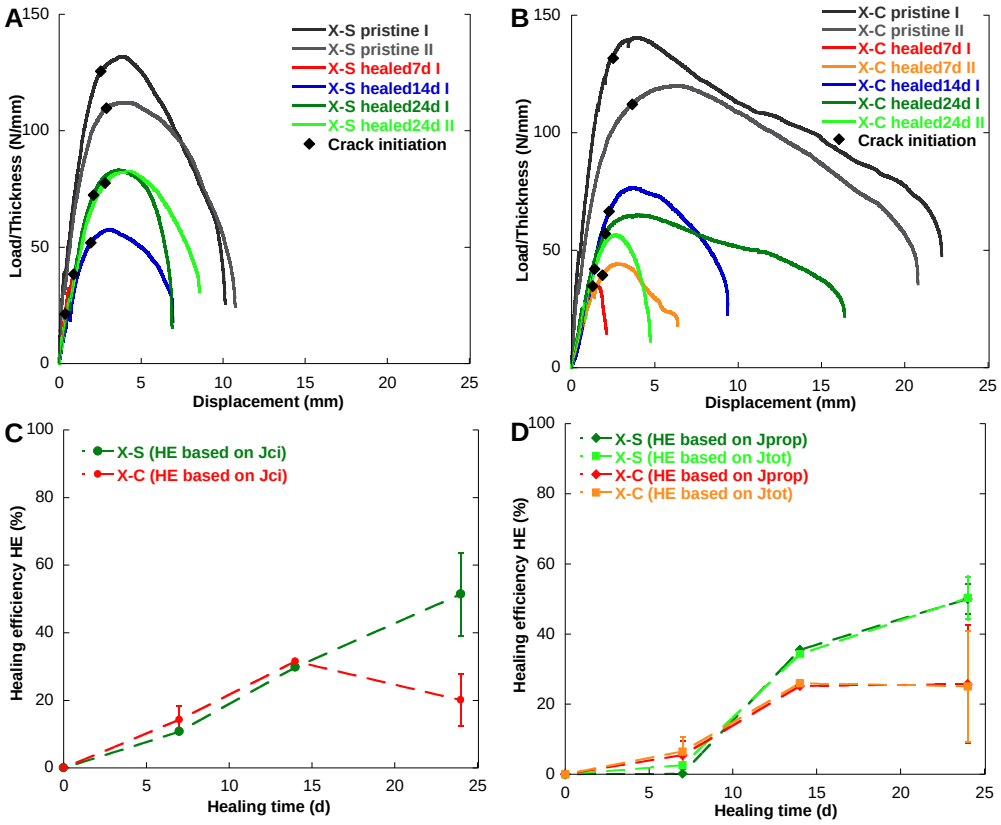

Figure A III.11. Load/Thickness-displacement curves (A: X-S, B: X-C) where crack initiation points for different samples are highlighted; and their healing efficiencies HE based on J_{ci} (C) and J_{prop} and J_{tot}-integrals (D) in function of healing time at 80ºC.

Abbreviations and acronyms

AC/DC/AC	Alternating Current / Direct Current / Alternating Current
a_T	Horizontal shift factor
b_T	Vertical shift factor
$C_2(Ph(CH_2)_3OH)_2$	1,2-[4-(3-Hydroxypropoxy)phenyl]ethane
CTOD	Crack Tip Opening Displacement
DA	Diels-Alder
DBA	Dibutylamine
DBTL	Dibutyltin dilaurate
DEA	Diethylamine
DETA	Diethylene triamine
DLS	Dynamic Light Scattering
DMA	Dynamic Mechanical Analysis
DMPA	2,2-Bis(hydroxymethyl)propionic acid
DMSO	Dimethyl sulfoxide
d_p	Particle size
DSC	Differential Scanning Calorimetry
D(t)	Creep compliance function
DTNB	5,5'-Dithiobis-(2-nitrobenzoic acid)
$\varepsilon_{(f)}$	Strain (at fracture)
E	Young's modulus
E'	Tensile storage modulus
E''	Tensile loss modulus
EHA	2-Ethylhexyl acrylate

EIS	Electrochemical Impedance Spectroscopy
EPR/ESR	Electron Paramagnetic/Spin Resonance spectroscopy
ESI	Electrospray Ionization
EtOAc	Ethyl acetate
FTIR	Fourier Transform Infrared spectroscopy
FRA	Frequency analyzer
G'	Shear storage modulus
G''	Shear loss modulus
$\|G^*\|$	Complex shear modulus
GPC	Gel Permission Chromatography
HCl	Hydrochloric acid
HDA	Hexane-1,6-diamine
HDC	Hydrodynamic chromatography
HE	Healing efficiency
HRMS	High-Resolution Mass Spectroscopy
IPDI	Isophorone diisocyanate
$J_{ci\ /\ prop\ /\ tot}$	Fracture energy based on crack initiation / propagation / total fracture
K_2CO_3	Potassium carbonate
LC/Q-TOF	Liquid Chromatography – Quadrupole Time-Of-Flight
NaCl	Sodium chloride
Na_2SO_4	Sodium sulfate
N_2	Nitrogen
NMP	*N*-Methylpyrrolidone

NMR	Nuclear Magnetic Resonance spectroscopy
MEK	Methyl ethyl ketone
MGP	Methyl α-D-glucopyranoside
MMA	Methyl methacrylate
M_n	Number average molecular weight
M_w	Weight average molecular weight
MWD	Molecular Weight Distribution
OCP	Open Circuit Potential
PEG	Polyethylene glycol
PMMA	Polymethyl methacrylate
PolyTHF	Polytetrahydrofuran
PP	Prepolymer
PS	Polystyrene
pSA	Polystearyl acrylate
PSD	Particle Size Distribution
PU	Polyurethane
PUD	Polyurethane dispersion
PUU	Poly(urethane-urea)
RAFT	Reversible addition-fragmentation chain transfer
RH	Relative Humidity
RI	Refractive Index
RT	Room temperature

$\sigma_{(y/f)}$	Stress (at yield/fracture)
SA	Stearyl acrylate
SC	Solids Content
SEC	Size Exclusion Chromatography
SENT	Single-edged Notch Tension specimen
$S_2(Ph(CH_2)_3OH)_2$	Bis[4-(3'-hydroxypropyloxy)phenyl]disulfide
$S_2(Ph(CH_2)_6OH)_2$	Bis[4-(3'-hydroxypropyloxy)phenyl]disulfide
$S_2(PhNH_2)_2$	Bis(4-aminophenyl)disulfide
$S_2(PhOH)_2$	Bis(4-hydroxyphenyl)disulfide
δ	Phase angle
T	Temperature
Tan δ	Tan delta (storage/loss modulus)
TBP	Tri-*n*-butylphosphine
τ_d	Relaxation time
T_d	Thermal degradation temperature
TEA	Triethylamine
TEMPO	2,2,6,6-Tetramethylpiperidine-1-oxyl
Tex	Texanol
T_g	Glass transition temperature
TGA	Thermogravimetric analysis
THF	Tetrahydrofuran
TNB	2-Nitro-5-thiobenzoate

T_m	Melting temperature
T_{ref}	Reference temperature
$t_{scratch}$	Time needed for scratch closure
TTS	Time Temperature Superposition
UPy	Ureidopyrimidone
UTS	Ultimate Tensile Strength
UV(-vis)	Ultraviolet(-visible)
V70	2,2'-Azobis(4-methoxy-2,4-dimethyl valeronitrile)
vGP	van-Gurp-Palmen
VOC	Volatile Organic Compound
$_d$	Crossover frequency
Z	Impedance